Departament d'Enginyeria Química
Escola Tècnica Superior d'Enginyeria Química
Universitat Rovira i Virgili

FUNCTIONAL OLIGONUCLEOTIDE RECOGNITION NANOMODULES FOR ELECTROCHEMICAL DNA BIOSENSORS

Mònica Campàs i Homs

Tarragona, 2002

Chapter II. Oligonucleotide immobilisation, characterisation and hybridisation detection on gold surfaces

Introduction

The goal of this thesis is to develop novel DNA analytical instruments in the form of DNA sensors and arrays. As explained, the development of such devices passes through the following prerequisite steps:

a) Immobilisation of probes.
b) Arraying.
c) Transduction and hybridisation detection.

This chapter of the thesis describes the preliminary work that led to the choice of solutions for items a) and c). To choose the immobilisation techniques used for arraying, item c) described in Chapters III and IV, it was necessary to examine the different possible routes.

The initial strategy examined for probe immobilisation and hybridisation detection is summarised in Scheme II.1.

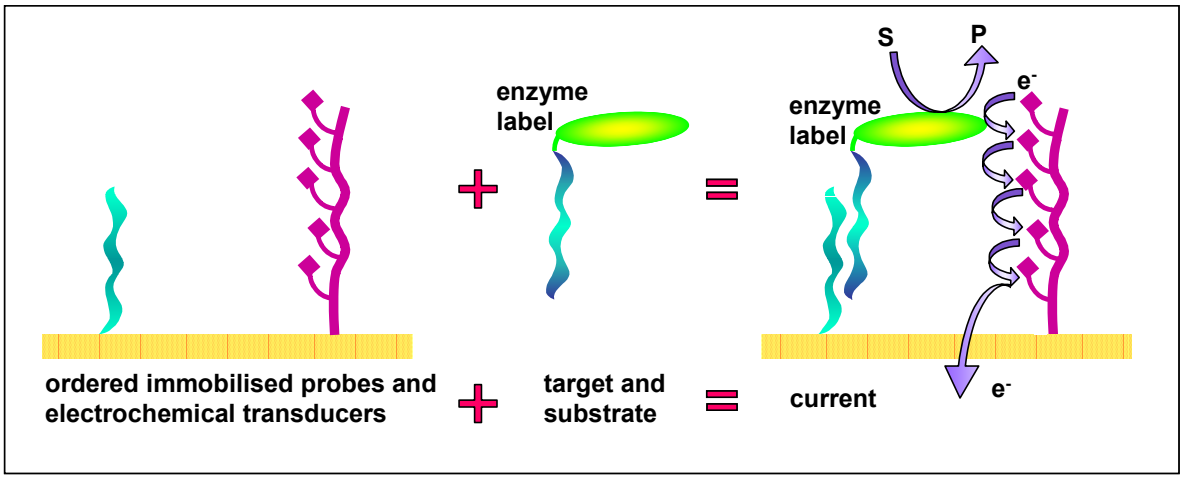

Scheme II.1. Immobilisation and hybridisation strategy.

The configuration described in Scheme II.1 consists of orderly immobilised probes in a mixed monolayer with redox polymers of controlled size. Upon hybridisation of the redox enzyme-labelled target, and in the presence of substrate, the electrons produced are transferred to the electrode surface thorough an electron hopping mechanism that is much more efficient than diffusional electron transfer. This improved electron collection efficiency combined with the reagentless nature of this configuration constitute a definitive advantage of these sensors compared to other available technologies.

Key to the success of this configuration is the ability to co-immobilise the recognition and transduction partners in such a way as to not impair their ability to hybridise whilst facilitating the transfer of electrons from relatively remote distances from the electrode surface. Thus, ordered monolayers on gold surfaces were chosen as the most appropriate strategy to fulfill these requirements.

The dative bonding of thiol-derivatised molecules on Au gives a significant flexibility for immobilisation and transduction. For example, mixed monolayers can achieve desirable spacing and orientation effects. The choice of gold as the immobilisation substrate has the additional advantage that it provides at the same time a transduction surface and the basis of the nanomodular arraying method described in subsequent chapters.

Related to the above is the ability to characterise the efficiency of immobilisation, functionality after immobilisation, and transduction. In the present chapter, these aspects are examined preliminarily. At first, the possibility to construct the SAMs described in Scheme II.1 is examined. Secondly, a survey of methods of quick and functional characterisation of the efficiency and functionality of immobilised biorecognition and transduction partners is made. Thirdly, optical and electrochemical strategies for hybridisation detection are surveyed.

Materials and methods

Materials. Gold (foils, wires, chips and quartz crystals) and glassy carbon were used as immobilisation substrates. Gold foil (0.05mm thickness, 99.99%) was purchased from Sigma. Gold wire (0.5mm diameter, 99.99%) was obtained from Incometal S.A. The National Microelectronics Research Centre (NMRC) of Ireland was the supplier of the 4 x 4mm gold chips on silicon substrate. Gold-covered quartz 5-MHz crystals were obtained from Universal Sensors Inc. 2-mercaptoethanol, 3-(2-pyridyldithio)propionic acid N-hydroxysuccinimide ester (SPDP), *p*-nitrophenyl phosphate (*p*NPP), 3,3',5,5'-tetramethyl-benzidine (TMB), polyoxyethylenesorbitan monolaurate (Tween 20), soybean peroxidase (SBP) and salmon testes DNA were purchased from Sigma. Thioctic acid, 4-mercaptopyridine, 3-mercapto-1-propanesulfonic acid sodium salt (MPS), glutaraldehyde and sodium borohydride ($NaBH_4$) were obtained from Aldrich. 2,2'-Azinobis(3-ethylbenzthiazoline-sulfonic acid) (ABTS), cystamine, 3,3'-dithiodipropionic acid di(N-succinimidyl ester) (DPS), 1-ethyl-3-(3-dimethylaminopropyl)carbodiimide hydrochloride (EDC) and N-hydroxisuccinimide (NHS) were purchased from Fluka. Antidigoxigenin-fluorescein-isothiocyanate Fab fragments (antidig-FITC) and antidigoxigenin-peroxidase Fab fragments (antidig-HRP) were obtained from Boehringer Mannheim. Antidigoxigenin-alkaline phosphatase Fab fragments (antidig-ALP) was purchased from Roche. 3' GTGCCAAGTCCCAATCGGTGTGAAACGCCC-SH 5' or 3' CTTTGTGGTTACTATAAATTTTTTTTTTTT-SH 5' (oligonucleotide-thiol), 3' FITC-GTGCCAAGTCC CAATCGGTGTGAAACGCCC-SH 5' (FITC-oligonucleotide-thiol), 3' GTGCCAAGTCCCAATCG

GTGTGAAACGCCC-amine 5' (amino-oligonucleotide), 3' GGGCGTTTCACACCGATTGGGACTTG GCAC 5' (complementary oligonucleotide), 3' digoxigenin-GGGCGTTTCACACCGATTGGGACTTG GCAC 5' (dig-labelled complementary oligonucleotide), 3' GGGCGTTTCACACCGATTGAGACTCG TAAC 5' (non-complementary oligonucleotide), 3' digoxigenin-GGGCGTTTCACACCGATTGAGA CTCGTAAC 5' (dig-labelled non-complementary oligonucleotide), 3' TTTATAGTAACCACAAAGCC CCCCCCCC CC-amine 5' (fully complementary amino-oligonucleotide), 3' ATAGTAGAAACCACAA AGCCCCCCCCCCCC-amine 5' (amino-oligonucleotide with 4-point mutations) were obtained from Isogen or Genosys. NAP^{TM}-10 columns (with Sephadex^{TM} G-25 DNA grade) were obtained from Amersham Pharmacia Biotech AB. [Os(2,2'-bipyridine)$_2$Cl(4-(aminomethyl)pyridine)]Cl, [Os(2,2'-bipyridine)$_2$Cl (pyridine-4-carboxylic acid)]Cl, [Os(2,2'-bipyridine)$_2$Cl(4-pyridylacetic acid)]Cl and Os(4,4'-dimethyl-2,2'-bipyridine)$_2$Cl$_2$ were synthesised as explained in Chapter V. The controlled size redox "wire" indicated in Scheme II.1 was synthesised by Peptide Technologies Corporation, and its structure was based on an oligopeptide (poly Lys) modified with isonicotinyl groups on the ε amino groups. This 15-mer was subsequently modified either on the electrode or in bulk with Os(4,4'-dimethyl-2,2'-bipyridine)$_2$Cl$_2$. The positive redox "wire" polymer used in the hybridisation detection was synthesised derivatising the PVP backbone with Os(2,2'-bipyridine)$_2$Cl$_2$ and 2-bromoethylamine hydrobromide, according to the procedure described by Katakis (1994).

Instrumentation. Cyclic voltammograms were obtained using either a BAS CV-1B or an AUTOLAB PGSTAT10 potentiostat in a conventional three-electrode cell, with Ag/AgCl as reference electrode and Pt as counter electrode. Frequency changes were measured with a Universal Sensors Inc. PZ-1000 quartz crystal microbalance (QCM). Colourimetric measurements were performed with a Molecular Devices 340PC 96-well plate reader. Fluorescence was measured with a Nikon E600FN fluorescence microscope equipped with a Sony CCD camera.

Electrode preparation. Gold wires, foils and chips were cleaned with "piranha's solution" (70% H_2SO_4 : 30% H_2O_2, 60ºC) and rinsed with distilled water to remove any adventitious organic and inorganic material prior to adsorption of the SAM as a precaution. Extreme caution should be used with this solution since it reacts violently with organic material and all work should be carried out in a fumehood. This cleaning process was inappropriate for the gold-covered quartz crystals because the drastic conditions removed the gold form the corresponding surface. Consequently, they were cleaned by immersion in 1.2M NaOH for 5min, rinsing with water, immersion in 1.2M HCl for 5min, rinsing with water, placing a 12.2M HCl drop on the gold for 5min, rinsing with water and letting them dry. The cleanliness of the gold was checked by cyclic voltammetry in 0.1M H_2SO_4. Glassy carbon electrodes were polished with 5, 1 and 0.3μm alumina on polishing clothes (Buehler), rinsed with water and sonicated for 15min.

SAMs formation and characterisation. SAMs were formed by immersion of the gold surface into a solution with thiol-containing molecules for different time periods (Scheme II.2). Cystamine SAMs

were obtained by immersion into a 100mM aqueous cystamine solution for 2h with stirring. Thioctic acid SAMs were obtained by immersion into a 10 or 100mM thioctic acid in 50% ethanol : 50% water for 12h with stirring. DPS SAMs were obtained by immersion into a 10mM DPS solution in DMF for 30min with stirring. MPS SAMs were obtained by immersion into a 2mM MPS in 50% ethanol : 50% water for 12h with stirring. Mixed monolayers with thioctic acid and blocking agents like mercaptoethanol and mercaptopyridine were formed simultaneously, by immersion of the solid surface into a solution with both thiol-containing molecules (10 or 100mM thioctic acid and 1mM blocking agent in 50% ethanol : 50% water) for 2h with stirring, or sequentially, by immersion firstly into the thioctic acid solution (10 or 100nM in 50% ethanol : 50% water) for 12h with stirring and afterwards into the blocking agent solution (1mM in ethanol) for 2h with stirring.

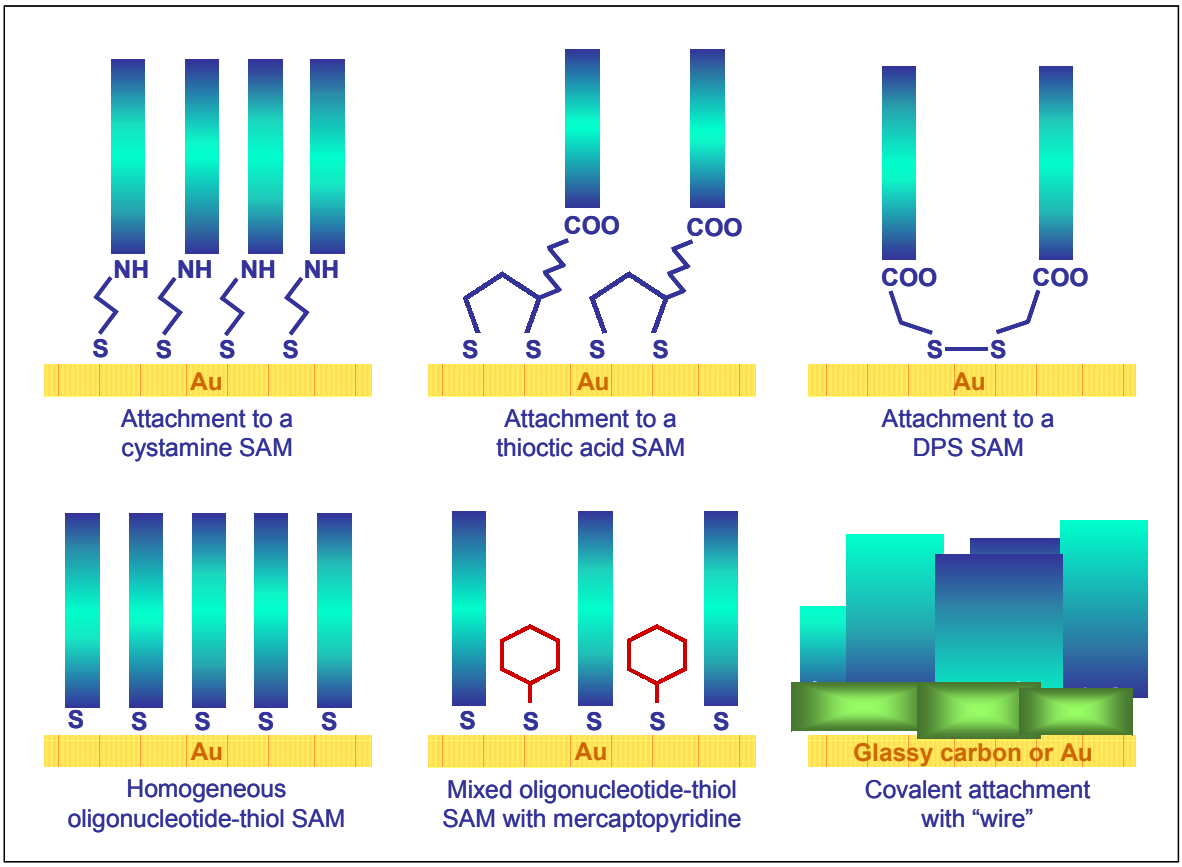

Scheme II.2. DNA immobilisation techniques.

The effectiveness of cystamine, thioctic acid, mercaptoethanol and mercaptopyridine SAMs was characterised by cyclic voltammetry in 0.5M KOH or in 0.1M phosphate buffer, 0.15M NaCl, pH 6.0, at 100mV s^{-1} and under argon to avoid oxygen reduction, which would interfere in the detection of the thiol reduction that takes place at around -0.7V (*vs.* Ag/AgCl). Cystamine and thioctic acid SAMs were also characterised measuring the surface coverage due to the non-specific adsorption of [Os(2,2'-bipyridine)$_2$Cl(4-(aminomethyl)pyridine)]Cl and [Os(2,2'-bipyridine)$_2$Cl(pyridine-4-carboxylic acid)]Cl (dissolved in water or DMF) after immersion for 2h. The surface coverage of adsorbed

complex was determined in 0.1M phosphate buffer, 0.15M NaCl, pH 6.0, at 100mV s^{-1} after washing the electrodes. It was assumed that non-specific adsorption occurred on the pinholes.

To study the ability of cystamine and thioctic acid SAMs to react with oligonucleotides, the redox complexes [Os(2,2'-bipyridine)$_2$Cl(4-(aminomethyl)pyridine)]Cl and [Os(2,2'-bipyridine)$_2$Cl(4-pyridylacetic acid)]Cl were covalently attached to the reactive groups of the cystamine and thioctic acid SAMs, respectively, via EDC reaction in 0.1M acetate buffer, pH 5.1, at 100mV s^{-1}, and the surface coverage due to the complexes was measured electrochemically

DNA immobilisation and characterisation. Amino-oligonucleotides were directly attached to the ester groups of the DPS SAM, simply by immersion of the DPS-modified surface into a 0.05, 0.5 or 50µg mL^{-1} amino-oligonucleotide solution for 2h with stirring. This binding was followed in real time by measuring the corresponding frequency change in the quartz crystal microbalance (QCM). In another characterisation technique, the amino-oligonucleotide was attached to a DPS SAM formed on a gold wire, hybridised with a dig-labelled complementary oligonucleotide (and with the dig-labelled non-complementary oligonucleotide as a control), and incubated with antidig-FITC.

FITC-oligonucleotide-thiol and oligonucleotide-thiol SAMs were obtained after immersion into 0.5 or 1ng mL^{-1} (for the FITC-oligonucleotide-thiol), and 0.2 or 90ng mL^{-1} (for the oligonucleotide-thiol) solutions in 0.1M phosphate buffer, pH 8.0, for 1h with stirring. Mixed monolayers with oligonucleotide-thiol and blocking agents like mercaptoethanol and mercaptopyridine were formed simultaneously, by immersion of the solid surface into a solution with both thiol-containing molecules (0.1ng mL^{-1} oligonucleotide-thiol and 1.1, 100, 110nM, 1, 10 or 11mM blocking agent) for 2h with stirring, or sequentially, by immersion firstly into the oligonucleotide-thiol solution and afterwards into the blocking agent solution. When sequential mixed monolayers were formed, the blocking agents were used at 2.2, 220nM or 22mM concentration for different times (15, 30, 45min, 1 or 2h) with stirring. FITC-oligonucleotide-thiol SAMs were characterised by measuring the fluorescence emitted by the FITC moiety. The surface coverage of oligonucleotide-thiol SAMs was characterised by the QCM technique, by cyclic voltammetry in 0.5M KOH or in 0.1M phosphate buffer, 0.15M NaCl, pH 6.0, at 100mV s^{-1} and under argon, and also by the electrochemical detection of guanine at +0.8V (*vs.* Ag/AgCl) in 10mM acetate buffer, 0.1M NaCl, pH 4.7.

Covalent attachment immobilisation technique was also attempted. Bare or MPS-modified electrodes were immersed into a solution containing 30µg mL^{-1} of the positive redox "wire" polymer for 6h with stirring. The electrode was then introduced into a 5µg mL^{-1} amino-oligonucleotide or 0.2ng mL^{-1} oligonucleotide-thiol solution, for 3h with stirring. Some electrodes were immersed in 1.5µg mL^{-1} SPDP (in 0.1M phosphate buffer, pH 8.0) for 30min with stirring, between the "wire" and the oligonucleotide steps in order to favour the cross-linking. This last procedure was also used with glassy carbon. The amino-oligonucleotide or oligonucleotide-thiol immobilisation efficiency and

functionality were characterised by hybridisation with SBP-labelled complementary oligonucleotide and electrochemical detection.

Amino-oligonucleotide labelling with SBP. The reaction procedure is depicted in Scheme II.3. 5mg of SBP were dissolved in 1mL of 0.1M phosphate buffer, pH 7.0, and 0.1mL of freshly dissolved sodium periodate in water (110mM) was added to a final concentration of 10mM. The mixture was left to react for 30min with stirring protected from light. Afterwards, the reaction was stopped by adding 0.11mL of ethylene glycol for 20min at 4ºC. The activated enzyme was purified by filtration with a G-25 Sephadex separation column. 1mL of the activated enzyme (7-fold molar excess) was added to 0.25mL of a 70.84µM amino-oligonucleotide solution (fully complementary or with 4 mutations, in 0.1M phosphate buffer, pH 7.8) and allowed to react for 3h at 4ºC with stirring protected from light. 0.5mL of 0.4M $NaBH_4$ were added to a final concentration 0.1M and the solution was allowed to react overnight at 4ºC with stirring protected from light. The final concentration of oligonucleotide was 10.12µM. The activity of the conjugated SBP was measured spectrophotometrically with the ABTS enzymatic assay, recording the absorbance change at 405nm. The activity of conjugated SBP was 33.58U mg^{-1}, 58.62% of native SBP. The loss of activity was presumably due to the periodate oxidation step.

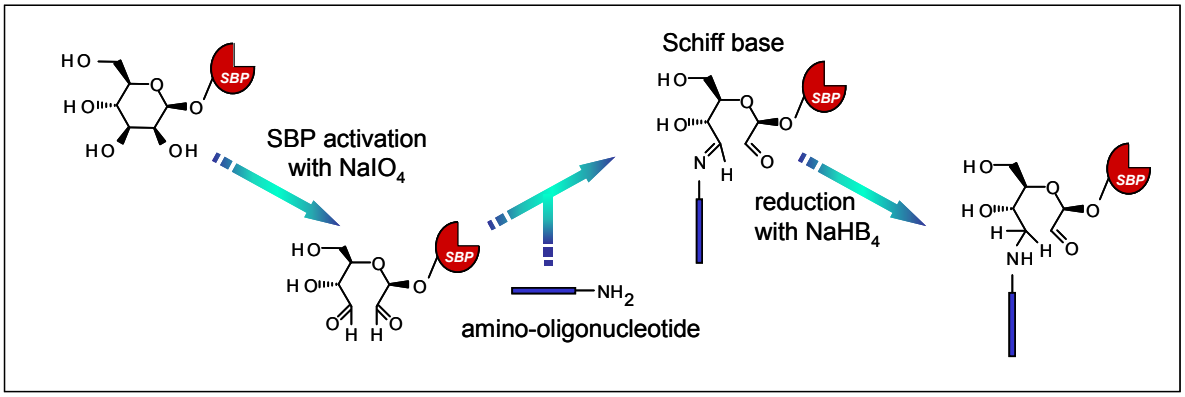

Scheme II.3. SBP-amino-oligonucleotide conjugation.

DNA hybridisation. Hybridisation was carried out with 0.04, 0.34, 0.4, 3.4 and 34ng mL^{-1} complementary oligonucleotide in 1 x SSC, 2.5 x Denhardt, 10mM tris-HCl, 1mM EDTA, pH 7.5, or 50mM tris-HCl buffer, 1M NaCl, pH 7.0, usually for 1h at 48 or 58ºC with stirring. Different blocking agents were used before (1% baby milk in 0.1M phosphate buffer, pH 7.0 for 1h at 37ºC with stirring) and/or during the hybridisation step (hybridisation buffer containing 1% baby milk, 0.2% Tween 20, 10ng mL^{-1} or 1µg mL^{-1} salmon testes DNA). Oligonucleotides were labelled with digoxigenin or SBP. Blanks were performed with non-complementary oligonucleotides or oligonucleotides with 4-point mutations depending on the needs.

DNA hybridisation measurement. For the hybridisation detection with dig-labelled oligonucleotides, after the hybridisation and a blocking step with BSA (1% in 50mM tris-HCl buffer,

150mM NaCl, pH 7.6, for 1h at 37ºC), the electrode was incubated in 50mM tris-HCl buffer, 150mM NaCl, pH 7.6, 1% BSA, containing antidig-ALP (1:2500 dilution) or antidig-FITC (1:5 dilution) conjugate for 1h at 37ºC with stirring. The fluorescence emitted by the antidig-FITC was detected by fluorescence microscopy. The electrodes with antidig-ALP were incubated with *p*NPP (1mg mL^{-1} in 0.1M DEA buffer, 50mM KCl, 1mM $MgCl_2$, pH 9.5) for 1h at 37ºC with stirring, and the reaction was stopped with H_2SO_4. Afterwards, the absorbance change was measured using a 96-well plate reader. Hybridisation with SBP-amino-oligonucleotide conjugate was detected by colourimetry, after incubation in TMB / H_2O_2 (100µL of TMB (10mg mL^{-1} in DMSO) + 2µL H_2O_2 + 10mL of 0.1M acetate buffer, pH 6.0) for 1h at 37ºC with stirring, or electrochemically, measuring the response to a saturated concentration of H_2O_2 in the presence of a positive redox polymer adsorbed *a posteriori* (in oligonucleotide-thiol SAMs) or cross-linked (in covalent oligonucleotide immobilisation) in 0.1M phosphate-acetate buffer, pH 5.0, and the working potential being at +0.1V (*vs.* Ag/AgCl). Scheme II.4 shows the global colorimetric system.

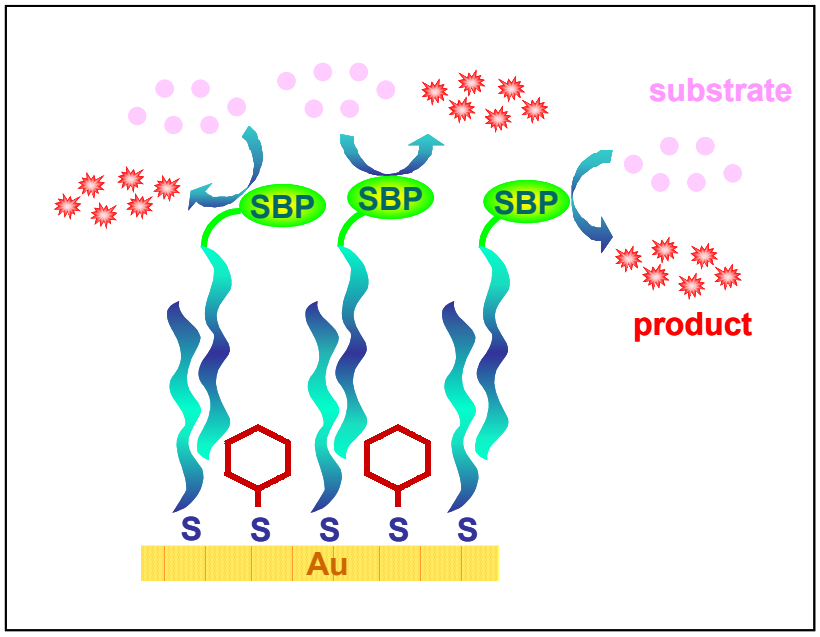

Scheme II.4. Colorimetric detection of hybridisation: mixed SAM / SBP-labelled complementary sequence / TMB + H_2O_2 / H_2SO_4.

Results and discussion

Electrode preparation. Gold electrode cleanliness was checked by cyclic voltammetry in 0.1M H_2SO_4, as the cyclic voltammogram of clean gold shows an oxidation peak at +1.3V (*vs.* Ag/AgCl) and a reduction peak at +0.9V (*vs.* Ag/AgCl) corresponding to metal oxide formation and reduction (Figure II.1). Furthermore, any residue of organic contaminant left by preceding cleaning treatments is removed during repeated oxidation and reduction of the gold. By finishing the scan at a negative potential an oxide-free gold surface was ensured. Although cleaning with “piranha’s solution” is a

very drastic treatment, it is necessary to mention that even under these extreme cleaning conditions, on some occasion adsorbed osmium complexes were difficult to remove and the repetition of the cleaning procedure was needed.

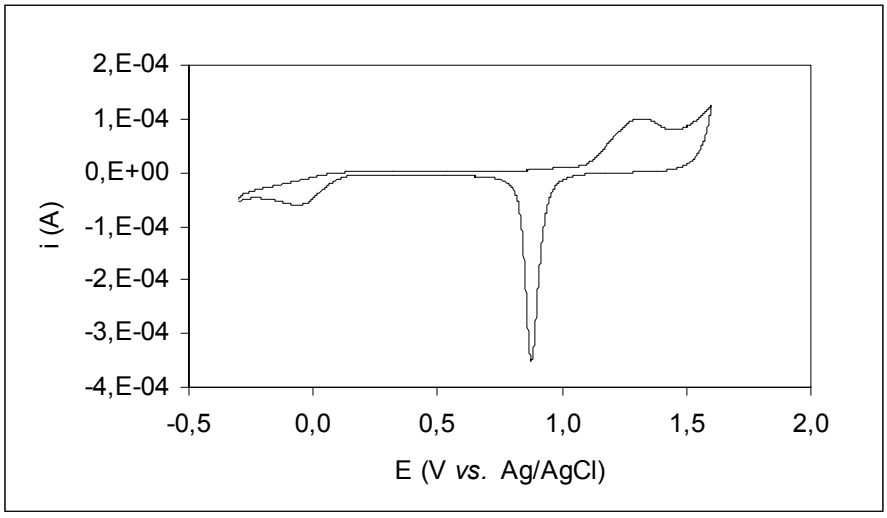

Figure II.1. Cyclic voltammogram of a gold electrode in 0.1M H_2SO_4 at 100 mV s^{-1}.

SAMs formation and characterisation. At sufficiently negative potentials the dative bond of thiol groups to Au can be reduced with consequent thiol desorption. Cystamine, thioctic acid and mercaptopyridine SAMs were characterised making use of this property. Cyclic voltammograms showed a reduction peak at -0.7V (*vs.* Ag/AgCl), indicating the SAM presence. By repetitive scans, the reduction peak intensity decreased, reflecting the desorption of thiols bound to the gold and, consequently, the loss of material assembled to the surface (Figure II.2).

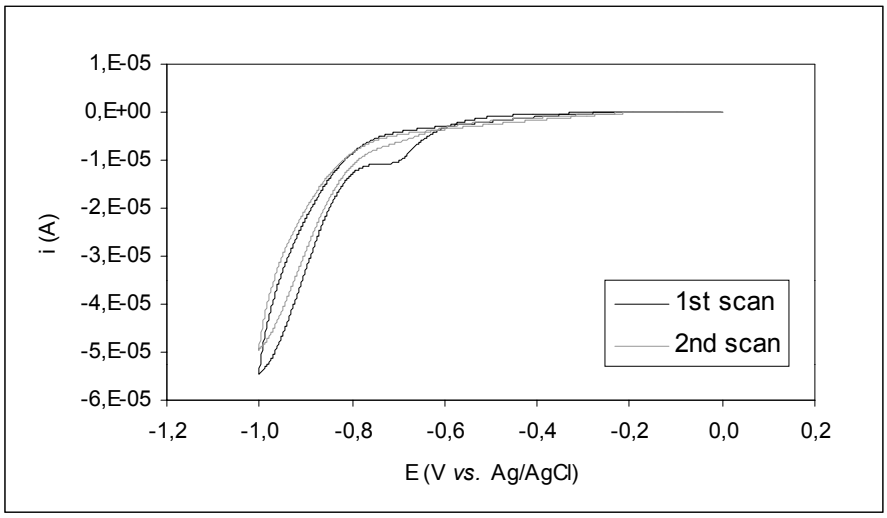

Figure II.2. 1st and 2nd cyclic voltammograms for the reduction of the Au-S bond in the mercaptopyridine SAM in 0.1M phosphate buffer, 0.15M NaCl, pH 6.0 at 100mV s^{-1}.

This technique, although useful to verify and quantify SAM formation, is destructive and does not allow the further use of the electrodes, but it was used to optimise the SAM formation assuming in subsequent experiments that equivalent SAMs were formed when the same conditions were used. This reduction peak, although prominent with mercaptopyridine SAMs, was not as clear or reproducible with cystamine or thioctic acid monolayers. For this reason, these compounds' self-assembly was characterised by the adsorption of osmium redox compounds on the pinholes or the SAM.

Ordered immobilisation of controlled size transduction oligomers. When the oligopeptide described in the experimental section was modified in bulk or on the surface of electrodes with Os redox compounds, identical surface coverage and low transduction efficiency even from redox enzymes led to the suspicion that the majority of the electrochemical signal was produced by a non-specific adsorption event of the Os complex directly on the gold surface. This phenomenon (if true) would prohibit exploitation of the ordered architecture for efficient electron transduction from the redox enzyme label. For this reason, two redox couples [Os(2,2'-bipyridine)$_2$Cl(4-(aminomethyl) pyridine)]Cl and [Os(2,2'-bipyridine)$_2$Cl(pyridine-4-carboxylic acid)]Cl were left to adsorb on differently modified Au surfaces. The results are summarised in Table II.1.

Table II.1. Adsorption of Os redox couples on Au-SAMs*.

Type of SAM	Adsorption solution	Redox couple	Os surface coverage (x 10^{11} mol cm^{-2})	Standard deviation
None	water	[Os(bipy)$_2$Cl(py-NH$_3^+$)]Cl	6.18	0.08
Cystamine	"	"	2.16	1.14
Thioctic acid	"	"	30.30	2.50
Mixed thioctic acid / mercaptoethanol	"	[Os(bipy)$_2$Cl(py-NH$_3^+$)]Cl	14.3	1.20
Mixed thioctic acid / mercaptopyridine	"	"	9.57	0.78
None	DMF	[Os(bipy)$_2$Cl(py-NH$_3^+$)]Cl	none	none
Cystamine	"	"	none	none
Thioctic acid	"	"	2.38	0.40
None	"	[Os(bipy)$_2$Cl(py-COOH)]Cl	none	none
Cystamine	"	"	none	none
Thioctic acid	"	"	0.32	0.08
Mixed thioctic acid / mercaptopyridine	"	"	0.15	0.004

* Surface coverage was determined by the integration of charge passed during CVs (200mV s^{-1}) in fresh buffer after washing the electrodes subsequent to modification as described in the experimental part.

Further to these results should be added the following observations: a) that sequential *vs.* simultaneous formation of the mixed monolayers did not result in any difference in the results, although sequential formation seemed to lead to more reproducibility and b) that protonation of the

thioctic acid SAM yielded one order of magnitude lower non-specific adsorption of [Os(2,2'-bipyridine)$_2$Cl(4-(aminomethyl)pyridine)]Cl.

The aforementioned demonstrates that a very high non-specific interaction exists between the osmium complexes and the gold surface, regardless of the existence of the SAM. This fact was underlined by the fact that Os-treated gold surfaces were almost impossible to clean even after repeated treatments in "piranha's solution". It was therefore determined that only the use of DMF solution for further SAM modification could lead to the type of architectures stipulated in Scheme II.1. Apparently, due to the low dielectric constant of DMF and the fact that it is a better solvent for the Os complexes (except for [Os(2,2'-bipyridine)$_2$Cl(4-pyridylacetic acid)]Cl), it is possible to achieve this ordered immobilisation procedure. A similar effect was observed if the thioctic acid-modified electrodes were immersed in a buffer of a lower pH before the mediator adsorption step, apparently due to the protonation of thioctic acid and the reduction of the electrostatic attraction of the SAM with the modifying Os moieties. For this reason, subsequent experiments to determine the capacity of selective (as opposed to non-specific) attachment of Os centres to SAMs were carried out under these conditions.

The reactivity of cystamine and thioctic acid SAMs was studied reacting [Os(2,2'-bipyridine)$_2$Cl(4-(aminomethyl)pyridine)]Cl and [Os(2,2'-bipyridine)$_2$Cl(4-pyridylacetic acid)]Cl with thioctic acid and cystamine SAMs, respectively, via EDC, the surface coverage providing an indication of the reaction yields. The surface coverage from the non-specific adsorption of these osmium complexes on the SAMs was compared with that after EDC. [Os(2,2'-bipyridine)$_2$Cl(4-pyridylacetic acid)]Cl was used instead of [Os(2,2'-bipyridine)$_2$Cl(pyridine-4-carboxylic acid)]Cl because the carboxylic group was more reactive towards activation with EDC. The conclusions were:

1) There were no differences between the EDC reaction in 0.1M acetate buffer, pH 5.1, between the cystamine SAM and the [Os(2,2'-bipyridine)$_2$Cl(4-pyridylacetic acid)]Cl complex ($\Gamma = 2.11 \times 10^{-11} \pm 0.21 \times 10^{-11}$mol cm^{-2}) and the non-specific adsorption in DMF ($\Gamma = 1.83 \times 10^{-11} \pm 0.82 \times 10^{-11}$mol cm^{-2}), suggesting that this could not be a suitable strategy for the ordered and selective modification of the SAM.

2) In the EDC reaction between [Os(2,2'-bipyridine)$_2$Cl(4-(aminomethyl)pyridine)]Cl in 0.1M acetate buffer, pH 5.1, and the carboxylic acid of thioctic acid / mercaptopyridine mixed SAMs, the non-specific adsorption in DMF was 53% ($\Gamma = 8.00 \times 10^{-11} \pm 1.46 \times 10^{-11}$mol cm^{-2} *vs.* $\Gamma = 4.2 \times 10^{-11} \pm 0.29 \times 10^{-11}$mol cm^{-2}). Although there results showed some promise, they did not guarantee a background-free measurement of hybridisation.

This high degree of Os adsorption combined with the low degree of reactivity of the cystamine and thioctic acid SAMs, also demonstrated for DPS SAMs by other techniques explained below, obliged a change of immobilisation strategy for the transduction chemistry. Additionally, it indicated that

direct oligonucleotide-thiol SAMs should be attempted, as they eliminate the low-yield EDC reaction step. Parallel experiments carried out by Narváez (1999) demonstrated that the surface coverage from osmium polymers covalently linked to previously formed SAMs was not higher than the surface coverage from covalently linked osmium monomers, indicating that these polymer redox sites had a low electrochemical transduction capability. Consequently, the initial strategy of having an ordered transduction monolayer of controlled size was abandoned.

DNA immobilisation and characterisation. QCM measurements showed frequency changes neither after the amino-oligonucleotide addition on DPS SAMs nor after subsequent hybridisations. These data suggested that the oligonucleotide was not attached, probably due to the deactivation of the ester groups of the DPS after DPS assembling and before frequency baseline stabilisation. The fluorescence measurement corroborated this result, as no fluorescence was observed after hybridisation with dig-labelled complementary oligonucleotide and incubation with antidig-FITC. Although reports in the literature indicate that the distance between the fluorophore and the Au surface is sufficient to avoid it, the absence of fluorescence emission could be due to the quenching effect due to the fluorescence resonance energy transfer (FRET) with the gold surface.

Supporting the FRET effect, FITC-oligonucleotide-thiols immobilised on gold did not emit any fluorescence signal either. It was therefore decided that an alternative method should be used to quantify fluorescing moieties immobilised on gold.

Since EDC activation of pre-formed SAMs proved unreliable, it was decided to use direct oligonucleotide SAMs. With the QCM technique, frequency changes on exposure to oligonucleotide-thiol solutions were observed to be 27 $\pm$ 4Hz for 1ng mL^{-1} and 13 $\pm$ 3Hz for 0.25ng mL^{-1} (*see example in Figure II.3*).

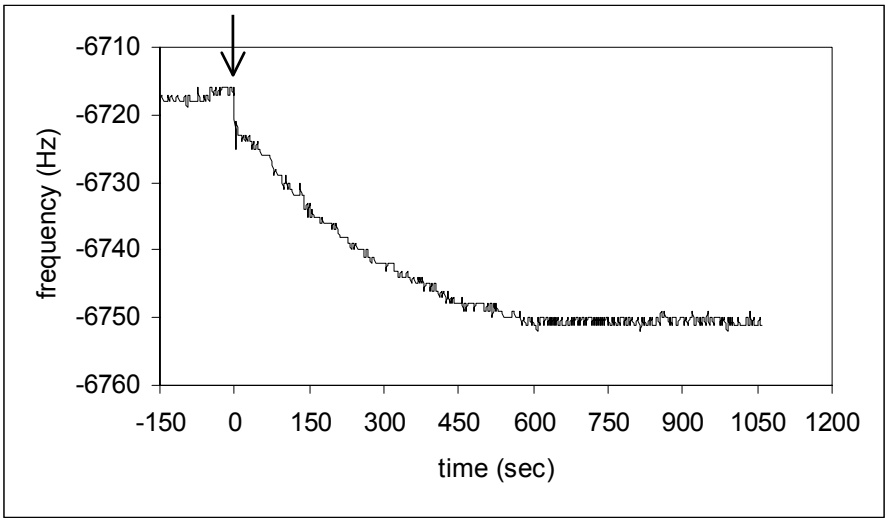

Figure II.3. Frequency change after oligonucleotide-thiol immobilisation (from a 1ng mL^{-1} solution) on a gold quartz crystal. Arrow indicates injection of oligonucleotide-thiol sample.

These results suggest successful oligonucleotide-thiol self-assembling. Moreover, the frequency stabilised 12min after the oligonucleotide-thiol solution injection, suggesting a quick monolayer formation. However, it was not possible to corroborate the surface coverage by the reduction of the thiol-Au bond or by the oxidation of guanine by cyclic voltammetry and thus, the gravimetric results were used to decide that the best strategy for probe immobilisation was the self-assembly of oligonucleotide-thiol, as it provides a direct, easy, simple, one-step probe immobilisation on gold surfaces.

DNA hybridisation measurement. A colorimetric assay technique was used to both verify and quantify the active functionality of immobilised oligonucleotides. In this technique, oligonucleotide-thiol homogeneous or mixed SAMs were immobilised on gold chips and hybridised with the dig-labelled complementary sequences. To detect hybridisation, chips were incubated with antidig-ALP and the absorbance change associated to the enzymatic reaction with the corresponding substrate was measured. Experiments showed a high non-specific adsorption of this conjugate on gold, on the oligonucleotide-thiol SAMs and on mercaptoethanol SAMs. Although a previous blocking step with BSA decreased this non-specific adsorption, no differences were observed in the hybridisation between complementary and non-complementary sequences. Consequently, the ALP label was changed by SBP, a thermostable peroxidase, in the hope to eliminate non-specific interactions. Furthermore, the modification according to Scheme II.3 allows the elimination of one step of the assay and ensures 1 SBP molecule per 1 complementary sequence, since the SBP was directly linked to an amino-oligonucleotide (fully complementary or with 4-point mutations). These experiments demonstrated that:

1) SBP-labelled oligonucleotides adsorbed non-specifically on the immobilised oligonucleotide SAMs. Nevertheless, the incorporation of baby milk (1%), Tween 20 (0.2%) and DNA salmon testes (1µg mL^{-1}) as blocking agents in the hybridisation step reduced this non-specific adsorption by 40%. The response from the non-complementary sequence was 65-82% of that of the complementary sequence, depending on the SBP-labelled oligonucleotide concentration, a fact that demonstrated the possibility to detect 4 mutations.

2) Mixed monolayers with different mercaptoethanol spacer concentrations in the oligonucleotide SAMs were attempted. When using mercaptopyridine concentrations higher than 50mM, the absorbance values obtained after the hybridisation and incubation step were lower than when using pure SAMs, due to the displacement of the oligonucleotide-thiol SAM to an extent higher than desired. Unexpectedly, lower mercaptopyridine concentrations did not change significantly the absorbance values, compared to pure oligonucleotide SAMs. Although the purpose of the mixed monolayers was to separate the immobilised strands in order to favour the complementary sequence transport, it was not

possible to observe such an effect. Therefore, the idea to construct mixed monolayers was abandoned for the rest of this thesis.

3) The hybridisation time needed for optimum spectrophotometric detection was optimised. At 20min, the absorbance values were only around 0.4, indicating that hybridisation had not reached saturation. At 40min, the response due to the complementary sequence was at maximum and the non-complementary sequence (4-point mutations) showed a non-specific adsorption of 81%. At longer times, no further differentiation was achieved and it was assumed that for the model oligonucleotides hybridisation had completed with 40min.

The final goal of this thesis is not a colorimetric DNA sensor, but an electrochemical DNA sensor. Although the colorimetric results serve for characterisation, the electrochemical detection strategy is outlined in Scheme II.1. However, the initial strategy of self-assemble osmium-derivatised polymers next to immobilised oligonucleotides in an organised structure was proven impossible as described before.

In order to achieve the same electrochemical communication, osmium redox polymers of uncontrolled MW were not self-assembled but cross-linked. Firstly, an osmium redox polymer was adsorbed *a posteriori* on the SBP-amino-oligonucleotide/oligonucleotide-thiol/gold system, as described in the “Materials and methods” section. Cyclic voltammetry showed oxidation and reduction peaks at +0.355 and +0.335V (*vs.* Ag/AgCl), respectively, indicating the presence of the redox polymer on the electrodes. However, chronoamperometry showed very low intensity values and no differences between complementary and non-complementary sequences. As these low intensity values could be due to the desorption of the redox mediator from the system, the osmium polymer was then adsorbed directly on gold or cross-linked to MPS modified electrodes. Afterwards, amine- or thiol-modified oligonucleotides were immobilised by covalent attachment. Electrochemical detection was then attempted. The gold electrodes showed the characteristic surface-immobilised redox species wave by cyclic voltammetry but very low intensity currents and no differences between complementary and non-complementary sequences upon SBP-oligonucleotide hybridisation. In order to improve the cross-linking efficiency of the redox polymer, SPDP was also added in the cross-linking step, but the same electrochemical behaviour was observed. These results demonstrated that a reliable electrochemical detection of hybridisation with these transduction chemistries is not possible. In Chapters IV and V, the possible integrated solutions to this problem are examined.

Conclusions

This chapter describes the preliminary studies to evaluate several probe immobilisation strategies and hybridisation detection. Although the presence of SAMs was demonstrated by cyclic voltammetry, they were not very reactive, which made them inappropriate for subsequent

oligonucleotide attachment. Additionally, the experiments showed a lack of electrical communication between ordered immobilised redox polymers and electrodes and a high non-specific adsorption of Os complexes on gold. Consequently, the strategy of ordered and controlled size transduction chemistry immobilisation was abandoned. In parallel, and to avoid the low yield of the oligonucleotide attachment step, direct oligonucleotide-thiol SAMs were attempted. QCM frequency changes and several colorimetric experiments proved the presence and functionality of these oligonucleotide-thiol monolayers on gold electrodes. This strategy provided a rapid, uniform and homogeneous immobilisation with only one step. Once the immobilisation step was demonstrated and optimised, the possibility to detect hybridisation was studied. In order to avoid an extra step and to reduce the analysis time, SBP-labelled complementary oligonucleotides were used in the hybridisation step. The experimental parameters concerning the presence of blocking agents, the hybridisation time and the effect of mixed monolayers were optimised by colourimetry. As the final goal of this thesis is the development of an electrochemical DNA sensor, an osmium polymer was incorporated into the system to act as electron transfer mediator. However, despite the successful colorimetric results, electrochemistry did not provide significant intensity currents, suggesting that a signal amplification method was necessary for the electrochemical hybridisation detection.

References

Katakis I., *Development and analysis of operation of enzyme electrodes based on electrochemically "wired" oxidoreductases*, Ph.D. thesis, University of Texas at Austin, USA, **1994**.

Narváez A., *Electrochemical communication between redox proteins and mediators: a rational approach for biosensor design*, Ph.D. thesis, Universidad de Alcalá, Spain, **1999**.

Abbreviations

A: adenine
ABTS: 2,2'-azinobis(3-ethylbenzthiazoline-sulfonic acid)
antidig: antidigoxigenin
ALP: alkaline phosphatase
BSA: bovine serum albumin
C: cytosine
CCD: charge-coupled device
DNA: deoxyribonucleic acid
DMF: dimethylformamide
DPS: 3,3'-dithiodipropionic acid di(N-succinimidyl ester)
EDC: 1-ethyl-3-(3-dimethylaminopropyl)carbodiimide hydrochloride
EDTA: ethylenediaminetetraacetic acid
FITC: fluorescein-isothiocyanate
G: guanine

HRP: horseradish peroxidase

MPS: 3-mercapto-1-propanesulfonic acid sodium salt

MW: molecular weight

NHS: N-hydroxysuccinimide

NMRC: National Microelectronics Research Centre

*p*NPP: *p*-nitrophenyl phosphate

PVP: poly(4-vinyl pyridine)

QCM: quartz crystal microbalance

SAM: self-assembled monolayer

SBP: soybean peroxidase

SPDP: 3-(2-pyridyldithio)propionic acid N-hydroxysuccinimide

SSC: saline-sodium citrate

T: thymine

TMB: 3,3',5,5'-tetramethyl-benzidine

tris-HCl: tris[hydroxymethyl]aminomethane hydrochloride

Chapter III. Functional biorecognition nanomodules

Abstract

The objective of this work is to create and characterise functional biorecognition nanomodules and define the conditions under which they form stable suspensions so that they can be subsequently used for microarraying.

It was found that 8.5mM carbonate, phosphate and citrate buffers gave the best results for the stabilisation of colloidal gold suspensions. However, when the particles were modified and for the necessary resuspension of the conjugates after centrifugation, 10mM phosphate buffer, 0.1M NaCl at pH 7.0 or 10-100mM tris-HCl buffer, 10-100mM KCl, 1%BSA, at pH 7.0-8.0 were more appropriate. High salt concentrations as well as divalent salts produced aggregation of the colloidal gold suspensions. Nevertheless, aggregation could be inhibited with 1% of BSA, which allowed to use 40mM buffer concentrations.

In this way, it was possible to produce biorecognition nanomodules with two model oligonucleotides (3' FITC-$(C)_{12}(T)_{20}(C)_{12}$-SH 5' and 3' digoxigenin-ACTTAACCGAGTCGACCGA-SH 5') that were used in a modified ELONA (Enzyme-Linked OligoNucleotide Assay) to demonstrate the efficiency of the conjugation, and in a hybridisation ELONA to demonstrate the functionality of the nanomodules. With these methods, it was possible to differentiate 4-point mutations in a target 19-mer oligonucleotide sequence. Furthermore, it was shown that the stability of the produced biorecognition nanomodules is sufficient for the purposes of mutation detection assays.

Keywords: colloidal gold, bioconjugation, nanomodules, suspension stabilisation, aggregation, thioctic acid SAMs, oligonucleotide-thiol, sandwich ELONA, hybridisation ELONA.

Introduction

Modification of colloidal particles with biomolecules has been extensively used for amplification of biorecognition reactions (Lin et al., 2000; Patolsky *et al.*, 2000; and Zhao *et al.*, 2001) or for the use of their electronic properties for biorecognition signal transduction (Powell *et al.*, 1997; Bubertret *et al.*, 2001; and Park *et al.*, 2002). Colloidal gold particles provide a convenient vehicle for the creation of biorecognition modular "libraries" (that are termed here "biorecognition nanomodules") that can be used at will for microarraying and development of biorecognition assays. They are readily available, easy to custom create (in terms of size and surface properties) and conducting, a property that provides arraying and recognition capacities. When aiming at the creation of such biorecognition nanomodules it is necessary to consider at first the nature of the colloidal gold nanoparticles. These particles are negatively charged due to adsorbed Cl^-, $AuCl_2^-$ or citrate ions left over from their synthesis procedure. When the suspension is stable, the repulsive forces of

electrostatic nature and the Van der Waals attraction forces maintain a high enough stability ratio so that the particles are essentially maintained in solution. However, changes in the ionic strength or the pH of the media will strongly influence the net charge of the colloidal particles or the degree of interaction between them, and therefore might lead to aggregation.

The DLVO theory of colloidal suspensions (Derjaguin and Landau (1941) and Verwey and Overbeek (1948)) helps to understand the nature of the interactions in colloidal suspensions. The stability of colloidal suspensions depends on the balance between the electrostatic potential (Langevin, 1908) given by:

$$V_r(H) = \frac{\pi\varepsilon_0\varepsilon r_1 r_2}{r_1 + r_2}\left[(\Psi_1 + \Psi_2)^2 \ln\{1 + \exp(\kappa H)\} + (\Psi_1 - \Psi_2)^2 \ln\{1 - \exp(-\kappa H)\}\right] \qquad \text{(Eq. III.1)}$$

where ε_0 is the permittivity in the vacuum, ε is the relative permittivity, $H = P - r_1 - r_2$ (the distance between particle surfaces = the distance between particle centres – radius of particle 1 – radius of particle 2), Ψ_1 and Ψ_2 are surface potentials of the two interacting particles, and κ^{-1} is the Debye length, and the Van der Waals attraction energy given by:

$$V_A(H) = -\frac{A}{12}\left[\frac{y}{x^2 + xy + x} + \frac{y}{x^2 + xy + x + y} + 2\ln\left\{\frac{x^2 + xy + x}{x^2 + xy + x + y}\right\}\right] \qquad \text{(Eq. III.2)}$$

where $x = H / 2r_1$, $y = r_2 / r_1$, and A is the Hamaker constant.

It can therefore be easily seen that the nature of the particle (size and Hamaker constant) is the most important parameter affecting the Van der Waals attraction forces while the conditions of the solution (e.g. ionic strength and dielectric constant) affect the electrostatic repulsive forces. The pH is a parameter that might influence both since it affects in principle the effective charge of the particles and the permittivity of the solution. The effects of modification of the surface of the particles have been studied with well-behaved model systems (Geoghegan *et al.*, 1977; Bonnard *et al.*, 1984; Brada and Roth, 1984; Morris and Saelinger, 1984; Slot and Geuze, 1985; De Waele *et al.*, 1989; Crumbliss *et al.*, 1992; O'Daly *et al.*, 1995; Elghanian *et al.*, 1997; Lyon *et al.*, 1998; Mucic *et al.*, 1998; Storhoff *et al.*, 1998; and Seelenbinder *et al.*, 1999). What is of interest here is to recognise that both the electrostatic repulsive forces and the London potential are affected due to these modifications because the effective charge and the apparent Hamaker constant are altered. However, DLVO considerations are not enough to explain these effects of surface modifications of the particles, and osmotic effects have been introduced by means of statistical thermodynamics. In many cases, quantitative predictions of stability have been made (deGennes, 1980, 1982 and 1987), although a rather detailed knowledge of the conformational multiplicity of the modifying molecules is necessary.

The above considerations also lead to the description of the kinetics of aggregation of colloidal particles. Mathematically, the rate of coagulation can be described by the stability ratio, which essentially gives the percentage of “fertile” collisions between particles, collisions that lead to aggregate formation. Again, since the stability ratio

$$W_{ij} = \frac{\beta_{ij}^{r}}{\beta_{ij}} \qquad \text{(Eq. III.3)}$$

where β^{r}_{ij} is the rapid collision frequency function with no interaction energy between particles of radii r_i and r_j and β_{ij} is the slower (observed) collision rate, the detail chosen to describe the potential function for the observed collision rate permits more or less accurate prediction of coagulation kinetics. However, it should be noted that the kinetics is also influenced by the evolution of the aggregates, and therefore an exact prediction should take these factors into account. Several works have appeared in the literature in this direction (Gardner and Theis, 1996 and Lin *et al.*, 2002).

The goal of this work is to rationally synthesise biorecognition nanomodules consisting of oligonucleotide probes conjugated to colloidal gold particles. These biorecognition modules, once characterised, will be used as nanoblocks in DNA arrays, as they will be site selectively deposited on different locations of a chip through electrophoresis. To conjugate biomolecules to colloidal gold, one takes advantage of either electronic attraction between the negatively charged colloidal gold particles and the positive sites on the protein, or adsorption between the metal surface and the hydrophobic pockets on the protein, or dative bonds between the gold and the sulfhydryl groups. The stability of the resulting conjugate suspensions depends, as mentioned above, on the kinetics and thermodynamics of the aggregation. Several authors have reported the conjugation of oligonucleotides to colloidal gold (Elghanian *et al.*, 1997; Mucic *et al.*, 1998; and Storhoff *et al.*, 1998). Here of particular importance it is to achieve the long-term stability of the suspensions.

Firstly, the conditions under which free colloidal gold suspensions are stable have been studied. As expected, the type, the pH and the concentration of the buffer play a significant role, not only because the buffer may change the nature of the ions adsorbed on the colloidal gold particles, but also because it can contribute to changes in the ionic strength of the media. It is further demonstrated that thiol-modified oligonucleotides can be conjugated to the colloidal particles, resulting in stable modified colloidal suspensions.

The modified colloids have been characterised in terms of functionality and ability to retain the biorecognition selectivity of the conjugated biomolecules with ELONA. It is demonstrated that the objective (to create “nanomodules” of biorecognition reagents) is satisfactorily achieved since the nanomodules are functional and have sufficient thermal stability (of the bond between oligonucleotides and colloidal gold particles) to allow their use under the hybridisation assay temperatures and times necessary for the detection of mutations.

Materials and methods

Materials. 20nm (21.7 ± 2.0nm) diameter colloidal gold was obtained from Sigma. The original concentration was 4.9 x 10^{11} particles mL^{-1} in about 0.01% $HAuCl_4$ suspended in 0.01% tannic acid with 0.04% trisodium citrate, 0.26mM potassium carbonate and 0.02% sodium azide as preservative. 3nm (3 ± 1nm) diameter colloidal gold was a gift from Dr. Ewen Smith. Bovine serum albumin (BSA), streptavidin-HRP, mercaptoethanol, dextran, polyethylene imine (PEI) and 3,3',5,5'-tetramethyl-benzidine (TMB) liquid substrate system for colour development (containing TMB and H_2O_2 in an slightly acidic buffer) were purchased from Sigma. Thioctic acid was bought from Aldrich. Polyethylene glycol (PEG) and cystamine were purchased from Fluka. Monoclonal antidigoxin was from Biodesign. Antidigoxigenin-HRP Fab fragments (antidig-HRP) were purchased from Roche. 3' FITC-$(C)_{12}(T)_{20}(C)_{12}$-SH 5' (FITC-oligonucleotide-thiol) and 3' digoxigenin-ACTTAACCGAGTCGA CCGA-SH 5' (dig-oligonucleotide-thiol) were from Genosys. 3' TCGGTCGACTCGGTTAAGT 5' (complementary), 3' TCGGTCGACTCGGTTAAGT-biotin 5' (biotin-labelled complementary) and 3' TCGGTGGGCTCGGGTGAGT-biotin 5' (4-mut-biotin) were from Eurogentec.

Instrumentation. Absorbance values or spectra were measured with an HP 8453 spectrophotometer or with a Molecular Devices 340PC 96-well plate reader. Chronoamperometries were performed using an AUTOLAB PGSTAT10 potentiostat in a conventional three-electrode cell, with Ag/AgCl as reference electrode and Pt as counter electrode. Fluorescence was measured with a Perkin Elmer LS-50 fluorometer or with a Nikon E600FN fluorescence microscope equipped with a Sony CCD camera.

Cystamine and thioctic acid SAMs on colloidal gold. 0.01 and 0.1M cystamine solutions were prepared in 0.1M carbonate buffer. 0.01, 0.05 and 0.1M thioctic acid solutions were prepared in 0.1M carbonate and phosphate buffer (10% ethanol). 12.5µL of each solution were put in separate eppendorfs. Afterwards, 125µL of 20nm colloidal gold commercial solution were added and mixed well. The final colloidal gold concentration was 4.5 x 10^{11} particles mL^{-1}. Absorbance spectra were monitored immediately after the mixing and after 24h. The suspensions were then centrifuged at 5000rpm and 4°C for 90min to remove unbound cystamine or thioctic acid. The supernatants were removed, and the pellets resuspended in 0.01M carbonate buffer, pH 9.3 or 10mM phosphate buffer, pH 7.0. Absorbance spectra of the resuspended solutions were monitored.

Studies of solution parameters on the stabilisation of the colloidal gold suspensions. For the effect of salts, buffers and salt/buffer combination, NaCl, KCl, KBr, KI, K_2SO_4, $CaCl_2$, $MgCl_2$ and $MgSO_4$ solutions (without and with 1% BSA), carbonate, phosphate and citrate buffers (without and with 10% ethanol, and at different pH), and several combinations of KCl with different buffers were prepared at 8.5, 40 and 85mM concentrations (without and with 1% BSA). In order to remove the original commercial buffer, 20nm colloidal gold was washed by two centrifugation steps at 5000rpm

and 4°C for 45min and resuspension in water. The 96-plate wells were filled with 85μL of the different salt and buffer solutions, and 15μL of washed colloidal gold were added and mixed well. The final colloidal gold concentration was 7.9 x 10^{11} particles mL^{-1} and the left over commercial buffer concentration was 240nM for these studies, concentration that could be neglected in comparison to the salts and buffers used. Absorbance spectra were then monitored immediately after the mixing and after 24h. For the effect of ethanol, 1mL solutions with the same 20nm colloidal gold concentration (4.9 x 10^{11} particles mL^{-1}) and different ethanol volumes (10, 30, 50, 70 and 90%) were prepared and mixed well. Absorbance spectra were then monitored immediately after the mixing and after 24h. For the effect of temperature, 200μL of a 20nm colloidal gold commercial solution (4.9 x 10^{11} particles mL^{-1}) were heated at 98°C for 1h. Absorbance spectra were monitored before and after heating.

To quantify the degree of stability of the colloidal gold or colloidal gold conjugate suspensions, the following parameter was used:

$$\% \text{ stability} = A_{523}(\text{sample}) / A_{523}(\text{blank}) \times 100 \qquad \text{(Eq. III.4)}$$

being A_{523}(sample) the absorbance at λ = 523nm of each one of the samples after mixing with salt, buffer, ethanol, or after heating, and A_{523}(blank) the absorbance at the same wavelength of a control after mixing with water or without heating. At 523nm is the maximum absorbance of the 20nm colloidal gold suspension. % aggregation (% aggregation = 100 - % stability) is also used.

Oligonucleotide conjugation to colloidal gold. 3 or 20nm colloidal gold (CG) commercial solutions were added into eppendorfs containing FITC-oligonucleotide-thiol (FOT) or dig-oligonucleotide-thiol (DOT) solutions in water and mixed well. The final colloidal gold concentrations were 0.46 x 10^{12}, 0.92 x 10^{12}, 2.31 x 10^{12}, 2.54 x 10^{12}, 3.23 x 10^{12} and 4.61 x 10^{12} particles mL^{-1} and the final oligonucleotide-thiol concentrations were 1, 1.5, 2, 3, 4 and 5μM. Mixtures were left to react for 40h at room temperature and protected from light. Afterwards, they were centrifuged twice unless otherwise mentioned at 5000rpm and 4°C for 30min. The supernatants were removed, and the pellets were resuspended in 50mM histidine buffer, pH 7.0 (for the FITC-oligonucleotide-thiol-colloidal gold conjugate) or 50mM tris-HCl buffer, 10mM KCl, pH 7.5 (for the dig-oligonucleotide-thiol-colloidal gold conjugate). Absorbance spectra of the resuspended solutions were monitored.

Characterisation of the FITC-oligonucleotide-thiol conjugation to colloidal gold (Scheme III.1). The protocol by Demers *et al.* (2000) was used. Mercaptoethanol was added to a small aliquot of the conjugate solution (12mM final concentration). The mixture was left to react for 18h at room temperature with intermittent shacking. Afterwards, it was centrifuged at 5000rpm and 4°C for 30min in order to separate the displaced oligonucleotides. The supernatant was then removed and 10-fold diluted, and the fluorescence emission was measured (excitation at 465nm and emission at 520nm).

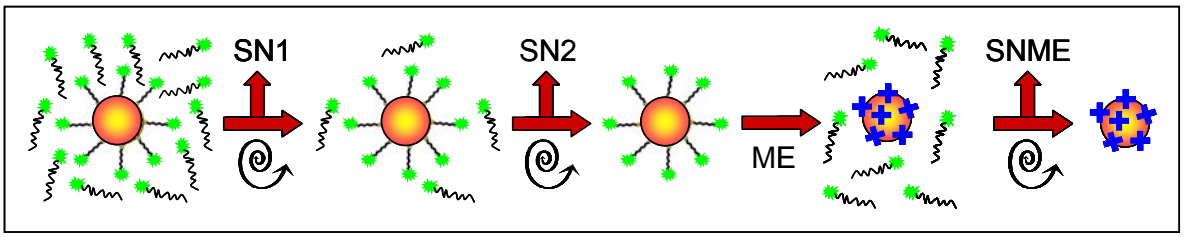

Scheme III.1. Procedure for the washing and removal of bound oligonucleotide by mercaptoethanol for the characterisation of the FITC-oligonucleotide-thiol conjugation to colloidal gold. means centrifugation. SN1: supernatant from the first washing step. SN2: supernatant from the second washing step. ME: mercaptoethanol addition. SNME: supernatant from the step of removal by mercaptoethanol.

The same experiment was used to study the stability of the modification. In this case, after three washing steps and before removal by mercaptoethanol, the sample was heated at 65°C for 1h, and an extra centrifugation step at 5000rpm and 32°C for 30min was carried out to separate the desorbed oligonucleotides. In the control, the sample was not heated but it was centrifuged. Parallel controls assured the lack of bleaching of the FITC under the same conditions.

Characterisation of the dig-oligonucleotide-thiol conjugation to colloidal gold (Scheme IIII.2).

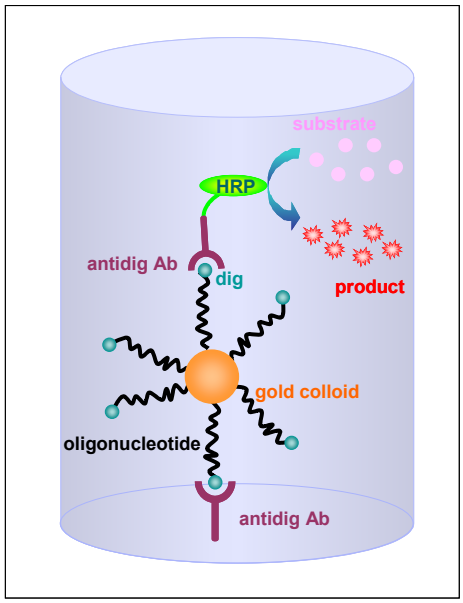

Scheme III.2. Sandwich ELONA on a well for the characterisation of the dig-oligonucleotide-thiol conjugation to colloidal gold. The well is coated by antidigoxigenin; the digoxigenin of the dig-oligonucleotide-thiol-colloidal gold conjugate recognises the antidigoxigenin; the antidig-HRP recognises the digoxigenin of the immobilised dig-oligonucleotide-thiol-colloidal gold conjugate; the HRP label reacts with its substrate to give a coloured product.

Modified ELONA with colloidal gold bioconjugates was performed. 96-well plates were coated with 50µL of an antidigoxin solution (5µg mL^{-1} in 0.01M phosphate buffer, 0.138M NaCl, 0.0027M KCl, pH 7.4). The remaining sites were blocked with 200µL of a BSA solution unless otherwise mentioned (1% in 0.05M tris-HCl buffer, 0.01M KCl, pH 7.5). 50µL of a dig-oligonucleotide-thiol-colloidal gold solution (2.94×10^{11} particles mL^{-1} in 0.05M tris-HCl buffer, 0.01M KCl, pH 7.5, with or

without 1% BSA) were incubated. FITC-oligonucleotide-thiol-colloidal gold (2.45 x 10^{12} particles mL^{-1}) was used as a control. The BSA blocking step was then repeated. 50µL of an antidig-HRP solution unless otherwise mentioned (1:2000 dilution from the commercial solution in 0.05M tris-HCl buffer, 0.01M KCl, pH 7.5, 1% BSA) were incubated. 50µL of commercial TMB liquid substrate were incubated. Each step was carried out for 1h at 37°C with stirring and protected from light. The wells were thoroughly rinsed between each step. Absorbance values were measured at 650nm.

Characterisation of the dig-oligonucleotide-thiol-colloidal gold functionality (Scheme III.3). A modified hybridisation ELONA with colloidal gold bioconjugates was performed. The protocol is the same as in the previous experiment but includes a hybridisation step after incubation with colloidal gold conjugate: 50µL of a solution of biotin-labelled complementary oligonucleotide, non-labelled complementary oligonucleotide or biotin-labelled oligonucleotide with 4-point mutations (5µg mL^{-1} in 10mM tris-HCl, 1mM EDTA, 0.3 x SSC, 2 x Denhardt's solution, pH 8.0) were incubated for 1h at 55°C with stirring and protected from light. Instead of antidig-HRP, 50µL of streptavidin-HRP (0.4µg mL^{-1} in 0.1M tris-HCl buffer, 0.1M KCl, pH 8.0, 1% BSA) were incubated for 1h at 37°C. In the wells was then added commercial TMB liquid substrate and incubated for 1h at 37°C. Between each step, the wells were thoroughly rinsed. Absorbance values were measured at 650nm.

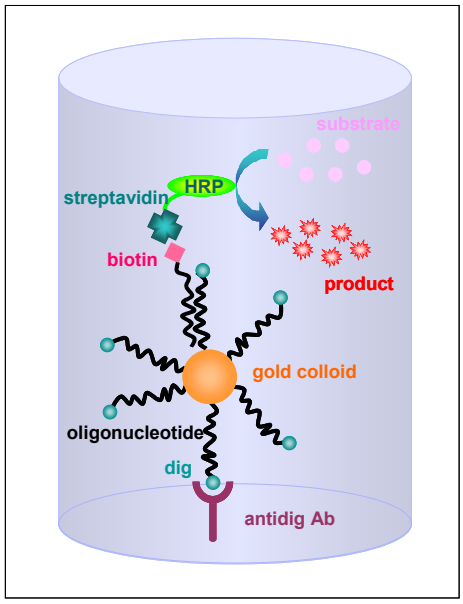

Scheme III.3. Hybridisation ELONA on a well for the characterisation of the dig-oligonucleotide-thiol-colloidal gold functionality. The well is coated by antidigoxigenin; the digoxigenin of the dig-oligonucleotide-thiol-colloidal gold conjugate recognises the antidigoxigenin; the oligonucleotide of the dig-oligonucleotide-thiol-colloidal gold conjugate hybridises with its complementary sequence; the streptavidin-HRP recognises the biotin of the complementary oligonucleotide; the HRP label reacts with its substrate to give a coloured product.

Results and discussion

Cystamine and thioctic acid SAMs on colloidal gold. Cystamine and thioctic acid SAMs on colloidal gold were tried in order to have amine or carboxylic acid functionalities on the particles and afterwards to react them with activated oligonucleotides via EDC reaction. Self-assembling of cystamine and thioctic acid (dissolved in water and 50% water : 50% ethanol, respectively) resulted in aggregation. Because several extreme concentrations were tried, one can affirm that the problem was not an inappropriate ratio between reactants. Nevertheless, as theory indicates, the media where the conjugation takes place also has an important role in the completion of a conjugation. Consequently, self-assembling was tried again in several buffers without ethanol for cystamine monolayers and with 10% ethanol for thioctic acid monolayers. Thioctic acid conjugations showed well-defined absorbance peaks at 523nm with 84 and 77% stability in carbonate and phosphate buffer, respectively, being the carbonate buffer slightly better. After 24 hours the stability percentages were 78 and 71%, suggesting a slow aggregation process. On the other hand, aggregation appeared when using cystamine in any buffer. In fact, Weisbecker *et al.* (1996), in their study of SAMs on gold colloids, reported that flocculation is a common phenomenon especially with short length alkanethiols. In the case of cystamine, the inversion of the charge of the particles' surface might be the reason for aggregation.

Thioctic acid / colloidal gold suspensions were washed in order to remove the unbound thioctic acid molecules, and several buffers were used to see if the suspensions were stable after the centrifugation step. Figure III.1 shows the spectra of the suspensions before the washing step and after resuspension of the pellets in carbonate and phosphate buffer.

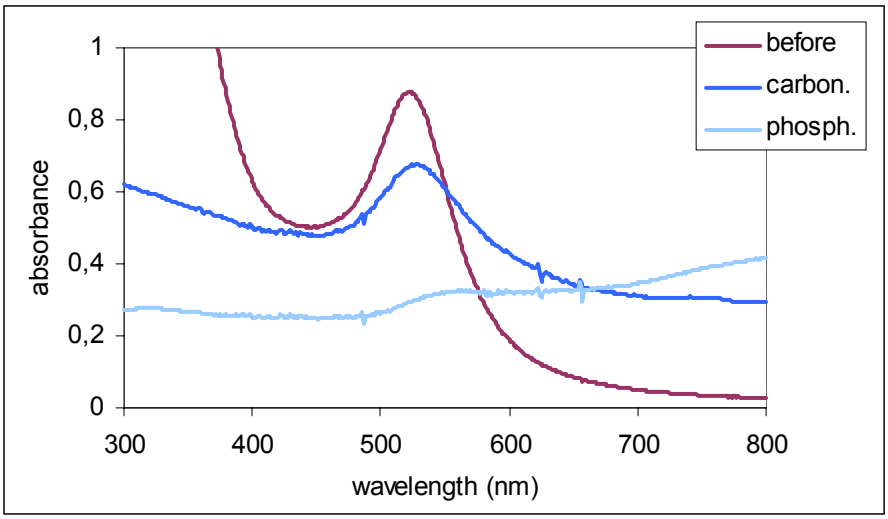

Figure III.1. Absorbance *vs.* wavelength for thioctic acid-colloidal gold suspensions (4.5×10^{11} particles mL^{-1}) before and after washing and resuspension in 0.01M carbonate buffer, pH 9.3 or 0.01M phosphate buffer, pH 7.0.

In carbonate buffer, a well-defined absorbance peak is observed at 523nm, although the 22% aggregation is evident. The suspension was not stable in phosphate buffer, and aggregates could be observed. Although neither carbonate nor phosphate buffers destabilised the colloidal gold suspension when thioctic acid was added, the election of the resuspension buffer after the centrifugation step was decisive, only carbonate buffer being useful. Although in this experiment, only one washing step was performed, in subsequent experiments (conjugations of oligonucleotides to colloidal gold) more than one washing steps were required to completely remove all the unbound material. If more than one washing steps are needed, a compromise should be taken between removal of unbound material and stability of the conjugate suspension, since repeated centrifugations were observed to destabilise the suspension.

As mentioned above, cystamine and thioctic acid SAMs on colloidal gold were attempted as a means to have functionality-modified colloidal gold to subsequently react with activated oligonucleotides via EDC reaction. However, this strategy was eventually abandoned in favor of direct self-assembling of oligonucleotide-thiol monolayers on colloidal gold particles, not only because of aggregation but also because of the EDC step, only 15% efficient.

Studies of solution parameters on the stabilisation of the colloidal gold suspensions. The conditions under which colloidal gold suspensions are stable were studied in order to proceed with the rational colloidal gold conjugation with oligonucleotides. All gold colloids offered by Sigma are produced by a modified method of Slot and Geuze (1985) and contain about 0.01% $HAuCl_4$, 0.01% tannic acid, 0.04% trisodium citrate, 0.26mM potassium carbonate and 0.02% sodium azide as preservative. Consequently, colloidal gold particles are supposed to have Cl^-, $AuCl_2^-$, citrate ions and tannic acid on their surface. In order to avoid the effects of the original commercial buffer, the colloidal gold suspensions were centrifuged twice, and after addition in the corresponding solutions, the total concentration of the original commercial buffer was only 240nM, negligible compared to 0.85-85mM salts and buffers concentrations used in this work. As the stabilisation of colloidal gold suspensions was desired to further modify the colloidal gold particles with different self-assembled chemistries, buffers, salts and combinations of both were prepared in the presence or not of 10% ethanol.

Table III.1 shows the salt effect in the colloidal gold suspensions. In this and the following tables, stability is considered when the stability percentage is higher than 85%, intermediate stability when the stability percentage is between 50 and 85%, and instability when the stability percentage is below 50%. If no BSA was present, all salt solutions at 85mM concentration destabilised the suspensions because the high ionic strength resulted in the screening of the supposedly negatives charges that are on the particles' surface, which arise from the synthesis procedure and help to maintain the stability of the suspensions. Nevertheless, when lower concentrations were used, only the salts with divalent positive counterions destabilised the colloidal gold suspensions, as expected

since the colloidal gold particles are negatively charged. The results of the stability of the colloidal gold suspensions in NaCl, KCl and KBr solutions reflect that the experimental critical coagulation concentration for these systems is between 8.5 and 8.5mM of electrolyte. Whereas suspensions in K_2SO_4 behave as in NaCl, KCl and KBr, suspensions in salt solutions with divalent cations are destabilised at lower ionic strengths, the experimental critical coagulation concentration being below 0.85mM, making obvious the "chemical" effects of the divalent cations, which can effectively reverse the surface charge. An evident further stabilising effect was observed when 1% BSA was present in the suspensions. In fact, BSA is expected to spontaneously adsorb on the surface of colloidal gold particles. It has an isoelectric point of approximately 5, and at the pH of the media (about 6) has a weak net negative charge that contributes to maintain the anionic atmosphere and avoid aggregation. This stabilising effect is expected when polymeric effects are taken into account. However, the effect might simply be "chemical" (i.e. lyophilisation of the lyophobic gold particles).

Table III.1. Colloidal gold suspension stability (✓), instability (×) or intermediate stability (⊙) in salt solutions at different concentrations without and with 1% BSA after 24h.

SALT	No BSA			1% BSA		
	85mM	8.5mM	0.85mM	85mM	8.5mM	0.85mM
NaCl	×	✓	✓	✓	✓	✓
KCl	×	✓	✓	✓	✓	✓
KBr	×	✓	✓	✓	✓	✓
K_2SO_4	×	✓	✓	✓	✓	✓
$CaCl_2$	×	×	×	⊙	✓	✓
$MgCl_2$	×	×	×	⊙	✓	✓
$MgSO_4$	×	×	×	⊙	✓	✓

Table III.2 summarises the results for the stability of colloidal gold suspensions in different buffers, at different pH and concentrations, without and with 10% ethanol. When using 85 or 40mM final buffer concentration, colloidal gold aggregated, independently of the pH. Only citrate buffer at 40mM and at the lowest pH (2.5) showed an intermediate destabilisation effect. At 8.5mM, any buffer could be used without destabilising the colloidal gold suspensions at any pH. Again, the general effect of buffer concentration can be explained in terms of charge screening and a shorter Debye length at higher concentrations, which leads to aggregation. Regarding the effect of ethanol, no differences were observed between suspensions with or without ethanol after 24 hours, although when absorbance spectra were measured immediately after mixing, suspensions without ethanol were slightly more stable (*results not shown*). Despite the shorter Debye length due to the lower dielectric constant of ethanol compared to water (24.3 *vs.* 80.0F m^{-1}), both the electrostatic repulsion between particles and the apparent Hamaker constant allow the stability of the suspension.

Table III.2. Colloidal gold suspension stability (✓), instability (×) or intermediate stability (⊙) in buffers at different pH and concentrations without and with 10% ethanol after 24h.

BUFFER	No ethanol						10% ethanol					
	85mM		40mM		8.5mM		85mM		40mM		8.5mM	
carbonate	11.5	×	10.5	×	8.5	✓	11.0	×	10.5	×	9.5	✓
	10.5	×	9.5	×	7.5	✓	10.5	×	10.0	×	7.0	✓
	9.5	×	9.0	×	7.0	✓	9.5	×	9.5	×	7.0	✓
phosphate	7.0.	×	7.5	×	7.0	✓	7.0.	×	7.5	×	7.0	✓
	6.5	×	6.5	×	6.5	✓	6.5	×	6.5	×	6.5	✓
	5.5	×	6.0	×	6.0	✓	6.0	×	6.0	×	6.0	✓
citrate	6.0	×	6.0	×	5.5	✓	5.5	×	6.0	×	6.0	✓
	4.0	×	4.5	×	4.5	✓	4.0	×	4.5	×	4.5	✓
	2.5	×	2.5	⊙	2.5	✓	2.5	×	2.5	⊙	3.0	✓

KCl was added to different buffers (without and with 1% BSA) at 85mM concentration to make sure that colloidal gold suspensions were stable under saline conditions, needed for electrochemistry. Whereas colloidal gold suspensions were not stable in any of the saline buffers without BSA, the presence of 1% of this protein resulted in stabilisation (Table III.3). Again, the protective action of BSA was demonstrated, as colloidal gold suspensions could be stable even under 85mM KCl concentration, result that correlates with the two previous independent experiments (effect of salts and effect of buffers).

Table III.3. Colloidal gold suspension stability (✓), instability (×) or intermediate stability (⊙) in buffers at different pH and concentrations with 85mM KCl without and with 1% BSA after 24h.

85mM KCl BUFFER	No BSA				10% BSA			
	40mM		8.5mM		40mM		8.5mM	
carbonate	10.5	×	9.0	×	10.0	✓	8.5	✓
	10.0	×	7.5	×	9.5	✓	7.5	✓
	9.5	×	7.0	×	9.0	✓	7.0	✓
phosphate	7.0	×	6.5	×	7.0	✓	7.0	✓
	6.5	×	6.0	×	6.5	✓	6.5	✓
	5.5	×	5.5	×	5.0	✓	5.5	✓
citrate	6.0	×	6.0	×	6.0	✓	6.0	✓
	4.0	×	4.5	×	4.5	✓	4.5	✓
	2.0	×	2.5	×	2.5	✓	4.0	✓

The stability of the colloidal gold suspension in different percentages of ethanol was studied to see if the presence of this solvent (necessary to dissolve the thioctic acid and consequently, to form thioctic acid SAMs on gold) had any aggregation effect on the colloidal gold. Initially, the colour of all the samples was pink and the absorbance spectra showed well-defined peaks at 523nm (Figure III.2). Although all samples seem stable, the sample with 90% ethanol showed an increase in the absorbance around 620nm and a decrease of the 523nm peak absorbance, corresponding to 22% aggregation.

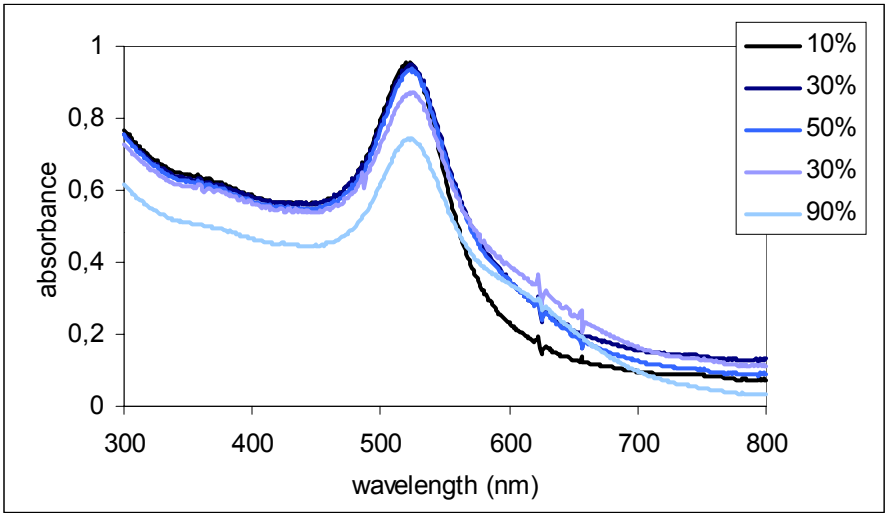

Figure III.2. Absorbance *vs.* wavelength for colloidal gold suspensions with different ethanol content.

After 24h, only the samples with 10 and 30% ethanol content were stable. The samples with higher ethanol content showed a darker purple colour as the percentage of ethanol increased (Figure III.3), reflected by the absorbance decrease at 523nm and the absorbance increase at 620nm.

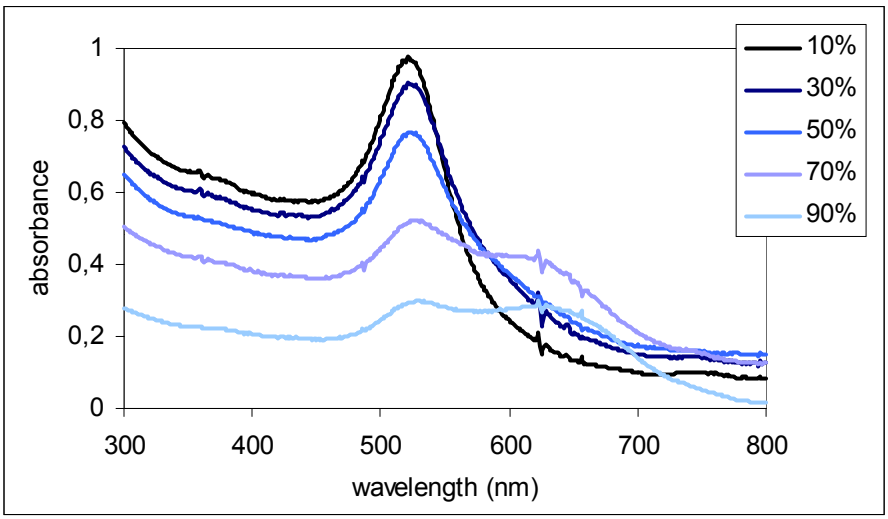

Figure III.3. Absorbance *vs.* wavelength for colloidal gold suspensions with different ethanol content after 24h.

In this case, the aggregation was 21, 46 and 69% for 50, 70 and 90% ethanol content, respectively. As mentioned above, this aggregation effect was expected because of the lower dielectric constant of ethanol, which shortens the Debye length. It is not easy to account for the slow kinetics of aggregation in ethanol. Theory suggests that for the conditions under investigation, doublet formation times should be of the order of magnitude of seconds. Agreement with theory should be examined by the explicit integration of the stability ratio given as

$$W_{ij} = 2a\int_{2a}^{\infty} \frac{exp(\Phi / kT)}{r^2 G(r)} dr \qquad \text{(Eq. III.4)}$$

where *a* is the particle radius, *r* is the centre-to-centre particle separation, $\frac{\Phi}{kT}$ is the dimensionless interparticle interaction potential, and *G*(*r*) is the probability density, of which the doublet formation depends.

The thermal stability of the colloidal gold suspension was studied to ensure that heating does not provoke any aggregation, as the biorecognition modules have to be stable during the hybridisation step. Although hybridisation is usually performed at lower temperatures, 98°C were used to study the thermal stability of colloid suspensions under extreme conditions. The absorbance spectrum for the colloidal gold solution after 1h at 98°C showed a well-defined peak at 523nm with only 19% aggregation. The well-defined peak indicated that the stability of the suspension was adequate.

Oligonucleotide conjugation to colloidal gold. The conjugation of FITC-oligonucleotide-thiol (3μM) to colloidal gold (2.31 x 10^{12} particles mL^{-1}) was performed in triplicate and the peak absorbance at 523nm showed only 3% standard deviation, demonstrating the high reproducibility of the stability of the conjugate suspension. The conjugations of dig-oligonucleotide-thiol (1.5μM) to colloidal gold (2.54 x 10^{12} particles mL^{-1}, 3 or 20nm in diameter) were performed in quadruplicate. Whereas peak absorbance values from 20nm colloidal gold conjugates showed 11% standard deviation, the standard deviation from 3nm colloidal gold conjugates was 22%, suggesting a lower reproducibility. Additionally, 3nm colloidal gold conjugates showed 32% lower peak absorbance than 20nm colloidal gold conjugates, suggesting a partial aggregation effect. Although 8.5mM carbonate, phosphate and citrate buffers gave the best results for the stabilisation of colloidal gold suspensions, 10mM phosphate buffer, 0.1M NaCl at pH 7.0 and 10-100mM tris-HCl buffer, 10-100mM KCl, 1%BSA, at pH 7.0-8.0 provided better results for resuspension of the conjugates.

Characterisation of the FITC-oligonucleotide-thiol conjugation to colloidal gold (Scheme III.1). Fluorescence measurements demonstrated that oligonucleotide solutions did not emit any fluorescence after their conjugation and washing (to remove unbound oligonucleotides). This effect indicated either the presence of fluorescence quenching or the non-successful conjugation. In order to characterise the conjugation by other methods, the bound oligonucleotides were removed from

the gold particles using mercaptoethanol and their fluorescence was measured, following the procedure of Demers *et al.* (2000). The aforementioned fluorescence quenching is due to the fluorescence resonance energy transfer (FRET) between the FITC and the gold. In the FRET, the FITC moiety (donor) is excited by absorption of a photon, but instead of emitting a fluorescence photon, the excitation is transferred by electronic coupling to the colloidal gold particle (acceptor). The result of this exchange is an excited acceptor and a ground state donor. In signal terms, the result is no fluorescence. Figure III.4 shows the fluorescence values from the supernatants corresponding to two washings and the removal by mercaptoethanol of five conjugations using different colloidal gold concentrations. As expected, the fluorescence values from the washing steps increased as colloidal gold concentration decreased, due to the less colloidal gold surface available for conjugation, and this effect was much more evident for the first washing than for the second one. The fluorescence values from the removal step showed the opposite trend because the higher the colloidal gold concentration, the higher the concentration of previously bound oligonucleotides. The total sum of the fluorescence emitted by the supernatants for each colloidal gold concentration was not significantly different between conjugations (8.1% standard deviation), which indicates a high reproducibility of the assay. In subsequent dig-oligonucleotide-thiol conjugations to colloidal gold, colloidal gold concentrations close to 2.31 x 10^{12} particles mL^{-1} were used, since Figure III.4 shows that for this concentration, the amount of oligonucleotide bound to the gold particles is significantly higher than the amount of free oligonucleotide that could be still present in the solution.

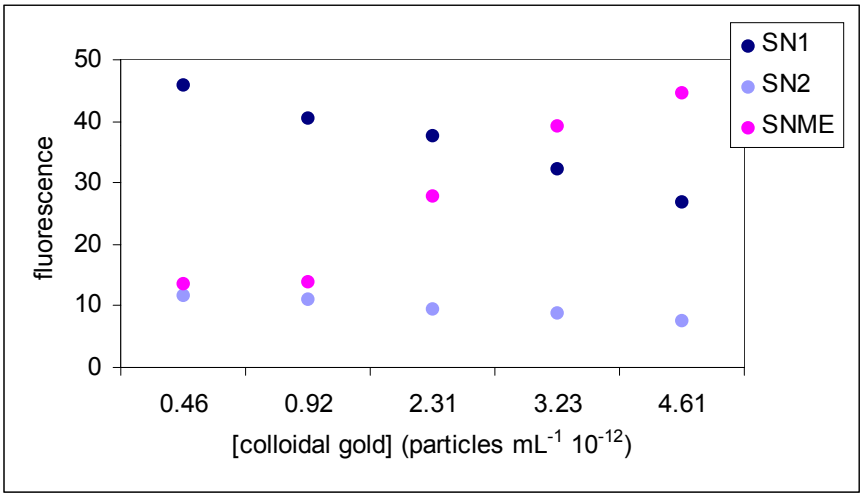

Figure III.4. Fluorescence emitted at 520nm by SN1, SN2 and SNME in the FITC-oligonucleotide-thiol-colloidal gold conjugate characterisation by mercaptoethanol for different colloidal gold concentrations and the same FITC-oligonucleotide-thiol concentration (3μM) (*see Scheme III.1*).

Figure III.5 shows the fluorescence values from the supernatants corresponding to five washings and the removal by mercaptoethanol of five conjugations using different FITC-oligonucleotide-thiol concentrations. Previous experiments with only two washing steps showed an increasing trend in the fluorescence emitted by removed oligonucleotide supernatants as the oligonucleotide concentration used in the conjugation increased. This would seem to indicate that at higher

oligonucleotide concentrations, the modification was more efficient due to displacement of the equilibrium towards the adsorbed state. However, it was postulated that the colloidal gold conjugate was not completely free of unbound FITC-oligonucleotide-thiol molecules. For this reason, more washing steps were carried out. Five washing steps were chosen because at the fifth centrifugation step, aggregates started to appear at the bottom of the eppendorfs. After five washings, the fluorescence emitted by the removed oligonucleotide supernatants (SNME) did not show any trend, demonstrating that the amount of oligonucleotide bound to the colloidal gold surface was the same independently of the initial oligonucleotide concentration. Additionally, from the SNME values, the surface coverage of bound oligonucleotides could be calculated assuming that no FITC bleaching occurred and essentially monodispersed gold. It was determined to be 14.87pmol cm^{-2}, or 159 oligonucleotides per particle, which corresponds to 37% coverage of the surface. Although it cannot be ruled out the possibility that the mercaptoethanol has not completely displaced all the oligonucleotides, it seems unlikely.

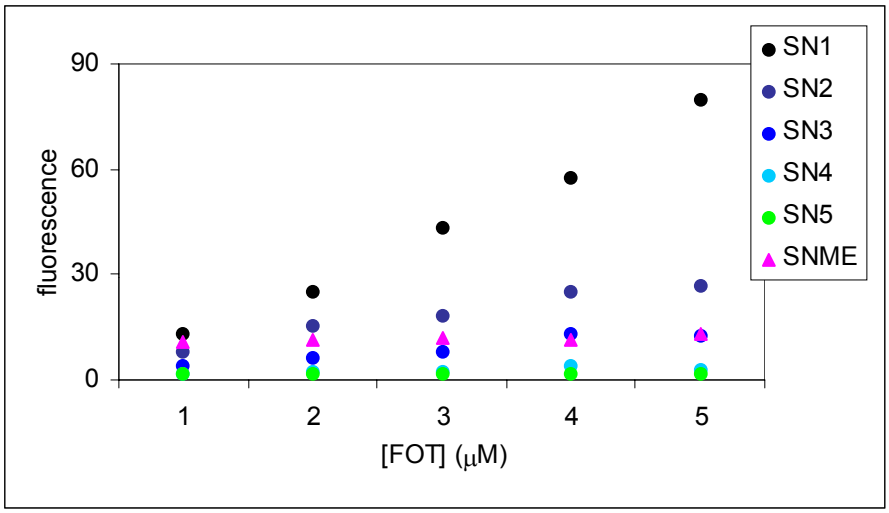

Figure III.5. Fluorescence emitted at 520nm by SN1, SN2, SN3, SN4, SN5 and SNME in the FITC-oligonucleotide-thiol-colloidal gold conjugate characterisation by mercaptoethanol for the same colloidal gold concentration (2.45 x 10^{12} particles mL^{-1}) and different FITC-oligonucleotide-thiol concentrations.

Characterisation of the dig-oligonucleotide-thiol conjugation to colloidal gold (Scheme III.2). Figure III.6 shows the absorbance results for the sandwich ELONA with dig-oligonucleotide-thiol-colloidal gold and FITC-oligonucleotide-thiol-colloidal gold used as a control (with 20nm colloidal gold). In the "total" set, the assay with dig-oligonucleotide-thiol-colloidal gold yield a coloured solution and the assay with FITC-oligonucleotide-thiol-colloidal gold did not produce any significant response different from the blank (set "no HRP"), demonstrating that the Scheme III.2 assay was valid. The "no colloid" set, which corresponds to the system without colloidal gold conjugate and which did not show any significant response, demonstrates that the antidig-HRP did not adsorb non-specifically on the BSA or on the antidigoxin coating. The bars associated to the FITC-oligonucleotide-thiol-colloidal gold conjugate present values close to the blanks, which indicates

that the antidig-HRP did not adsorb non-specifically on the colloidal gold conjugates. Consequently, the absorbance values are entirely due to the dig-antidig recognition. These observations lead to the conclusion that the dig-oligonucleotide-thiol conjugation to colloidal gold was successful and that the digoxigenin label was functional (able to recognise the antidigoxin of the coated surface and the antidig-enzyme). Comparing the "total" and the "no coat" sets, the bars associated to the dig-oligonucleotide-thiol-colloidal gold conjugate decreased when there was not antidigoxin on the well surface, and this effect was more pronounced when there was BSA in the conjugate solution. If there is not BSA in the conjugate solution, the conjugate adsorbs non-specifically on the non-coated well because this well is coated by BSA (from the first blocking step) and the tendency of the conjugate is to adsorb on this protein. Therefore, BSA in the conjugate suspension has both a stabilisation effect and a protective effect against non-specific adsorption. The results also show that an additional coating BSA step was not necessary.

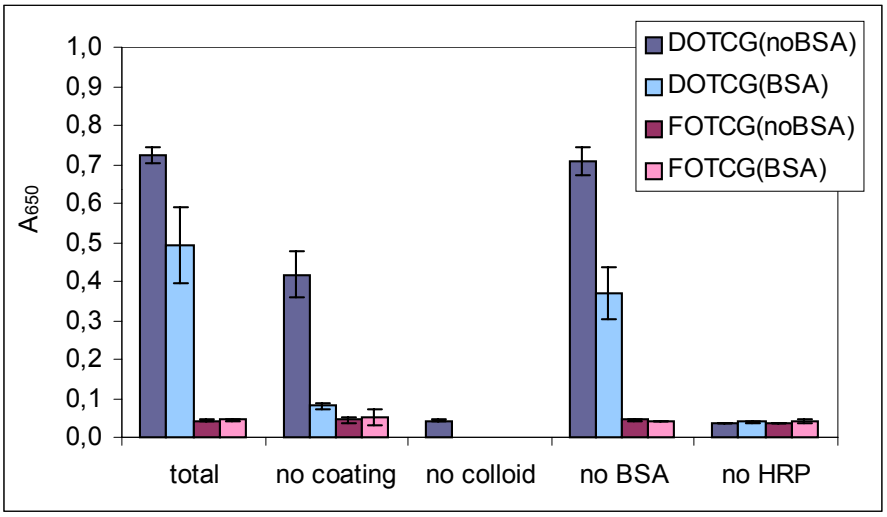

Figure III.6. Absorbance at 650nm obtained in the sandwich ELONA for the dig-oligonucleotide-thiol-colloidal gold (20nm colloidal gold) conjugate characterisation; total: system as depicted in Scheme III.2; no coating: blank without antidigoxigenin on the surface; no colloid: blank without conjugate; no BSA: blank without the blocking step; no HRP: blank without antidig-HRP. FITC-oligonucleotide-thiol-colloidal gold conjugate was used as a control.

Despite the partial aggregation of the suspensions of dig-oligonucleotide-thiol conjugated to 3nm colloidal gold, sandwich ELONA was also carried out with these conjugates. Figure III.7 compares the results for both types of conjugates, with 3 and 20nm colloidal gold. The absorbance obtained in the "total" set and the low absorbance values for the controls and blanks ("no colloid" and "no HRP" sets) demonstrate the effectiveness of both conjugations. However, the 3nm colloidal gold conjugates present lower absorbance values for the "total" system (76% of the corresponding value for the 20nm colloidal gold conjugate). Regarding the reproducibility of the functionality assay, whereas the assay with 20nm colloidal gold conjugates has a standard deviation of 6%, in the assay with 3nm colloidal gold conjugates the standard deviation is of 14% in accordance with the conjugation results for the colloids of this size.

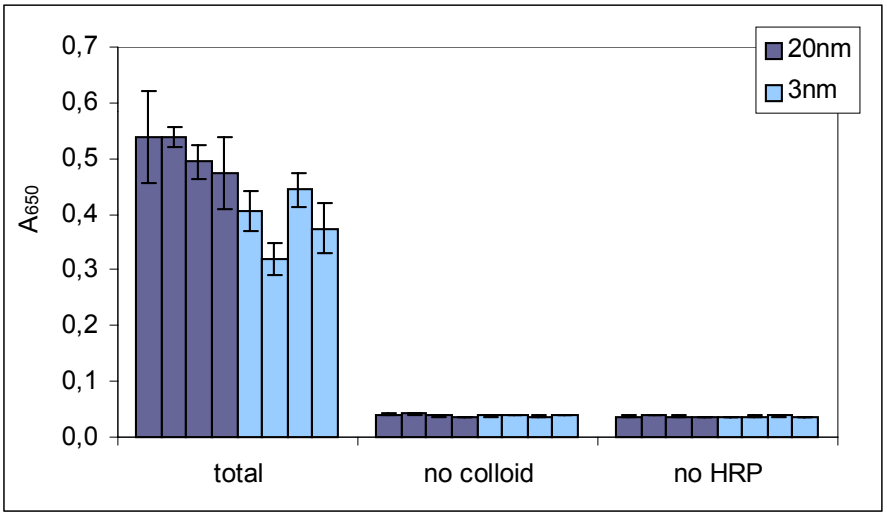

Figure III.7. Absorbance at 650nm obtained in the sandwich ELONA for the dig-oligonucleotide-thiol-colloidal gold (3 and 20nm colloidal gold) conjugate characterisation; total: system as depicted in Scheme III.2; no colloid: blank without conjugate; no HRP: blank without antidig-HRP.

In order to find the best blocking agent to avoid the non-specific adsorption of the dig-oligonucleotide-thiol-colloidal gold conjugate on the 96-well plate, a sandwich ELONA was performed using 1% BSA, PEG, PEI, dextran or glycerol in the dig-oligonucleotide-thiol-colloidal gold conjugate solution. As PEI provoked the aggregate formation, this polymer was not used as blocking agent in subsequent assays. The best results, i.e. higher absorbance values from the "total" set and lower absorbance values from the "no coating" set (*results not shown*), were obtained with BSA as blocking agent. Consequently and also due to the results obtained in the studies of the stability of colloidal gold suspensions, 1% of BSA was used in the dig-oligonucleotide-thiol-colloidal gold conjugate solutions in subsequent experiments.

Characterisation of the dig-oligonucleotide-thiol-colloidal gold functionality (Scheme III.3). Figure III.8 shows the results for the hybridisation ELONA with dig-oligonucleotide-thiol-colloidal gold and FITC-oligonucleotide-thiol-colloidal gold as a control. The dig-oligonucleotide-thiol-colloidal gold bar for the "total" set, significantly different from the rest of bars, demonstrated the hybridisation event with the dig-oligonucleotide-thiol-colloidal gold conjugate. The set associated to the system without colloidal gold conjugate presents a value close to the blanks ("no HRP"), demonstrating that the streptavidin-HRP did not adsorb non-specifically on BSA or on the antidigoxin coating. The set corresponding to the system without the hybridisation oligonucleotide presents values close to the blanks, which proves that the streptavidin-HRP did not adsorb non-specifically on the colloidal gold conjugates. As expected, the bars associated to the FITC-oligonucleotide-thiol-colloidal gold conjugate also present values similar to the blanks, because this conjugate has no digoxigenin and consequently, it cannot be immobilised on the antidigoxin-coated surface. All the controls and blanks prove that the absorbance value in the "total" set with dig-oligonucleotide-thiol colloidal gold is entirely due to the biotin-streptavidin recognition from oligonucleotides hybridised to colloidal gold conjugates. These results indicated that the

oligonucleotides conjugated to the colloidal gold are functional, i.e. able to recognise their complementary sequence. This experiment also included the hybridisation with other sequences: the fully complementary sequence without the biotin label ("no biotin" set) and the labelled oligonucleotide sequence with 4-point mutations ("4-mut" set). The low absorbance value for the hybridisation with the oligonucleotide with 4-point mutations compared to the absorbance value for the hybridisation with the fully complementary sequence showed the sensitivity of the assay, which is able to detect 4 mutations in 19-mer oligonucleotides working at 55°C. The experiment with the non-labelled complementary oligonucleotide shows that the streptavidin-HRP did not adsorb non-specifically on the complementary oligonucleotide.

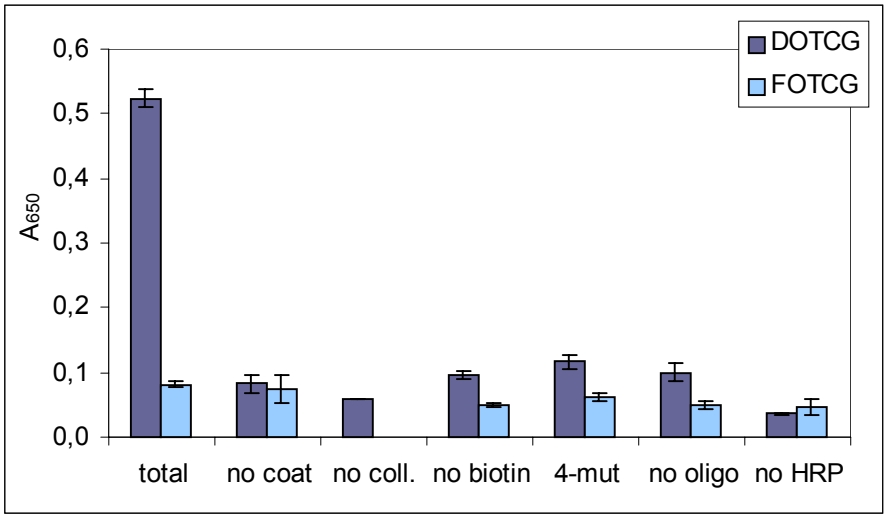

Figure III.8. Absorbance at 650nm obtained in the hybridisation ELONA for the dig-oligonucleotide-thiol-colloidal gold (20nm colloidal gold) conjugate functionality characterisation; total: system as depicted in Scheme III.3; no coating: blank without antidigoxigenin on the surface; no coll.: blank without conjugate; no biotin: blank with non-labelled complementary oligonucleotide; 4-mut: blank with biotin-labelled oligonucleotide with 4-point mutations; no oligo: blank without complementary oligonucleotide; no HRP: blank without streptavidin-HRP. FITC-oligonucleotide-thiol-colloidal gold conjugate was used as a control.

Oligonucleotide-colloidal gold thermal stability. The thermal stability of the biorecognition nanomodules, i.e. of the conjugation between oligonucleotides and colloidal gold, was studied, since the biomodules have to be stable under hybridisation temperatures. Firstly, FITC-oligonucleotide-thiol thermal stability was studied in order to ensure that fluorescence does not decay with heat. FITC-oligonucleotide-thiol fluorescence did not vary significantly with heating, proving the stability of this fluorescent moiety with temperature (*results not shown*). As FITC-oligonucleotide-thiol and colloidal gold were stable with temperature, the effect observed in the FITC-oligonucleotide-thiol-colloidal gold conjugate thermal stability, if any, had to be due to the desorption of the fluorescent oligonucleotides from the gold particle. The absorbance spectra demonstrated that the conjugate suspension did not aggregate with heating (*results not shown*). Table III.4 shows the fluorescence values for the sample and the control after three washing steps, heating and removal by mercaptoethanol.

Table III.4. Fluorescence emitted at 520nm by the supernatants from the three washings, from heat + centrifugation or only centrifugation, and from removal by mercaptoethanol.

	1st washing	2nd washing	3rd washing	After 1h	After ME	Total
Sample (heat + centrifugation)	68.5 ± 6.7	41.2 ± 1.3	15.8 ± 3.1	8.8 ± 2.5	11.1 ± 3.0	145.4 ± 16.6
Control (centrifugation)	68.6 ± 2.1	45.8 ± 6.7	13.2 ± 0.8	5.9 ± 1.0	12.7 ± 2.0	146.2 ± 12.6

The sample and the control fluorescence balances close, as indicate the total sums of the fluorescence emitted, with an experimental error of 10%. Comparing the "After 1h" values, there is a 32.9% oligonucleotide desorption from the colloid, however the experimental error in this column is 23.8%. Comparing the "After ME" values, there is a 12.6% oligonucleotide desorption from the colloid, the experimental error in this column being 21.0%. Consequently, there is between 12.6 and 32.9% oligonucleotide desorption from the colloid due to heating, but the experimental error is considerable. The group is working on new chemistries to attach the oligonucleotides to the colloidal gold particles, which may confer stronger or more bonds between DNA and colloids, and would overcome the problem of thermal stability of the interaction. Nevertheless, despite the partial oligonucleotide desorption from the colloid, the biorecognition modules have demonstrated to be functional in ELONA hybridisations.

Conclusions

The conditions under which colloidal suspensions are stable (no aggregation occurs) have been established. It was found that 8.5mM carbonate, phosphate and citrate buffers gave the best results for the stabilisation of colloidal gold suspensions. However, 10mM phosphate buffer, 0.1M NaCl at pH 7.0 or 10-100mM tris-HCl buffer, 10-100mM KCl, 1%BSA, at pH 7.0-8.0 provided better results for resuspension of the conjugates. The study of several parameters on the stability of colloidal gold suspensions, and the observation of the aggregation after 24h in some experiments, showed that aggregation could be a slow process and that can be inhibited when using protective agents, like BSA in the colloidal gold suspension.

Two model oligonucleotides, with FITC and digoxigenin as labels, were conjugated to 20nm colloidal gold, resulting in stable and reproducible colloidal gold suspensions, with 3% standard deviation for FITC-oligonucleotide-thiol-colloidal gold conjugates and 11% standard deviation for dig-oligonucleotide-thiol-colloidal gold conjugates. When 3nm colloidal gold was used, both the stability and the reproducibility of the conjugate suspension were lower (32% lower peak absorbance and 22% standard deviation). The effectiveness of the conjugations was demonstrated

by fluorescence for FITC-oligonucleotide-thiol-colloidal gold conjugates and by sandwich ELONA for dig-oligonucleotide-thiol-colloidal gold conjugates. BSA was found to act as an effective blocking and protecting agent in the oligonucleotide-thiol-colloidal gold conjugate suspensions and assays. Hybridisation ELONA demonstrated the functionality of the bionanomodules and the ability to differentiate 4-point mutations in 19-mer oligonucleotide sequences.

The thermal stability corresponding to the interaction of colloidal gold with oligonucleotide-thiol was studied by fluorescence methods in order to know if the nanomodules were suitable for hybridisation at high temperatures. Between 12.6 and 32.9% of FITC-oligonucleotide-thiol desorbed from the colloids surface after 1 hour at 65°C. Nevertheless, the experimental error is considerable and the biorecognition modules still worked in hybridisation assays.

The stability of the oligonucleotide-colloidal gold conjugate suspensions, the functionality of these conjugates, and the thermal stability of the modification or interaction between the two components (oligonucleotides and colloidal gold), make the rationally designed biorecognition nanomodules suitable for use in DNA sensors. By taking benefit from the colloidal gold properties, these conjugates will be selectively electrodeposited on arrays and the hybridisation event will be detected by electrochemical techniques, providing a promising integrated approach for DNA arrays, competitive with the current arraying technologies.

References

Bonnard C., Papermaster D.S., and Kraehenbuhl, J.-P., in *Immunolabelling for Electron Microscopy*, ed. Elsevier, New York, USA, **1984**, pp. 95-111.

Brada D. and Roth J., *Anal. Biochem.*, **1984**, 142, 79.

Crumbliss A.L., Perine S.C., Stonehuerner J., Tubergen K.R., Zhao J., Henkens R.W., and O'Daly J.P., *Biotechnol. Bioeng.*, **1992**, 40 (4), 483.

deGennes P.-G., *Macromolecules*, **1980**, 13, 1069.

deGennes P.-G., *Macromolecules*, **1982**, 15, 492.

deGennes P.-G., *Adv. Colloid Interface Sci.*, **1987**, 27, 189.

Demers L.M., Mirkin C.A., Mucic R.C., Reynolds R.A., Letsinger R.L., Elghanian R., and Viswanadham G., *Anal. Chem.*, **2000**, 72 (22), 5535.

Derjaguin B.V. and Landau L., *Acta Physiochim.*, **1941**, 14, 633.

De Waele M., Renmans W., Segers E., De Valck V., Jochmans K., and Van Camp B., *J. Histochem. Cytochem.*, **1989**, 37 (12), 1855.

Dubertret B., Calame M., and Libchaber A.J., *Nature Biotechnol.*, **2001**, 19, 365.

Elghanian R., Storhoff J.J., Mucic R.C., Letsinger R.L., and Mirkin C.A., *Science*, **1997**, 277, 1078.

Gardner K.H. and Theis T.L., *J. Colloid Interface Sci.*, **1996**, 180, 162-173.

Geoghegan W.D. and Ackerman G.A., *J. Histochem. Cytochem.*, **1977**, 25 (11), 1187.

Langevin P., *C. R. Acad. Sci. Paris*, **1908**, 146, 530.

Lin L., Zhao H.Q., Li J.R., Tang J.A., Duan M.X., and Jiang L., *Biochem. Biophys. Res. Commun.*, **2000**, 274, 817.

Lin B., Sureshkumar R., and Kardos J.L., *Ind. Eng. Chem. Res.*, **2002**, 41, 1189.

Lyon L.A., Musick M.D., and Natan M.J., *Anal. Chem.*, **1998**, 70 (24), 5177.

Morris R.E. and Saenlinger C.B., *J. Histochem. Cytochem.*, **1984**, 32, 124.

Mucic R.C., Storhoff J.J., Mirkin C.A., and Letsinger R.L., *J. Am. Chem. Soc.*, **1998**, 120 (48), 12674.

O'Daly J.P., Henkens R.W., Zhan J., and Zhang H., *U.S. Patent 5,391,272*, **1995**.

Park S.J., Taton T.A., and Mirkin C.A., *Science*, **2002**, 295, 1503.

Patolsky F., Ranjit K.T., Lichtenstein A., and Willner I., *Chem. Commun.*, **2000**, (12), 1025.

Powell R.D., Halsey C.M.R., Spector D.L., Kaurin S.L., McCann J., and Hainfield J.F., *J. Histochem. Cytochem.*, **1997**, 45 (7), 947.

Seelenbinder J.A., Brown C.W., Pivarnik P., and Rand A.G., *Anal. Chem.*, **1999**, 71 (10), 1963.

Slot J.W. and Geuze H.J., *European J. Cell Biol.*, **1985**, 38, 87.

Storhoff J.J., Elghanian R., Mucic R.C., Mirkin C.A., and Letsinger R.L., *J. Am. Chem. Soc.*, **1998**, 120 (9), 1959.

Verwey E.J.W. and Overbeek J.T.G., *Theory of the stability of lyophobic colloids*, ed. Elsevier, New York, USA, **1948**.

Weisbecker C.S., Merritt M.V., and Whitesides G.M., *Langmuir*, **1996**, 12 (16), 3763.

Zhao H.Q., Lin L., Li J.R., Tang J.A., Duan M.X., and Jiang L., *J. Nanoparticle Res.*, **2001**, 3, 321.

Abbreviations

antidig: antidigoxigenin

BSA: bovine serum albumin

CCD: charge-coupled device

dig: digoxigenin

DLVO: Derjaguin - Landau - Verwey - Overbeek

DNA: deoxyribonucleic acid

EDC: 1-ethyl-3-(3-dimethylaminopropyl)carbodiimide hydrochloride

EDTA: ethylenediaminetetraacetic acid

ELONA: enzyme-linked oligonucleotide assay

FITC: fluorescein-isothiocyanate

FRET: fluorescence resonance energy transfer

HRP: horseradish peroxidase

ME: mercaptoethanol

PEG: polyethylene glycol

PEI: polyethylene imine

pI: isoelectric point

SAM: self-assembled monolayer

SN: supernatant

SSC: saline-sodium citrate

TMB: 3,3',5,5'-tetramethyl-benzidine

tris-HCl: tris[hydroxymethyl]aminomethane hydrochloride

Chapter IV. Site-directed electrodeposition of biorecognition nanomodules as biochip arraying technique

Abstract

The goal of the present work is to selectively electrodeposit oligonucleotide-modified colloidal gold conjugates (biorecognition nanomodules) with photolithographic resolution to yield a new arraying method for the production of high-density multi-addressable biosensing chips.

It is shown by light and electron microscopy that selective electrodeposition of colloidal gold on 5µm interdigitated electrodes (IDEs) can be achieved. Selective electrodeposition on indium-tin oxide (ITO) electrodes was proven by spectrophotometry. In all the cases, colloidal gold could be selectively deposited in short times (from 1 to 5min) applying from +0.8 to +1.2V (*vs.* Ag/AgCl). Piezoelectric techniques also demonstrated the selective electrodeposition of colloidal gold.

Oligonucleotide-colloidal gold biorecognition nanomodules were then electrodeposited on several electrode surfaces. Light microscopy proved the selective electrodeposition on IDEs and 3-electrode arrays, the optimal conditions being +0.8V (*vs.* Ag/AgCl) for 10min. Electrochemical techniques proved the selective deposition on glassy carbon electrodes in 2min with +1.1V (*vs.* Ag/AgCl) applied potential. The conjugates were also electrodeposited on carbon screen-printed electrodes applying +1.2V (*vs.* Ag/AgCl) for 2min, and the immobilisation was proved by colourimetric and electrochemical methods, showing a non-specific adsorption of 14%.

Electrodeposited nanomodules were functional after their electrodeposition, and able to differentiate 4-point mutations in 19-mer oligonucleotide sequences, demonstrating that this arraying strategy can be used in low cost DNA sensor arrays.

Keywords: colloidal gold, biorecognition nanomodules, HRP-colloidal gold conjugate, oligonucleotide-colloidal gold conjugate, DNA chip array, mutation detection.

Introduction

There is little doubt that low cost biosensors can change the way in which analytical procedures are performed in clinical diagnosis, environmental and food analysis. Key to the utility and low cost of these analytical devices is the ability to make multi-analyte sensors. Miniaturisation and integration are therefore the most urgent requirements for biosensors and biochips, in order to minimise sample volumes, invasiveness, reagent and other general costs, and to obtain ready-to-use portable devices.

One of the key parameters in the DNA chip design is the immobilisation step. Not only it is necessary to retain the functionality of the biomolecule after the immobilisation, but also to achieve

a high attachment efficiency and density. Site-specific immobilisation at high density has been attempted for several years. Specific arraying methods, like ink-jetting (Castellino *et al.*, 1997), pin deposition (Yershov *et al.*, 1996; Drobyshev *et al.*, 1997; and Guschin *et al.*, 1997; Sakai *et al.*, 2000; and Zammatteo *et al.*, 2000), polypyrrolisation (Livache *et al.*, 1994, 1995 and 1998; and Roget *et al.*, 1995) and photolithography (Fodor *et al.*, 1991; and Pease *et al.*, 1994), provide ordered arrangement of different oligonucleotides fixed to specific positions on a solid surface with varying resolution. However, each one of the techniques presents relative disadvantages. The main problem of ink-jetting is the ease and robustness of the method. Air bubbles or clogging reduce the repeatability and reliability of the system, and lead to maintenance problems. Poor uniformity of the deposit may result, which can cause crossover contamination between probes. In the pin deposition technique, excessive splashing is also a problem leading to variability in spot size and in probe concentration. Polypyrrolisation presents the drawbacks of wet chemistry, which increases the irreproducibility of the system, and the necessity of a washing step after each polypyrrole synthesis to avoid cross-contamination with residual oligonucleotides. In photolithography, the main drawback is the inability to control the sequence quality, and the fact that possible mistakes in the synthesis make necessary a high number of redundant sites. This work is focused on the development of a new immobilisation and arraying method, based on the site-directed electrodeposition of biorecognition modules. These biorecognition modules are formed by the conjugation of the biorecognition element or functional biomolecule to a colloidal gold particle that acts as immobilisation vehicle. Despić and Pavlović (1984) took benefit of the electrophoretic mobility of colloidal gold to deposit it at a carbon electrode. Apart from bare colloidal gold, several scientists used colloidal gold to immobilise enzymes on their sensors by electrodeposition. For example, Crumbliss *et al.* (1992) conjugated glucose oxidase (GOx), horseradish peroxidase (HRP) and xanthine oxidase to colloidal gold and electrodeposited these conjugates onto platinum or glassy carbon by applying +1.6V (*vs.* Ag/AgCl) for 2h. These enzyme electrodes gave an electrochemical response to the corresponding enzyme substrates in the presence of ferrocene mediators, demonstrating the utility of colloidal gold as biocompatible matrix suitable for the fabrication of enzyme electrodes. Following the same strategy, our work is focused to the selective electrodeposition of bio/nanoconjugates of colloidal gold with oligonucleotides. The nanomodular approach presented in this paper can be used to build DNA sensor microarrays with high resolution (only limited by the electrode pattern, i.e. with photolithographic resolution) and the possibility to previously control the quality of the probes. Arraying with these characteristics is achieved with low cost equipment once the photolithographed substrate is available. Furthermore, the technique is compatible with well-developed processes in the semiconductor industry. With both arraying and measurement by electrochemical methods, overall fabrication costs can be lower. Moreover, the versatility of the strategy makes it a generic approach, useful for any kind of sensing chip, where high resolution might be needed, be it enzymatic, affinity or chemical. Of importance in this technique is the avoidance of non-specific adsorption.

Relating to this, it is considered to briefly examine what is known about deposition of colloidal suspensions on solid surfaces. Colloidal gold particles have a negatively charged surface, property that can be used to deposit them on surfaces under applied electric fields (Despić and Pavlović, 1984; Giersig and Mulvaney, 1993; and Bailey *et al.*, 2000). When like-charged colloidal particles are immobilised on a surface of opposite charge, the interparticle repulsion decreases due to electrohydrodynamic and electroosmic effects, favouring the ordered and close packing (Giersig and Mulvaney, 1993), unlike simply adsorbed colloidal particles on neutral surfaces (Grabar *et al.*, 1996). In fact, although several particle adsorption models, e.g. Random Sequential Adsorption (RSA), describe an irreversible particle adsorption (Adamczyk *et al.*, 1994 and 1997, and Adamczyk and Weroński, 1997), the aforementioned electrohydrodynamic and electroosmic effects might favour the mobility of the adsorbed particle. In fact, these models are being refined to consider not only these effects, but also transport mechanisms, such as diffusion and convection (Lavalle *et al.*, 1999; Wojtaszczyk *et al.*, 1997; and Faraudo and Bafaluy, 1999).

In this work, the electrodeposition of colloidal gold and biorecognition nanomodules on different electrode surfaces and the detection of selective deposition by a variety of methods are described. Firstly, bare colloidal gold was electrodeposited on photolithographed gold interdigitated electrodes (IDEs), indium-tin oxide (ITO) and gold-covered quartz crystals, and the selective electrodeposition was detected by microscopic, spectrophotometric and piezoelectric methods, respectively. Secondly, HRP-colloidal gold conjugate was deposited on screen-printed electrodes and the deposition was characterised by colourimetry. Finally, selective depositions of oligonucleotide biorecognition nanomodules on photolithographed gold IDEs and photolithographed gold 3-electrode arrays were shown by microscopy, depositions on glassy carbon were shown by electrochemistry, and depositions on carbon screen-printed electrodes were shown by colourimetry and electrochemistry. For each one of the electrodepositions, the operational parameters were optimised in order to use minimum potential and short deposition times. Hybridisation of electrodeposited oligonucleotide-colloidal gold conjugates with complementary sequences and sequences with 4-point mutations was followed by electrochemistry, demonstrating the functionality of the bio/nanomodules after their immobilisation.

Materials and methods

Materials. 5nm (4.9 $\pm$ 0.7nm) and 20nm (21.7 $\pm$ 2.0nm) diameter colloidal gold, and HRP-10nm colloidal gold conjugate (9.3 $\pm$ 0.5nm) were obtained from Sigma. The original concentrations were 4.4 x 10^{13}, 4.9 x 10^{11} and 3.2 x 10^{13} particles mL^{-1} for 5, 20nm colloidal gold and HRP-10nm colloidal gold, respectively. Unconjugated gold colloids contained about 0.01% $HAuCl_4$ suspended in 0.01% tannic acid with 0.04% trisodium citrate, 0.26mM potassium carbonate and 0.02% sodium azide as preservative. HRP-colloidal gold was a suspension in 50% glycerol with 0.15M NaCl, 0.01M MES, pH 6.5, 0.25% BSA (no sodium azide was added because it inhibits the peroxidase

activity). 3nm (3 ± 1nm) diameter colloidal gold was a gift from Dr. Ewen Smith (University of Strathclyde, Glasgow, United Kingdom). Polyoxyethylenesorbitan monolaurate (Tween 20), bovine serum albumin (BSA), streptavidin-HRP and 3,3',5,5'-tetramethyl-benzidine liquid substrate system for ELISA (TMB) (containing TMB and H_2O_2 in an slightly acidic buffer) were also purchased from Sigma. Antidigoxigenin-HRP Fab fragments (antidig-HRP) were obtained from Roche. FITC-oligonucleotide-thiol-colloidal gold conjugate, the oligonucleotide being 3' FITC-$(C)_{12}(T)_{20}(C)_{12}$-SH 5', and digoxigenin(dig)-oligonucleotide-thiol-colloidal gold conjugate, the oligonucleotide being 3' digoxigenin-ACTTAACCGAGTCGACCGA-SH 5', were obtained by conjugation of 3 or 20nm colloidal gold with oligonucleotides from Genosys and Eurogentec, respectively. 3' TCGGTCGACTCGGTTAAGT 5' (complementary), 3' TCGGTCGACTCGGTTAAGT-biotin 5' (biotin-labelled complementary) and 3' TCGGTGGGCTCG GGTGAGT-biotin 5' (biotin-labelled with 4-point mutations) were from Eurogentec. Indium-tin oxide (ITO) surfaces were purchased from Delta Technologies, Ltd. 5μm interdigitated gold electrodes (IDEs) were from ABTECH Scientific Inc. 1.5mm diameter glassy carbon electrodes were from Cypress Systems. 5MHz gold-covered quartz crystals were purchased from Maxtek, Inc. Photolithographed 1mm diameter gold 3-electrode arrays were in-house designed and fabricated by NMRC (National Microelectronics Research Centre) of Ireland.

Instrumentation. Electrodepositions and chronoamperometries were performed using an AUTOLAB PGSTAT10 potentiostat in a conventional three-electrode cell, with Ag/AgCl as reference electrode and Pt as counter electrode or in a two-electrode system (for the screen-printed electrodes), with screen-printed Ag/AgCl as reference and counter electrode. Absorbance values and full spectra were measured with an HP 8453 spectrophotometer or with a Molecular Devices 340PC 96-well plate reader. Fluorescence was measured with a Perkin Elmer LS-50 fluorimeter or with a Nikon E600FN fluorescence microscope equipped with a Sony CCD camera. The fluorescence microscope in the transmittance mode was used for light microscopy. Electron microscopy was performed with a Zeiss 10 Ca electron microscope. All solutions were made from distilled water purified through a Milli-Q water system. Frequency measurements were performed with a PM-710 Electrochemical Quartz Crystal Microbalance plating monitor from Maxtek, Inc. The flow-cell used in the removal of non-specifically adsorbed particles from photolithographed gold surfaces was a loan of Trace Biotech AG.

Site-directed colloidal gold electrodeposition on photolithographed gold IDEs, ITO electrodes and gold-covered quartz crystals. For the electrodeposition of 5nm colloidal gold on photolithographed gold IDEs, firstly the IDEs were cleaned with "piranha's solution" (70% H_2SO_4 : 30% H_2O_2) and cyclic voltammetry (10 scans between -0.3 and +1.7V (*vs.* Ag/AgCl) at 0.5V s^{-1} in 0.33M H_2SO_4). Afterwards, the IDEs were immersed in a three-electrode cell containing 5nm colloidal gold suspension (4.4×10^{11}, 2.2×10^{12} and 4.4×10^{12} particles mL^{-1} in 10mM phosphate buffer, 0.1M NaCl, pH 7.0), and from +1.0 to +1.6V (*vs.* Ag/AgCl) was applied at one of the two sets

for 10, 20 and 30min. The set at which no potential was applied was used as control to measure non-specific adsorption. The deposition was characterised by light microscopy, electron microscopy and electrochemistry. For the electrochemical detection, linear sweep voltammetry (LSV) was performed between -0.3 and +1.7V (*vs.* Ag/AgCl) at 0.05mV s^{-1} in 0.1M H_2SO_4.

Transparent ITO electrodes were cleaned as follows: sonication in Alconox for 15min, sonication in 2-propanol for 15min and sonication in water for 15min twice. Two different detection modes were set up. *Sampling:* the electrodeposition (+0.8 and +1.6V (*vs.* Ag/AgCl) for 1, 2, 5, 10, 20, 25 and 30min) was performed in a three-electrode conventional cell containing 5 or 20nm colloidal gold suspension (4.4 x 10^{13} and 5.2 x 10^{11} particles mL^{-1}, respectively, in 10mM phosphate buffer, 0.1M NaCl, pH 7.0) and the ITO electrode was then immersed in a spectrophotometric cuvette filled with water or with colloidal gold suspension for absorbance measurement. *Real-time monitoring:* the electrodeposition (+0.8V (*vs.* Ag/AgCl) for 30min) was carried out at the same time as the detection, the counter and the reference electrode being included in a three-electrode spectrophotoelectrochemical thin cuvette / cell (200µL of volume, 0.05cm light path) containing 5nm colloidal gold suspension (4.4 x 10^{13} particles in 10mM phosphate buffer, 0.1M NaCl, pH 7.0). No potential was applied at the controls.

Colloidal gold was also electrodeposited on 5MHz gold-covered quartz crystals in an in-house made electrochemical flow-cell at a rate of 75µL min^{-1}. Firstly, 10mM tris-HCl buffer, 10mM KCl, 1% BSA, pH 7.0, was circulated trough the cell and the frequency was monitored. Once the frequency stabilised, +1.2V (*vs.* Ag/AgCl) was applied to the gold-covered quartz crystal. Once the frequency stabilised again, the solution was changed by a colloidal gold suspension (4.2 x 10^{11} particles in the same buffer). 10min after the colloidal gold injection, the potential was stopped.

Removal of non-specifically adsorbed colloidal gold particles. Some preliminary experiments were performed in a flow system to study the effect of the Reynolds number on the removal of non-specifically adsorbed colloidal gold on photolithographed gold electrodes. After deposition of a 50-µL drop of the colloidal gold suspension (8.5 x 10^{11} particles mL^{-1} in 10mM tris-HCl buffer, 10mM KCl, 1% BSA, pH 7.0) on the electrode and application of +1.6V (*vs.* Ag/AgCl) for 10min (no potential was applied to the blanks), the arrays were introduced into the flow-cell and the same buffer without colloidal gold was circulated firstly for 10min at 0.07mL min^{-1}, and afterwards for 10min at 6.20mL min^{-1}. Electrodes were observed under light microscopy before and after each experiment. Phase analysis was performed with the microscope AnalySIS software.

HRP-bionanomodule arraying. A 2-µL drop of HRP-colloidal gold conjugate suspension (3.2 x 10^{13} particles mL^{-1} in 50% glycerol with 0.15M NaCl, 0.01% MES, pH 6.5, 0.25% BSA) was deposited on screen-printed electrodes and +0.8V (*vs.* Ag/AgCl) was applied for 1 and 5min. No potential was applied at the control electrodes. After rinsing, the electrodes were incubated in

commercial TMB liquid substrate for 1h at 37°C with stirring, and the reaction was stopped with H_2SO_4. The colourimetric response was monitored at the 96-well plate reader.

Biorecognition nanomodule electrodeposition. The FITC-oligonucleotide-thiol-colloidal gold conjugate (1.8 x 10^{12} particles mL^{-1} in 10mM phosphate buffer, 0.1M NaCl, pH 7.0) was deposited on one of the sets of the IDEs (+1.6V (*vs.* Ag/AgCl) for 2h) and the deposition was characterised by light microscopy. The set at which no potential was applied was used as control.

The FITC-oligonucleotide-thiol-colloidal gold conjugate (7.7 x 10^{11} particles mL^{-1} in 10mM phosphate buffer, 0.1M NaCl, pH 7.0) was also electrodeposited on glassy carbon electrodes by applying +1.1V (*vs.* Ag/AgCl) for 2min, +0.8V (*vs.* Ag/AgCl) for 5min, and +0.6V (*vs.* Ag/AgCl) for 10min. No potential was applied at the controls. None of the microscopy characterisation techniques could be used and the electrodeposition was detected by cyclic voltammetry (CV) at 0.05V s^{-1} in 0.1M H_2SO_4.

The dig-oligonucleotide-thiol-colloidal gold conjugate was firstly used in sandwich ELONA on screen-printed electrodes (Scheme IV.1).

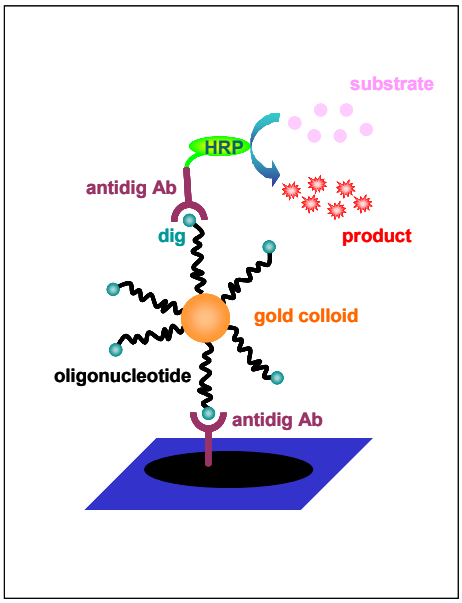

Scheme IV.1. Sandwich ELONA with dig-oligonucleotide-thiol-colloidal gold (20nm) on a carbon screen-printed electrode. The electrode is coated by antidigoxigenin; the digoxigenin of the dig-oligonucleotide-thiol-colloidal gold conjugate recognises the antidigoxigenin; the antidig-HRP recognises the digoxigenin of the immobilised dig-oligonucleotide-thiol-colloidal gold conjugate; the HRP label reacts with its substrate to give a coloured product.

The dig-oligonucleotide-thiol-colloidal gold conjugate was electrochemically deposited on screen-printed electrodes (Scheme IV.2). The electrodes were firstly blocked with BSA. After rinsing, a 0.5-µL drop of dig-oligonucleotide-thiol-colloidal gold conjugate (1.3 x 10^{12} particles mL^{-1} in 0.1M tris-HCl buffer, 0.1M KCl, pH 8.0, 1% BSA) was placed on the screen-printed electrode and +1.2V (*vs.* Ag/AgCl) was applied for 2min. No potential was applied at the controls. FITC-oligonucleotide-thiol-

colloidal gold conjugate (1.2 x 10^{12} particles mL^{-1} in 0.1M tris-HCl buffer, 0.1M KCl, pH 8.0, 1% BSA) was also used as control. The electrodes were then rinsed and incubated in antidig-HRP. For the colourimetric detection, dig-oligonucleotide-thiol-colloidal gold conjugate was used, and the electrodes were incubated in commercial TMB liquid substrate and absorbance values were measured at 650nm. For the electrochemical detection, dig-oligonucleotide-thiol-colloidal gold conjugate was used, and 1µL of H_2O_2 (1:500 dilution in 50mM acetate buffer, 0.15M NaCl, pH 5.1) and 1µL of [Os(2,2'-bipyridine)$_2$Cl(4-(aminomethyl)pyridine)]Cl (0.2mM in water) were mixed and placed on the working electrode. After 2-min incubation, -0.1V (*vs.* Ag/AgCl) was applied for 1min and the current values at different times were measured (control and blank electrodes were examined as stated).

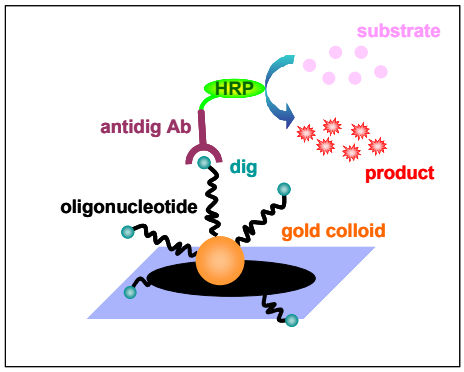

Scheme IV.2. Electrodeposited dig-oligonucleotide-thiol-colloidal gold (20nm) on a carbon screen-printed electrode. The dig-oligonucleotide-thiol-colloidal gold conjugate is electrodeposited on the carbon screen-printed electrode; the antidig-HRP recognises the digoxigenin of the electrodeposited dig-oligonucleotide-thiol-colloidal gold conjugate; the HRP label reacts with its substrate to give a coloured product.

The dig-oligonucleotide-thiol-colloidal gold conjugate was also electrochemically deposited on photolithographed gold 3-electrode arrays. A 15-µL drop of dig-oligonucleotide-thiol-3nm colloidal gold conjugate (1.3 x 10^{12} particles mL^{-1} in 0.05M tris-HCl buffer, 0.05M KCl, pH 8.0, 1% BSA) was placed on two gold electrodes of the 3-electrode array and from +0.8 to +1.9V (*vs.* Ag/AgCl) was applied for 1-10min to one of them. No potential was applied at the other gold electrode. The third gold electrode was used as blank (no potential, no colloidal gold conjugate). The array was then rinsed and observed under light microscopy, and the brightness was evaluated with the phase analysis of the microscope AnalySIS software.

Functionality of electroarrayed biorecognition nanomodules. The dig-oligonucleotide-thiol-colloidal gold conjugate was used in a hybridisation ELONA on carbon screen-printed electrodes (Scheme IV.3, but measuring the colourimetric response instead of the electrochemical one). For the hybridisation step, after the colloidal gold incubation like in the previous section, the electrodes were introduced in 70µL of a solution of biotin-labelled complementary oligonucleotide, non-labelled complementary oligonucleotide or biotin-labelled oligonucleotide with 4-point mutations (5µg mL^{-1} in 10mM tris-HCl, 1mM EDTA, 0.3 x SSC, 2 x Denhardt's solution, pH 8.0, corresponding to 4.7 x 10^{14} oligonucleotide molecules per mL) for 1h at 55°C with stirring, and rinsed with water and with

0.1mM tris-HCl buffer, 0.1% Tween 20. The electrodes were then incubated in 50μL of a streptavidin-HRP solution (0.4μg mL^{-1} in 0.1M tris-HCl buffer, 0.1M KCl, pH 8.0, 1% BSA) for 1h at 37°C with stirring, and rinsed with water and with 0.1mM tris-HCl buffer, 0.1% Tween 20. Finally, the electrodes were incubated in 50μL of commercial TMB liquid substrate for 1h at 37°C with stirring protected from light and absorbance values were measured at 650nm. Appropriate blanks and control experiments were performed as mentioned.

The dig-oligonucleotide-thiol-colloidal gold conjugate was electrochemically deposited on carbon screen-printed electrodes like in the previous section and hybridisation was detected electrochemically (Scheme IV.3). No potential was applied at the controls. In the hybridisation step, biotin-labelled complementary sequences and oligonucleotides with 4-point mutations were used. After incubation in streptavidin-HRP, hybridisation from electrodeposited conjugates was detected electrochemically following the same detection system as for the antidig-HRP label.

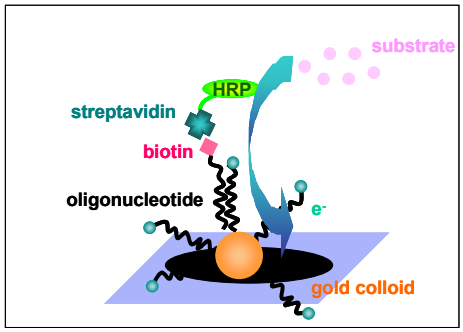

Scheme IV.3. Electrodeposited dig-oligonucleotide-thiol-colloidal gold (20nm) on a carbon screen-printed electrode and subsequent hybridisation. The dig-oligonucleotide-thiol-colloidal gold conjugate is electrodeposited on the carbon screen-printed electrode; the oligonucleotide of the dig-oligonucleotide-thiol-colloidal gold conjugate hybridises with its complementary sequence; the streptavidin-HRP recognises the biotin of the complementary oligonucleotide; the HRP label reacts with its substrate to give an electrochemical signal.

Results and discussion

Site-directed colloidal gold electrodeposition on photolithographed gold IDEs, ITO electrodes and gold-covered quartz crystals. Firstly, microarraying with photolithographic resolution using unmodified colloidal gold has been attempted. Light and electron microscopy demonstrated the site-directed deposition of the colloidal gold on interdigitated electrodes (5-μm width gap and lines). Figure IV.1 shows a portion of the gold IDEs before and after immersion in a colloidal gold suspension (4.4 x 10^{12} particles in 10mM phosphate buffer, 0.1M NaCl, pH 7.0) and application of +1.0V (*vs.* Ag/AgCl) for 30min at one of the sets. Lower concentrations and times did not provide detectable electrodeposition with light microscopy, and higher applied potentials provoked colloidal gold aggregation. The pink lines correspond to the electrodes and the blue lines to the gap between them. It can be clearly seen that whilst the lines corresponding to the set at which no potential has been applied remain at the same colour (small differences due to the imaging set up), the lines associated to the set at which +1.0V (*vs.* Ag/AgCl) has been applied for

30min show a different colour (orange). This observation demonstrates the selective electrodeposition of 5nm colloidal gold on 5μm electrodes.

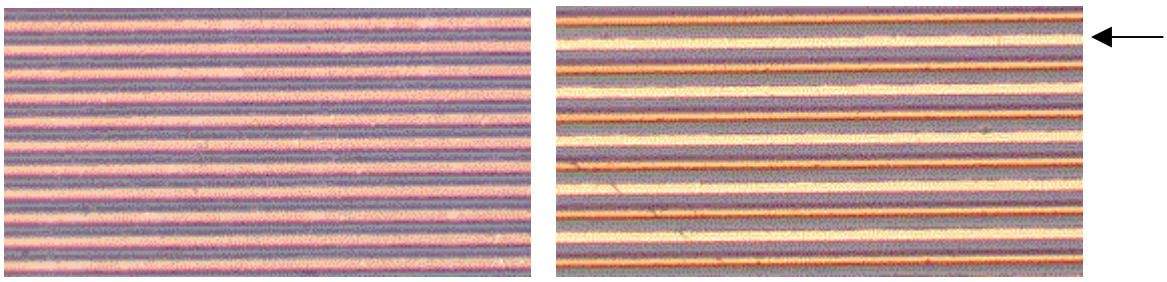

a) b)

Figure IV.1. Gold IDEs (5-μm width electrodes and gap) under light microscopy a) before and b) after immersion in a 5nm colloidal gold suspension in a three-electrode cell and application of +1.0V (*vs.* Ag/AgCl) for 30min at one of the sets. No potential was applied at the control set. Arrow indicates control set.

Under these conditions, a thick multilayer of colloidal gold has been formed. Surface hydrodynamic stresses of this structure led to detachment of the electrodeposited material as if it were a new dense phase (Figure IV.2). This observation settles to some extent the controversy on the reversibility of the deposition phenomenon. Since for the application of DNA sensors a multilayer structure is not necessary, in subsequent experiments it has been tried to limit the extent of electrodeposition by lowering the exposure time in the hope that the non-specific adsorption phenomena would also be limited.

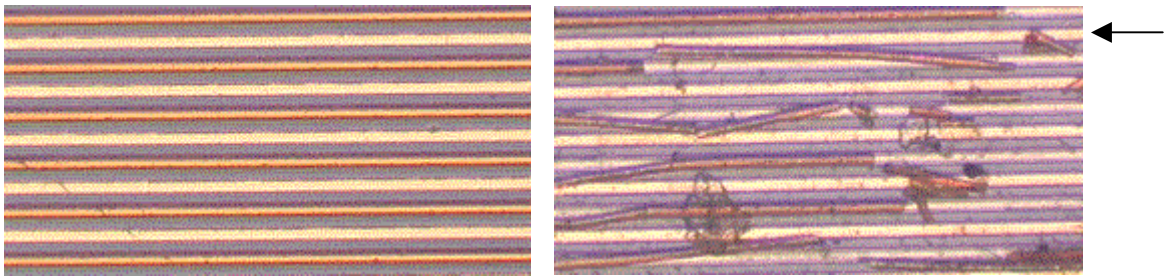

a) b)

Figure IV.2. Gold IDEs (5-μm width electrodes and gap) under light microscopy after immersion in a 5nm colloidal gold suspension in a three-electrode cell, application of +1.0V (*vs.* Ag/AgCl) for 30min at one of the sets and a) carefully rinsing or b) water-jet rinsing. No potential was applied at the control set. Arrow indicates control set.

Electron microscopy was also used to characterise the site-directed electrodeposition of colloidal gold on gold IDEs. Figure IV.3 shows a portion of the IDEs after electrodeposition under the same conditions. The white lines correspond to the electrodes and the black lines to the gaps between them. The electrode lines at which the potential has been applied present a rougher surface, with an irregular silhouette representing electrodeposited colloidal gold particles. This site-directed electrodeposition was also detected with electrochemistry. At the electrode where potential was applied, it was possible to see an oxidation peak at approximately +1.2V (*vs.* Ag/AgCl) that

corresponds to the electrodeposited colloidal gold oxides formation (Figure IV.4). The intensity of this peak is substantially higher than the intensity of the peak corresponding to the electrode where no potential was applied. This increase in intensity corresponds most likely to the surface area increase and the higher catalytic efficiency of the nanostructured material. Additionally, the peak intensity corresponding to the passive adsorption does not differ from the peak intensity of the background caused by the gold IDEs (*result not shown*). Another oxidation peak at approximately +1.5V (*vs.* Ag/AgCl) appears in the linear sweep voltammetry on the electrode where potential was applied. This peak could correspond to another gold oxidation mechanism that appears when there is electrodeposited material on the electrode. These site-directed electrodeposition experiments on IDEs have demonstrated that the strategy is suitable for arraying colloidal gold with photolithographic resolution.

Figure IV.3. Gold IDEs (5-µm width electrodes and gap) under electron microscopy after immersion in a 5nm colloidal gold suspension in a three-electrode cell and application of +1.0V (*vs.* Ag/AgCl) for 30min at one of the sets. No potential was applied at the control set. Arrow indicates control set.

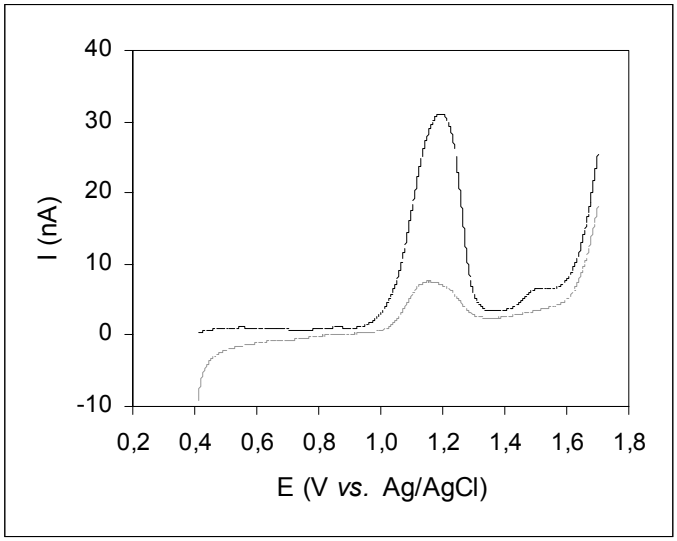

Figure IV.4. Linear sweep voltammetry at 0.05mV s^{-1} in 0.1M H_2SO_4 after selective electrodeposition of 20nm colloidal gold by immersion of the gold IDEs in a three-electrode cell and application of +1.0V (*vs.* Ag/AgCl) for 30min at one set (dark blue). No potential was applied at the control set (light blue).

Colloidal gold deposition on transparent ITO electrodes was characterised by *sampling* and *real-time monitoring* spectrophotometric techniques (*see experimental section*). The *sampling* mode showed absorbance peaks at 523nm only when potential had been applied (Figure IV.5). This peak corresponds to the electrodeposited colloidal gold particles on the ITO, since the colloidal gold suspension absorbs at this wavelength. Although after 1min differences between electrodeposition and passive adsorption were not observed (no absorbance peaks at 523nm in any of the spectra, *results not shown*), after 2min the differences were noticeable and at higher times more evident. The highest differences between electrodeposited and non-specifically adsorbed colloids were achieved at longer times. However, since at short times the absorbance of non-specifically adsorbed particles is negligible, it seems that they are advantageous for arraying. However, the detection limit of this method should be taken into consideration when making this assertion. The short-time regime is interesting from two points of view. Firstly, it is very probable that the kinetics of non-specific adsorption and of electrodeposition are different. It is expected that during electrodeposition, a plateau coverage can be reached in short times, whilst the non-specific adsorption is slower. Secondly, if electrodeposition can be done at 1-min range, arraying can be fast enough to compete with pin deposition or ink-jetting. Higher electrodeposition potentials (+1.6V (*vs.* Ag/AgCl)) resulted in aggregation of the colloidal gold suspension in the spectroelectrochemical cell the colour of the solution changing from pink to blue.

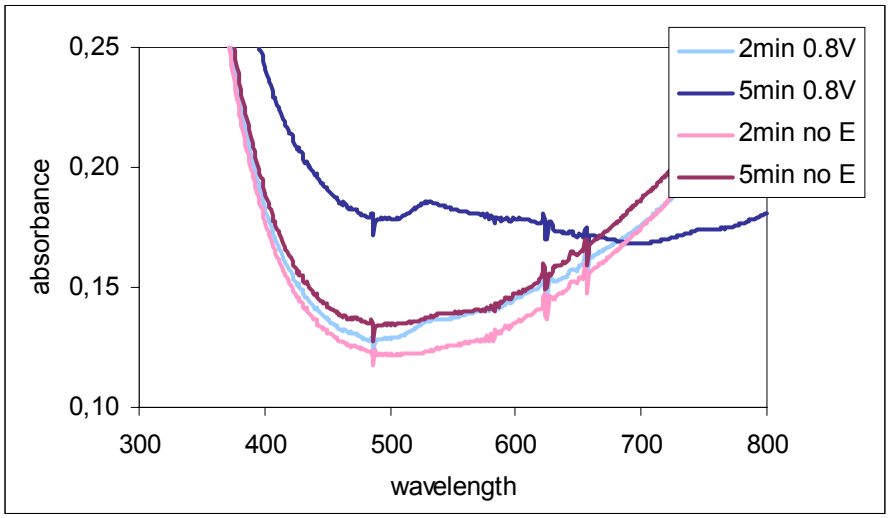

Figure IV.5. Absorbance *vs.* wavelength of 20nm colloidal gold electrodeposited or adsorbed on ITO electrodes in *sampling* mode. Electrodeposition conditions: application of +0.8V (*vs.* Ag/AgCl) for 2 and 5min to a working ITO electrode immersed in a three-electrode cell containing 20nm colloidal gold suspension (5.2 x 10^{11} particles mL^{-1} in 10mM phosphate buffer, 0.1M NaCl, pH 7.0). No potential was applied at the controls.

The *sampling* mode was also used in other experiments, where the spectrophotometric cuvette was filled with colloidal gold suspension during the measurement. Figures IV.6 and IV.7 show the absorbance at 523nm *vs.* electrodeposition time for 5 and 20nm colloidal gold particles. The absorbance change is higher for 20nm colloidal gold than for 5nm colloidal gold, although absolute absorbance values are higher for the 5nm colloidal gold electrodeposition, probably due to the

higher colloidal particle concentration in the spectrophotometric cuvette. Both plots show that short electrodeposition times (less than 5min) are preferable.

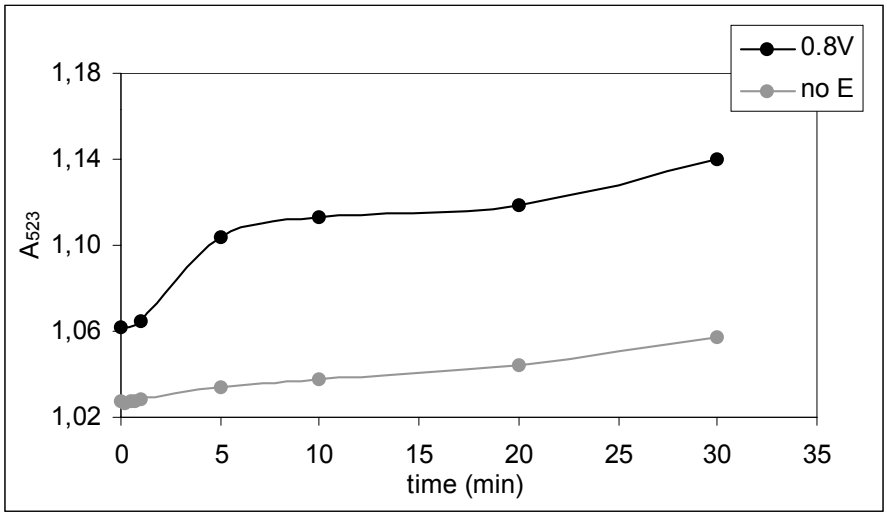

Figure IV.6. Absorbance at 523nm *vs.* time of 5nm colloidal gold electrodeposited or adsorbed on ITO electrodes in *sampling* mode. Electrodeposition conditions: application of +0.8V (*vs.* Ag/AgCl) for different times to a working ITO electrode immersed in a three-electrode cell containing 5nm colloidal gold suspension (4.4×10^{13} particles mL^{-1} in 10mM phosphate buffer, 0.1M NaCl, pH 7.0). No potential was applied at the controls.

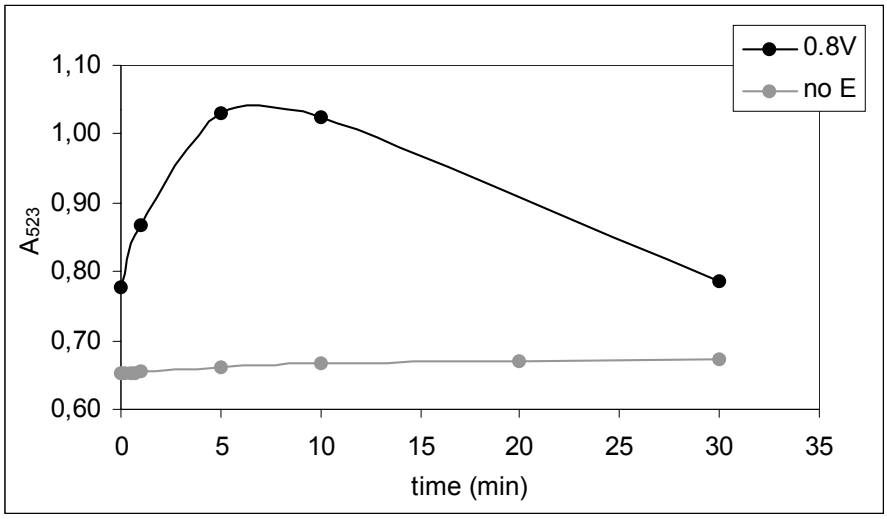

Figure IV.7. Absorbance at 523nm *vs.* time of 20nm colloidal gold electrodeposited or adsorbed on ITO electrodes in *sampling* mode. Electrodeposition conditions: application of +0.8V (*vs.* Ag/AgCl) for different times to a working ITO electrode immersed in a three-electrode cell containing 20nm colloidal gold suspension (5.2×10^{11} particles mL^{-1} in 10mM phosphate buffer, 0.1M NaCl, pH 7.0). No potential was applied at the controls.

The *real-time monitoring* mode provided similar results but higher reproducibility since the same area of the electrode was addressed continuously. Figure IV.8 shows the absorbance values for the electrodeposition of 5nm colloidal gold. It is possible to observe a different slope depending on if potential was applied or not, the slope of the electrodeposition being higher. No non-specific adsorption could be appreciated spectrophotometrically. Although in this case the measurement is

taken in a thin spectroelectrochemical cell, the difference in absorbance can still be appreciated probably due to the increased back scattering of the now immobilised particles.

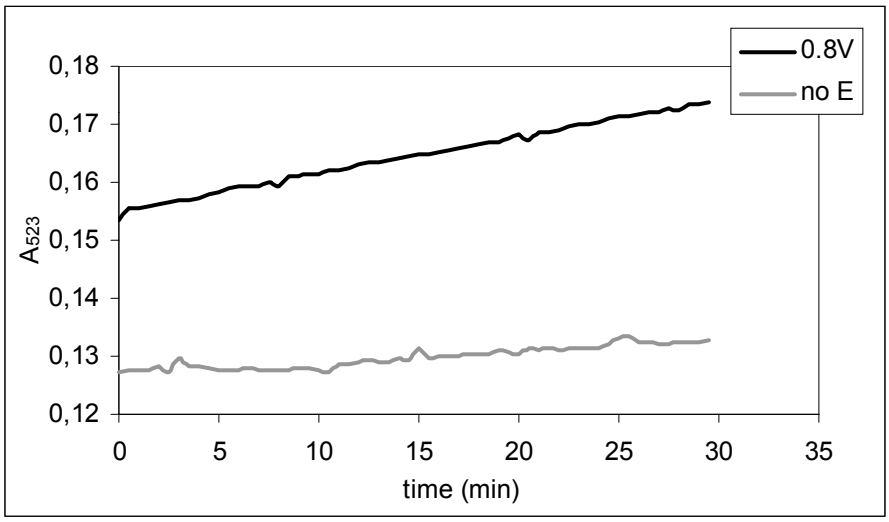

Figure IV.8. Absorbance at 523nm *vs.* time of 5nm colloidal gold electrodeposited or adsorbed on ITO electrodes in *real-time monitoring* mode. Electrodeposition conditions: application of +0.8V (*vs.* Ag/AgCl) in continuous to a working ITO electrode immersed in a three-electrode spectrophotoelectrochemical thin cuvette/cell containing 5nm colloidal gold suspension (4.4 x 10^{13} particles mL^{-1} in 10mM phosphate buffer, 0.1M NaCl, pH 7.0). No potential was applied at the controls.

It is interesting to note that in all the experiments with ITO, the first absorbance value for the electrodeposition was always higher than the corresponding non-specific adsorption one. This observation suggests that the highest electrodeposition rates may be occurring at times shorter than the time necessary to start the spectrophotometric measurement on this material.

Piezoelectric measurements with the electrochemical quartz crystal microbalance were also performed to study the colloidal gold electrodeposition. After injection of the colloidal gold suspension, there was a shift in frequency of 60Hz in 10min when applying +1.2V (*vs.* Ag/AgCl), while there was a flat line when potential was not applied (Figure IV.9). Our calculations, applying the Sauerbrey equation (1959), indicate that when a monolayer of colloidal gold particles is deposited on the electrode surface, the expected shift in frequency should be between 1140 and 1450Hz, depending on the packing density agreeing with other experimental results reported in the literature. Consequently, according to the observed shift in frequency, the electrodeposited colloidal gold particles correspond to approximately 5% of a monolayer. Although this result is difficult to explain and the experimental set up has to be optimised in order to make sure the observation is not an artefact, it indicates again that the application of potential selectively directs the electrodeposition of colloidal particles, whilst its absence leads to very little (if at all) non-specific adsorption.

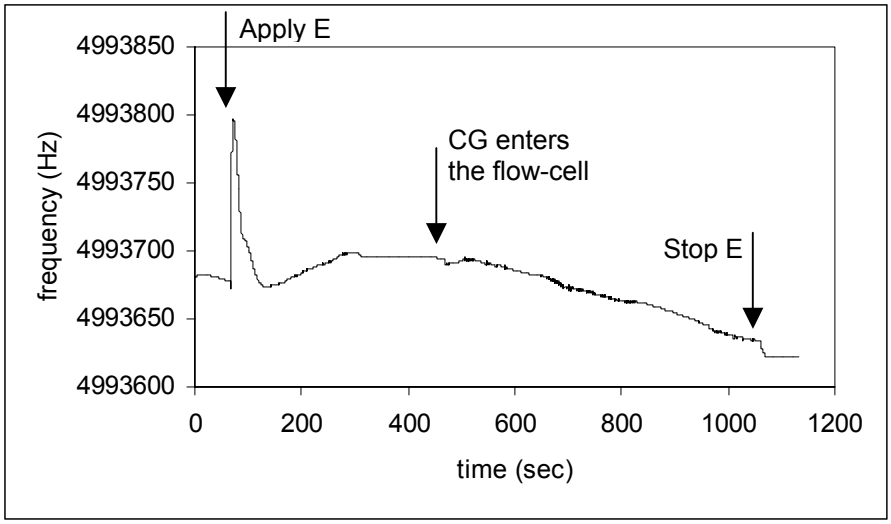

Figure IV.9. Frequency *vs.* time for the electrodeposition of 20nm colloidal gold on gold-covered quartz crystals. Experiment conditions: injection of 10mM tris-HCl buffer, 10mM KCl, 1% BSA, pH 7.0, at 75µL min^{-1}, application of +1.2V (*vs.* Ag/AgCl), and injection of the colloidal gold suspension (4.2 x 10^{11} particles mL^{-1} in the same buffer).

Removal of non-specifically adsorbed colloidal gold particles. It is necessary to mention that the experiments reported so far were performed under quiescent conditions (except the electrodeposition on gold-covered quartz crystals). However, the effect of shear stresses on the stability of colloidal gold suspensions is well known and quantified (Russel *et al.*, 1986). It is also of interest that Burdick *et al.* (2001) have shown that deposition is also a function of the Reynolds number of the mobile phase in contact with the electrode, especially when the roughness of the electrode surface is comparable or smaller than the particle characteristic dimension. Preliminary experiments were performed to observe if after the electrodeposition, non-specifically adsorbed particles could be removed if the electrodes were exposed to a flowing buffer solution at different Re. After the slow flow (Re = 1.85) the amount of electrodeposited material did not change significantly but unexpectedly, there was a 17-fold increase in the amount of non-specifically adsorbed material. In fact, the light microscopy images seem to show aggregation of the non-specifically adsorbed particles, which may interfere the phase analysis and give an artefact associated with the mobility that some authors have observed when particles deposit on surfaces (Trau *et al.*, 1996 and 1997). However, after the fast flow (Re = 164.48), whilst the amount of electrodeposited material decreased only by 25%, the amount of non-specifically adsorbed material decreased by 53% compared with the amount before any flow or 73% compared with the amount after the slow flow. Although experimental set-up and results analysis have to be optimised, these first observations are indicative of the possibility to remove non-specifically adsorbed particles by using flows with the appropriate Re values, or making the deposition under controlled hydrodynamic conditions.

HRP-bionanomodule arraying. Figure IV.10 shows the absorbance values from the colourimetric response of commercial TMB liquid substrate after electrodeposition or non-specific adsorption of HRP-colloidal gold on these electrodes. Absorbance values are higher when using 5min instead of 1min, due to the higher electrodeposition or non-specific adsorption of HRP-colloidal gold. However, whereas with 5min the absorbance value from the non-specific adsorption is 69% the value from the electrodeposited material, with 1min this non-specific adsorption is reduced to 58%. As noticed with free colloidal gold and spectrophotometry, at short times the difference between electrodeposition and non-specific or passive adsorption is higher. With this experiment it has been demonstrated that the electrodeposition of biorecognition nanomodules, in this case with HRP as a "proof of concept", is feasible.

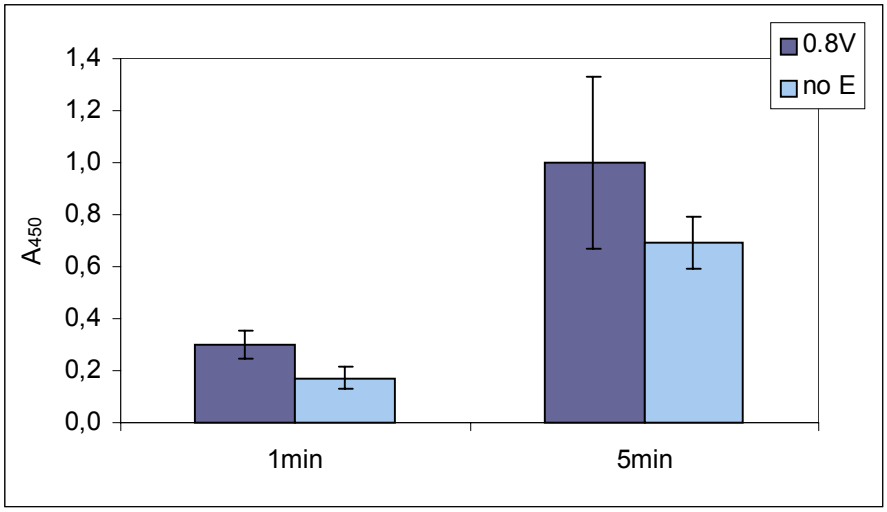

Figure IV.10. Absorbance at 450nm from the colourimetric reaction of the electrodeposited or adsorbed HRP-colloidal gold (10nm) with TMB on carbon screen-printed electrodes. Electrodeposition conditions: application of a 2-µL drop of HRP-colloidal gold conjugate suspension (3.2×10^{13} particles mL^{-1} in 50% glycerol with 0.15M NaCl, 0.01% MES, pH 6.5, 0.25% BSA) on the screen-printed electrodes, followed by application of +0.8V (*vs.* Ag/AgCl) for 1 and 5min. No potential was applied at the controls. Detection conditions: incubation of the modified electrodes in commercial TMB liquid substrate for 1h at 37°C with stirring, stopping of the reaction with H_2SO_4, and monitoring of the absorbance at 450nm.

Biorecognition nanomodule electrodeposition. The experiments described with colloidal gold suspensions with FITC-oligonucleotide-thiol-colloidal gold biorecognition nanomodules were repeated but in this case with electrodeposited conjugates. The FITC-oligonucleotide-thiol-colloidal gold conjugates were successfully deposited on the set of the IDEs at which potential had been applied (*results not shown*), showing the same appearance as the electrodeposition of bare colloidal gold. However, more extreme conditions (+1.6V (*vs.* Ag/AgCl) for 2h) had to be used in the electrodeposition, since milder conditions (+1.0V (*vs.* Ag/AgCl) for 30min) resulted in deposited material that was not detectable by microscopy. The electrodeposition was more difficult probably due to the coating of colloidal gold with biomolecules, which decreased the ability of the gold particles to be attracted by the potential wall or attached to gold. The FITC-oligonucleotide-thiol-colloidal gold-modified IDE was observed under fluorescence microscopy. However, the deposited

oligonucleotide did not emit any fluorescent signal. This quenching effect was probably due to the fluorescence resonance energy transfer (FRET) between FITC and gold.

The FITC-oligonucleotide-thiol-colloidal gold deposition on glassy carbon electrodes was detected electrochemically. Electrodes at which +1.1V (*vs.* Ag/AgCl) had been applied for 2min showed an oxidation peak at +1.6V (*vs.* Ag/AgCl), corresponding to the gold oxides formation, and a reduction peak at +1.3V (*vs.* Ag/AgCl), which might correspond to their reduction (Figure IV.11). The electrode at which no potential had been applied also showed lower oxidation and reduction peaks. Comparing the surface coverage, these peaks represented 26% of the specific electrodeposition. Lower potentials for higher times, +0.8V (*vs.* Ag/AgCl) for 5min and +0.6V (*vs.* Ag/AgCl) for 10min, resulted in higher non-specific adsorption ratios.

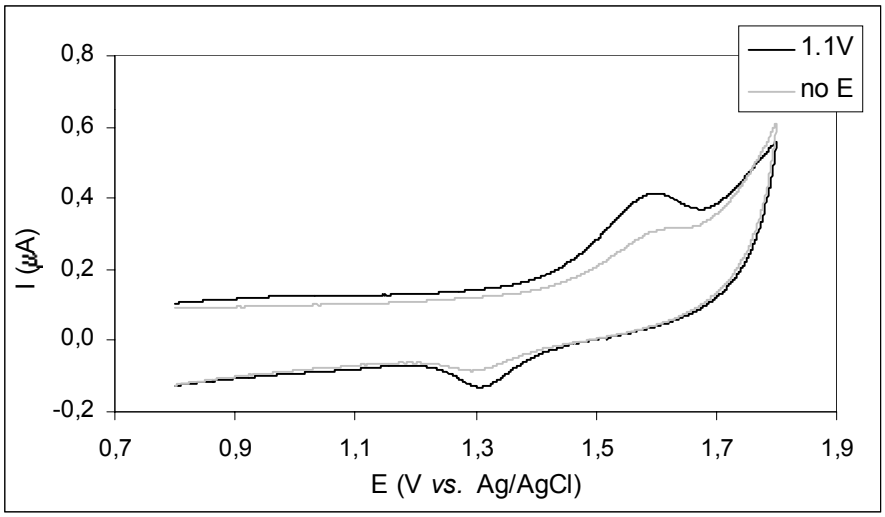

Figure IV.11. Cyclic voltammetry at 0.05mV s^{-1} in 0.1M H_2SO_4 of 1.5mm diameter glassy carbon electrodes after immersion of the electrode in a three-electrode cell containing a FITC-oligonucleotide-thiol-colloidal gold (20nm) conjugate suspension (7.7 x 10^{11} particles mL^{-1} in 10mM phosphate buffer, 0.1M NaCl, pH 7.0) and application of +1.1V (*vs.* Ag/AgCl) for 2min (dark blue). No potential was applied at the controls (light blue).

Sandwich ELONA was used on carbon screen-printed electrodes to verify the technique has the detection limit necessary to observe the electrodeposited biorecognition nanomodules and to verify the functionality of the same (Scheme IV.1). Figure IV.12 shows the results for this experiment. Although absorbance values were quite low and the background (blank) signal high, the total system with dig-oligonucleotide-thiol-colloidal gold gave higher response than the blanks without one of the steps or with FITC-oligonucleotide-thiol-colloidal gold conjugate, indicating that the sandwich can be built on the carbon screen-printed electrodes and detected colourimetrically. The results show that non-specific adsorption of the dig-oligonucleotide-thiol-colloidal gold conjugate on the screen-printed electrode surface (“no coating” bar) could not be appreciated, probably due to the presence of 1% BSA in the dig-oligonucleotide-thiol-colloidal gold conjugate suspension and on the electrode surface. BSA in the conjugate suspension blocks any possible remaining free sites of the dig-oligonucleotide-thiol-colloidal gold, inhibiting the subsequent adsorption on the BSA-coated

electrode. Moreover, there is not non-specific adsorption from the antidig-HRP label on any of the components of the system. Experiments with FITC-oligonucleotide-thiol-colloidal gold did not give any response, as expected since the conjugate does not have digoxigenin.

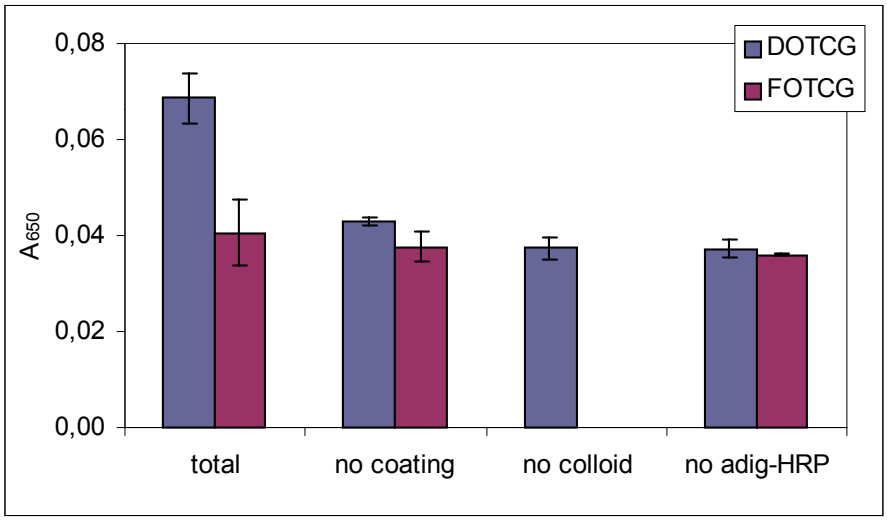

Figure IV.12. Absorbance at 650nm from the colourimetric reaction of the antidig-HRP with TMB in the sandwich ELONA on carbon screen-printed electrodes. Total: system as depicted in Scheme IV.1 with dig-oligonucleotide-thiol-colloidal gold (DOTCG) (20nm) (2.5 x 10^{10} particles mL^{-1} in 0.1M tris-HCl buffer, 0.1M KCl, pH 8.0, 1% BSA); no coating: blank without antidigoxigenin on the surface; no colloid: blank without conjugate; no adig-HRP: blank without antidig-HRP. FITC-oligonucleotide-thiol-colloidal gold (FOTCG) (20nm) conjugate suspension (2.3 x 10^{10} particles mL^{-1} in 0.1M tris-HCl buffer, 0.1M KCl, pH 8.0, 1% BSA) was used as a control. Detection conditions: incubation of the modified electrodes in commercial TMB liquid substrate for 1h at 37°C with stirring and monitoring of the absorbance at 650nm.

As can be seen in Figure IV.13, the electrodeposition experiment with colourimetric detection proved the selective deposition of the dig-oligonucleotide-thiol-colloidal gold conjugate on carbon screen-printed electrodes. Whilst the electrodes were only passive adsorption of the dig-oligonucleotide-thiol-colloidal gold conjugate show absorbance values not different from the blanks (with FITC-oligonucleotide-thiol-colloidal gold conjugate, without colloid or without antidig-HRP), the ones exposed to electrodeposition of the conjugate are almost three-fold higher, although the reproducibility achieved was low. The dig-oligonucleotide-thiol-colloidal gold conjugate did not adsorb non-specifically neither on the BSA-coated carbon electrode surface, probably due to the presence of 1% BSA in the dig-oligonucleotide-thiol-colloidal gold conjugate solution, nor on the non-coated carbon electrode surface. Moreover, the BSA coating of the electrode surface did not inhibit the electrodeposition, the same results as in the non-coated electrodes being obtained.

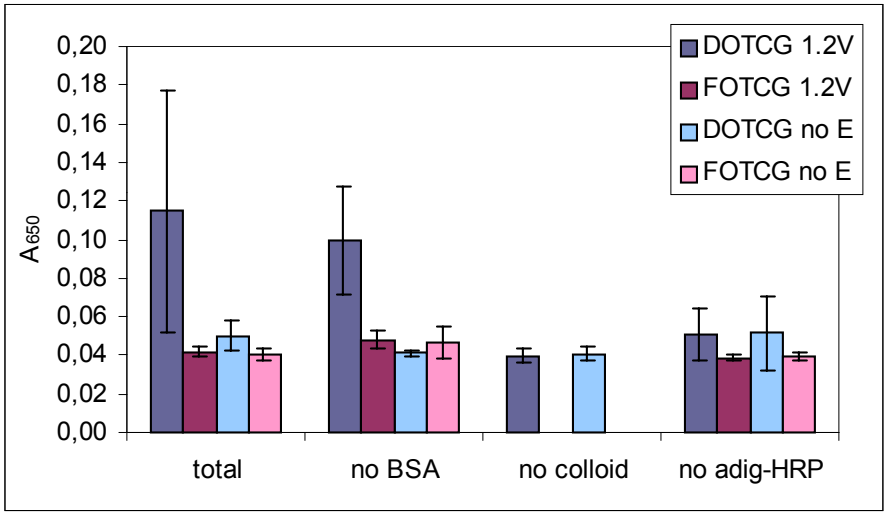

Figure IV.13. Absorbance at 650nm from the colourimetric reaction of the antidig-HRP with TMB due to the electrodeposited or adsorbed dig-oligonucleotide-thiol-colloidal gold (DOTCG) (20nm) on carbon screen-printed electrodes. Total: system as depicted in Scheme IV.2; no BSA: blank without the blocking step with BSA; no colloid: blank without conjugate; no adig-HRP: blank without antidig-HRP. Electrodeposition conditions: immersion of the carbon screen-printed electrode in a three-electrode cell containing a dig-oligonucleotide-thiol-colloidal gold (20nm) conjugate suspension (1.3 x 10^{12} particles mL^{-1} in 0.1M tris-HCl buffer, 0.1M KCl, pH 8.0, 1% BSA) and application of +1.2V (*vs.* Ag/AgCl) for 2min. No potential was applied at the controls. FITC-oligonucleotide-thiol-colloidal gold (FOTCG) (20nm) conjugate suspension (1.2 x 10^{12} particles mL^{-1} in 0.1M tris-HCl buffer, 0.1M KCl, pH 8.0, 1% BSA) was also used as a control. Detection conditions: incubation of the modified electrodes in commercial TMB liquid substrate for 1h at 37°C with stirring and monitoring of the absorbance at 650nm.

Figure IV.14 shows the background-subtracted electrochemical results with dig-oligonucleotide-thiol-colloidal gold conjugate for different measurement times to see if there is an optimal reading time with the highest signal/background ratio. Although electrodeposition intensity values are very low (20-24nA), it is possible to see that non-specific adsorption values are considerably lower. Whereas the electrodeposition currents are independent on the reading time, the non-specific adsorption intensity values show an increasing trend, the percentage compared to the electrodeposition being 14, 18, 20, 26 and 31% for 10, 15, 20, 30 and 60sec, suggesting that shorter times are the optimal reading conditions. This increase is related to the amplification due to the enzymatic reaction of the label. This 14% non-specific adsorption value demonstrates the viability of the strategy as arraying method and the use of amperometric detection. It is important to note that the non-specific adsorption is as important as the detection method used allows it to be. In this work, the detection method was not optimised and in fact, it can be appreciated from the high values of blanks (around 5nA) that it barely allows the detection of the electrodeposited nanomodules.

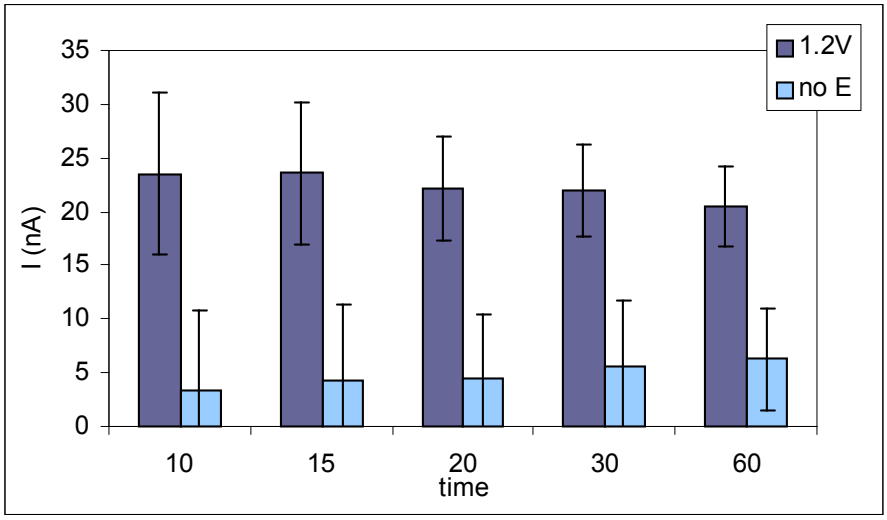

Figure IV.14. Currents obtained from the enzymatic reaction of the antidig-HRP with osmium complex due to the electrodeposited or adsorbed dig-oligonucleotide-thiol-colloidal gold (20nm) on carbon screen-printed electrodes. Intensity values are background-subtracted. Electrodeposition conditions: immersion of the carbon screen-printed electrode in a three-electrode cell containing a dig-oligonucleotide-thiol-colloidal gold (20nm) conjugate suspension (1.3 x 10^{12} particles mL^{-1} in 0.1M tris-HCl buffer, 0.1M KCl, pH 8.0, 1% BSA) and application of +1.2V (*vs.* Ag/AgCl) for 2min. No potential was applied at the controls. Detection conditions: incubation of 1µL of H_2O_2 (1:500 dilution in 50mM acetate buffer, 0.15M NaCl, pH 5.1) and 1µL of [Os(2,2'-bipyridine)$_2$Cl(4-(aminomethyl)pyridine)]Cl (0.2mM in water) on the working electrode for 2min, application of -0.1V (*vs.* Ag/AgCl) for 1min, and measuring of the current values at different times.

The dig-oligonucleotide-thiol-colloidal gold conjugate was also electrodeposited on photolithographed gold 3-electrode arrays. The two gold electrodes where the drop was placed were 1mm in diameter and the distance between them was 2mm. Due to evaporation effects, short deposition times (to 10min) were used. Figure IV.15 shows the light microscopy images for the blank electrodes whre no sample (a) or potential (b) were applied and the working electrode at which +0.8V (*vs.* Ag/AgCl) was applied for 10min (c).

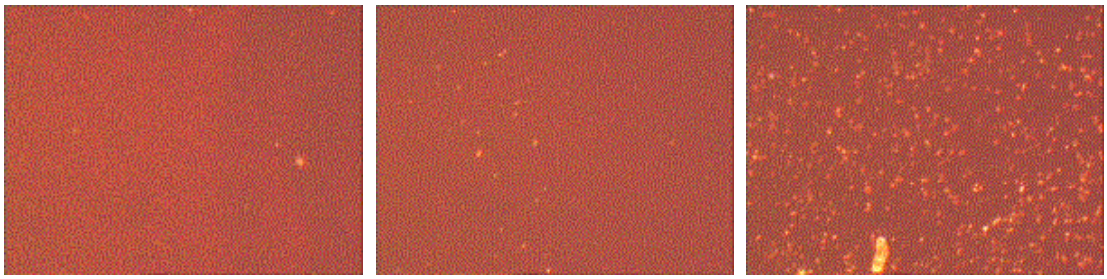

Figure IV.15. Light microscopy images of the electrodeposition of dig-oligonucleotide-thiol-colloidal gold (3nm) on photolithographed gold 3-electrode arrays. a) Bare gold electrode; b) gold electrode after incubation with dig-oligonucleotide-thiol-colloidal gold for 10min; c) gold electrode after electrodeposition with dig-oligonucleotide-thiol-colloidal gold for 10min at +0.8V (*vs.* Ag/AgCl).

The light dots, much more abundant when applying potential, demonstrate that the dig-oligonucleotide-thiol-colloidal gold conjugate was electrodeposited to a much higher extent than non-specifically adsorbed. Using the phase analysis of the microscope AnalySIS software, the

percentage of the area covered by colloidal gold was approximately 0.05, 0.30 and 3.99% for the bare electrode, the electrode where no potential was applied and the electrode where +0.8V (*vs.* Ag/AgCl) was applied for 10min, respectively. These values show that the non-specific adsorption is 7.5% of the specific deposition. It should be noted that these observations also give an indication of some nucleation phenomena upon deposition (the observed dots are approximately 20μm in diameter), probably on surface imperfections.

In Figure IV.16, +1.6V (*vs.* Ag/AgCl) was applied to the working electrode for 10min. In this case, the number of light dots increases, suggesting that there is more electrodeposited material. However, the deposition is less homogeneous, and the presence of aggregates is noticeable. Using the phase analysis, the percentage of the area covered by colloidal gold is approximately 0.05, 1.81 and 53.21% for the bare electrode, the electrode where no potential was applied and the electrode where +1.6V (*vs.* Ag/AgCl) was applied for 10min, respectively. In this case, the non-specific adsorption is 3.4% of the specific deposition. At higher potentials (+1.9V (*vs.* Ag/AgCl)), depositions were more evident and moreover and they could be achieved at shorter times (1min), but they lacked homogeneity. Despite the experimental error in the percentages (as evidenced by the difference between the 0.30 and the 1.81% obtained for the electrodes where no potential was applied in Figures IV.15 and IV.16), the values demonstrate the successful directed electrodeposition of the biorecognition nanomodules. It was decided that for this system, the optimum dig-oligonucleotide-thiol-colloidal gold conjugate electrodeposition conditions are +0.8V (*vs.* Ag/AgCl) for 10min.

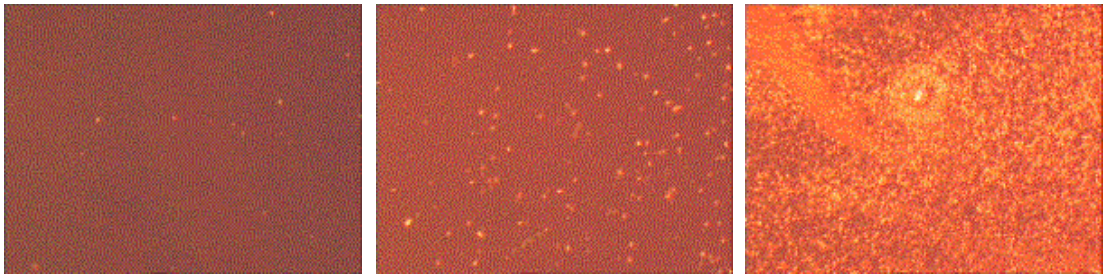

Figure IV.16. Light microscopy images of the electrodeposition of dig-oligonucleotide-thiol colloidal gold (3nm) on photolithographed gold 3-electrode arrays a) Bare gold electrode; b) gold electrode after incubation with dig-oligonucleotide-thiol-colloidal gold for 10min; c) gold electrode after electrodeposition with dig-oligonucleotide-thiol-colloidal gold for 10min at +1.6V (*vs.* Ag/AgCl).

Functionality of electroarrayed biorecognition nanomodules. The *hybridisation* ELONA with the dig-oligonucleotide-thiol-colloidal gold conjugate was performed also on carbon screen-printed electrodes. Although the *hybridisation* ELONA was successful in plate wells (*see Chapter III*), in the case of spectrophotometric detection of hybridisation on the surface of carbon screen-printed electrodes, there was little difference between signal and background. Control experiments indicated that there was a high non-specific adsorption of streptavidin-HRP either on the electrode

surface or on the polycarbonate substrate on which the electrodes were screen-printed. Several experiments demonstrated that high non-specific adsorption of streptavidin-HRP was produced on the polycarbonate substrate.

Although the colourimetric detection was not suitable, the electrochemical detection offered the possibility to detect the hybridisation event on screen-printed electrodes because in the electrochemical mode only the response from the working electrode (and not from the substrate surface) is measured. Figure IV.17 plots the background-subtracted electrochemical responses at 10sec for the electrodeposition and non-specific adsorption of the dig-oligonucleotide-thiol-colloidal gold conjugate followed by hybridisation with biotin-labelled complementary and oligonucleotides with 4-point mutations (background currents being around 5nA).

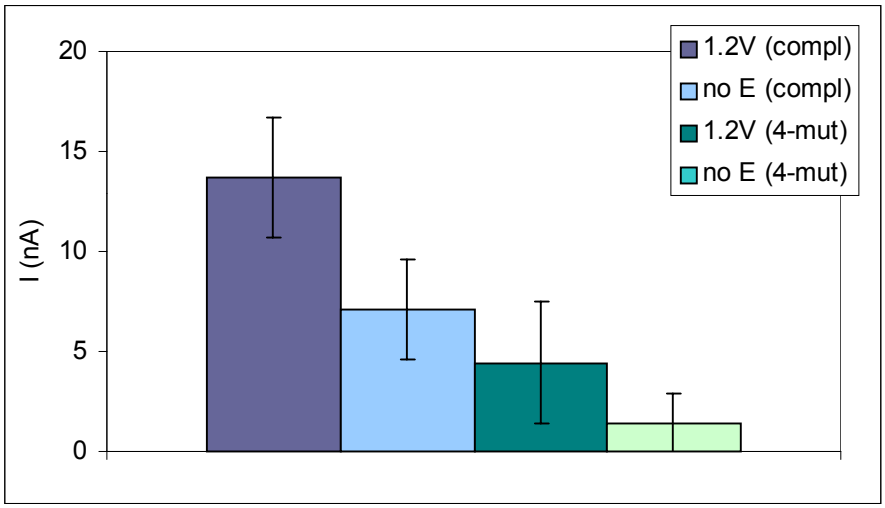

Figure IV.17. Currents obtained from the enzymatic reaction of the streptavidin-HRP with osmium complex due to the electrodeposited or adsorbed dig-oligonucleotide-thiol-colloidal gold (20nm) on carbon screen-printed electrodes and subsequent hybridisation. Intensity values are background-subtracted. Electrodeposition conditions: immersion of the carbon screen-printed electrode in a three-electrode cell containing a dig-oligonucleotide-thiol-colloidal gold (20nm) conjugate suspension (1.3 x 10^{12} particles mL^{-1} in 0.1M tris-HCl buffer, 0.1M KCl, pH 8.0, 1% BSA) and application of +1.2V (*vs.* Ag/AgCl) for 2min. No potential was applied at the controls. Hybridisation conditions: incubation with a solution of biotin-labelled complementary oligonucleotide, non-labelled complementary oligonucleotide or biotin-labelled oligonucleotide with 4 point mutations (5μg mL^{-1} in 10mM tris-HCl, 1mM EDTA, 0.3 x SSC, 2 x Denhardt's solution, pH 8.0) for 1h at 55°C. Detection conditions: incubation of 1μL of H_2O_2 (1:500 dilution in 50mM acetate buffer, 0.15M NaCl, pH 5.1) and 1μL of [Os(2,2'-bipyridine)$_2$Cl(4-(aminomethyl)pyridine)]Cl (0.2mM in water) on the working electrode for 2min, application of -0.1V (*vs.* Ag/AgCl) for 1min, and measuring of the current values at 10sec.

As expected, the current intensity values from hybridisation of electrodeposited biorecognition nanomodules with complementary sequences are the highest ones, the values from hybridisation of non-specifically adsorbed biorecognition modules with the same complementary sequences being 52%. The current from hybridisation of electrodeposited biorecognition nanomodules with mutated sequences is 32% (compared with the hybridisation with complementary sequences), and the current from hybridisation of non-specifically adsorbed biorecognition nanomodules with mutated sequences is also 32% (compared with the hybridisation with complementary sequences). It can be seen that there is selective electrodeposition of the dig-oligonucleotide-thiol-colloidal gold conjugate

on carbon screen-printed electrodes, this oligonucleotide-colloidal gold conjugate can be hybridised, and the response can be monitored electrochemically. Moreover, the electrochemical DNA sensor can differentiate 4-point mutations in a 19-mer oligonucleotide. Electrochemical amplification systems are being investigated in order to increase the current arising from the hybridisation detection, which will provide the possibility of further miniaturisation.

Conclusions

Oligonucleotide biorecognition nanomodules can be site selectively electrodeposited on IDEs, glassy carbon electrodes, gold 3-electrode arrays and carbon screen-printed electrodes, and the selective electrodeposition can be followed by light microscopy, colourimetry and electrochemical methods. Despite the clear differences between electrodeposition and non-specific adsorption, the later still gives a “stray” 14% signal in the electrochemical detection. Absorbance and currents were very low compared to blanks, suggesting the necessity for a signal amplification system. Preliminary experiments suggested that non-specifically adsorbed particles could be removed by using a flow system with an appropriate Re. Finally, electrodeposited biorecognition nanomodules were functional and able to differentiate 4 mutations in a 19-mer oligonucleotide sequence, demonstrating that the strategy can be used in low-cost DNA sensor arrays. Again, electrochemical currents were very low, suggesting that signal amplification is required for efficient amperometric detection of hybridisation events.

References

Adamczyk Z., Siwek B., Zembala M., and Belouschek P., *Adv. Colloid. Interface Sci.*, **1994**, 48, 151.

Adamczyk Z., Siwek B., Zembala M., and Weroński P., *J. Colloid. Interface Sci.*, **1997**, 185, 236.

Adamczyk Z. and Weroński P., *J. Colloid. Interface Sci.*, **1997**, 189, 348.

Bailey R.C., Stevenson K.J., and Hupp J.T., *Adv. Mater.*, **2000**, 12 (24), 1930.

Burdick G.M., Berman N.S., and Beaudoin S.P., *J. Nanoparticle Res.*, **2001**, 3, 455.

Castellino A.M., *Genome Res.*, **1997**, 7, 943.

Crumbliss A.L., Perine S.C., Stonehuerner J., Tubergen K.R., Zhao J., Henkens R.W., and O’Daly J.P., *Biotechnol. Bioeng.*, **1992**, 40 (4), 483.

Despić A.R. and Pavlović M.G., *J. Electroanal. Chem.*, **1984**, 180, 31.

Drobyshev A., Mologina N., Shik V., Pobedimskaya D., Yershov G., and Mirzabekov A., *Gene*, **1997**, 188, 45.

Faraudo J. and Bafaluy J., *Europhys. Lett.*, **1999**, 46 (4), 505.

Fodor S.P.A., Read J.L., Pirrung M.C., Stryer L., Lu A.T., and Solas D., *Science*, **1991**, 251, 767.

Giersig M. and Mulvaney P, *J. Phys. Chem.*, **1993**, 97, 6334.

Grabar K.C., Smith P.C., Musick M.D., Davis J.A., Walter D.G., Jackson M.A., Guthrie A.P., and Natan M.J., *J. Am. Chem. Soc.*, **1996**, 118 (5), 1148.

Guschin D., Yershov G., Zaslavsky A., Gemmell A., Shick V., Proudnikov D., Arenkov P., and Mirzabekov A., *Anal. Biochem.*, **1997**, 250, 203.

Lavalle P., Schaaf P., Ostafin M., Voegel J.-C., and Senger B., *Prot. Natl. Acad. Sci. USA*, **1999**, 96, 11100.

Livache T., Roget A., Dejean E., Barthet C., Bidan G., and Téoule R., *Nucleic Acids Res.*, **1994**, 22 (15), 2915.

Livache T., Roget A., Dejean E., Barthet C., Bidan G., and Téoule R., *Synthetic Metals*, **1995**, 71, 2143.

Livache T., Fouque B., Roget A., Marchand J., Bidan G., Téoule R., and Mathis G., *Anal. Biochem.*, **1998**, 255, 188.

Pease A.C., Solas D., Sullivan E.J., Cronin M.T., Holmes C.P., and Fodor S.P.A., *Proc. Natl. Acad. Sci.*, **1994**, 91, 5022.

Roget A., Livache T., Marchand J., and Téoule R., *Nucleosides Nucleotides*, **1995**, 14 (3-5), 943.

Russel W.B., Saville D.A., and Schowalter W.R., *Colloidal dispersions*, Cambridge University Press, Cambridge, United Kingdom, **1989**.

Sakai K., Higuchi H., Matsubara K., and Kato K., *Anal. Biochem.*, **2000**, 287, 32.

Sato T. and Ahmed H., *Appl. Phys. Lett.*, **1997**, 70 (20), 2759.

Sauerbrey G.Z., *Z. Phys.*, **1959**, 155, 206.

Trau M., Saville D.A., and Aksay I.A., *Science*, **1996**, 272, 706.

Trau M., Saville D.A., and Aksay I.A., *Langmuir*, **1997**, 13 (24), 6375.

Wojtaszczyk P., Bonet Ávalos J., and Rubí J.M., *Europhys. Lett.*, **1997**, 40 (3), 299.

Yershov G., Barsky V., Belgovskiy A., Kirillov E., Kreindlin E., Ivanov I., Parinov S., Guschin D., Drobishev A., Dubiley S., and Mirzabekov A., *Proc. Natl. Acad. Sci.*, **1996**, 93, 4913.

Zammatteo N., Jeanmart L., Hamels S., Courtois S., Louette P., Hevesi L., and Remacle J., *Anal. Biochem.*, **2000**, 280, 143.

Abbreviations

BSA: bovine serum albumin

CCD: charge-coupled device

CV: cyclic voltammetry

dig: digoxigenin

DNA: deoxyribonucleic acid

DOTCG: digoxigenin-oligonucleotide-thiol colloidal gold

ELONA: enzyme-linked oligonucleotide assay

FITC: fluorescein-isothiocyanate

FOTCG: FITC-oligonucleotide-thiol colloidal gold

GOx. glucose oxidase

HRP: horseradish peroxidase

IDEs: interdigitated electrodes

ITO: indium-tin oxide

LSV: linear sweep voltammetry

MES: 2-morpholinoethanesulfonic acid

TMB: 3,3',5,5'-tetramethyl-benzidine

tris-HCl: tris[hydroxymethyl]aminomethane hydrochloride

Tween 20: polyoxyethylenesorbitan monolaurate

Chapter V. Rational design of mediators for optimising electron transfer rates between redox enzymes and electrodes

Abstract

Glucose oxidase (GOx) was used as a model enzyme to study the electron transfer between enzymes and redox mediators. Since this enzyme can be used in many biosensor configurations where electrochemical signal amplification is required such as in DNA sensors, high electron transfer rate constants, which result in high currents and low limits of detection, are desired.

Osmium complexes of the type [Os(2,2'-bipyridyl)$_2$LL'] and [Os(4,4'-dimethyl-2,2'-bipyridyl)$_2$LL'] were rationally designed and synthesised to study the effect of charge, potential, ionic strength and pH on the electron transfer rate constant. The effect of the mediator global charge from 0 to +5 on the electron transfer rate constant was studied and experimental results showed an exponential dependence of the constant in the mediator global charge, from 0.66 x 10^5 to 6.67 x $10^5 M^{-1}s^{-1}$.

Electron transfer rate constants achieved with osmium mediators having different redox potentials, from 175 to 650mV (*vs.* Ag/AgCl), also showed an exponential dependence on the donor-acceptor potential difference from 0.68 x 10^5 to 1.81 x $10^6 M^{-1}s^{-1}$, in accordance to Marcus' theory. A theoretical maximum electron transfer rate constant k_{ET} = 1.87 x $10^6 M^{-1}s^{-1}$ for a mediator having E_{redox} = 848mV (*vs.* Ag/AgCl) was obtained. Moreover, with the experimental results it was possible to obtain the Marcus reorganisation energy λ = 0.87eV and the distance decays constants β = 2.62 and 0.57Å^{-1} for Os(bpy)$_2$Cl(pyNH$_3^+$) and Os(bpy)$_3$, respectively.

The study of the ionic strength effect demonstrated the influence of the glucose oxidase and osmium mediators charge screening on the kinetics of electron transfer, being these constants higher when using lower ionic strength conditions. Plots of the logarithm of the electron transfer rate constant *vs.* the ionic strength function for Os(bpy)$_2$Cl(pyNH$_3^+$) (E_{redox} = 272mV (*vs.* AgAgCl)) and Os(bpy)$_3$ (E_{redox} = 647mV (*vs.* AgAgCl)) allowed to obtain its infinite ionic strength rate constant k_0 = 3.9 x $10^3 M^{-1}s^{-1}$ and 5.1 x $10^5 M^{-1}s^{-1}$, the radius of the enzyme R_{enz} = 2.5 and 23.6Å and the charge of the enzyme Z_{enz} = -5.3 and -31.9, respectively.

The effect of pH of the media on the kinetics was also studied, the electron transfer rate constant at pH 4.0 decreasing 96% compared to the value at pH 8.0. Studies with negatively and positively charged osmium complexes suggested that a local His residue, which could be on the enzyme surface or close to the active site, may be playing a decisive role in the mechanism of electron transfer between redox mediators and glucose oxidase.

Keywords: homogeneous electron transfer rate constant, redox enzyme electrochemistry, osmium redox mediator, rational mediator design, electrochemical amplification schemes.

Introduction

Most of electrochemical biosensors use enzymes as biorecognition elements or as labels that produce an electrochemical signal proportional to the biorecognition event. In electrochemical DNA sensors, where the biorecognition element is the DNA probe, the enzymatic label can be included in the system by direct attachment of the enzyme to the complementary strand (target) or by incubation with enzyme-antibody conjugates after the hybridisation, which recognise the antigen-modified complementary strands. Additionally, enzymes can be used as part of a cascade that amplifies the signal from the label. These enzymes have to be able to transfer electrons with the electrode surface in order to generate detectable currents. Glucose oxidase is a ubiquitous enzyme that can be used in such schemes of amplification (DellaCiana *et al.*, 1995; Male *et al.*, 1998; and Gooding *et al.*, 2000).

Due to the fact that most of redox enzymes do not exchange directly electrons with electrodes, a wide range of chemical compounds have been described are used as mediators, which allow enzymes to transfer electrons to electrodes (Fultz and Durst, 1982 and Johnson *et al.*, 1983). The requirements for the mediators are: suitable solubility in aqueous or organic solvents, well-known and reversible electrochemical behaviour, chemical stability in both oxidised and reduced forms, appropriate redox potential allowing to work at potentials lower than the oxidation potentials of interfering substances, absence of direct reaction with the enzyme substrates or other substances, and insensitivity to pH and ionic strength effects of the media. Ferrocene derivatives have been extensively used as electron donors/acceptors for redox enzymes, due to their well-known, reversible and pH-independent redox behaviour. Apart from these characteristics, it is possible to introduce active groups on either or both of the cyclopentadienyl rings while retaining the redox properties. These redox couples have been shown to have high electron transfer rate constants for their reaction with oxidoreductases (Cass *et al.*, 1984, 1985; Green and Hill, 1986; Jönsson and Gorton, 1989; and Liaudet *et al.*, 1990). Zakeeruddin *et al.* (1992) and Fraser *et al.* (1993) synthesised Rh and Os complexes, and demonstrated that they can act as electron transfer acceptors for these enzymes. And not only did they demonstrate their electrocatalytic capacity, but also studied the mediator global charge optimisation for glucose oxidase mediation, observed the role of redox potential, pH and ionic strength in mediation, and incorporated the synthesised mediators in enzyme electrodes in order to compare the current intensities. Apart from metal complexes, some other molecules have been used as electron acceptors/donors. Kulys *et al.* (1994) studied the kinetics between glucose oxidase and phenothiazines, phenoxazines and Wurster's salts, and their dependence on the redox potential. Scheller *et al.* (1989) used benzoquinone to study the effect of the capacity of transferring electrons and protons on the electron transfer rate constant, since the relation between single- and double-electron transfer is of great interest in the chemistry of flavin oxidases. The same objective was pursued by Kulys and

Čénas (1983 and 1988), who used a series of quinonic acceptors and studied the effect of the working pH and of the redox potential and global charge of the mediator. Coury *et al.* (1990, 1991 and 1993) applied cyclic voltammetry to sulphite oxidase reactions and studied the kinetics of reactions between sulphite oxidase and several kinds of electron transfer mediators, like Rh and Co complexes, cytochrome *c* and different dyes. Apart from studying the influence of the mediator redox potential, the global charge and the ionic strength on the electrocatalytic voltammetry, they investigated the effect of sulphite stabilisers in solution and they used chronoamperometry for quantification of sulphite concentration and determination of both sensitivity and dynamic range. With these studies, they elucidated the mechanism of the catalytic cycle of the enzyme and they determined the apparent self-exchange rate constants of the enzyme heme site, which contributed to rationally design new biosensors.

In electrochemical sensors, one of the most important requirements for a mediator is to present a high electron transfer rate constant (k_{ET}) with the enzyme in order to obtain high currents. One of the main problems in DNA electrochemical sensors is the limit of detection of the system. On one hand, the amount of hybridised DNA that has to be detected is usually in the femtomolar or attomolar range. On the other hand, the sensitivity of the system has a crucial importance, for example, in the detection of 1 mismatch in a complementary sequence. The need for a low limit of detection and a high sensitivity is solved when high currents are obtained, and this requirement explains the increasing interest in electrochemical signal amplification methods. In these schemes, the optimisation of the homogeneous electron transfer rate constant between the label (enzyme) and the transducer (electrode) by the choice of the appropriate mediator, is the first step to consider to obtain high current densities, which may lower the limit of detection several orders of magnitude. That is why the study of electron transfer kinetics is important for the optimisation of amperometric mediated biosensors (Frew and Hill, 1988; Pishko *et al.*, 1990a, b; Katakis and Heller, 1994; Csöregi *et al.*, 1994, 1995; Ye *et al.*, 1994; Taylor *et al.*, 1995; Narváez *et al.*, 1996, 1997; Ruzgas *et al.*, 1996; Kenausis *et al.*, 1996; Hedenmo *et al.*, 1996, 1997; and Popescu *et al.*, 1999). Apart from the direct improvement of the limit of detection and the sensitivity, other advantages from the fast electron exchange between enzyme and mediator and the consequent high currents are, as it is demonstrated elsewhere, (Katakis and Heller, 1992 and Katakis, 1994) the lower competition from O_2 (for oxidase-based electrodes) and from electrooxidisable interfering substances, such as ascorbate (vitamin C), urate and acetaminophen (Johnson *et al.*, 1983). Moreover, high current densities make possible the miniaturisation of the sensors, a necessary condition for DNA arrays. The miniaturisation of the hybridisation detection device, together with the miniaturisation of the sample volume, pre-treatment and amplification systems, allow the integration of the processes in microfluidic devices.

Accessibility is an important factor for electron transfer. It includes steric effects, orientation and distance dependence. For an electron transfer reaction to occur, the reactants must approach each

other to facilitate electron coupling. Apart from accessibility, other factors that influence the electron transfer are the redox potential and the electrostatic interactions, and the pH and the ionic strength of the media. Marcus' semiclassical theory (1965) describes the biological electron transfers and postulates an expression that includes the parameters that influence the electron transfer rate constant:

$$k_{ET} = 10^{13} \exp(-\beta (r - r_0)) \exp - \left(\frac{(\Delta G^0 + \lambda)^2}{4RT\lambda} \right) \qquad \text{(Eq. V.1)}$$

where β is the distance decay constant in $Å^{-1}$, r is the distance between donor and acceptor in Å, r_0 is the value of r at which the frequency of motion of the nuclei equals $10^{13}s^{-1}$ in Å, ΔG^0 is the free energy of the reaction, and λ is the Marcus reorganisation energy, both energies in eV. This equation describes a decay of the electron transfer constant with distance. However, some deviations from this dependence have been observed. It has been demonstrated experimentally that the deviations could be due to the existence of electronic-coupling "pathways", through polypeptide sigma bonds and hydrogen bonds present inside the protein, where an electron tunnelling effect is produced. The existence of these "pathways" in proteins like cytochrome *c* and myoglobin was experimentally verified using semi-synthesised proteins with incorporated redox complexes (Mayo *et al.*, 1986; and Wuttke *et al.*, 1992; and Casimiro *et al.*, 1993). Moreover, Beratan and Onuchic (1987, 1989, 1991a and 1992) described a theoretical model for the electron transfer rate constant that included these electronic "pathways" and their model was successfully applied to the study of the electron transfer between proteins and metal complexes (Cowan *et al.*, 1988; Beratan *et al.*, 1990, 1991b; Jacobs *et al.*, 1991; Onuchic *et al.*, 1992a, b; and Ullmann and Kostić, 1995).

The thermodynamic driving force depends on the redox potential of the two partners of the reaction, which has an influence on the kinetics of electron transfer. It has been mentioned above than one of the requirements for a mediator in an electrochemical biosensor is to have a low redox potential in order to work at potentials that decrease the oxidation currents from interfering compounds. But on the contrary, a high thermodynamic driving force, which results in a high electron transfer rate, is desired. Consequently, it is necessary to compromise between low interfering currents and high rates. The electrostatic interactions also intervene on the electron transfer, favouring or disfavouring the approach and orientation of the reactants. The pH and the ionic strength of the media can change the role or the importance of these interactions, increasing or decreasing the electron transfer rate constants.

This work examines the effect of the global charge and the redox potential of several osmium mediators, the ionic strength and the pH of the media on the electron transfer rate constant between glucose oxidase and these mediators. Rational design of the mediator by the choice of

their ligands allowed the synthesis of two series of osmium complexes. The first series differs only on the mediator global charge, from 0 to +5, as the mediators have similar sizes and redox potentials. A second series includes mediators with the same size and global charge, differing only on the redox potential, varying from 175 to 650mV *vs.* Ag/AgCl. These studies demonstrate how this data can be used for the elaboration of enzymatic mechanisms and for rationally designing amplification schemes for affinity sensors.

Materials and methods

Materials. The enzyme glucose oxidase (GOx) from *Aspergillus Niger* (EC 1.1.3.4.) was obtained from Sigma (G-7141). Enzymatic activity was monitored periodically by spectrophotometric assay at pH 7.0. Enzyme solutions were made by dissolving weighed amount of enzyme in standard buffer solution of 0.05M tris[hydroxymethyl]amino methane hydrochloride (Sigma, T-3253) containing 0.2M NaCl (Panreac, 131659) and titrating to pH 7.0 using NaOH (Panreac, 131687). Enzyme concentrations were calculated by spectrophotometry. Glucose solutions were made by preparing a 0.25M solution of anhydrous D-(+)-glucose (Panreac, 131341) in the standard buffer. This solution was always left to mutarotate overnight.

K_2OsCl_6 was obtained from Alfa (Stk. 12177). 2,2'-Bipyridyl, pyridine-3,5-dicarboxylic acid and isonicotinic acid were purchased from Fluka (14454, 82794, and 58930). 4,4'-Dimethyl-2,2'-bipyridyl, 2,2'-bipyridine-4,4'-dicarboxylic acid, pyridine, 3-pyridinepropanol, 4-(aminomethyl)pyridine and 1-(3-aminopropyl)imidazole were obtained from Aldrich (24,573-9; 28,281-2; 36,057-0; P7,120-7; A6,560-3; and 27,226-4). Sodium dithionite was obtained from Panreac (211685). Mediator solutions were made dissolving weighed amount of mediator in Milli-Q water.

Instrumentation. Spectrophotometry was conducted with a Hewlett Packard HP-8452A photodiode-array spectrometer interfaced to a PC. Cyclic voltammetry experiments were performed using an AUTOLAB PGSTAT10 potentiostat connected with a single-compartment and three-electrode electrochemical cell with a glassy carbon working electrode, Ag/AgCl reference electrode and Pt counter electrode. Before each experiment the surface of the working electrode was polished with alumina of 5, 1 and 0.3μm (Buehler, 40-6351-006, 40-6361-006 and 40-6363-006), rinsed with water and sonicated in Milli-Q water. Working electrode areas (3.08 ± 0.02 and $4.46 \pm 0.10 mm^2$) were determined by chronoamperometry experiments from background-subtracted Cottrell plots.

Synthesis of mediators. Figure V.1 shows the chemical structure of the osmium mediators, which were characterised electrochemically.

$Os(bpy)_2Cl_2$[1], $Os(dmebpy)_2Cl_2$[2] and $Os(dcarbpy)_2Cl_2$. These complexes were synthesised by refluxing K_2OsCl_6 with 2,2'-bipyridyl (bpy), 4,4'-dimethyl-2,2'-bipyridyl (dmebpy) or 2,2'-bipyridine-

4,4'-dicarboxylic acid (dcarbpy) (complex : ligand, 1 : 2) for 1h in DMF. Then, the precipitated KCl was filtered and the product was reduced by sodium dithionite.

$[Os(bpy)_2ClL]Cl$ and $[Os(dmebpy)_2ClL]Cl$[3] (L = pyridine, pyridine-3,5-dicarboxylic acid, isonicotinic acid, 3-pyridinepropanol, 4-(aminomethyl)pyridine or 1-(3-aminopropyl)imidazole). They were prepared by refluxing [1] or [2] with the corresponding ligand (complex:ligand, 1:1) for 30min in ethylene glycol. To introduce an imidazole derivative, L = 1-(3-aminopropyl)imidazole (complex : ligand, 1 : 5), the mixture was heated at 120˚C for 1h. The product was isolated as PF_6^- salt and ion-exchanged with Cl^- for use.

$[Os(dmebpy)_2LL']Cl_2$ (L = pyridine or 4-(aminomethyl)pyridine and L' = 1-(3-aminopropyl) imidazole). [3] was refluxed the ligand L' (complex : ligand, 1 : 6) for 2h in ethylene glycol. The product was isolated as PF_6^- salt and ion-exchanged with Cl^-.

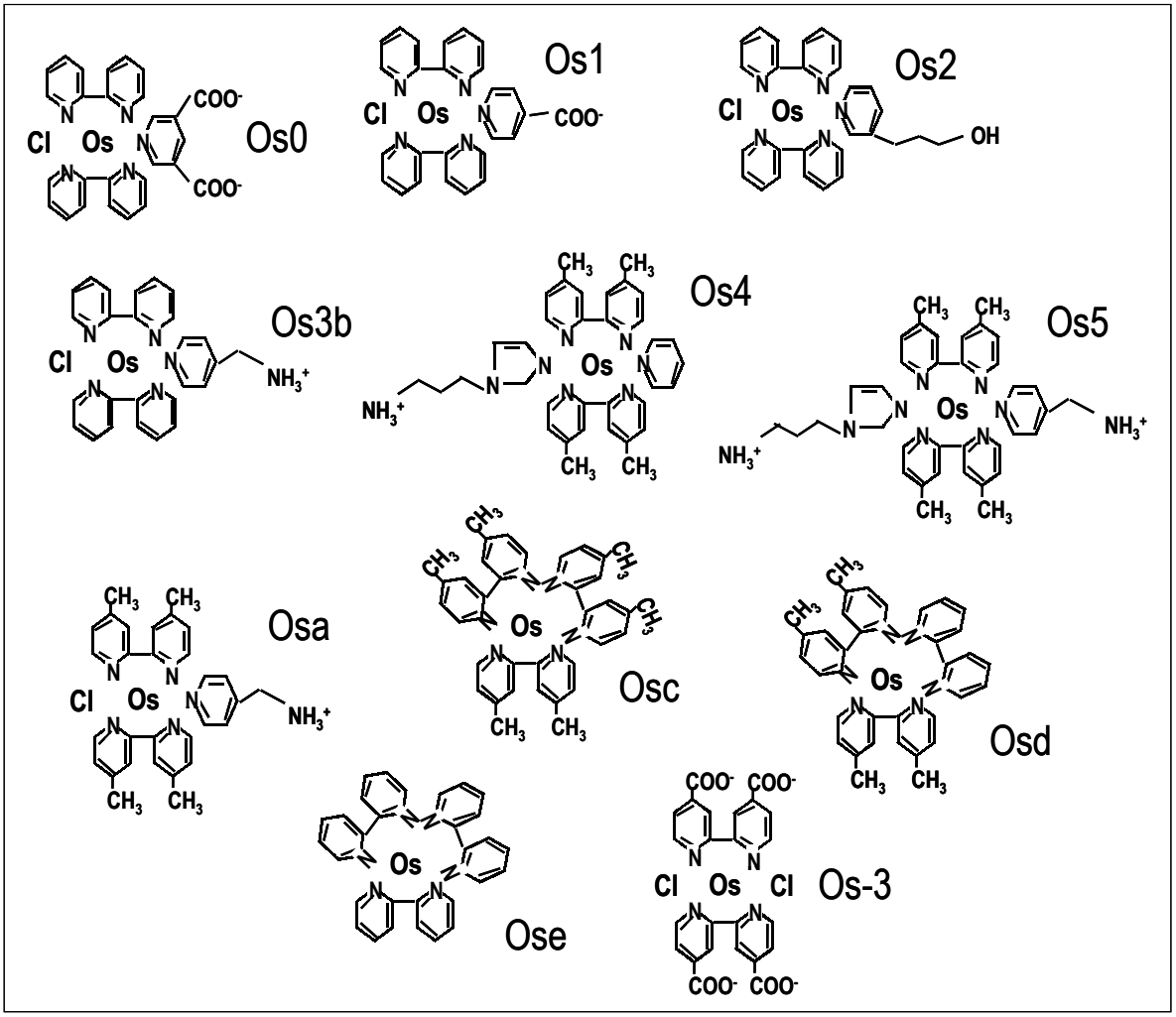

Figure V.1. Chemical structure of the osmium mediators. Os0 = $Os(bpy)_2Cl(py2COO^-)$; Os1 = $Os(bpy)_2Cl(pyCOO^-)$; Os2 = $Os(bpy)_2Cl(pyOH)$; Os3b = $Os(bpy)_2Cl(pyNH_3^+)$; Os4 = $Os(dmebpy)_2(py)(imNH_3^+)$; Os5 = $Os(dmebpy)_2(pyNH_3^+)(imNH_3^+)$; Osa = $Os(dmebpy)_2Cl(pyNH_3^+)$; Osc = $Os(dmebpy)_3$; Osd = $Os(dmebpy)_2(bpy)$; Ose = $Os(bpy)_3$; Os-3 = $Os(dcarbpy)_2Cl_2$.

$[Os(bpy)_2(L\text{-}L)]Cl_2$ and $[Os(dmebpy)_2(L\text{-}L)]Cl_2$ (L-L = 2,2'-bipyridyl, 4,4'-dimethyl-2,2'-bipyridyl or 1,10-phenanthroline-5,6-dione). Synthesis were performed by refluxing [1] or [2] with the corresponding ligand (complex : ligand, 1 : 3) for 3h in ethylene glycol. The product was isolated as PF_6^- salt and ion-exchanged with Cl^-.

Determination of electron transfer rate constants. Electron transfer rate constants were derived from steady-state cyclic voltammetry, which was conducted in a 400µL standard 3-electrode cell with 0.05M tris-HCl buffer solution, 0.2M NaCl and pH 7.0 unless otherwise mentioned. The buffer was Ar-saturated, containing 0.25M glucose, at 25˚C. Initially, cyclic voltammograms of the corresponding mediator were obtained (from 0.05 to 1mM final concentration). Upon addition of increasing concentrations of glucose oxidase (from 0.015 to 22.371µM final concentration), electrocatalytic voltammograms were recorded. For each mediator concentration, the GOx concentration range was adjusted in order to obtain an electrocatalytic plateau for each enzyme addition and to accurately determine the rate constant. Care was taken to avoid bubbling of Ar through solutions when cyclic voltammograms were recorded. Experiments were performed at scan rates of 2, 10 and 20mV s^{-1} in unstirred solutions. Measurements for rate constant determination were taken at 2mV s^{-1}.

Results and discussion

Mediators characterisation. Mediator redox potentials obtained from cyclic voltammetry are summarised at Table V.1. Mediator global charges in their oxidised form are also shown.

Table V.1. Global charges and mediator redox potentials (E_{redox} in mV *vs.* Ag/AgCl) for osmium complexes obtained by cyclic voltammetry.

	Os0	*Os1*	*Os2*	*Os3b*	*Os4*	*Os5*	*Osa*	*Osc*	*Osd*	*Ose*	*Os-3*
Z_{med}	0	+1	+2	+3	+4	+5	+3	+3	+3	+3	-3
E_{redox}	286	283	280	272	280	280	178	463	570	647	120

* Os0 = $Os(bpy)_2Cl(py2COO^-)$; Os1 = $Os(bpy)_2Cl(pyCOO^-)$; Os2 = $Os(bpy)_2Cl(pyOH)$; Os3b = $Os(bpy)_2Cl(pyNH_3^+)$; Os4 = $Os(dmebpy)_2(py)(imNH_3^+)$; Os5 = $Os(dmebpy)_2(pyNH_3^+)(imNH_3^+)$; Osa = $Os(dmebpy)_2Cl(pyNH_3^+)$; Osc = $Os(dmebpy)_3$; Osd = $Os(dmebpy)_2(bpy)$; Ose = $Os(bpy)_3$; Os-3 = $Os(dcarbpy)_2Cl_2$.

Mediators Os0, Os1, Os2, Os3, Os4 and Os 5 belong to the same series. They have similar size (approximately 12Å in diameter) and similar redox potential, about 280mV *vs.* Ag/AgCl, but they differ on the global charge, from 0 to + 5. This series was useful for the evaluation of the effect of the global charge on the kinetics of electron transfer between mediator and enzyme. These mediators were also used in the study of the effect of the ionic strength of the media. Additional results were obtained with the $Os(dcarbpy)_2Cl_2$ mediator (Os-3), which has negative global charge (-3) and more negative redox potential (120mV *vs.* Ag/AgCl). Mediators Osa, Osb (Os3), Osc, Osd and Ose belong to the other series. They have similar size and the same global charge (+3), and

differ on their redox potential, varying from 175 to 650mV *vs.* Ag/AgCl. With this series it was possible to study the effect of the mediator redox potential and the pH of the media on the electron transfer rate constant.

Determination of the electron transfer rate constants. The principle of the enzymatic catalysis is shown at Scheme V.1. GOx catalyses the oxidation of ß-D-glucose to glucono-D-lactone (FAD and $FADH_2$ are the oxidised and reduced form of the flavin adenine dinucleotide group of GOX). After this reaction, the reduced GOx is regenerated (oxidised) by the redox mediator. Then, the reduced mediator transfers its electrons to the electrode, which is held at an oxidising potential, and it is regenerated (oxidised). Since the glucose/gluconolactone and $FADH_2$/FAD couples are $2e^- + 2H^+$ systems, 2 equivalents of osmium complex are involved in the mediation.

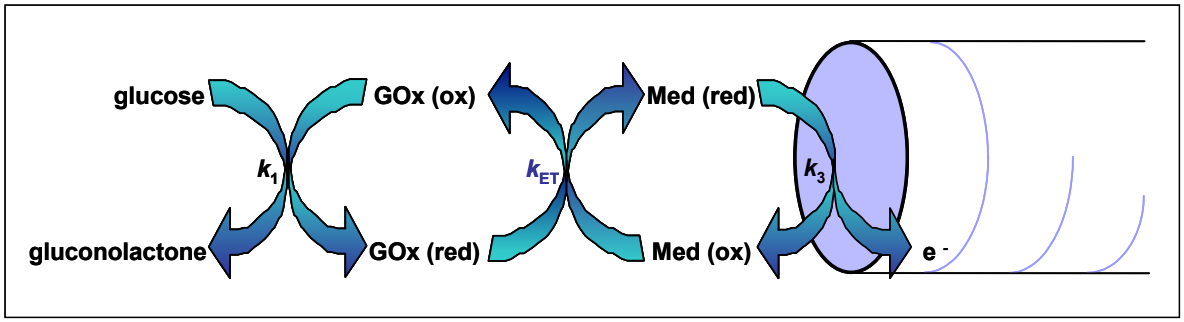

Scheme V.1. Electrocatalytic reaction mechanism between GOx and a redox mediator.

The homogeneous electron transfer rate constant corresponding to the reaction between a mediator and an enzyme in solution can be determined by cyclic voltammetry according to Nicholson and Shain theory (1964). In order to apply this theory to the determination of the electron transfer rate constant between GOx and an osmium complex, two criteria have to be fulfilled: the electrode reaction of the mediator must be fast compared to the rate between the mediator and the enzyme, and saturated glucose concentration is required to ensure a pool of reduced enzyme. If these hypotheses are fulfilled, the limiting step of the overall mechanism will be the reaction between the reduced glucose oxidase and the oxidised mediator, which will facilitate the calculation of the electron transfer rate constant between these two partners.

Figure V.2 illustrates the systematic increase of electrocatalytic currents for the Ose mediator as the concentration of GOx increases. In the absence of GOx, the only species in solution are glucose and mediator. In this case, cyclic voltammetry shows a reversible wave with an oxidation and a reduction peak, corresponding to the oxidation and reduction of the mediator, since glucose is not electroactive in this redox potential window. The anodic peak current is proportional to the square root of the scan rate, indicating a diffusional system. Addition of GOx increases the oxidation peak intensity and decreases the reduction peak intensity. When the reaction between the reduced enzyme and the oxidised mediator is so fast than the diffusion of the reduced mediator from the

bulk to the electrode is limiting, the oxidation catalytic intensity reaches a plateau, the reduction disappears completely and the cyclic voltammogram acquires a sigmoidal shape. Since the diffusion is limiting, the plateau intensity does not depend on the scan rate (at time scales where the assumptions are fulfilled). Experiments must be performed under anaerobic conditions to avoid the competitive reaction of O_2 for the reduced GOx.

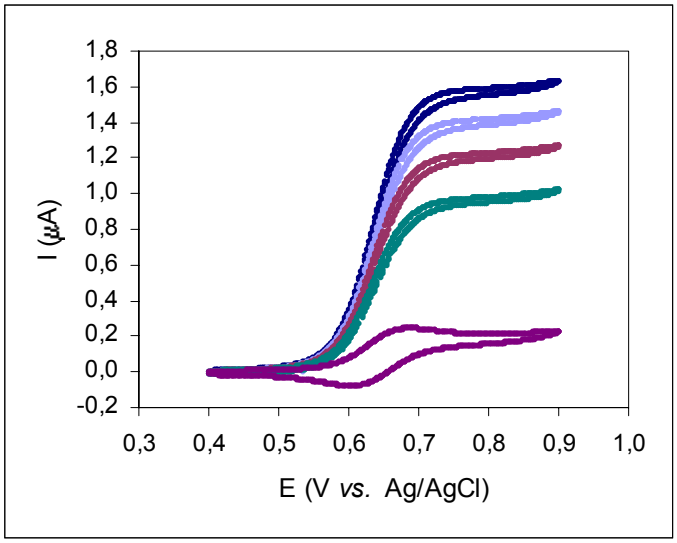

Figure V.2. Cyclic voltammetry for the Ose mediator at 2mV s^{-1} in 400µL of a 0.05M tris-HCl buffer solution, 0.2M NaCl, pH 7.0, Ar-saturated, containing 0.25M glucose, at 25°C. Initially, the cyclic voltammogram of 0.25mM Ose was obtained (no GOx). Upon addition of increasing concentrations of GOx (0.15, 0.22, 0.29 and 0.36µM final concentrations), electrocatalytic voltammograms were recorded.

The theoretical treatment of Nicholson and Shain (1964) for the reactions of the type EC_{cat}:

$$Z + O \rightarrow R$$

$$R \leftrightarrow O + ne^-$$

where O and R are the respective oxidised and reduced forms of the mediator and Z is the reduced enzyme, provides an equation for the steady-state current, i_{SS}, which is an expression derived from the Savéant and Vianello equation (1965):

$$i_{SS} = nFAC_{med}^*(D_{med}k_{ET}C_{enz}^*)^{1/2} \qquad \text{(Eq. V.2)}$$

where i_{SS} is the steady-state current, A is the electrode area, C_{med}^* is the mediator concentration, D_{med} is the mediator diffusion coefficient, k_{ET} is the electron transfer rate constant, and C_{enz}^* is the enzyme concentration. This equation predicts a scan rate-independent steady-state intensity and a dependence of this intensity on the square root of the concentration of the enzyme. Plots of i_{SS} *vs.* $C_{enz}^{*1/2}$ for constant C_{med}^* are linear and according to this equation will provide the k_{ET} values.

The linear dependence predicted by Equation V.2 is confirmed by experimental data (*results not shown*). Slight negative deviations from linearity at high GOx concentrations suggest that at fast

enzyme turnover, the electrocatalytic reaction sequence is not limited by the reaction between mediator and enzyme. Possible reasons could be accumulation of systematic errors, loss of mediator, adsorption of mediator on the walls of the electrochemical cell, or poisoning and blocking of the electrode surface, due to an accumulation of GOx. Another possibility, perhaps more probable, could be that a fast consumption of oxidised mediator breaks down the assumptions. In order to determine the electron transfer rate constants, values that disturb the linearity were neglected, assuming linear regressions with $r^2 = 0.99$ as acceptable results. Such plots were used to calculate the rate constants in what follows.

Effect of the mediator global charge on the electron transfer rate constant. As previously mentioned, the effect of the mediator global charge on the rate constant of electron transfer was studied with mediators Os0, Os1, Os2, Os3, Os4 and Os5, which have similar size (approximately 12Å in diameter) and redox potential (about 280mV *vs.* Ag/AgCl), and differ on the global charge, from 0 to +5. Results for electron transfer rate constants are shown in Figure V.3. Experimental data shows an exponential increase on the electron transfer rate constant from 0.66×10^5 to $6.67 \times 10^5 M^{-1}s^{-1}$ that can be explained as the result of the electrostatic attraction, since GOx is negatively charged at pH 7.0 (pI = 4.2).

Apart from the global charge, the local charges can also have an important role in the kinetics of electron transfer. In fact, observations of electron transfer mechanisms show that the global charges dominate the electrostatic interactions at large distances, but the local charges become more important as the distance decreases. Moreover, theory postulates that a precursor complex between the two reactant species might be formed, and that the electron transfer rate constant may increase proportionally to that complexation constant. GOx contains many groups, such as amine, imidazole or sulfhydryl groups, which can interact with oxidised mediators and form this precursor complex. Although both cationic and anionic groups are located on the GOx surface, as mentioned above at pH 7.0 the enzyme has an essentially negative electrostatic surface potential, because of excess of glutamate and aspartate over lysine and arginine. This fact favours the idea of the electrostatic complexation between mediators with positively charged groups and anionic sites of the enzyme. Experimental results also support this hypothesis, since the observed trend for the electron transfer rate constant between GOx and Os mediators is Os5 (with two amine groups) > Os 4 (with one amine group and global charge +4) > Os 3 (with one amine group and global charge +3) > Os 2 (with one hydroxyl group) > Os 1 (with one carboxylic group) > Os 0 (with two carboxylic groups). In fact, it has been reported that the formation of this complex seems to be more favourable with mediators having amino or hydroxyl groups than with mediators having carboxylic groups (Bourdillon *et al.*, 1993; and Fraser *et al.*, 1993).

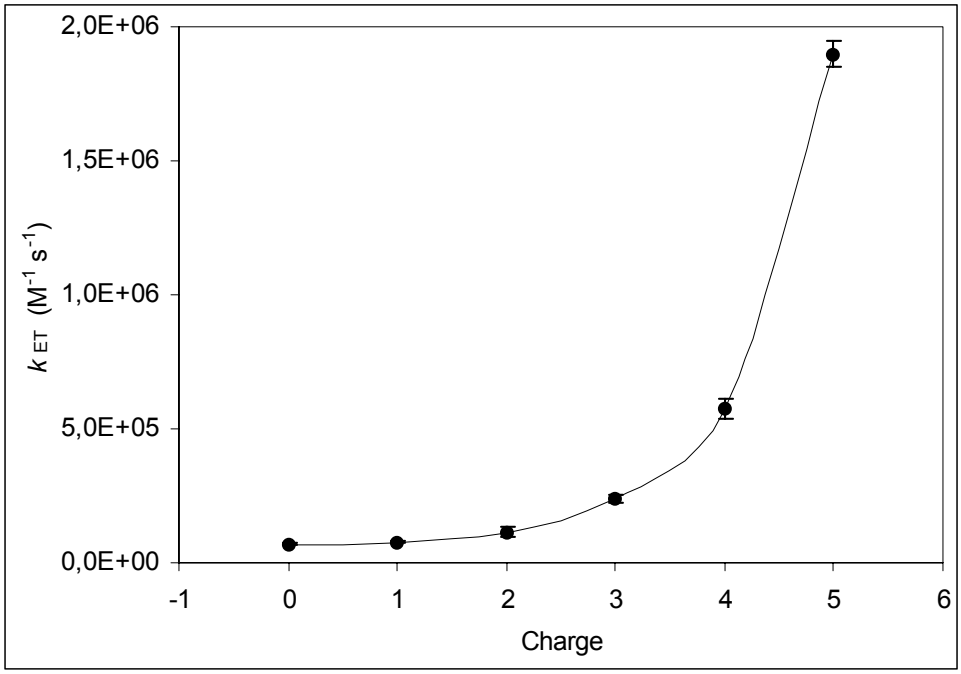

Figure V.3. Variation of the electron transfer rate constant (k_{ET}) with the mediator global charge. Electron transfer rate constants were derived from steady-state cyclic voltammetry at 2mV s^{-1} in 400μL of a 0.05M tris-HCl buffer solution, 0.2M NaCl, pH 7.0, Ar-saturated, containing 0.25M glucose, at 25°C. Initially, cyclic voltammograms of the corresponding mediator were obtained. Upon addition of increasing concentrations of GOx, electrocatalytic voltammograms were recorded. Plots of i_{SS} *vs.* $C_{enz}{}^{*1/2}$ for constant $C_{med}{}^{*}$ provided the k_{ET} values according to Equation V.2.

Although it has been observed that the funnel where the active centre of GOx is located is quite inaccessible, the effect of the residues of the active centre on the electron transfer must be considered. Takabe *et al.* (1986) (although not with GOx but with cytochrome) studied the influence of the positive local charges. Their work showed that residues next to prosthetic group play a more important role on the electrostatic interactions than other residues and global charge. Consequently, if the electronic contacts between mediators and enzymes mentioned above could occur close to the active site, the kinetics would be even more favoured.

Another possible explanation for the mechanism of mediation takes into account the conducting "pathways" in the enzyme. In general terms, the GOx shell is insulating in order to inhibit the indiscriminate electron transfer with other biomolecules present in physiological conditions. However, the shell can be crossed by electronic-coupling "pathways", through which the electron transfer is possible. According to Wuttke *et al.* (1992) and Casimiro *et al.* (1993), the effective electron tunnelling distance can be reduced not only through physical contact between the redox partners, but also through these electron conducting "pathways", whose termini are on the enzyme surface. In this way, the observed trend could be due to the preferential approach, or even the complexation, of the mediator to negatively charged groups of residues located at the enzyme surface, which are the terminal extremes of electron conducting "pathways" that cross the insulating enzyme. This explanation is highly likely because the channel to the active centre of glucose

oxidase is not very accessible to the solvent and probably even less to the mediator. In fact, from the tertiary structure of glucose oxidase, it is known that the FAD centre is located at 13Å from the surface, at the bottom of a funnel that has a cross section of 10 x 10Å at the top (Hecht *et al.*, 1993). Consequently, access to the flavin site seems rather difficult for the osmium mediators, as their diameter is approximately 12Å. It can be therefore speculated that a surface local charge close to such a conducting "pathway" explains the behaviour observed in Figure V.3.

Effect of the pH on the electron transfer rate constant. Several authors have studied the reaction mechanism between oxidoreductases and the natural acceptor O_2, and have predicted the formation of a complex between the active centre and the dioxygen (Bright and Appleby, 1969; Yamasaki and Yamano, 1973; Choong and Massey, 1980; Massey and Hemmerich, 1980; Voet and Andersen, 1984; Ghisla and Massey, 1986; Schreuder *et al.*, 1990; Hecht *et al.*, 1993; and Meyer *et al.*, 1998). All the models converge in the importance of a His in the electron transfer reaction between GOx and O_2. But unlike O_2, the entrance of the osmium complex through the funnel towards the active centre seems unlikely, which rules out the hypothesis of a precursor complex with FAD. Nevertheless, Bourdillon *et al.* (1993) suggested the formation of a precursor complex between a ferrocene mediator and the GOx enzyme site, the energetics or kinetics of which may influence the kinetics of electron transfer, and proposed a His residue or a thiol group that are in the close vicinity of the flavin as responsible for the enzyme binding site to the ferrocene mediator. To obtain more information about the electron transfer mechanism between GOx and osmium complexes, the effect of pH on the rate constant was studied.

GOx shows a broad activity plateau between pH 4.0 and pH 7.0, presenting its maximum activity at pH 5.5 when the acceptor is dioxygen. By contrast and like results reported by other authors (Nakamura *et al.*, 1976; and Zakeeruddin *et al.*, 1992), kinetic experiments with synthetic mediators show an increase of the overall rate constant k_{ET} with pH, presenting the highest electron transfer rate constants at pH 8.0, and a sharp drop as the medium becomes acidic to give only 4% of the response at pH 4.0. This distinct dependence indicates that the factors that influence the electron transfer with redox mediators are different to those that influence the reaction with dioxygen. In Figure V.4, normalised results of the variation of the electron transfer rate constant with the pH for the Osa and Ose mediators are plotted and for qualitative comparison, the pH activity profile when O_2 is the acceptor. The electron transfer rate constants with Ose were at least 25-fold higher than those with Osa (18.10 x 10^5 $M^{-1}s^{-1}$ for Ose and 0.74 x 10^5 $M^{-1}s^{-1}$ for Osa, at pH 7.0), due to the higher difference in redox potential, as expected from Equation V.2. However, the observed pH trend was the same for both mediators. The reaction between glucose oxidase and mediator is a multistep reaction, where two electrons and two protons are exchanged between the reduced form of the enzyme ($FADH_2$) and two molecules of oxidised mediator and the buffer. The observed trend could be explained in different terms. Regarding the redox potential, when pH increases, the redox potential value of the osmium mediator does not change, but the redox potential of the $FADH_2$

becomes more negative (Stankovich *et al.*, 1978). This implies that at higher pH, the thermodynamic driving force is larger, which favours the electron transfer kinetics. Additionally, at pH above the pI, glucose oxidase has a global negative charge, which favours the attraction with the positively charged mediators. Finally, the sharp jump around pH 7.0 could be related to the pK_a for the deprotonation of the neutral to the anionic semiquinone (pK_a = 7.3), the FAD$^{\bullet}$ being more reactive towards the osmium mediator than the FADH and, consequently, accelerating the electron transfer. This is so because above pH 7.3, it is not necessary to transfer a proton from the reduced form of FAD, a proton that in any case the mediator is not able to abstract. The $Os(dmebpy)_2(phen)$ mediator was used to test the effect that a proton-abstracting mediator of similar characteristics would have on electron transfer. No improvement of the electron transfer rate constant was observed. Therefore, it seems certain that direct or close contact between FAD and mediator can be ruled out. So, one possible explanation for the observed pH behaviour is the effect of the driving force on the electron transfer, although the abrupt change, even if it coincides with the semiquinone pK_a, it cannot be explained.

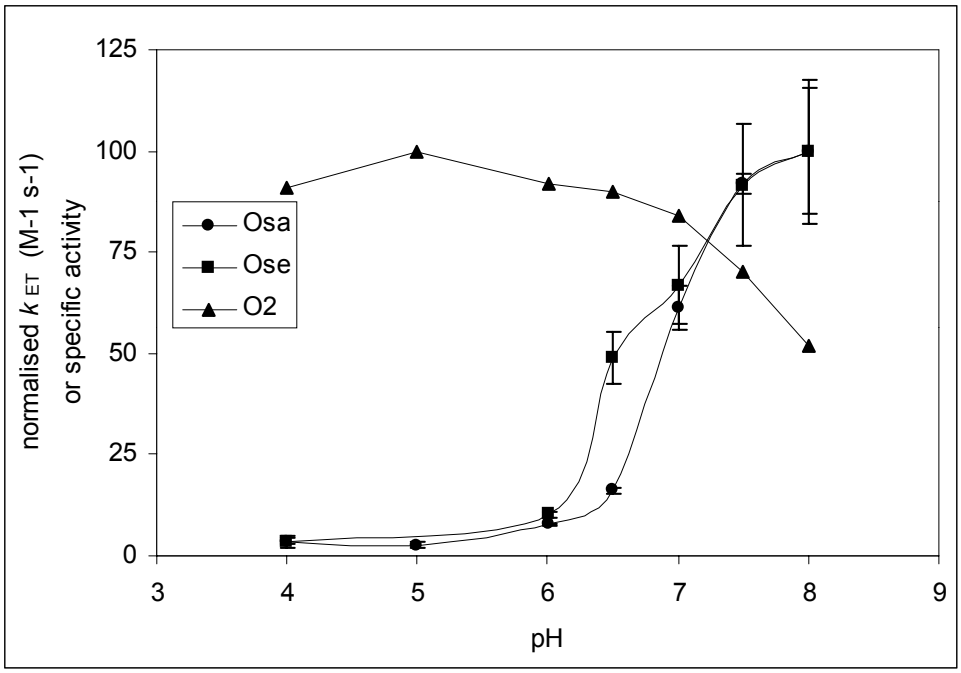

Figure V.4. Variation of the normalised electron transfer rate constant (k_{ET}) and specific activity with the pH for the Osa and Ose mediators and O_2. Electron transfer rate constants were derived from steady-state cyclic voltammetry at 2mV s^{-1} in 400µL of a 0.05M tris-HCl buffer solution, 0.2M NaCl, at different pH values, Ar-saturated, containing 0.25M glucose, at 25˚C. Initially, cyclic voltammograms of the corresponding mediator were obtained. Upon addition of increasing concentrations of GOx, electrocatalytic voltammograms were recorded. Plots of i_{SS} *vs.* $C_{enz}{}^{*1/2}$ for constant $C_{med}{}^{*}$ provided the k_{ET} values according to Equation V.2. For comparison, the pH activity profile when O_2 is the acceptor is given (pH activity profile from Toyobo Co., Ltd.).

However, it is also necessary to remember the importance of the local charges of the enzyme. As mentioned above, His may intervene on the kinetics of electron transfer. There are several His on the GOx surface and at the active site participating in the catalytic mechanism, which have an imidazole group. At pH higher than ~6.8, this group is deprotonated and may favour the approach

or interaction with positive mediators. At pH lower than ~6.8, the imidazole is protonated and the electrostatic repulsion with positive mediators may contribute to decrease the electron transfer rate constant. It is very unlikely that the pK_a of the active site buried histidine is 6.8. To clarify this point, additional experiments were performed with the $Os(dcarbpy)_2Cl_2$ (Os-3) mediator. This osmium mediator is negatively charged due to the four carboxylic groups, which are deprotonated at pH 7.0, conferring a negative total charge to the complex (-3). As expected, at pH 7.0 it was not possible to observe electrocatalysis, because both GOx and the Os-3 mediator are negatively charged and mediation does not occur due to the electrostatic repulsion between them. The same kinetic experiments were performed at pH 5.0, and it was possible to detect electrocatalytic currents. Moreover, the electron transfer constant obtained in this experiment was 8.54 x $10^5 M^{-1}s^{-1}$, higher than expected taking into account that the Os-3 mediator has a redox potential of 120mV *vs.* Ag/AgCl (lower than any mediator used in this work). As at this pH, GOx is still overall negative, the observed mediation cannot be explained in terms of global electrostatic interaction. However, this high electron transfer rate constant could be explained if considering the approach or complexation of Os-3 to a local residue of GOx. This local residue could be a His of the GOx surface, which moreover could be an ending of a conducting "pathway", or of the GOx active centre but, as mentioned, the pK_a of the active site His is unlikely to be unchanged. Unlike when positively charged mediators are used, at pH lower than ~6.8, the protonated His could favour the approach (by local electrostatic interactions) or the complex formation (between the carboxylic groups and active local residues) between mediator and enzyme. Although these experiments do not demonstrate the precursor or complex formation, they do suggest the importance of the His residues in the electron transfer kinetics and most likely they prove the terminus of the electron conducting "pathways" discussed above.

Another factor that may have an important role on the electron transfer are steric effects. It has been reported that acidic pH can provoke a change in the tertiary structure of the GOx, which would facilitate the accessibility to the active centre and the penetration of the redox mediator, increasing the kinetic rate constant (Kulys and Cénas, 1983). At pH 7.0, the distance from the active site to the surface is 13Å, whilst at pH 5.0 the distance is 8Å. The groups responsible for such changes in the conformation of the enzyme could be carboxylic residues or groups of the ionic bridges that bind the two protein subunits (Akulova *et al.*, 1978). However, the general results do not follow this trend because at low pH the electron transfer rate constants are lower than at high pH. Although the effect of structure change would have been present in these experiments, the effects of the thermodynamic driving force or most likely the electrostatic interaction with a surface residue with pK_a close to 7.0 have a more important contribution to the overall rate constant.

Effect of the mediator redox potential on the electron transfer rate constant. The effect of the mediator redox potential on the electron transfer rate constant was examined using the mediators Osa, Osb, Osc, Osd and Ose, with the same global charge (+3) and approximately the same size

(around 12Å in diameter), and with redox potential varying from 175 to 650mV *vs.* Ag/AgCl. Results are plotted in Figure V.5. Experimental data showed an exponential increase on the electron transfer rate constant from 0.68 x 10^5 to 1.81 x $10^6 M^{-1}s^{-1}$.

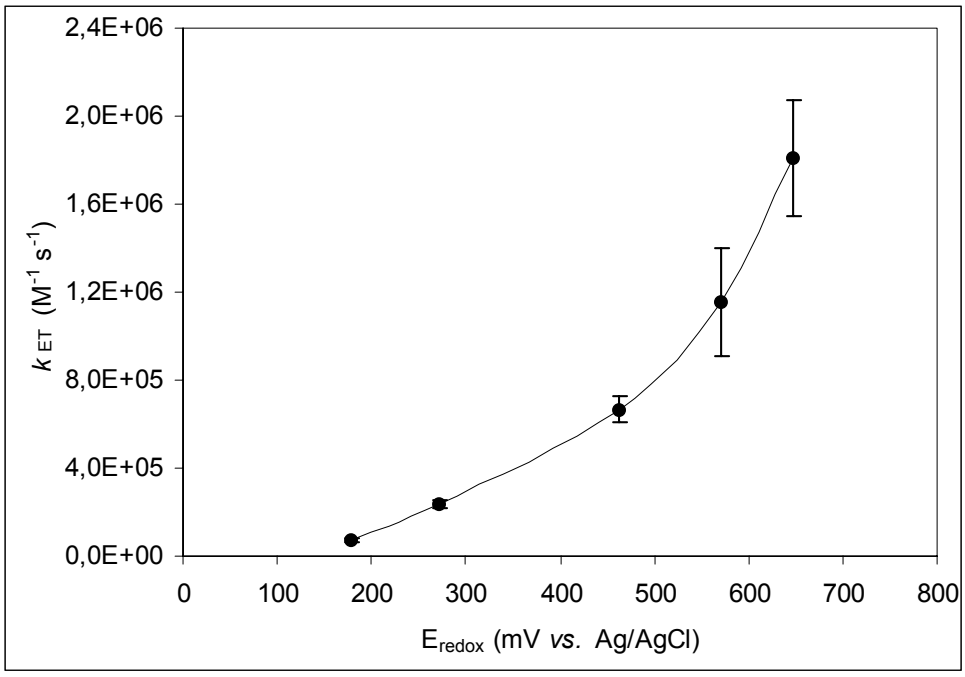

Figure V.5. Variation of the electron transfer rate constant (k_{ET}) with the mediator redox potential (E_{redox} *vs.* Ag/AgCl). Electron transfer rate constants were derived from steady-state cyclic voltammetry at 2mV s^{-1} in 400µL of a 0.05M tris-HCl buffer solution, 0.2M NaCl, at pH 7.0, Ar-saturated, containing 0.25M glucose, at 25°C. Initially, cyclic voltammograms of the corresponding mediator were obtained. Upon addition of increasing concentrations of GOx, electrocatalytic voltammograms were recorded. Plots of i_{SS} *vs.* $C_{enz}{}^{*1/2}$ for constant $C_{med}{}^*$ provided the k_{ET} values according to Equation V.2.

In Figure V.6, the logarithm of the obtained rate constants *vs.* the difference in redox potentials between mediators and the active centre of GOx is plotted. At high mediator redox potentials, the logarithm of the constant changes slowly. Nevertheless, no “inverted region” was observed, since the maximum mediator redox potential was only 650mV *vs.* Ag/AgCl. In general, the data follow the trend expected from the Marcus theory of electron transfer, which postulates that electron transfer rate constants increase with increasing thermodynamic driving force (due to the higher difference between the reversible potentials of FAD/$FADH_2$ and the electron acceptor couple). The standard redox potential of the FAD/$FADH_2$ couple in a pH 7.0 solution can be assumed to be -245mV *vs.* Ag/AgCl (Stankovich *et al.*, 1978). Consequently, the shift of the mediator redox potential in the positive direction results in an increase in the thermodynamic driving force and larger electron transfer rate constants.

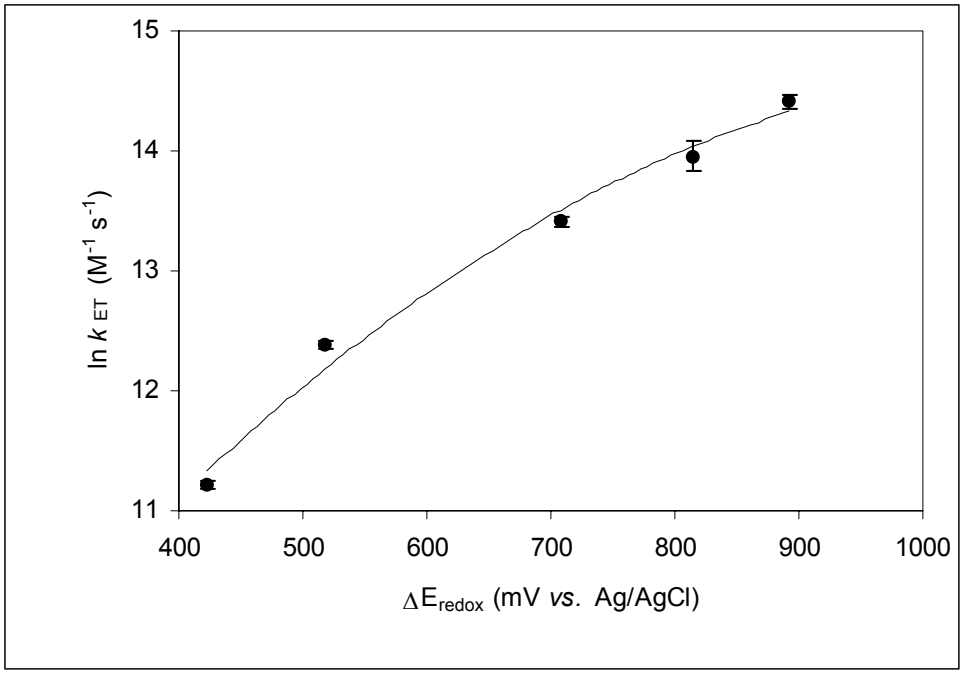

Figure V.6. Variation of the logarithm of the electron transfer rate constant (k_{ET}) with the difference in redox potentials between mediator and GOx active centre (ΔE_{redox} *vs.* Ag/AgCl).

The results obtained in Figure V.6 give an experimental equation, $y = -7\ 10^{-6}\ x^2 + 0.0153\ x + 6{,}083$. With this experimental equation and Equation V.1, it is possible to obtain $\lambda = 0.87$eV. Although the reorganisation energy varies from system to system, this value can be assumed to be the same for all the mediators used in this section because they are similar in structural terms.

With the experimental equation and Equation V.1, and assuming r_0 = 3Å (the distance at Van der Waals contact) and r = 8.9 and 30Å (distance between redox partners, obtained in next section with the effect of the ionic strength on the electron transfer between GOx and the mediators Osb and Ose, respectively), it is possible to obtain $\beta = 2.62$ and $0.57 Å^{-1}$, respectively. The exponential distance decay constant, β, describes the effectiveness of the medium (separating donor and acceptor) in coupling the fixed redox sites. $\beta = 2.62 Å^{-1}$ indicates a very weak coupling and $\beta = 0.57 Å^{-1}$ a very strong coupling, which is translated in higher rates for Ose than for Osb (*see next section*). Both values are very extreme, since in proteins it is reasonable to expect distance decay constants in the vicinity of $1 Å^{-1}$. These extreme values indicate that the electron transfer distances obtained (and used to calculate the distance decay constants) may be perturbed by experimental errors. The difference in β for the two mediators, although is due to the different assumed distances between redox partners, may also reflect a different electron transfer "pathway", i.e. a different intervening polypeptide structure. However, since the most important difference between these two mediators is their redox potential (272mV for Osb and 647mV for Ose), another possibility would be that β depends on this parameter. Apart from the reorganisation energy and the distance decay constant, the experimental equation provides a hypothetical maximum electron transfer rate constant, $k_{ET} = 1.87 \times 10^6 M^{-1} s^{-1}$, for a mediator with E_{redox} = 848mV (*vs.* Ag/AgCl).

Although all the mediators have the same global charge, one could think about the nature of these local charges. Whereas Osa and Osb have amino groups, which could be favouring the docking of the mediatior, Osc, Osd and Ose present higher electron transfer rate constant without having amino groups. The observed trend however suggests that the redox potential plays a more important role than local charges.

Effect of the ionic strength on the electron transfer rate constant. An experimental approach to estimate the magnitude of the electrostatic component of donor-acceptor interaction is the determination of the electron transfer constant as a function of the ionic strength. High ionic strength conditions disfavour the association of oppositely charged species and favour the association of like-charged molecules. This effect was observed using the mediators of both series in order to see the effect of the charge and the redox potential independently. In the ionic strength range from 0.2 to 1.0M, the enzyme glucose oxidase does not change its activity when assayed with glucose, O_2 and the *o*-dianisidine dye. This observation implies that the differences observed on the electron transfer rate constant are only due to the effect of the ionic strength on the reaction rate constant of glucose oxidase with mediator.

In Figure V.7, results for the normalised electron transfer rate constants for mediators Os0, Os2 and Os3, with similar redox potential (280mV (*vs.* Ag/AgCl)) but with different global charge, are shown.

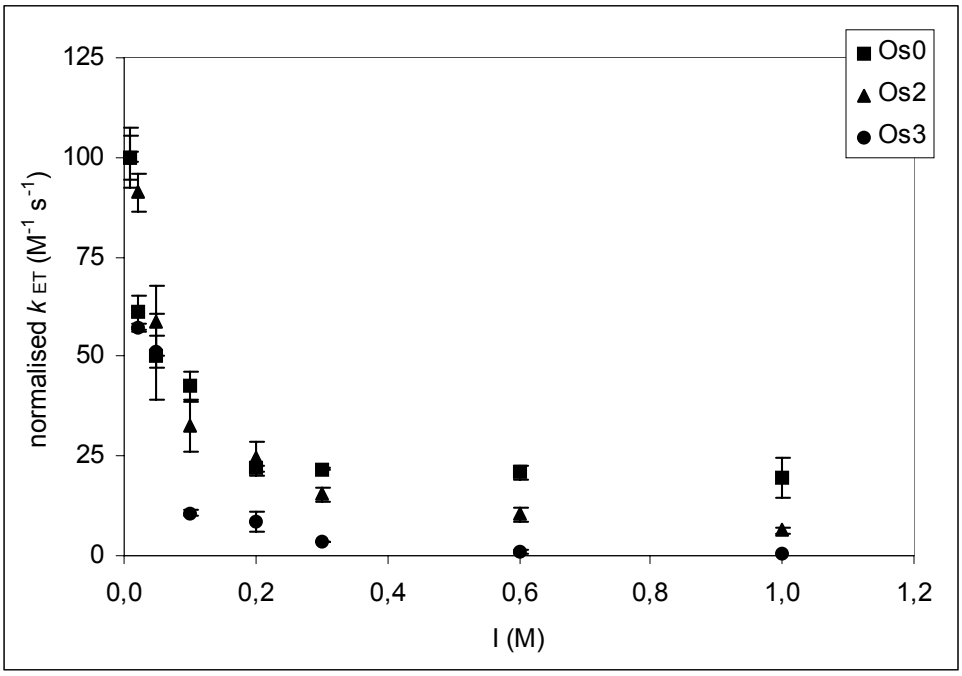

Figure V.7. Variation of the normalised electron transfer rate constant (k_{ET}) with the ionic strength (I) for the Os0, Os2 and Os3 mediators. Electron transfer rate constants were derived from steady-state cyclic voltammetry at 2mV s^{-1} in 400µL of a 0.05M tris-HCl buffer solution, different NaCl concentrations, at pH 7.0, Ar-saturated, containing 0.25M glucose, at 25°C. Initially, cyclic voltammograms of the corresponding mediator were obtained. Upon addition of increasing concentrations of GOx, electrocatalytic voltammograms were recorded. Plots of i_{SS} *vs.* $C_{enz}{}^{*1/2}$ for constant $C_{med}{}^{*}$ provided the k_{ET} values according to Equation V.2.

It can be clearly seen that the electron transfer rate constant increases as the ionic strength decreases, and this effect is much more drastic with the mediator of charge +3 (Os3) than with the mediator of charge +2 (Os2), and more important with the mediator of charge +2 (Os2) than with the neutral mediator (Os 0) at ionic strengths ≥ 0.1M (at lower ionic strengths, the error associated to the measurement does not allow one to appreciate significant differences). Comparing the results at 0.01 and 0.1M, whereas the constant for Os3 decreases 89%, for Os2 it decreases 67% and for Os3 it decreases 58%. High ionic strength produces an environment that screens glucose oxidase and mediator global charges, decreasing the electrostatic forces and slowing the kinetics of electron transfer. As expected, this masking effect is much more evident when using more positively charged mediators because the electrostatic interactions represent a higher contribution to electron transfer. In fact, there should not exist such effect for the Os0 mediator, since the global charge is 0. However, there is a trend, and the explanation would be the effect of the local charges, in this case the carboxylic groups of this mediator and the still positive charge of the central ion.

In Figure V.8, results for the electron transfer rate constant with mediators Osa, Osb and Ose, having different redox potentials but the same global charge (+3) are shown.

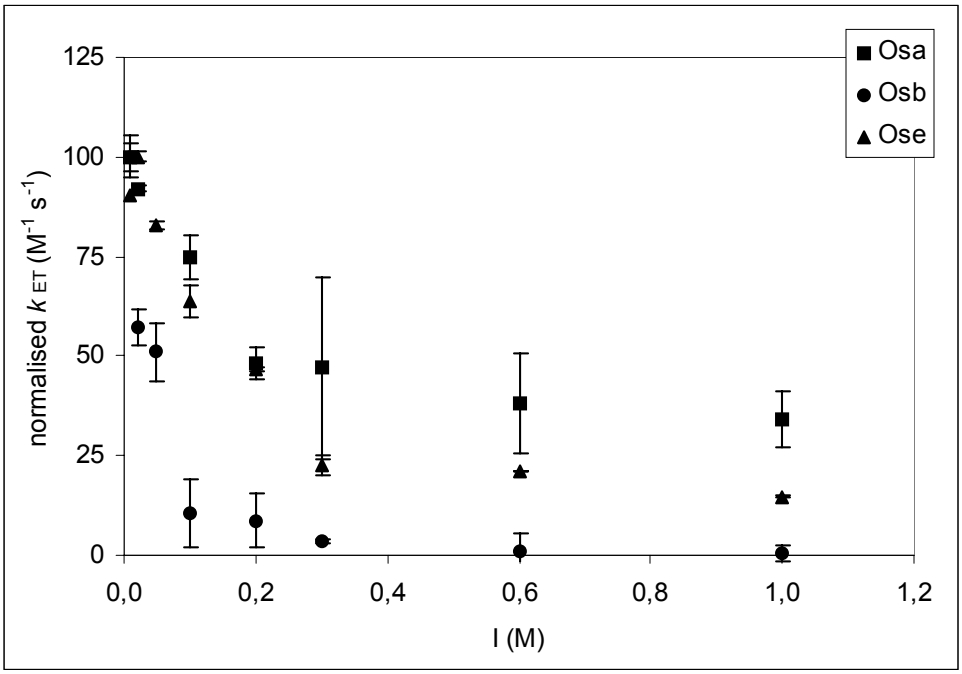

Figure V.8. Variation of the normalised electron transfer rate constant (k_{ET}) with the ionic strength (I) for the Osa, Osb and Ose mediators. Electron transfer rate constants were derived from steady-state cyclic voltammetry at 2mV s^{-1} in 400μL of a 0.05M tris-HCl buffer solution, different NaCl concentrations, at pH 7.0, Ar-saturated, containing 0.25M glucose, at 25°C. Initially, cyclic voltammograms of the corresponding mediator were obtained. Upon addition of increasing concentrations of GOx, electrocatalytic voltammograms were recorded. Plots of i_{SS} *vs.* $C_{enz}{}^{*1/2}$ for constant $C_{med}{}^{*}$ provided the k_{ET} values according to Equation V.2.

In these results, there is no direct correlation between mediator redox potential and effect of the ionic strength, as at ionic strengths ≥ 0.1M the influence of the ionic strength follows the trend Osb >

Ose ≥ Osa (as before, at lower ionic strengths, the error associated to the measurement does not allow one to appreciate the differences). Comparing the results at 0.01 and 0.1M, whereas the constant for Osa and Ose decreases 25 and 33%, respectively, for Osb it decreases 89%. The differences between Osb and Ose cannot be explained in terms of mediator global charge, but they can be explained in terms of side ligand groups in the mediators. Whereas Ose has no side groups, Osb has one amine group that could be more susceptible to ionic strength changes. This local charge phenomena may explain that the effect of ionic strength on the kinetics of Osb is much more drastic than the effect on Ose. The problem appears with Osa, which has also one amine group but it is the less influenced than Osb. The dimethyl groups of Osa make the mediator more hydrophobic, which might be decreasing the effect of screening on the rate constant or the orientation of the mediator during electron transfer.

Figures V.9 and V.10 show the variation of the logarithm of the electron transfer rate constant with the ionic strength function, f(I), defined by Wherland and Gray (1976), for Osb and Ose, respectively:

$$\ln k_{ET} - \ln k_0 = f(I) = -3.576 \left[\frac{e^{-KR_{enz}}}{1+KR_{med}} + \frac{e^{-KR_{med}}}{1+KR_{enz}} \right] \left[\frac{Z_{enz} Z_{med}}{R_{enz} + R_{med}} \right] \qquad \text{(Eq. V.3)}$$

where k_{ET} is the electron transfer rate constant, k_0 is the infinite ionic strength electron transfer rate constant, K = 0.329 $(I)^{½}$ $Å^{-1}$, R_{med} and R_{enz} are the radii of the mediator (theoretical value of 6.4 Å), and the enzyme, respectively, and Z_{med} and Z_{enz} are the charges of the mediator and the enzyme, respectively. Figure V.9 shows a linear plot for the variation of the logarithm of the electron transfer rate constant with the ionic strength function for Osb. From this regression line it is possible to obtain the infinite ionic strength rate constant when all the electrostatic contributions are screened out (f(I) = 0): k_0 = 3.9 x $10^3 M^{-1}s^{-1}$. The Figure V.9 inset shows the squared correlation coefficients for a series of plots at different R_{enz}. The statistically best value, which is obtained for the maximum r^2, gives R_{enz} = 2.5Å. This value is very low compared to the hydrodynamic enzymatic radius of 43Å (Schreuder *et al.*, 1990) or its structural determination (60 x 52 x 77Å) (Savéant and Vianello, 1965). The discrepancy may be due to the scatter of the data and the accumulated errors. It may however reflect the specific docking of the mediator to an electron conducting "pathway" as explained before. In any case, assuming the best-fit enzyme radius, it is possible to obtain Z_{enz} = -5.3. This value is lower than the global enzyme charge, -80 (Voet *et al.*, 1981), because it considers the charge given by the residues inside a sphere of radius 2.5Å, again possibly reflecting the very specific docking of this mediator. Still, this value is negative, which correlates with the expected anionic active centre of GOx. Assuming the theoretical mediator radius and the experimental enzyme radius, the distance between these two redox partners is $r = R_{enz} + R_{med}$ = 2.5 + 6.4 = 8.9Å, which reflects the distance at which the electron travels from one partner to the other. Although the best fit has provided

enzyme experimental radius R_{enz} = 2.5Å, as mentioned above experimental errors could change this value. For example, with R_{enz} = 3, 5, 7, 9 and 11Å, the R^2 value is still 0.99, and provides Z_{enz} = -5.8, -8.1, -11.2, -15.4 and -20.6, respectively. As expected, the negative charge increases as the radius increases, as more residues are being considered. This uncertainty in the distance value could explain the high value obtained for β in the previous section. Simply using R_{enz} = 11Å, β = 1.07$Å^{-1}$ would be obtained.

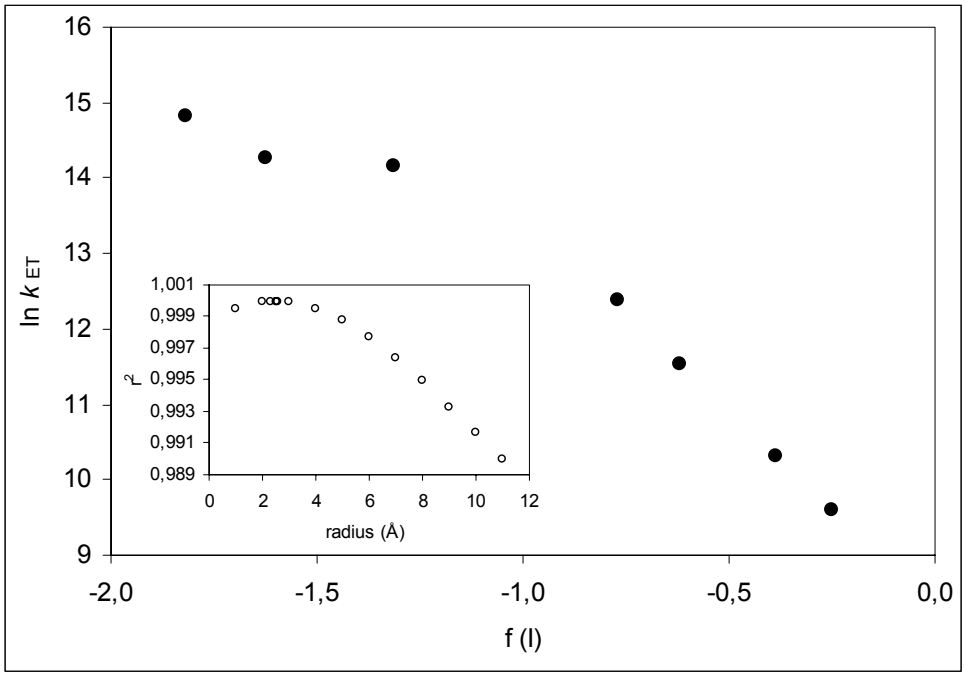

Figure V.9. Variation of the logarithm of the electron transfer rate constant (k_{ET}) with the ionic strength function (f(I)) for the Osb mediator. Inset: variation of the squared correlation coefficients for the ionic strength function with the radius of the enzyme.

On the other hand, whereas Osb produces a linear plot, Ose does not (Figure V.10). In this case, the logarithm of the electron transfer rate constant deviates from the linearity at low ionic strengths. In fact, since this mediator is the most oxidizing, the electron transfer rate constant achieves the internal electron transfer rate constant value at 0.05M, and consequently, lower ionic strength values do not increase the electron transfer rate constant in a significant way. Calculating the regression line for the four points corresponding to the highest ionic strengths, the infinite ionic strength rate constant k_0 = 5.1 x $10^5 M^{-1}s^{-1}$ has been obtained for Ose. This value is higher than the corresponding value for Osb (k_0 = 3.9 x $10^3 M^{-1}s^{-1}$) because this mediator possesses a higher internal electron transfer, due to its more positive redox potential. Moreover, from Figure V.10 inset, it is possible to obtain R_{enz} = 23.6Å and Z_{enz} = -31.9. In this case, r^2 shows less fitting to the regression line. As mentioned above, again experimental errors can be assumed or a less specific docking of the mediator might explain the results. In the same way, considering for example R_{enz} = 19, 21, 26, 28 and 30Å, where the r^2 is still 0.89, Z_{enz} = -20.6, -25.2, -38.8, -45.0 and -51.5, are obtained respectively. The statistically optimum distance between these two redox partners is *r* =

R_{enz} + R_{med} = 23.6 + 6.4 = 30Å. This distance is higher than the distance obtained for Osb (8.9Å), indicating that Ose allows the electron transfer to occur at higher distances with the same efficiency. As with Osb, simply using R_{enz} = 19Å, β = 0.90Å^{-1} would be obtained.

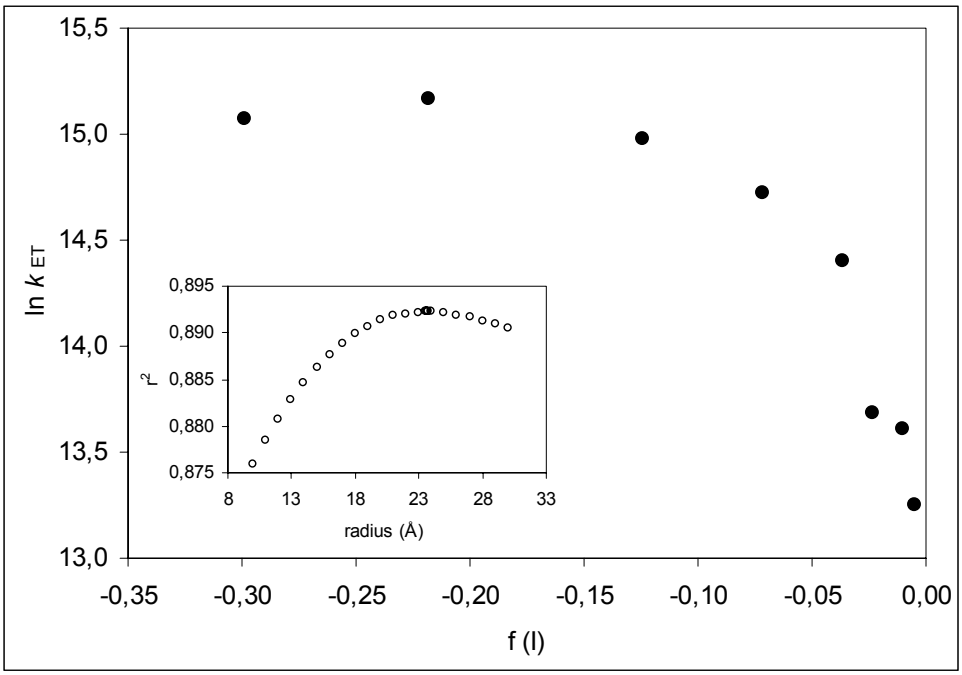

Figure V.10. Variation of the logarithm of the electron transfer rate constant (k_{ET}) with the ionic strength function (f(I)) for the Ose mediator. Inset: variation of the squared correlation coefficients for the ionic strength function with the radius of the enzyme.

Implications of findings to the design of affinity sensors. It was shown that mediators with more positive global charge result in higher electron transfer rate constants, which could lower the limit of detection of affinity sensors several orders of magnitude. When incorporating these mediators to the final configuration, an amperometric DNA sensor with GOx as label or as part of the amplifying cascade, more factors have to be considered. In principle, since hybridisation is usually carried out at pH 7.0-8.0, GOx is negatively charged and does not interact with the DNA (negatively charged due to the phosphate groups). However, the interaction between the positive charged mediators and DNA is possible. In this case, the way to incorporate the mediator in the system is crucial. For example, in a reagentless DNA sensor where the redox mediator is already attached to the electrode surface, its charge may increase the non-specific adsorption of the target DNA. If instead of having the mediator immobilised, it is incorporated to the system at the same time as the hybridisation step, the electrostatic interaction of the mediator with the probe may also increase the non-specific adsorption of the target DNA and/or decrease the hybridisation yield. In these two examples, it will be necessary to compromise between the kinetics of the mediator and its charge, trying to achieve an electron transfer rate constant as high as possible but without having non-specific electrostatic interactions. If, on the other hand, the mediator is incorporated after the

hybridisation step, there will be no interferences. However, the system will not be reagentless and will not allow real-time measurements.

Regarding the mediator redox potential, once again it is necessary to compromise. Although the higher the mediator redox potential, the higher the electron transfer rate constant and the lower the limit of detection, high mediator redox potential implies amperometric steady-state measurements at high fixed potential, which increases the interference currents from other oxidisable compounds that may be present in the real sample, such as ascorbic acid. However, since direct DNA analysis is rarely performed, samples can be cleaned from interfering substances.

Finally, using low ionic strength in the DNA “hybridisation + real-time detection” step, not only favours the kinetics of electron transfer between the enzymatic label and the redox mediator, but also increases the hybridisation stringency conditions because the electrostatic repulsion between the probe and the target is higher. Consequently, low ionic strengths decrease the limit of detection and increase the selectivity of the DNA sensor. But it is still necessary to have a certain amount of salt in the “hybridisation + real-time detection” solution to allow the base pairing to occur and to carry out electrochemical measurements.

Conclusions

Electron transfer between GOx and osmium mediators has been studied as a means to better understand the mechanisms of the redox reactions and to further use the redox system in electrochemical signal amplification schemes. Electron transfer rate constants between GOx and mediators showed an increasing trend with the positive mediator global charge. The trend can be explained in terms of global (at large distances) and local (at small distances) electrostatic interactions, or existence of redox conducting “pathways” inside the enzyme that accelerate the electron transfer kinetics. Whereas mediators contribute to the local interactions through the active groups of their ligands, the enzyme contributes through its residues, which appear to be on the surface rather than in the active site. The increase of electron transfer rate constants at high pH can be due to different effects: the higher thermodynamic driving force, the positive global charge of the enzyme and/or a more reactive deprotonated $FAD^{\bullet}$ (compared to the $FADH_2$). Nevertheless, the assumption of a His residue that contributes to the proton transfer is also possible. As when a negatively charged mediator was used, the trend was the opposite, His could be in this case favouring electrostatic attraction or complexation between GOx and the mediator. The effect of the redox potential of the mediator on the electron transfer rate constant showed a dependence according to Marcus’ theory of electron transfer, where the electron transfer rate constants increase with increasing thermodynamic driving force. This trend allows to calculate the theoretical maximum electron transfer rate constant, the reorganisation energy for a series of osmium complexes and the distance decay constants for particular osmium complexes. The study of the effect of the ionic

strength demonstrated that high ionic strength screens the charges of redox enzymes and mediators, decreasing the electron transfer rate constants. Calculations of the ionic strength function defined by Wherland and Gray allowed to obtain infinite ionic strength constants for particular mediators, the radius of the enzyme and its charge. Moreover, the non-dependence of the kinetics on the ionic strength at I < 0.05M, shown that the internal kinetic limit has been achieved, demonstrating the fast intrinsic electron transfer kinetics of the rationally designed osmium mediators.

Summarising, complexes more positively charged and complexes with higher redox potential exhibit larger electron transfer rate constants in their reaction with glucose oxidase, and even larger at low ionic strength and high pH conditions. Rationally designing the mediators for a detection system, it is possible to amplify, in a simple way, the electrochemical response from DNA amperometric biosensors with oxidoreductase labels. This rational design is an easy, promising and applicable tool to obtain high current densities from the hybridisation in the DNA arrays, where miniaturisation is pursued.

References

Akulova V.F., Vaitkekevičius R.K., Kurtinaitiene B.S., and Kulys J.J., *Proc. Biochim. Mikrobiol.*, **1978**, 14, 377.

Beratan D.N., Betts J.N., and Onuchic J.N., *Science*, **1991a**, 252, 1285.

Beratan D.N., Betts J.N., and Onuchic J.N., *J. Chem. Phys.*, **1992**, 96, 2852.

Beratan D.N. and Onuchic J.N., *Photosynth. Res.*, **1989**, 22, 173.

Beratan D.N., Onuchic J.N., Betts J.N., Bowler B., and Gray H.B., *J. Am. Chem. Soc.*, **1990**, 112, 7915.

Beratan D.N., Onuchic J.N., and Gray H.B., *Metal Ions Biol. Syst.*, **1991b**, 27, 97.

Beratan D.N., Onuchic J.N., and Hopfield J.J., *J. Chem. Phys.*, **1987**, 86, 4488.

Bourdillon C., Demaille C., Moiroux J., and Savéant J.-M., *J. Am. Chem. Soc.*, **1993**, 115, 2.

Bright H. J. and Appleby M., *J. Biol. Chem.*, **1969**, 244, 3625.

Casimiro D.R., Wong L.-L., Colón J.L., Zewert T.E., Richards J.H., Chang I.-J., Winkler J.R., and Gray H.B., *J. Am. Chem. Soc.*, **1993**, 115, 1485.

Cass A.E.G., Davis G., Francis G.D., Hill H.A.O., Aston W.J., Higgins I.J., Plotkin E.V., Scott L.D.L., and Turner P.F., *Anal. Chem.*, **1984**, 56, 667.

Cass A.E.G., Davis G., Green M.J., and Hill H.A.O., *J. Electroanal. Chem.*, **1985**, 190, 117.

Choong Y.S. and Massey V., *J. Biol. Chem.*, **1980**, 255 (18), 8672.

Coury Jr. L.A., Murray R.W., Johnson J.L., and Rajagopalan K.V., *J. Phys. Chem.*, **1991**, 95, 6034.

Coury Jr. L.A., Oliver B.N., Egekeze J.O., Sosnoff C.S., Brumfield J.C., Buck R.P., and Murray R.W., *Anal. Chem.*, **1990**, 62, 452.

Coury Jr. L.A., Yang L., and Murray R.W., *Anal. Chem.*, **1993**, 65, 242.

Cowan J.A., Upmacis R.K., Beratan D.N., Onuchic J.N., and Gray H.B., *Ann. N. Y. Acad. Sci.*, **1988**, 550, 68.

Csöregi E., Laurell T., Katakis I., Gorton L., and Heller A., *Mikrochim. Acta*, **1995**, 121, 31.

Csöregi E., Quinn C., Lindquist S.-E., Schmidtke D., Pishko M., Ye L., Katakis I., Hubbel J., and Heller A., *Anal. Chem.*, **1994**, 66, 3131.

DellaCiana L., Bernacca G., Boudin F., Fenu S., and Garetto F., *J. Electroanal. Chem.*, **1995**, 382, 129.

Fraser D.M., Zakeeruddin S.M., and Grätzel M., *J. Electroanal. Chem.*, **1993**, 359, 125.

Frew J.E. and Hill H.A.O., *J. Biochem.*, **1988**, 172, 261.

Fultz M.L. and Durst R.A., *Anal. Chim. Acta*, **1982**, 140, 1.

Ghisla S. and Massey V., *Biochem.*, **1986**, 239, 1.

Ghisla S. and Massey V., *Eur. J. Biochem.*, **1989**, 181, 1.

Gooding J.J., Pugliano L., Hibbert D.B., and Erokhin P., *Electrochem. Commun.*, **2000**, 2, 217.

Green M.J. and Hill H.A.O., *J. Chem. Soc., Faraday Trans. I*, **1986**, 82, 1237.

Hecht H.J., Kalisz H.M., Hendle J., Schmid R.D., and Schomburg D., *J. Mol. Biol.*, **1993**, 229, 153.

Hedenmo M., Narváez A., Domínguez E., and Katakis I., *Analyst*, **1996**, 121, 1891.

Hedenmo M., Narváez A., Domínguez E., and Katakis I., *J. Electroanal. Chem.*, **1997**, 425, 1.

Jacobs B.A., Mauk M.R., Funk W.D., MacGillivray R.T.A., Mauk A.G., and Gray H.B., *J. Am. Chem. Soc.*, **1991**, 113, 4390.

Johnson J.M., Halsall H.B., and Heineman W.R., *Anal. Biochem.*, **1983**, 133, 186.

Jönsson G. and Gorton L., *Electroanalysis*, **1989**, 1, 49.

Katakis I. and Heller A., *Anal. Chem.*, **1992**, 64, 1008.

Katakis I., *Development and analysis of operation of enzyme electrodes based on electrochemically "wired" oxidoreductases*, Ph.D. thesis, University of Texas at Austin, USA, **1994**.

Katakis I., Ye L., and Heller A., *J. Am. Chem. Soc.*, **1994**, 116, 3617.

Kenausis G., Taylor C., Katakis I., and Heller A., *J. Chem. Soc., Faraday Trans.*, **1996**, 92, 4131.

Kulys J. and Čénas N. K., *Biochim. Biophys. Acta*, **1983**, 744, 57.

Kulys J. and Čénas N. K., *J. Mol. Catal.*, **1988**, 47, 335.

Kulys J., Buch-Rasmussen T., Bechgaard K., Razumas V., Kazlauskaite J., Marcinkeviciene J., Christensen J.B., and Hansen H.E., *J. Mol. Catal.*, **1994**, 91, 407.

Liaudet E., Battaglini F., and Calvo E.J., *J. Electroanal. Chem.*, **1990**, 293, 55.

Male K.B., Saby C., and Juong J.H.T., *Anal. Chem.*, **1998**, 70, 4134.

Marcus R.A., *J. Chem. Phys.*, **1965**, 43, 679.

Massey V. and Hemmerich P., *Biochem. Soc.*, *Trans. Biochem. Rev.*, **1980**, 8, 246.

Mayo S.L., Ellis Jr. W.R., Crutchley R.J., and Gray H.B., *Science*, **1986**, 233, 948.

Meyer M., Wohlfahrt G., Knäblein J., and Schomburg D., *J. Comput.-Aided Mol. Design*, **1998**, 12, 425.

Nakamura S., Hayashi S., Koga K., *Biochim. Biophys. Acta*, **1976**, 445, 294.

Narváez A., Domínguez E., Katakis I., Katz E., Ranjit K., and Willner I., *J. Electroanal. Chem.*, **1997**, 430, 227.

Narváez A., Parellada J., Domínguez E., and Katakis I., *Quím. Anal.*, **1996**, 15, 75.

Nicholson R.S. and Shain I., *Anal. Chem.*, **1964**, 36, 706.

Onuchic J.N., Beratan D.N., Winkler J.R., and Gray H.B., *Ann. Rev. Biophys. Biomol. Struct.*, **1992**, 21, 349.

Onuchic J.N., Beratan D.N., Winkler J.R., and Gray H.B., *Science*, **1992**, 258, 1740.

Pishko M.V., Katakis I., Lindquist S.-E., Heller A., and Degani Y., *Mol. Cryst. Liq. Cryst.*, **1990a**, 190, 221.

Pishko M.V., Katakis I., Lindquist S.-E., Ye L., Gregg B., and Heller A., *Angew. Chem. Intl. Ed. Eng.*, **1990b**, 102, 109.

Popescu I.C., Domínguez E., Narváez A., Pavlov V., and Katakis I., *J. Electroanal. Chem.*, **1999**, 464, 208.

Ruzgas T., Csöregi E., Katakis I., Kenausis G., and L. Gorton, *J. Mol. Recog.*, **1996**, 9, 480.

Savéant J.-M. and Vianello E., *Electrochim. Acta*, **1965**, 10, 905.

Scheller F.W., Hintsche R., Neuman B., and Bogdanovskaya V., *Studia Biophys.*, **1989**, 132, 93.
Schreuder H.A., Hol W.G.J., and Drenth J., *Biochem.*, **1990**, 29, 3101.
Stankovich M.T., Schopfer L. M., and Massey V., *J. Biol. Chem.*, **1978**, 253, 4971.
Takabe T., Takenaka K., Kawamura H., and Beppu Y., *J. Biochem.*, **1986**, 99, 833.
Taylor C., Kenausis G., Katakis I., and Heller A., *J. Electroanal. Chem.*, **1995**, 396, 511.
Ullmann G.M. and Kostić N.M., *J. Am. Chem. Soc.*, **1995**, 117, 4766.
Voet J.G. and Andersen E.C., *Archiv. Biochem. Biophys.*, **1984**, 233 (1), 88.
Voet J.G., Coe J., Epstein J., Matossian V., and Shipley T., *Biochem.*, **1981**, 20, 7182.
Wherland S. and Gray H.B., *Proc. Natl. Acad. Sci. U.S.A.*, **1976**, 73, 2950.
Wuttke D.S., Bjerrum M.J., Winkler J.R., and. Gray H.B, *Science*, **1992**, 256, 1007.
Yamasaki M. and Yamano T., *Biochem. Biophys. Res. Commun.*, **1973**, 51 (3), 612.
Ye L., Katakis I., Schuhmann W., Schmidt H.-L., Duine J.A., and Heller A., *Diagnostic Biosensor Polymers.*, eds. Usmani A.M. and Akmal N., ACS Symposium Series 556, Washington, USA, **1994**.
Zakeeruddin S.M., Fraser D.M., Nazeeruddin M.-K., and Grätzel M., *J. Electroanal. Chem.*, **1992**, 337, 253.

Abbreviations

bpy: 2,2'-bipyridyl
dcarbpy: 2,2'-bipyridine-4,4'-dicarboxylic acid
dmebpy: 4,4'-dimethyl-2,2'-bipyridyl
DMF: dimethylformamide
enz: enzyme
FAD: oxidised flavin adenine dinucleotide
$FADH_2$: reduced flavin adenine dinucleotide
GOx: glucose oxidase
His: histidine
$imNH_3^+$: 1-(3-aminopropyl)imidazole
L: ligand
med: mediator
O: oxidised mediator
phen: 1,10-phenanthroline-5,6-dione
pI: isoelectric point
py: pyridine
$pyCOO^-$: isonicotinic acid
$py2COO^-$: pyridine-3,5-dicarboxylic acid
$pyNH_3^+$: 4-(aminomethyl)pyridine
pyOH: 3-pyridinepropanol
R: reduced mediator
Z: reduced enzyme

Chapter VI. Conclusions

This thesis examined oligonucleotide immobilisation strategies, the stability of colloidal gold suspensions, the electrodeposition of the biorecognition nanomodules and the signal amplification for electrochemical hybridisation detection. The most important findings in each one are described.

Regarding oligonucleotide probe immobilisation:

➢ Several methods to immobilise oligonucleotides on gold electrodes as probes for DNA sensors were studied. The low reactivity of cystamine and thioctic acid SAMs on gold, demonstrated using redox mediators and cyclic voltammetry, led to the direct self-assembling of oligonucleotide-thiol probes. This self-assembling was demonstrated by piezoelectric and colourimetric techniques. The strategy provided a rapid, uniform and homogeneous immobilisation with only one step.

➢ A simple system to demonstrate oligonucleotide immobilisation and hybridisation detection before the use of biorecognition nanomodules as probes was used. Although several operating parameters, such as blocking agent type and concentration, mixed monolayer concentrations, and hybridisation time, were optimised, the high limits of detection suggested that signal amplification was necessary for the hybridisation detection.

Regarding colloidal gold suspension stability and conjugations:

➢ The best stabilising buffer conditions for bare gold and for resuspension of the centrifuged biorecognition nanomodules were found, which allowed to modify the colloidal gold maintaining the stability of the suspensions.

➢ Two model thiol-oligonucleotides, with FITC and digoxigenin as labels, were successfully conjugated on colloidal gold, resulting in stable and reproducible colloidal gold suspensions. Additionally, the conjugation was stable under hybridisation temperatures and times and the nanoconjugates were functional and able to differentiate 4-point mutations in 19-mer oligonucleotide sequences, allowing their use as probes as probes for DNA sensors and arrays.

Regarding the site-directed electrodeposition of functional nanomodules:

➢ Colloidal gold was site-directed on several electrode surfaces by electrodeposition and characterised by several methods. Light and electron microscopy and electrochemistry demonstrated the selective electrodeposition on photolithographed gold IDEs of 5-μm width and gap electrodes, which proved the viability of the strategy for array manufacturing with photolithographic resolution. Spectrophotometric characterisation of the deposition of colloidal gold on ITO electrodes demonstrated the benefits of using short arraying times. Colloidal gold selective deposition was also demonstrated by piezoelectric techniques.

➢ After the ”proof-of-concept” with bare colloidal gold, light microscopy, colourimetric and electrochemical techniques demonstrated the site-directed electrodeposition of oligonucleotide biorecognition nanomodules on photolithographed gold IDEs and 3-electrode arrays, and carbon screen-printed electrodes. Despite the clear electrodeposition over the non-specific adsorption, the values from the system were too close to the values from the blanks, indicating that signal amplification was required.

➢ The electrodeposited oligonucleotide biorecognition nanomodules were functional and able to detect 4-point mutations in 19-mer oligonucleotide sequences, demonstrating their suitability as probes in DNA sensors. Again, the low current intensities showed the necessity for signal amplification.

➢ Preliminary experiments suggested the possibility to decrease the non-specific adsorption yields by exposing the conjugate-modified electrodes to a flowing buffer solution at the appropriate Re.

Regarding electron transfer kinetics optimisation:

➢ The effect of the global charge and the redox potential of the osmium complexes, as well as the effect of the pH and the ionic strength of the media on the electron transfer rate constant between mediators and redox enzymes were evaluated, in order to subsequently apply the acquired knowledge to the design of electrochemical signal amplification schemes for DNA sensors.

➢ The study of the global charge of the osmium mediator led to the conclusion that more positively charged mediators presented higher electron transfer rate constant as a consequence of the electrostatic interactions, and the existence of electron conducting “pathways”. The pH dependence, which provided higher electron transfer rates at higher pH, was explained in terms of higher driving force and the effect on the pK_a of the enzyme active site and His residues. The effect of the redox potential correlated satisfactorily with the Marcus theory. The ionic strength showed an effect according to the screening of the charges of enzyme and mediator. The evaluation of the mentioned effects yielded several system parameters, such us the theoretical maximum electron transfer rate constant, the Marcus reorganisation energy, the electron transfer decay constants, the infinite ionic strength rate constants, and the radius and the charge of the enzyme. These parameters were used to understand the mechanisms of electron transfer for subsequent application in electrochemical signal amplification schemes for amperometric DNA sensors.

Summarising, the biorecognition nanomodules were successfully synthesised, and the stability of the suspensions, the functionality of the conjugates and the thermal stability of the modification were demonstrated. These biorecognition nanomodules were selectively electrodeposited on electrodes with photolithographic resolution. Consequently, the initial proposed strategy of selective electrodeposition of biorecognition nanomodules as arraying method for DNA sensors is viable.

Chapter VII. Future work - extensions

One of the main requirements of DNA sensors and arrays is a high sensitivity, as at physiological levels DNA is usually at the femtomolar or attomolar range. Experiments in Chapters II and IV have clearly demonstrated the necessity for electrochemical signal amplification, and not only to detect hybridisation (the final goal of this work) but also to detect any biorecognition event in which a redox enzymatic label is involved. In fact, in Chapter IV, the low sensitivity has been a problem in the characterisation of the site-directed electrodeposition by electrochemical methods. Although clear evidence of selective electrodeposition was observed, the current intensities from the system were very close to current intensities from the blanks. Having realised this problem, efforts were focused to intrinsically increase the kinetics of electron transfer between redox enzymes and osmium mediators, as can be seen in Chapter V. However, the optimised operating conditions should be incorporated into DNA hybridisation detection methods and signal amplification recycling systems. Our group is also working on other signal amplification schemes. One of them is based on the inclusion of redox enzymes and osmium mediators into liposomes, which are modified with antibodies able to recognise antigen-labelled target sequences. The other one is based on the derivatisation of polymers, like dextran, with antibodies, redox enzymes and osmium mediators. In both cases, the goal is to increase the number of enzyme molecules per recognition event.

Apart from the electrochemistry, label-free techniques for the characterisation of the selective electrodeposition should be developed. Electrochemical quartz crystal microbalance and electrochemical surface plasmon resonance are two firm candidates. These combined techniques will allow both the electrochemical deposition of oligonucleotide-colloidal gold conjugates and the characterisation of the site-directed deposition. These techniques do not require any label, are highly sensitive and are able to follow measurements in real-time. Although some preliminary experiments have been performed with the piezoelectric detection, the experimental set up has to be optimised.

Regarding the experiments where the electrodeposition has been characterised by light microscopy, it is obvious that the experimental set up as well as the image analysis have to be improved in order to avoid possible artefacts that might be compromising the limit of detection.

The still present non-specific adsorption of oligonucleotide-colloidal gold conjugates on the electrodes were no potential has been applied should be completely avoided to guarantee a completely site-directed deposition. The article “Describing hydrodynamic particle removal from surfaces using the particle Reynolds number” by Burdick *et al.* (2001) suggests the possibility to use the flow to remove fine particles form surfaces when surface roughness is small compared to particle diameter. This effect can be studied using the conjugates of different size that have been synthesised (3 and 20nm diameter colloidal gold) and the photolithographed gold arrays, whose

roughness has been observed to be around 10nm from laser beam scanning experiments performed with Trace Biotech AG. Preliminary flow experiments have been performed. However, difficulties to evaluate the proper Re on the electrode surface have appeared and a new flow-cell with controlled flow should be designed.

Modelling of electrodeposition of bare colloidal gold and colloidal gold conjugates is another pending task. Most of the existing models are focused on adsorption of colloidal particles, and although some other models include the presence of charged walls and the electrophoretic phenomena, none of them use oligonucleotide-modified colloidal gold particles. A simulation more close to our experimental system and including all the processes and existing forces would probably clarify the mechanisms of electrodeposition.

Related to the previous pending task is the study of the kinetics of aggregation. In Chapter III, the different kinetics of aggregation have been qualitatively observed. The kinetics essentially depends on the collision frequency and the collision efficiency, being the latter difficult to quantify because it is a complex function of the diffuse layer, the Van der Waals potentials, the hydration forces and other interparticle interactions that cannot be fully accounted for. Nevertheless, a semi-empiric model could be developed in order to establish the conditions under which colloidal gold and colloidal gold conjugates suspensions are stable.

Regarding the electron transfer kinetics studies, recombinant glycosylated GOx could be used to evaluate the steric accessibility of the flavin active centre. Apart from GOx, other model enzymes could also be studied. In fact, our group is working with HRP, as this redox enzyme is more commonly used in detection systems. The kinetics of dehydrogenase enzymes, able to transfer electrons and protons simultaneously, could also be studied as they intervene in many signal amplification schemes. Simulation of the interaction between enzymes and osmium mediators is also an interesting approach to visualise the dominating interactions.

Finally, a hybridisation detection method should be established. In the ideal strategy, the target does not require to be labelled. This could be achieved using a sandwich format, where apart from the first immobilised probe, a second signalling probe would recognise the unpaired segment of the sequence hybridised with the first probe. This kind of format confers more selectivity to the system, as two target hybridisation steps are involved. Moreover, the mutation discrimination should be studied, as the ideal system should be able to differentiate one-point mutation. Obviously, real samples should be also used to evaluate the viability of the DNA array.

Burdick G.M., Berman N.S., and Beaudoin S.P., *J. Nanoparticle Res.*, **2001**, 3, 455.

IOANNIS KATAKIS, Professor Titular del Departament d'Enginyeria Química de la Universitat Rovira i Virgili

FAIG CONSTAR

que el present treball que porta per títol

FUNCTIONAL OLIGONUCLEOTIDE RECOGNITION NANOMODULES FOR ELECTROCHEMICAL DNA BIOSENSORS

que presenta na MÒNICA CAMPÀS i HOMS per optar al Grau de Doctora en Enginyeria Química, ha estat realizat sota la meva direcció en els laboratoris del Departament d'Enginyeria Química de la Universitat Rovira i Virgili, i que tots els resultats presentats i la seva anàlisi són fruit de la investigació realitzada per l'esmentada doctoranda.

I per a que se'n pregui coneixement i tingui els efectes que correspongui signo aquesta certificació.

Tarragona, 1 de juliol de 2002

Dr. Ioannis Katakis
Professor Titular d'Universitat

Agraïments

En aquest parell de fulls voldria agrair la col·laboració de tots aquells que han fet que aquesta tesi hagi arribat finalment a bon port.

Gràcies, en primer lloc, al meu director de tesi, el Dr. Ioanis Katakis, per donar-me l'oportunitat de treballar amb ell i per ensenyar-me com n'és de fascinant la ciència.

Gràcies als membres del tribunal, que tan amablement han acceptat llegir-se aquesta tesi.

Gràcies a la *Comisión Interministerial de Ciencia y Tecnología* per la beca associada al projecte "*Desarrollo de Biosensores de la Cuarta Generación: Cables en Ingeniería Molecular*" (*Programa Nacional de Biotecnología*, BIO97-1204-C02-02) i a la Comissió Europea per la beca associada al projecte "DISSARM" (*Quality of Life and Management of Resources Program*, QLK2-CT- 2000-00765).

Gràcies a tots els membres que han passat pel BBG, en especial al Juanjo (el meu mestre), al Valeri (malgrat la seva tossuderia en demostrar-me què és l'entropia), a la Mikaela (i la seva altra manera de veure les coses), al Dr. Dani Martorell (malgrat el poc temps) i al Dr. Christophe Bengoa (per fer una mica de germà gran). Gràcies també al Lluís Masip, al Josep Pàmies i al Carlos Nieto per ajudar-me amb les constants de transferència i la deposició de l'or col·loidal. Gràcies als "becaritos", sobretot al Vicenç, a l'Òscar, a la Lolo, a la Bego, al Pau, al Josep Lluís i al Paul, per les bones estones que m'han fet passar. I finalment, gràcies als "katakids", la Kristin, l'Alex i la Mònica, amb qui comparteixo tant les preocupacions dels experiments fallits com les alegries dels exitosos (?).

Gràcies també a tots els membres del BBCAT (com oblidar el "no me diga más... pase, pase que ya se lo ha ganado"?), sobretot a la Dra. Arantxa Narváez i a la directora del gup de la Universitat de Alcalá de Henares, la Dra. Elena Domínguez, que em van ensenyar a donar les primeres passes pel camí de la recerca.

Gràcies al Prof. George G. Guilbault, a la Dra. Ciara K. O'Sullivan (ara la meva companya de despatx i la "help" que resol sempre els meus dubtes) i a tot el lab B16 per la meva immillorable estada al University College Cork, en especial al Dr. Philip O'Connell i a la Dra. Sabina Susmel per haver-me fet veure "això de fer una tesi" d'una manera més atractiva.

Gràcies a la gent que ha estat al meu costat durant el dia a dia. Com oblidar la vida a la Imperial? M'ho he passat molt bé i en guardo molts bons records: l'Ingrid (i la definició dels objectius), l'Alvarito (el meu conseller orgànic i informàtic), el Maxi (i el "verdad o mentira"), el Gökhan (i les classes de castellà), l'Albert (i els campionats de "Shangai"), el Jordi i la Neus (i el cine i els concerts), la Clàudia (i les xerrades a la "baticueva"), l'Ana (i la crònica social). La vida està feta de

petits moments i és amb tota aquesta gent amb qui els he estat compartint aquests darrers sis anys. I gràcies també a tots els altres companys del departament, amb qui he compartit el dinar de cada dia, les xerrades pels passadissos, els viatges amb bus, els histerismes de la tesi (Montse i Silvia, ja veureu com s'acabarà), la llista "precaris"...

Gràcies a tota la gent del Departament d'Enginyeria Química i, en general, de l'Escola Tècnica Superior d'Enginyeria Química i de la Universitat Rovira i Virgili. Gràcies també a tot el Personal d'Administració i Serveis de la URV, tant la gent de secretaria i als dels laboratoris, com als informàtics i als de recursos científics, per ajudar a fer-me la vida més fàcil. Gràcies també a la gent que neteja tot el que s'embruta i es desordena com per art de màgia. I als vigilants de nit, sense ells no hauria acabat.

Gràcies a la gent que m'han fet sortir de la facultat per anar al cine, a prendre "algo", a fer un cafè, a sopar, a cantar...: l'Anna, la Lolo (un altre cop), la Rosa, el Javi, la Inma i la Marga, i sobretot a la Núria (la meva amiga de l'ànima) i al Xavier, perquè amb ells puc parlar de tot i perquè m'ajuden a racionalitzar les coses.

Gràcies a la meva mare, al meu pare, al Sàndal i a l'Àngels, que em fan tocar de peus a terra cada cap de setmana, que em fan veure el meravellosa que és la vida i la sort que tinc de tenir una família així. Gràcies també a la iaia, als tiets i tietes i cosins, per connectar-se de tant en tant i alegrar-me el dia.

Gràcies al Desi, per fer la tesi amb mi, i amb qui sóc tal com sóc.

Table of contents

Abstract

The goal of this thesis has been to design, characterise and optimise an electrochemical DNA sensor array. In order to investigate the oligonucleotide probe immobilisation and the hybridisation detection, preliminary experiments with an easy system were performed. This system demonstrated the suitability of oligonucleotide self-assembled monolayers (SAMs) on gold as immobilisation method. Due to the rapid DNA sensor development towards DNA arrays, a modified strategy was proposed. This strategy was based on the site-directed and selective electrodeposition of biorecognition nanomodules on electrodes of photolithographic resolution. These biorecognition nanomodules, oligonucleotide-modified colloidal gold particles, were rationally synthesised previously studying the conditions under which colloidal gold suspensions were stable. Fluorescence and colourimetric techniques proved the effectiveness of the conjugation, the functionality of the conjugated probes, and the thermal stability of the modification, which made the biorecognition nanomodules suitable for hybridisation detection. After their characterisation, the biorecognition nanomodules were electrodeposited on different electrode surfaces and the site-directed immobilisation was clearly demonstrated by several techniques, such as light and electron microscopy, and colourimetric, piezoelectric and electrochemical techniques. Additionally, the site-directed deposited biorecognition nanomodules were functional and able to differentiate 4-point mutations in 19-mer oligonucleotides. Despite the promising results, which demonstrated the viability of the directed electrodeposition as arraying technique, the necessity for signal amplification was observed, as system values were very close to blank values. Following two parallel objectives for the electrochemical signal amplification (to intrinsically increase kinetic rates between enzymes and electrodes, and to optimise electrochemical recycling systems), osmium complexes were rationally designed and the kinetics of electron transfer with redox enzymes was evaluated. These kinetic studies showed that more positively charged mediators and with higher redox potentials yielded higher rates, also favoured at high pH and low ionic strength, demonstrating the possibility to amplify electrochemical signals.

This thesis is structured in seven chapters. Chapter I establishes the basis of DNA sensors and arrays, colloidal gold stability, conjugations and deposition, and signal amplification. It also presents the thesis. Chapter II describes the preliminary system for the immobilisation characterisation and hybridisation detection. Chapters III, IV and V correspond to the synthesis and characterisation of the functional biorecognition nanomodules, the site-directed electrodeposition of these nanomodules, and the electron transfer kinetics optimisation for signal amplification. Finally, Chapters VI and VII summarise the conclusions and the future work.

List of tables

List of schemes

Chapter I. Introduction

1.1. DNA sensors and arrays

1.1.1. Introduction and definitions

The detection of specific DNA sequences has always been an important issue in the biomedical field due to its application in DNA sequencing and diagnostics. Thirty years ago, the method by excellence to identify DNA was "sequencing by digestion", which was laborious and time-consuming. Soon thereafter, membrane-supported methods appeared based on "sequencing by hybridisation" (SBH), which were simpler (Wallace *et al.*, 1979 and 1981). However, the most important advance did not appear until the last decade, with the advent of DNA sensors and arrays (Fodor *et al.*, 1991; Pease *et al.*, 1991; and Southern *et al.*, 1992). These two approaches overcame the problems of the previous technologies, such as low hybridisation efficiency, low sequence discrimination, long analysis time and laborious procedures. Additionally, DNA arrays allow simultaneous multi-site detection, which further reduces the analysis time and facilitates genetic analysis. Miniaturised arrays allow small sample volumes and can be mass-produced.

DNA sensors are analytical devices that consist of two components in intimate contact: the biorecognition molecule and the transducer. The biorecognition molecule is immobilised on the transducer and recognises the DNA target, and the transducer is the component that converts the biorecognition event into a quantifiable signal. DNA arrays or chips can be defined as the integration of several DNA sensors in the same device. In other words, DNA arrays are ordered sets of known biorecognition molecules immobilised on precisely defined locations of a solid substrate. In most cases, these biorecognition molecules are oligonucleotides of known sequence and the recognition event is the hybridisation with the complementary sequences. The advantages of this high throughput analysis tool are obvious and represent a drastic reduction in effort, time and costs. Microarrays can be applied to both genomics and proteomics. Whilst genomics is focused on the identification, sequencing and study of the function of genes, proteomics includes the identification and quantification of proteins, and the determination of their function, localisation, modifications and interactions. Proteomics array technology is still one step behind that of the genomics arrays. These are now almost routinely applied in old and new DNA analysis areas that can be loosely divided into four main inter-related groups:

1. **Sequencing.** Gene discovery or identification by sequencing requires arrays modified with probes that include all possible combinations of nucleotides for a determined length. Usually, an n-mer sequence is chosen as the basic identification unit and the array must have 4^n probes, corresponding to all the possible combinations with the 4 bases. The target DNA fragment is broken into smaller pieces labelled and hybridised with the immobilised

oligonucleotides or probes. Detecting the location of hybridised probes and using appropriate analysis, the total sequence can be identified.

2. **Expression analysis.** Gene expression is the process by which gene coded information is converted into the structures present and operating in the cell. Expression analysis includes both identification of differentially expressed genes and quantitation of expression levels, important in growth, metabolism, development, behaviour and adaptation of living systems. In a simple gene expression array, also known as a gene array, the messenger RNA (mRNA) is extracted and reverse-transcribed into more stable complementary DNA (cDNA). These cDNAs are marked with different labels and subjected to SBH on the array. Scanning of the array provides information about the position and intensity of the hybridisation events and, therefore, the level of expression of genes. Expression analysis contributes to find correlations between the genetic profiles of patients and the therapeutic responses to drugs (pharmacogenomics) or to toxic agents (toxicogenomics), which act at the protein level to disrupt or alter protein function. Consequently, microarrays for the analysis of gene expression can be used as powerful tools to understand the action of drugs and toxic agents at the molecular level and to tailor drug design to individuals.

3. **Disease diagnosis and mutation detection.** Microarray technology can be used in viral infection and mutation detection, and in identification of genes that have been upregulated or downregulated (Yershov *et al.*, 1996; Drobyshev *et al.*, 1997; Healey *et al.*, 1997; Head *et al.*, 1999; and Proudnikov *et al.*, 2000). The identification of these pathogens, infectious species and drug-resistant mutants at molecular level is based on SBH technology and can contribute to a better understanding of the disease processes and to diagnosis.

Related with the three areas is **polymorphism identification** (Gentalen and Chee, 1999), which uses SBH technology to detect differences in DNA sequences among individuals. These genetic mutations, commonly referred to as single nucleotide polymorphisms (SNPs), are often diagnostic of particular genetic predisposition towards disease and drug-response, so that can be linked to the genotype and phenotype information of individuals.

This thesis contributes to the development of methods for the construction of DNA arrays and sensors. The development of DNA arrays is already having a profound effect on various aspects of social, economic and scientific activity. When combined with the results of the human genome and other sequencing projects, it is accelerating the changes in these aspects of human activity that together contribute to the new technological revolution based on the combination of silicon technology and biotechnology, which is widely believed that will characterise the XXI century. It is only appropriate that at this point an effort is made to systematically define the steps involved in DNA or biochip array development. Although the limits are not clearly delineated between them, for the sake of a systematic approach these are defined as:

- Probe immobilisation (and characterisation).
- Arraying.
- Biorecognition event detection (and amplification).
- Data analysis (a field that is widely known as bioinformatics).

This thesis makes a contribution to the state-of-the-art of the three first, and for this reason they are further examined in what follows.

1.1.2. Probe immobilisation and characterisation

DNA sensors and chips are made using different types of probes. The most commonly used probes are **single-stranded deoxyribonucleic acid** (ssDNA) sequences or **oligonucleotides**, which are synthesised *in situ* or obtained synthetically with DNA synthesisers and afterwards immobilised on solid substrates. Probe oligonucleotides are usually linear. However, hairpin oligonucleotides with dangling ends are being used with increasing frequency, as they have been observed to display higher rates of hybridisation and larger equilibrium amounts of captured targets than linear probes (Riccelli *et al.*, 2001). Additionally, hairpin-target complexes are thermodynamically more stable. Molecular beacons, scorpions and light-up probes are special types of DNA probes that will be defined later. **Messenger ribonucleic acid** (mRNA) is less commonly used, due to its higher instability compared to DNA. mRNA is obtained from cells and afterwards purified. Consequently, mRNA analysis provides information about gene expression. Moreover, as mRNA is a copy of the DNA coding regions, it can be also used to identify polymorphisms in these coding regions. However, mRNA information in probe form is usually reverse-transcribed into more stable cDNA. **Peptide nucleic acid** (PNA), a probe that has found increasing recent application, deserves special mention. PNA is a linear polymer that, unlike DNA, contains a neutral, achiral backbone of repeating *N*-(2-aminoethyl)glycine units linked by amide bonds, with the purine and pyrimidine bases attached by methylene carbonyl linkages. In other words, it is a sequence made up of derivatives of the four nucleobases found in DNA but without 2'-deoxy-D-ribose residues and phosphodiester bonds, having instead a neutral backbone that reduces the electrostatic repulsion during duplex formation (Chandler *et al.*, 2000). PNA forms hybrids stabilised by hydrogen bonding and base stacking with distances similar to the DNA double helix structure but, unlike DNA/DNA hybrids, PNA/DNA hybrids are resistant to nuclease and protease attack due to the inability of nuclease and proteolytic enzymes to recognise the peptide backbone, have higher thermal stability and their melting temperature (T_m) is approximately 10ºC higher than the corresponding DNA/DNA duplex, and are relatively insensitive to ionic strength, due to the neutral charge of PNA. Additionally, single base mismatched duplexes are less stable than their corresponding DNA/DNA hybrids, a fact that makes them perfectly suitable for specific mutation detection (Jensen *et al.*, 1997 and Schwarz *et al.*, 1999).

1.1.2.1. Probe immobilisation

The most commonly used immobilisation methods for DNA sensors, summarised in Table I.1 and described below, are retention in a polymeric matrix, covalent attachment on a functionalised support, affinity immobilisation, physical adsorption on a solid surface, and monolayer self-assembling. Among these well-known and traditional methods, self-assembled monolayer (SAM) immobilisation is finding more followers, as it provides advantages in terms of simplicity, efficiency, ordered immobilisation and cost.

Table I.1. DNA immobilisation methods.

Method	Technique	Imm. site	Orientation	Access	Advantages	Drawbacks	Ref.
Retention in a polymeric matrix	Entrapment or cross-linking	Random	Random	Low	High amounts of probes	Surface treatment needed Low hybridisation yields	Hasebe,1997
Covalent attachment	EDC reaction	Activated terminal	Ordered	High	High stability	Surface treatment needed Low immobilisation yields	Millan,1993 Caruana,1999
Silanisation – covalent attachment	EDC reaction	Activated terminal	Ordered	High	Possible probe density control	Surface treatment needed Possible non-specific interactions Low immobilisation yields	Joos,1997 Potyrailo,1998 Berney,2000 Balladur,1997 Barendrecht,1990
Affinity	Biotin-avidin/ streptavidin interaction	Biotinylated terminal	Ordered	High	High stability Simplicity	Surface treatment needed Possible non-specific interactions	Lucas,2000
Adsorption	Adsorption	Random	Random	Low	Simplicity	Low hybridisation yields	Krznaric,1986 Cai,1996 Fojta,1996 Oliveira-Brett,1996,1997 Wang,1996,1997 Zhao,1997 Pang,1998 Marrazza,1999 Armistead,2000 Azek,2000
Inclusion in a composite	Entrapment	Random	Random	Low	Possible ordered attachment	Low hybridisation yields	Millan,1994
Direct SAMs	Dative binding	Thiolated terminal	Ordered	High	Simplicity Possible probe density control	Possible non-specific interactions	Okahata,1992 Hashimoto,1994 Caruso,1997b Nakano1997 Napier,1997 Steel,1998 Bardea,1999 Patolsky,1999 Bonn,2000 Ketterer,2000
Indirect SAMs	EDC reaction	Activated terminal	Ordered	High	Possible probe density control	Surface treatment needed Low immobilisation yields	Napier,1997 Steel,1998

Four effects have to be taken into account with probe immobilisation. Firstly, it is necessary that the immobilisation chemistry is stable during subsequent assay steps, which means that the immobilised biorecognition molecules should not desorb from the transducer surface. Secondly, the probes have to be functional after attachment, which means that the immobilisation technique should not change the chemical structure of the probe, as the biorecognition function could be modified and inhibited. Thirdly, biomolecules have to be immobilised with an appropriate orientation and configuration so that base pairing is not restrained. Finally, even with the appropriate orientation, there should not exist steric impediments or lack of accessibility due to the dense packing of the immobilised probes.

a) Retention in a polymeric matrix

The biorecognition biomolecules are entrapped or cross-linked with bifunctional agents, which have been activated chemically, electrochemically, photochemically or thermally (Hasebe *et al.*, 1997). The support matrix for entrapment is formed by polymers that can be organic, inorganic or organometallic, and are immobilised on a surface by chemisorption or physical adsorption. The advantage of this technique is the high amounts of oligonucleotides that are covalently attached. The main disadvantage is that the matrix does not provide any orientation, all the strands being randomly immobilised, which decreases their mobility and accessibility and inhibits the hybridisation event. This problem can be solved linking the oligonucleotides to the polymer by one of their terminals, which increases hybridisation efficiency (Caruana and Heller, 1999) (*see next section*).

b) Covalent attachment

To immobilise the biorecognition molecules on the transducer via covalent attachment it is usually necessary to pre-treat both the oligonucleotide and the surface, in order to introduce the reactive groups necessary for attachment. As the reactive group can be introduced in one of the extremes of the oligonucleotide without inhibiting its hybridisation capability, this approach confers more mobility and better orientation to the immobilised strands. Depending on the transducer surface and the reactive groups available on the oligonucleotide, different strategies have been proposed. In the strategy mentioned in the previous section, the oligonucleotide is EDC-activated and reacted with hydrazide functions of a polymer previously deposited on the electrode surface (Caruana and Heller, 1999). In the covalent immobilisation of oligonucleotides on glassy carbon, this surface can be activated with 1-ethyl-3-(3-dimethylaminopropyl)carbodiimide hydrochloride (EDC) and N-hydroxysuccinimide (NHS) in order to react with the deoxyguanosine residues of the DNA strand (Millan and Mikkelsen, 1993). Among the different transducer modification methods, silanisation is the most popular. The hydroxide or oxide layer of the substrate, which can be glass (Joos *et al.*, 1997 and Potyrailo *et al.*, 1998), silicon (Berney *et al.*, 2000), silica (Balladur *et al.*, 1997) and metals, is firstly activated with an organosilane, usually introducing amine groups (Barendrecht, 1990). Afterwards, the oligonucleotide strands are attached via EDC. Depending on the

organosilane molecule, the packing density can be controlled. However, electrostatic interactions between the aminated groups on the silanes and the negatively charged DNA are difficult to control, and this can result in non-orientated immobilisation and non-specific adsorption of possible target sequences in the hybridisation step.

c) Affinity

This immobilisation technique is based on the interaction between biomolecules, one being immobilised on the transducer surface and the other one being attached to one of the extremes of the oligonucleotide. The avidin/streptavidin-biotin affinity system is the most commonly used due to the high affinity complexation constant (K_d = 10^{-15}M) (Ebersole *et al.*, 1990; Abel *et al.*, 1996; Kolakowski *et al.*, 1996; Caruso *et al.*,1997a; Okahata *et al.*,1998; and Trabesinger *et al.*,1999). This binding force is almost equal to that of a covalent bond and can be only broken under drastic conditions. This high binding force combined with the simplicity of the procedure, makes the technique very attractive to immobilise DNA strands. However, the attraction between the positively charged lysines or arginines on the large surface of streptavidin (70kDa) and the negatively charged backbone of DNA may cause non-specific adsorption, compromising the sensitivity and selectivity of the sensor (Lucas and Harding, 2000).

d) Adsorption

In this immobilisation technique, DNA is attached by irreversible adsorption via the multiple interactions between the transducer surface and the phosphate backbone. The adsorption can be performed on different substrates, such as gold (Zhao *et al.*, 1997 and Pang and Abruña, 1998), indium-tin oxide (ITO) (Armistead and Zhorp, 2000) and screen-printed electrodes (Marrazza *et al.*, 1999 and Azek *et al.*, 2000). However, glassy carbon electrodes are more commonly used (Oliveira-Brett, 1996 and 1997). The electrodes can be covered by a drop of probe oligonucleotide and allowed to dry, or immersed in a DNA solution. In this last strategy, the oligonucleotide can be pre-concentrated on the electrode by applying a positive potential for a pre-determined time (dependent on the DNA concentration). This potential makes the electrode positively charged, improving the interaction with the negatively charged DNA backbone (Cai *et al.*, 1996; and Wang *et al.*, 1996a, b, c, 1997a, b, c). The main advantage of this method is the simplicity, but it has the inconvenience of non-ordered immobilisation and multiple-point attachment, which inhibits the recognition event. In addition to this, the immobilisation is not very stable, as depending on the hybridisation conditions the nucleic acid may be desorbed from the electrode surface.

e) Inclusion in a composite

In this immobilisation technique, the biomolecule is mixed with a matrix material, such as graphite powder, and the carbon paste mixture is introduced into an electrode body and pressed. This methodology is widely used in enzyme sensors, but it is not very commonly used in DNA sensors

due to the limited accessibility of the immobilised strands. However, in order to give more mobility to the strand, oligonucleotides can be attached to the surface of this composite paste (Millan *et al.*, 1994).

f) SAMs formation

Self-assembled monolayers (SAMs) are molecular layers formed on a surface when it is immersed in a solution containing molecules that specifically interact with this surface. Although different molecules can be immobilised (silanes, carboxylic acids, pyridines, sulphites and thiols) on different surfaces (gold, silver, platinum, copper, mercury and glass), thiols are the most commonly used especially in conjunction with gold surfaces. The stability and organisation of the SAMs depend on the forces of attraction between the immobilised molecules, the interaction between terminal groups and their local environment, and the binding force between the surface and the binding group. Oligonucleotide SAMs can be formed directly on the surface (Okahata *et al.*, 1992; Hashimoto *et al.*, 1994; Caruso *et al.*, 1997b; Nakano *et al.*, 1997; Napier and Thorp, 1997; Steel *et al.*, 1998; Patolsky *et al.*, 1999; Bonn *et al.*, 2000; and Ketterer *et al.*, 2000), when the oligonucleotides contain a pendant thiol group, or can be attached to reactive and previously formed SAMs via EDC (Napier and Thorp, 1997; and Steel *et al.*, 1998). The direct strategy reduces the number of steps required for immobilisation and avoids the EDC reaction, which usually results in considerably lower immobilisation efficiency. However, the indirect strategy (SAMs + EDC) is an alternative when non-saturated monolayers are desired.

As mentioned above, SAMs are commonly used in DNA sensor formats, as they confer ordered, stable, simple, easy and cost effective immobilisations. However, the packing density has to be controlled if optimum hybridisation efficiency is to be achieved. Too densely packed monolayers (although sometimes difficult to achieve, due to the repulsion between negatively charged probes) can be avoided using mixed monolayers, formed by the same method as pure monolayers but using oligonucleotides and spacers such as mercaptopyridine, mercaptoethanol or mercaptohexanol (Bardea *et al.*, 1999). These spacers not only block the free remaining sites, called pinholes, that could have been formed during SAM formation, but also compete with the thiol-oligonucleotides, separating them, facilitating the transport of complementary strands and increasing hybridisation efficiency.

1.1.2.2. Probe immobilisation characterisation

During the development of a biosensor or biochip, it is necessary to characterise the immobilisation efficiency and immobilised probe functionality to rationally design sensors and arrays. The techniques used for the characterisation of the probe immobilisation in DNA sensors are reviewed below.

a) Piezoelectric methods

The quartz crystal microbalance (QCM) is the most commonly used piezoelectric or microgravimetric device. This device consists of a piezoelectric quartz crystal with a determined frequency of oscillation under an applied potential. When the oligonucleotide is immobilised on the surface, the frequency of oscillation changes proportionally to the immobilised mass. The dependence of the frequency modulation with the mass change is described by the Sauerbrey equation (1959):

$$\Delta F = -2.3 \times 10^{-6} F^2 \Delta M / A \qquad \text{(Eq. I.1)}$$

ΔF being the change in the frequency (MHz), F the characteristic resonant frequency of the crystal (MHz), ΔM the mass deposited (g) and A the area of the quartz crystal (cm^2). The advantages of this technique are not only the high sensitivity and low limit of detection, but also the labelless operation. Additionally, frequency changes can be followed in real time. Caruso *et al.* (1997a, b) and Okahata *et al.* (1998) immobilised oligonucleotides directly on the gold quartz crystals, by forming a direct SAM, and also used biotin-oligonucleotides to immobilise them on streptavidin-modified gold quartz crystals. By real-time frequency measurement, they compared the two methods in terms of immobilisation kinetics. As previously mentioned, the immobilisation step is a key factor in the performance of the sensor, as it has an influence on the hybridisation kinetics. In this direction, Zhou *et al.* (2001) compared different immobilisation methods (direct chemical bonding, avidin-biotin interaction and electrostatic adsorption on polyelectrolyte films) and different immobilisation architectures (oriented oligonucleotide monolayers and multilayers created by self-assembling of alternating DNA and polymers). They observed that biotinylated DNA films provided fast sensor responses and high hybridisation efficiencies, due to the spacer group that conferred better accessibility, and that multilayered films increased the sensor sensitivity, indicating that the complementary DNA can penetrate into the multilayered sensing film, but also increased the sensor response time because of the more difficult transport of the complementary sequence.

b) Electrochemical methods

The oligonucleotide immobilisation efficiency can be determined using different electrochemical techniques. The oldest method is based on the detection of the direct oxidation of guanine by chronopotentiometry (Cai *et al.*, 1996). This technique requires the presence of guanines in the sequence, which restricts its common use. Additionally, as the direct oxidation requires a rather high potential and the reproducibility of the analysis is usually a difficult issue, mediators such as $Ru(bpy)_3^{3+}$ are commonly used as catalyst that enhance the Faradaic currents and can allow one to detect attomole quantities of immobilised DNA (Napier *et al.*, 1997; Ontko *et al.*, 1999; and Armistead and Thorp, 2000). Apart from chronopotentiometry, DNA immobilisation can be characterised by cyclic voltammetry (CV), linear sweep voltammetry (LSV) or alternating current

(AC) impedance spectroscopy of redox complexes, like $Co(bpy)_3^{3+}$, $Co(phen)_3^{3+}$ and $[Fe(CN)_6^{4-/3-}]$, or dyes, like Hoechst 33258, that present different electrochemical behaviour depending on the absence or presence of ssDNA on the electrode surface (Millan and Mikkelsen, 1993; Millan *et al.*, 1994; Hashimoto *et al.*, 1994; and Zhao *et al.*, 1997 and 1999).

SAMs can also be characterised by electrochemical methods. Cyclic voltammetry allows the observation of the reduction of the thiol-gold bond at approximately -1V (*vs.* Ag/AgCl) (Yang *et al.*, 1996 and 1997a; Imabayashi *et al.*, 1997; and Madoz *et al.*, 1997). This is a destructive technique because the thiol-gold bond is broken during reduction. Cyclic voltammetry can also be used to determine the effect of an immobilised monolayer on the electrochemical behaviour of a redox compound, which has been previously adsorbed or attached to it. Surface coverage measurements can provide data about the formation, capacitance and packing density of the DNA SAM (Chidsey *et al.*, 1990; Katz and Solov'ev, 1990; Hickman *et al.*, 1991; Miller *et al.*, 1991; Katz *et al.*, 1992; Acevedo *et al.*, 1994; Bretz and Abruña, 1995 and 1996; Cheng and Braiter-Toth, 1996; Maskus and Abruña, 1996; and Tirado and Abruña, 1996).

c) Optical methods

Immobilisation of ssDNA has been characterised by several spectroscopy techniques, such as *in situ* Ultra-Violet/visible (UV/vis), reflection spectroscopy, X-ray photoelectron spectroscopy (XPS), scanning tunnelling microscopy (STM), Raman spectroscopy and surface-enhanced Raman scattering (SERS), each one of them providing complementary structural information (Zhao *et al.*, 1999). Surface plasmon resonance (SPR) is an optical technique based on the change in the refractive index of a surface when a biomolecule is immobilised or when an affinity interaction occurs. The main advantages are that it does not require any label and that measurements can be carried out in real time (Caruso *et al.*, 1997b). Fluorescence can also be used to characterise probe immobilisation, but the oligonucleotide has to be tagged with a fluorescent label, and thus labelling efficiency and lifetime have to be taken into consideration.

1.1.3. Arraying

In making the step from DNA sensors to arrays, the ability to spatially direct the immobilisation of distinct probes is essential. Therefore, the resolution of the DNA immobilisation technique is crucial for arraying and miniaturisation. Microarraying technologies thus have to fulfil several requirements: easy implementation, robustness, consistency, automation, high speed of fabrication, versatility, repeatability, regularity, uniformity, accuracy, high precision, high resolution, high array density, durability and cost effectiveness. This long list makes it difficult to find one technique that fulfils all the conditions. In this competitive field, technologies are quickly consolidated and reduced to practice. For this reason, technology breakthroughs are usually represented by manufacturing

systems used by different companies. Table I.2 summarises some of the systems commonly used in the area as well as their advantages and drawbacks.

Table I.2. Leader companies and systems in microarraying technology.

Company	Technique	Probe	Spatial resolution	Detection	Advantages	Drawbacks	Application
Synteni / Incyte Pharmaceuticals Inc.	Ink-jetting on glass	500nt DNA samples PCR fragments	10000 spots on 3.6cm^2	Fluorescence Radioisotopic	Off synthesis	Low density Low cost	Expression profiling, gene identification, diagnostics, polymorphism analysis
Hyseq	Pin deposition on membranes	5nt oligos 500-2000nt DNA samples	1024 spots on 1.15cm^2 64 spots on 0.6cm^2	Fluorescence Radioisotopic	High density Off synthesis	Low cost	Expression profiling, gene identification, diagnostics, sequencing, polymorphism analysis
Affymetrix	Photolithography with activated nucleotides	25nt oligos	9000 spots on 1.6cm^2	Fluorescence	High density	High cost *In situ* synthesis	Expression profiling, diagnostics, polymorphism analysis
Clinical Micro Sensors	Pin deposition on electrodes or Photolithography with activated oligonucleotides	Small DNA/RNA fragments	36 targets on a chip	Impedance	Off synthesis Low cost	Low density Low cost or High cost	Expression profiling, gene identification, diagnostics, sequencing, polymorphism analysis
Nanogen	Electronically-driven binding of biotin on streptavidin-modified agarose	20nt oligos	99 locations on 2mm^2	Fluorescence	High density Off synthesis	Low cost	Expression profiling, gene identification, diagnostics, short tandem repeat identification

Immobilisation can be carried out on many different substrates: glass, agar, gels or membranes (nitrocellulose or nylon). Usually, they have to be previously treated in order to introduce the functional groups necessary for the biomolecule attachment. The probes can be either synthesised *in situ* (like in the photolithographic technique) or pre-made and afterwards immobilised. Although *in situ* construction of arrays by lithography is advantageous in terms of resolution, this technique implies lack of quality control of the sequences. On the other hand, techniques that use pre-made oligonucleotides allow the previous testing of the sequence, in order to see if there are some errors that could produce false responses. Below, different arraying methods will be reviewed.

a) Ink-jetting

Ink-jetting is a non-contact printing technology, where the DNA probes are dispensed in small volumes on a slide without touching it, reducing the risk of possible contamination. During ink-jetting, the DNA sample is withdrawn from the source, introduced into the print head, moved to the pre-determined site of deposition, and deposited through ejection onto the surface. Usually, this

surface is pre-treated in order to covalently attach the DNA. There are two different types of ink-jet printing: piezoelectric, where a piezoelectric crystal biased by a voltage squeezes the capillary containing the sample and causes its ejection (Incyte Pharmaceuticals), and syringe-solenoid, where the microsolenoid dispenses low volumes ejected by a syringe pump (Cartesian Technologies). Whilst in the syringe-solenoid technique the minimum dispense volume is in the order of 4-8nL, with a spot size of 250-500μm and a density of 200-400 spots cm^{-2}, in the piezoelectric technique the spot volume is on the order of 50pL, with a spot size of 125-175μm and a density of 500-2500 spots cm^{-2}. Moreover, the delivery speed is 10-50 spots sec^{-1} with the syringe-solenoid technique and 100-500 spots sec^{-1} with the piezoelectric device. However, despite the larger volumes and the lower array densities, the reliability of the syringe-solenoid technique is higher and the equipment is cheaper and more robust. In general, despite the advantages of ink-jet arraying, the main disadvantages are the air bubbles, which reduce the repeatability and reliability of the system; the difficult sample changing; maintenance problems related to the obstruction of the inlet tubing and capillaries or syringes; excessive splashing; clogging of the nozzle; and poor uniformity of the deposit, which can cause cross-over contamination between probes. The ink-jet technology has been used for the *in situ* synthesis of oligonucleotides of 40-50 bases in length on an array (Castellino, 1997). In this case, the printer dispenses one of the four bases onto a coated surface, where it is anchored by standard chemistry. Following washing and deprotection, the next dispense adds the following base and the cycle is repeated until the complete sequence is immobilised. Nevertheless, this strategy, although feasible, is laborious, requires many washing steps and lacks control of the quality of the sequence.

b) Pin deposition

Pin deposition is a contact printing technique, as there is direct contact between the dispenser and the surface. Pin tools are immersed in the DNA probe source, which results in the adherence of small volumes onto the tip of the pins. When the pin touches the surface, a drop is transferred from the tip to the sensor surface. The number and the diameter of the spots, between 50 and 360μm, depend on surface and solution properties, the velocity of the pin, the diameter of the tip and its geometry. Different pin geometries are available: tweezers, split tip, micro spotting pin (Hyseq and TeleChem International) or Pin-and-Ring™ (Genetic MicroSystems). As a practical example, Zammatteo *et al.* (2000) used different strategies to covalently attach DNA onto glass surfaces. After comparison between amino-silane, carboxylic acid and aldehyde-covered glass slides, they chose the aldehyde-modified surfaces to build, using 250-μm pins, DNA microarrays for human cytomegalovirus (HCMV) detection. Apart from this functionalised glass substrate, many authors have also used glass modified with poly-L-lysine[6] or polyacrylamide gel (Guschin *et al.*, 1997) as substrate. Usually, the dispensed volume is in the range of 0.5-2.5nL. This technique allows 400-625 locations on an area of $1cm^2$, a density that depends on the spatial resolution of the robotics and the dispersion of the deposit. The delivery speed is 64 spots sec^{-1}, slower than the non-contact

printing techniques. However, pin deposition is more robust, simpler and cheaper. Nevertheless, a common disadvantage to all the printing techniques is the splashing or the poor uniformity of the deposit. The variability in spot size and in probe concentration diminishes the reliability on the measurement, and the variability in spot location produces cross-contamination, also generating false measurements.

c) Polypyrrolisation

Polypyrrolisation is based on the co-polymerisation of pyrrole and oligonucleotides bearing a pyrrole moiety introduced via phosphoramidite chemistry at their 5' termini. The different pyrrole-modified oligonucleotide sequences can be electrochemically immobilised on specific sites by sequentially switching on the different electrodes. These arrays have been demonstrated, going from 4 working electrodes and using radioisotopic detection (Livache *et al.*, 1994 and 1995) to 10 and even 48 electrodes (4 x 12-electrode matrix in a 50 x 50-μm^2 chip), and using fluorescence microscopy detection (Roget *et al.*, 1995 and Livache *et al.*, 1998). This arraying technique presents the drawbacks of wet chemistry, which increases the irreproducibility of the system, and the necessity of a washing step after each polypyrrole synthesis to avoid cross-contamination with residual oligonucleotides, which makes the arraying procedure time-consuming. However, the advantage of this method is the low instrumentation costs for the manufacturing of the array unlike other methodologies involving photolithography or robotic deposition. Guedon *et al.* (2000) used a strategy to create a polypyrrole-based DNA sensor in which they combined polypyrrolisation and spotting, strategy called "electrospotting". In this arraying strategy, they filled a pipette tip incorporating a platinum wire with pyrrole-oligonucleotide and moved it to a precise location on a gold layer used as the electrode. After depositing a droplet of solution, an electrochemical pulse allowed the synthesis of the polypyrrole film. By successive co-polymerisations with different oligonucleotides, they constructed a 500-µm diameter four-spot oligonucleotide array. This "electrospotting" process allows an easy and rapid preparation of oligonucleotide matrices onto a gold substrate without the need for multi-step synthesis, but with loss of the possible resolution.

d) Photolithography

Affymetrix was the pioneer in applying photolithography to microarrays (Fodor *et al.*, 1991). Their first chip was an array of 106 probes on $1cm^2$. The photolithographic DNA arrays are fabricated by *in situ* synthesis of oligonucleotides on Si wafers. The pattern of exposure to light through a mask determines which regions of the support are activated for chemical coupling. Activation by light is due to the removal of photolabile protecting groups from selected areas. After deprotection, activated nucleic acid monomers are exposed to the entire surface, but reaction takes place only with regions that were addressed by light in the previous step. The substrate is then illuminated by a second mask, which activates other sites for reaction with the following nucleic acid monomers. The procedure is repeated until the whole oligonucleotide sequence is synthesised. Pease *et al.*

(1991) improved the initial configuration and fabricated a 1.28 x 1.28-cm^2 array of 256 different tetranucleotides in 16 chemical reaction cycles, requiring 4 hours to complete. Now, their Genechip® allows the immobilisation of 9000 oligonucleotide sequences up to 30 bases in length on a glass area of 1.6cm^2. The number of compounds that can be attached by this technique is limited only by the number of synthesis sites that can be addressed with appropriate resolution. In this case, the physical limit is the radiation wavelength used for patterning. The high arraying density is the main advantage of this technique, as none of the techniques used by other companies can achieve such resolution. However, the main drawback is the *in situ* synthesis and the consequent inability to control the sequence quality. This makes the existence of a high number of redundant sites necessary. The errors in synthesis can be due to problems with the alignment of the photolithographic masks, the removal of photoprotecting groups or the phosphoramidite coupling. In order to overcome the problem of the lack of quality control, Beier and Hoheisel (2000) developed a method to check the quality of each individual DNA microarray position after the synthesis, using removable fluorescent tags. With this method, only full-length oligonucleotides were labelled. However, any previously failed deprotection leaving protected molecules could be deprotected in a succeeding step, resulting in internally deleted oligonucleotides still capable of incorporating the fluorophore, and making the hybridisation with known sequences necessary for the identification of false sequences.

e) Affinity and capture with electronic addressing

This technique has been developed by Nanogen. In principle, it is based on the immobilisation of biotinylated oligonucleotides on streptavidin sites of the array. Because DNA oligonucleotides are negatively charged, the application of an electric field favours their migration, accumulation and immobilisation to determined locations on the array (and once immobilised, the high streptavidin-biotin affinity makes the coupling essentially irreversible). In addition, these sequences can be moved away from negatively charged sites if no immobilisation is desired (Sosnowski *et al.*, 1997 and Radtkey *et al.*, 2000). This approach allows the simultaneous use of a variety of probes of different content, length and chemical composition on the same chip. Additionally, as the electric field control can also be used in the hybridisation step, the approach has significant advantage over passive arrays, where the hybridisation is limited by diffusion.

f) Selective electrodeposition

This thesis is examining a new approach for oligonucleotide arraying (Campàs and Katakis, 2002). It is based on the selective electrodeposition of biorecognition nanomodules on photolithographically defined electrodes. These biorecognition nanomodules consist of oligonucleotide molecules conjugated to colloidal gold particles. The selective deposition of these biorecognition nanomodules on electrodes held at an applied potential, permits the location of specific oligonucleotide sequences on determined electrode locations. This means that the

technique has lithographic resolution, only limited by the photolithographic limit needed to pattern the electrodes and consequently, it can be competitive with the present techniques used by the leading DNA array companies. Additionally, this approach is generic, since it can be used to construct other biochip arrays such as arrays of enzymes, antibodies, aptamers, and any other chemical of biochemical recognition elements. This deposition method, although it uses wet chemistry, is fully compatible with manufacturing and testing procedures common in the microelectronics industry, making large-scale fabrication possible. The selective deposition can be performed in short times, therefore it is conceivable that the streaming of the process can be effected at speeds that match even the most extensive contact and non contact printing heads. The main disadvantage of the method is that there is about 10% non-selective deposition between sites. This fact makes the technique unsuitable for extensive gene arrays. However, it makes it perfectly competitive for applications where 2-25 sites are needed for common diagnostics allowing the use of sample volumes from 20 to 200nL. These characteristics make the technique suitable for most common affinity or enzymatic diagnostic tests.

1.1.4. Hybridisation detection and amplification in DNA sensors and arrays

The sensitive and discriminating detection of the hybridisation event is an important feature of the successful DNA sensor or array. The biorecognition event in DNA sensors and arrays is based on the pairing affinity between complementary DNA sequences. The immobilised DNA probe recognises its complementary sequence, if the target is present in the sample. The transducer converts the biological interaction into a measurable signal, proportional to the degree of hybridisation and, consequently, to the amount of target in the sample. Whereas in direct detection techniques, the target DNA does not need to be labelled, in indirect detection techniques, labelling is a requirement to translate the hybridisation event into a signal. Label-free strategies are desirable as they facilitate reduced analysis times, and there are no undesirable effects from the label, such as steric impediments and instability of the label. However, the instrumentation cost and operational requirements of label-free techniques tend to be elevated, therefore electrochemical and fluorescence label-dependent techniques are also broadly used. In fact, most DNA chips use fluorescence methods for detection.

1.1.4.1. Hybridisation detection techniques

Several reviews describe the different transducers and detection methods used in DNA sensors (Mikkelsen, 1996; Palanti *et al.*, 1996; Yang *et al.*, 1997b; and Pividori *et al.*, 2000). Table I.3 summarises the most commonly used techniques that are briefly examined in what follows.

a) Piezoelectric methods

Piezoelectric sensors provide label-free detection. Piezoelectric transducers demonstrate high sensitivity, as they are capable of measuring sub-nanogram levels of mass change. The

transduction is based on the change in the frequency of the piezoelectric crystal when the target complementary sequence hybridises with the immobilised probe, the frequency of oscillation of the piezoelectric crystal changing proportionally to the hybridisation efficiency (Ebersole *et al.*, 1990; Caruso *et al.*, 1997a, b; Okahata *et al.*, 1992 and 1998; Ketterer *et al.*, 2000; and Bardea *et al.*, 1999). This technique allows real-time measurements, which is of great interest in DNA sensing, facilitating the determination of association constants and binding and dissociation rate constants (Okahata *et al.*, 1998 and Zhou *et al.*, 2001). Additionally, the effect of mismatches in the target sequences, hybridisation temperature or ionic strength of the hybridisation media on the kinetic parameters can be studied. Summarising, the advantages of this technique compared to fluorescence techniques are: non-requirement of probe treatment, possibility to obtain absolute binding amount and in real time, relatively rapid measurement, re-usability (removing the target oligonucleotide by heating or alkali treatment) and relatively inexpensive instrument.

Although it is not very common, piezoelectric devices can be found in a multi-array format. Tatsuma *et al.* (1999) developed four-channel QCMs, each channel giving an independent measurement. Although this is in an early step, the applicability to genetic disease diagnosis seems to be possible.

Table I.3. DNA hybridisation detection techniques.

Transducer	Techniques	Label	Real-time measurement	Multi-analysis	Ref.
Piezoelectric	Piezoelectric	Not needed	Yes	Possible	Ebersole,1990 Caruso,1997 Okahata,1992,1998 Bardea,1999 Tatsuma,1999 Ketterer,2000 Zhou,2001
Electrochemical	Chronopotentiometry Linear sweep voltammetry Cyclic voltammetry Impedance	Cationic complexes Redox compounds	Possible	Possible	Millan,1994 Palanti,1996 Marrazza,1999 Wang,1996a,1997 Napier,1997
Electrochemical	Chronoamperometry	Redox enzymes	Possible	Possible	Caruana,1999
Electrochemical	Capacitance	Not needed	Yes	Possible	Berney,2000
Optical	Colourimetry	Enzymes	Possible	Possible	Jablonski,1986 Li,1987 Kaway,1993
Optical	Surface plasmon resonance	Not needed	Yes	Possible	Jensen,1997 Georgiadis,2000 Heaton,2001
Optical	Surface plasmon resonance imaging	Not needed	Yes	Yes	Guedon,2000 Nelson,2001
Optical	Electrochemical chemiluminescence	Ruthenium chelate	No	Difficult	Blackburn,1991 Gudibande,1992 Kenten,1992 Yu,1995 Hsueh,1996
Optical	Fluorescence	Fluorophores	Yes	Possible	Abel,1996 Piunno,1995 Trabesinger,1999 Svanvik,2000b

b) Electrochemical methods

Electrochemical transduction is very useful due to its simplicity, low instrumentation costs and high sensitivity, which is comparable to fluorescence techniques. There are several electrochemical methods to detect DNA hybridisation, the use of electroactive hybridisation indicators being the most commonly used. These indicators are cationic metal complexes, like $Co(bpy)_3^{3+}$, $Co(phen)_3^{3+}$ and $Ru(bpy)_3^{3+}$, or organic compounds, like Hoechst 33258 and daunomycin, that recognise the DNA helix and intercalate selectively and reversibly into double-stranded DNA (dsDNA) (Millan *et al.*, 1994; Palanti *et al.*, 1996; Wang *et al.*, 1996a, 1997a, b, c; Napier *et al.*, 1997; and Marrazza *et al.*, 1999). This technique, although useful for obtaining general information, is not very suitable for mutation discrimination, which makes it inappropriate for diagnosis applications. Capacitance can also be used to detect specific label-free sequences, as hybridisation induces charge effects, altering the dielectric properties of the biolayer (Berney *et al.*, 2000). However, most electrochemical detection techniques include enzymatic labels. Enzymes are usually conjugated to intercalators or to avidin or streptavidin, which recognises its corresponding biotin-modified oligonucleotide, and results in an electrochemical response proportional to the hybridisation efficiency. Due to the high sensitivity of electrochemical techniques, the detection limits are always lower compared to the traditional colourimetric hybridisation assays in microtiter plates. In an advantageous strategy, Caruana and Heller (1999) labelled the target oligonucleotide directly with soybean peroxidase (SBP), a thermostable enzyme able to work at the temperatures needed in the hybridisation step. When hybridisation occurred, the enzyme was brought close to the surface, reacting with a previously deposited redox “wire” and resulting in an amperometric current proportional to the amount of hybridised strands. As no current was obtained from the enzyme-modified oligonucleotide in solution (due to the large distance between this enzyme and the redox polymer immobilised on the electrode surface), no washing step was needed and the format provided measurements in real time.

Although fluorescence is the most common detection choice for DNA arrays, some companies use electrochemical techniques. The work of Clinical Micro Sensors deserves special attention, as they have developed a versatile platform for the electronic detection of nucleic acids on microarrays (Tatsuma *et al.*, 1999). Each biochip has several electrodes, each one with a different DNA capture probe that recognises its complementary sequence. When the target hybridises with the oligonucleotide probe, a ferrocene-labelled DNA sequence (signalling probe) also hybridises with the target oligonucleotide. This implies that there is no need to incorporate a label into the target. The double hybridisation event is detected by the change in impedance. Carefully choosing the capture and signalling probes, multiple-target detection is possible, even at room temperatures. This method is not inhibited by common components of blood, serum, saliva, plasma and urine, and is compatible with PCR amplification. Moreover, since no washing is necessary, the detection works in real time. Clinical Micro Sensors have successfully applied their technology to sequence-specific

detection of amplicons, mismatch discrimination for the characterisation of single nucleotide polymorphisms, and gene expression monitoring. Additionally, the low manufacturing costs make the development of a disposable chip possible. Currently, Clinical Micro Sensors is developing the integration of specimen preparation with a new amplification method (to obviate PCR) in the same system to develop a portable device.

c) Optical methods

In DNA sensors, to use optical techniques as hybridisation detection methods, it is necessary to label the oligonucleotide with an indicator dye, a fluorophore or an enzyme that will produce a coloured product. The most commonly used techniques are based on Ultra-Violet (UV), visible (vis) or Infra-Red (IR) absorption, fluorescence and surface plasmon resonance (SPR). Below, some optical DNA sensors are reviewed.

In colourimetric DNA sensors, the enzyme is directly linked to the oligonucleotide or to antibodies, which in an affinity reaction interact with the antigen-labelled oligonucleotides. In these assays, a washing step is necessary to remove the non-hybridised oligonucleotides or the antibody-enzyme in excess, respectively. The enzyme converts its substrate into a coloured product so the change in the absorbance is directly proportional to the hybridisation efficiency (Jablonski *et al.*, 1986; Li *et al.*, 1987; and Kaway *et al.*, 1993). It is also possible to obviate the use of enzymes, by taking advantage of the absorbance of some intercalators that recognise dsDNA.

Surface plasmon resonance (SPR) is much more sensitive and moreover, it does not require any label and allows real-time measurements. In DNA sensors, the refractive index of the sensing layer changes depending on the amount of DNA in proximity with the surface. The SPR system is particularly useful for the determination of binding and dissociation kinetics, and it has been demonstrated to be sensitive enough to detect the presence of mismatches (Jensen *et al.*, 1997 and Georgiadis *et al.*, 2000). SPR can also be combined with electrochemical techniques. In this direction, Heaton *et al.* (2001) used the electric field to easily control the electrostatic forces on a surface-bound oligonucleotide monolayer. They used this field in a reversible manner to increase or decrease the rate of oligonucleotide hybridisation. Additionally, they demonstrated that a repulsive potential preferentially denatures mismatched DNA hybrids within a few minutes, while leaving the fully complementary hybrids largely intact. This sequence selectivity imparted an extremely high stringency for mutation detection based purely on electrostatic effects. However, unlike Clinical Micro Sensors, they used the strategy for DNA sensors and not for DNA arrays.

A slightly modified SPR system, called “SPR imaging”, can be used in array formats. “SPR imaging” is based on the same SPR principle, with the exception that the metal surface is imaged on a CCD camera via an imaging lens. This slight modification allows the sensing on several areas of the gold surface at the same time. Additionally, the detection is only limited by a spatial resolution of a few

micrometers. Guedon *et al.* (2000) used this system to detect the hybridisation of target sequences to four-spot polypyrrole oligonucleotide matrices and the sensitivity was a few pg mm^{-2}. Nelson *et al.* (2001) applied "SPR imaging" to the multiple detection of sequence-specific ribosomal RNA (rRNA), which is not very common and has applicability in the identification of microbial populations.

Electrogenerated chemiluminescence (ECL) is a highly sensitive technique that combines both optics and electrochemistry. It has mainly been used to detect and quantify PCR products as it increases the sensitivity and reduces routine analysis time (Blackburn *et al.*, 1991; Kenten *et al.*, 1992; Gudibande *et al.*, 1992; Yu *et al.*, 1995; and Hsueh *et al.*, 1996). In this technique, a chemiluminescence reaction is initiated by an electrical stimulus generated from the label of the complementary strand, which is a ruthenium chelate, tris(2,2'-bpy)ruthenium (II) (TBR). This technology benefits from simplicity, short analysis times, low detection limits, wide dynamic range for label quantification, and extremely stable labels.

Fluorescence is the optical technique with the highest sensitivity and lowest background noise, as weak signals are easily detected against a dark background. Fluorophores, such as acridine orange (AO) and fluorescein-isothiocyanate (FITC), are attached to the target oligonucleotide, allowing real-time monitoring of the hybridisation event and subsequent evaluation of association and dissociation kinetics (Trabesinger *et al.*, 1999). Fiber-optic sensors, based on fluorescence excitation and detection in the evanescent field of a quartz fiber, coupled to fluorescence microscopes and/or photomultipliers provide ways to detect the hybridisation of oligonucleotides. The complementary strand can be labelled with a fluorophore that in the case of biorecognition increases the emission signal (Abel *et al.*, 1996), or the double helix can be recognised by an intercalating dye, such as ethidium bromide (EB) (Piunno *et al.*, 1995), cyanine dimer YOYO or PicoGreen (Kleinjung *et al.*, 1997).

Fluorescence techniques can also be applied to homogeneous assays by using molecular beacons, scorpions and light-up probes. Molecular beacons are probes with a fluorescent moiety at one end and a quenching moiety at the other. When they are not hybridised with the target, they form a hairpin or stem-and-loop structure so that the termini are close and quenching occurs. In the presence of the target the hairpin opens because the loop portion of the molecule is complementary to the target, the two ends are then separated, and fluorescent signal results. Molecular beacons have been widely applied to real-time DNA-RNA hybridisation detection in living cells (Sokol *et al.*, 1998), to single base-pair mutation detection in PCR systems (Giesendorf *et al.*, 1998 and Chen *et al.*, 2000) and to DNA-protein binding assays (Stühmeier *et al.*, 2000). Molecular beacons have also been immobilised onto solid supports in order to apply their advantages to the DNA array format (Liu *et al.*, 2000 and Steemers *et al.*, 2000). When using molecular beacons as probes, the main advantage is that no labelling of the target is required. An interesting approach is described by Frutos *et al.* (2002), who did not use molecular beacons, but rather bimolecular beacons. In this

case, they immobilised a fluorophore-labelled probe that was hybridised with a quencher-containing sequence that was complementary except for an artificial mismatch. Hybridisation with the perfectly complementary target brought about a displacement of the mismatched sequence and a consequent increase in fluorescence. Scorpions are similar to molecular beacons, but their structure promotes a unimolecular probing mechanism instead of the common bimolecular mechanism because their amplicon specific region is attached to a PCR primer. This unimolecular mechanism makes them faster and more efficient. Additionally, scorpion primers are selective enough to give high sensitivity and to detect single-base mutations (Whitcombe *et al.*, 1999 and Thelwell *et al.*, 2000). Light-up probes are another kind of probes also used in DNA fluorescence detection in homogeneous solutions. A light-up probe is a PNA to which a dye is tethered. Upon probe hybridisation the dye binds to the target DNA, which results in a large enhancement of the dye fluorescence. These probes have several advantages as it is sufficient to measure the increase in fluorescence intensity, instead of measuring the change in the fluorescence intensity distribution (measured when energy transfer probes are used), they do not change conformation (unlike molecular beacons), and they hybridise faster and stronger than oligonucleotide probes, due to the lack of negative charges on their backbone (Ortiz *et al.*, 1998; Nikiforov *et al.*, 1999; and Svanvik *et al.*, 2000a, b).

1.1.4.2. Amplification systems

Even with all the different detection techniques, the main limiting factor for the development of DNA sensors and arrays is the sensitivity. For a viral infection, for example, the amount of DNA that has to be detected is at femtomolar (10^{-15}M) or attomolar (10^{-18}M) level. To achieve these low detection limits reliably it is possible to increase the amount of sample or to amplify the signal although, in reality, many of the approaches do both at the same time. Polymerase chain reaction (PCR) is the most commonly used technique to increase the amount of DNA in a sample. However, this procedure is time consuming. Nowadays, PCR is being integrated into sensors and arrays, in order to minimise assay time. On the other hand, signal amplification methods, like Rolling Circle Amplification (RCA), labelling or multi-labelling of the oligonucleotides with enzymes or fluorophores, Tyramide signal amplification (TSA), modified-liposomes or electrochemical amplification can be incorporated in the detection system. In the following, PCR and signal amplification methods are described.

a) Polymerase chain reaction (PCR)

PCR is the technique most commonly used for sample amplification. During PCR, the amount of DNA is exponentially amplified by repetitive cycles. PCR is also used as a method to label the target with antigens, fluorophores and labile groups, in the case that the detection technique used to measure hybridisation is not label-free (Zhu and Waggoner, 1997). Attempts have been made to

reduce the amplification time, by using small volume PCR chambers (Giordano *et al.*, 2001) or integrating the PCR step in the detection chip (Tillib *et al.*, 2001).

b) Rolling circle amplification (RCA)

RCA is a hybridisation signal amplification technique that uses padlock probes (circularising oligonucleotides). Once the probe is immobilised, the complementary target sequence is added and it hybridises. Afterwards, a second probe is added. It hybridises with part of the target and is linked to the first probe by a DNA ligase. Then, the target is removed and the padlock probe is added. In the presence of a strand-displacing DNA-polymerase, the primer is extended and, after one complete revolution of the circularised probe, the primer is displaced itself at its 5' termini. Continued polymerisation and displacement generates a single-stranded concatameric (repetitive) DNA copy of the original probe. To detect hybridisation, fluorescent complementary tags are added that hybridise at the multiple repeated sites in the elongated DNA sequence. This kind of amplification is rapid, technically simple and enables the detection of infrequent mutations in the presence of a large excess of wild-type DNA (Lizardi *et al.*, 1998 and Hatch *et al.*, 1999). RCA is a generic amplification technique, as it can also be used in antibody/antigen assays. Schweitzer *et al.* (2000) and Wiltshire *et al.* (2000) combined RCA with immunochemistry: "immunoRCA". In this technique, an oligonucleotide primer is covalently attached to an antibody. Once bound to the antigen and in the presence of circular DNA, DNA polymerase and nucleotides, amplification results in a long chain with repetitive sequences that remain attached to the antibody and that allow the antigen detection.

c) Branched DNA

Another way to amplify the hybridisation response is using branched DNA (bDNA), which is a hyperpolymeric DNA. Depending on the superstructure it is possible to find different types of bDNA: cascades, silvanes, arboranes or dendrimers. Their characteristics are uniformity, homogeneity, controlled composition and relatively large size. However, it is also possible to incorporate strands with different lengths, different orientations and even different sequences by using different blocking groups. The amplifier bDNA is commonly used after two hybridisations: a first hybridisation between the immobilised probe and the target, and a second hybridisation between the target and some preamplifiers. After this, amplifier bDNA structures are hybridised to the preamplifiers. The bDNA has multiple single-stranded arms either available for consecutive conjugation reaction with labels or for further hybridisation with labelled sequences (Collins *et al.*, 1997; Shchepinov *et al.*, 1997; Iqbal *et al.*, 1999; and Stears *et al.*, 2000). The use of bDNA amplifies the hybridisation signal and lowers the detection limit. A special case of dendritic amplification of DNA is the one based on the oligonucleotide-functionalised gold-nanoparticles used in piezoelectric techniques (Patolsky *et al.*, 2000a and Zhao *et al.*, 2001). These nanoparticles contain oligonucleotide fragments that hybridise with the target once it has already hybridised with the immobilised probe, amplifying the frequency

change. Additionally, a second amplifying step can be included by the use of a second gold-nanoparticle able to hybridise with the oligonucleotide fragments of the first one. Appropriately choosing the nanoparticle size, a detection limit of 10^{-14}M can be achieved.

d) Tyramide signal amplification™ (TSA™)

TSA™ is a signal amplification system that increases the sensitivity without loss of resolution or increase in background noise. After hybridisation between the immobilised probes and complementary oligonucleotides labelled with the epitopes biotin or dinitrophenol (DNP), streptavidin- or anti-dinitrophenol-HRP conjugates are added. Cyanide-tyramide fluorescent reagent is then added, thereby providing a fluorescent signal. In the presence of hydrogen peroxide, the HRP oxidises the phenolic ring of these cyanide-tyramide conjugates. This oxidation produces highly reactive free radical intermediates that subsequently form covalent bonds with tyrosine residues of nearby proteins used to block the immobilisation surface. In a short period, multiple depositions are possible through HRP-catalysed substrate conversion. The main advantages of this indirect labelling method are the simplicity, low cost, the 10- to 100-fold signal amplification over direct fluorescence techniques, the non-contamination of the target, and the possibility of multi-target detection by incorporating various fluorophores. Furthermore, it can be used in slide-based immunohistochemistry, *in situ* hybridisation assays and nucleic acid microarrays. TSA technology rivals *in situ* PCR particularly for detection of single copy viral nucleic acid because reproducibility and reliability are much better, and because it does not provide false positive from artefacts or back-diffusion of amplicons. However, the main drawback is the low precision for comparative analysis because of the different labelling efficiencies and protein binding affinities of the epitopes (Adler *et al.*, 2000). TSA can be also used with electrochemical detection techniques, especially impedance spectroscopy (Patolsky *et al.*, 1999).

e) Functionalised liposomes

Patolsky *et al.* (2000b) amplified oligonucleotide recognition events by using functionalised liposomes. There are two different approaches, although both are based on inhibition of the electron transfer between the redox probe $[Fe(CN)_6]^{3-}/[Fe(CN)_6]^{4-}$ and the electrode surface where the probe is immobilised. In the first approach, the liposomes are functionalised with oligonucleotides, which make them negatively charged. Before hybridisation, electron transfer from the redox probe in solution to the electrode is possible and measurable in terms of Faradaic impedance spectroscopy. However, after hybridisation, the negatively charged liposome electrostatically repels the redox probe, inhibiting the electron transfer. In the second approach, the liposomes are functionalised with biotin. Before hybridisation, the redox probe can interact with the electrode. After hybridisation with biotinylated oligonucleotides, avidin molecules are added to the system. These molecules not only interact with the hybridised biotinylated oligonucleotides, but also with the multiple biotinylated liposomes, which in turn interact with other functionalised liposomes.

This large structure inhibits the accessibility of the redox couple to the electrode surface due to steric effects.

f) Electrochemical amplification

Electrochemical amplification is based on enzyme redox cycles. There are many different strategies, which combine different enzymes and transduction chemistries. One example is the cycle that uses diaphorase and dehydrogenase enzymes (Tang and Johansson, 1995). The trigger for the system is alkaline phosphatase, which could be the label of the target. This enzyme reacts with NADPH producing NADH that is oxidised by diaphorase, and the produced NAD^+ is reduced again by a dehydrogenase enzyme (alcohol dehydrogenase, glycerol dehydrogenase, etc.). The diaphorase enzyme can be then reoxidised by a redox mediator, which is in turn oxidised on the electrode surface, providing an electron flux. Because the dehydrogenase is continuously producing NADH, each molecule of NADPH can give rise to many reduced mediator molecules that amplify the signal when oxidised on the electrode. In another example, tyrosinase and dehydrogenase enzymes are used (Bauer *et al.*, 1996 and 1998). In this case, the substrate for alkaline phosphatase is phenyl phosphate, which is converted to phenol. The phenol is oxidised to catechol by the tyrosinase, which also converts the catechol to *o*-quinone. The *o*-quinone is then recycled to catechol by glucose dehydrogenase. In this amplification scheme, the O_2 consumption by tyrosinase on a Clark-type electrode is measured.

1.1.5. Stringency, imaging systems and bioinformatics

It is not within the scope of this work to provide insights to the reliability of hybridisation events and signals. On a purely informative level the possible hybridisation and detection artefacts are mentioned here. These possible artefacts together with the formidable amount of data that is generated with DNA arrays have given rise to bioinformatics that is also briefly reviewed.

The basic requirement for a functional array system is the ability of all different probes to hybridise to their target sequences with high specificity at a single temperature. Since all the different immobilised oligomers are under the same stringency conditions, signal generation may be observed even if there is not an exact binding match. This is particularly relevant for mutation discrimination. In general, it is possible to find hybridisation conditions that give quite strong signals for hybridisation and weak signals for mismatches. For example, since A and T bind more weakly than G and C, sometimes a false GC match can give a stronger signal than a true AT match. Nanogen has solved this problem by the combination of electrophoretic propulsion and electronic stringency control (Sosnowski *et al.*, 1997 and Radtkey *et al.*, 2000). Using this technique, hybridisation stringency conditions can be controlled electrochemically, approaching the analyte to the immobilised probes and repulsing the non-complementary or low-affinity sequences by

reversing the potential. In addition to this advantage, this technique accelerates the transport of DNA and concentrates it to the corresponding locations, thereby increasing the hybridisation rates.

The most extensively used detection method is fluorescence (Pease *et al.*, 1991; Yershov *et al.*, 1996; Drobyshev *et al.*, 1997; Guschin *et al.*, 1997; Healey *et al.*, 1997; Sosnowski *et al.*, 1997; Livache *et al.*, 1998; Proudnikov *et al.*, 1998 and 2000; Gentalen and Chee, 1999; Vo-Dinh *et al.*, 1999; and Tillib *et al.*, 2001). There are two different detection systems for fluorescence that have simplified data analysis and reduced costs: scanners that use lasers to illuminate one pixel at one determined time and that are coupled to photomultiplier tubes detectors, and charge-coupled devices (CCD) with continuous light source for excitation. CCD systems allow simultaneous acquisition of large images but they have the drawback of using broadband xenon bulb technology and spectral filtration for excitation, which makes the effective separation of excitation and emission light more difficult. Some CCD-based systems, in order to solve the problem of limited light collection, integrate the signal over a significant amount of time to allow collection of enough emitted photons to create an acceptable image. However, the time required for this operation is usually longer than the time that a scanning system uses to capture a comparable area. On the contrary, the laser scanning systems use defined excitation wavelengths, which provide many more excitation and emission photons generated and collected for each pixel in a given amount of time, improving the sensitivity of the detection system.

As mentioned, arraying technology, stringency control, and imaging accuracy and time have to continue to improve to efficiently take advantage of the data generated by the new generations of biochips.

Related to data acquisition is data analysis, giving rise to another branch of expertise that has had to satisfy the demands originated by the high amounts of data obtained with biochips. Bioinformatics develop algorithms that, on one hand, are fed with the construction characteristics of the biochips and, on the other hand, take advantage of the vast and expanding genomic and expression databases. Tools are therefore being developed by the same companies and institutions that produce DNA arrays, as a result of the necessity to extract results from the huge datasets that microarray hybridisations generate. These companies develop their own software for their own array schemes, as for example Synteni's GemTools and Affymetrixís LIMS. Bioinformatics includes relational databases, data storage systems, data analysis software (which requires the development of the appropriate algorithms for handling DNA and protein sequences, with results validated against reference data and expected behaviour), mathematics and graphing packages, and interpretation and visualisation programs (as for example evolutionary trees and metabolic, signalling and transport pathway diagrams). Although these bioinformatic tools require large capacity servers linked to workstations, the state-of-the-art of informatics and the continuously improved computational capabilities are rapidly making the use of biochips easier. The importance

of bioinformatics technology in the development and use of biochips is just one more demonstration of the multidisciplinary effort required to associate the data obtained to the medical, pharmacological, toxicological and environmental information and progress in these areas.

1.1.6. Conclusions and future directions

Development of DNA sensing devices is the main focus of many research groups and high technology companies. The extensive work done in this field is particularly due to the broad versatility of these DNA sensing devices. From probes to transducer substrates, from immobilisation to characterisation and detection methods, from single to multi-analyte formats, this wide range of possibilities makes the research field very diversified and competitive.

DNA chips are rapidly replacing other DNA analysis techniques, due to the obvious advantages in terms of potential applicability in rapid DNA sequencing, expression analysis and other high throughput applications. Although research is still focused on probe immobilisation for DNA sensors and new strategies appear every day, it cannot be forgotten that the main focus is now on DNA chip arraying and detection. None of the arraying techniques described above is ideal but the best resolution is achieved by the photolithographic technique developed by Affymetrix. However, despite its high resolution, it lacks probe sequence quality control, an advantage that the other arraying techniques described can provide. Pin deposition and ink-jetting are very useful printing techniques as they provide short arraying times, although they suffer from both poor uniformity of the deposits and operational problems. The arraying technique based on capture with addressing is advantageous in terms of integration, as the control by the electric field can be applied both to immobilisation as well as hybridisation. This technique, based on the streptavidin/biotin interaction for immobilisation, uses the electric field to attract the negatively charged probes and, subsequently, to accelerate the transport of complementary DNA and repel the mismatched sequences. The present work introduces a new technique based on the selective electrodeposition of biorecognition nanomodules, consisting of colloidal gold particles modified with oligonucleotide probes. This strategy allows high resolution and fast selective deposition, is an integrated and generic approach, benefits from low manufacturing costs, is compatible with the microelectronics industry and, once optimised, can lead to miniaturisation.

Regarding the detection of hybridisation, the technique most commonly used in DNA arrays is fluorescence. In this field, new probes such as molecular beacons, scorpions and light-up probes, although not still fully developed for their use in solid-supported DNA arrays, seem to be powerful tools for sensitive, fast and label-free hybridisation measurements. The approach developed by Clinical Micro Sensors, based on electrochemical detection, is especially interesting due to several advantages: no need for a label, multiple target detection possible even at room temperatures, no interferences from common components of blood, serum, saliva, plasma and urine, compatibility with PCR amplification, no washing, real-time detection, reusability, low manufacturing costs and

possibility to miniaturise. Although fluorescence techniques are very difficult to compete with, Clinical Micro Sensors possesses at the time of writing the most competitive DNA sensor technology based on electrochemistry, although it might only be applicable to a small number of sensors, mainly for diagnostic applications.

References

Abel A.P., Weller M.G., Duveneck G.L., Ehrat M., and Widmer H.M., *Anal. Chem.*, **1996**, 68, 2905.

Acevedo D., Bretz R.L., Tirado J.D., and Abruña H.D., *Langmuir*, **1994**, 10, 1300.

Adler K., Broadbent J., Garlick R., Joseph R., Khimani A., Mikulskis A., Rapiejko P., and Killian J., in *Microarray Biochip Technology*, ed. M. Schena, BioTechniques Books, Natick, MA, USA, **2000**, pp. 221-230.

Armistead P.M. and Thorp H., *Anal. Chem.*, **2000**, 72, 3764.

Azek F., Grossiord C., Joannes M., Limoges B., and Brossier P., *Anal. Biochem.*, **2000**, 284, 107.

Balladur V., Theretz A., and Mandrand B., *J. Colloid Interface Sci.*, **1997**, 194, 408.

Bardea A., Dagan A., and Willner I., *Anal. Chim. Acta*, **1999**, 385, 33.

Barendrecht E., *J. Appl. Electrochem.*, **1990**, 20, 175.

Bauer C.G., Eremenko A.V., Ehrentreich-Förster E., Bier F.F., Makower A., Halsall H.B., Heineman W.R., and Scheller F.W., *Anal. Chem.*, **1996**, 68, 2453.

Bauer C.G., Eremenko A.V., Kühn A., Kürzinger K., Makower A., and Scheller F.W., *Anal. Chem.*, **1998**, 70, 4624.

Beier M. and Hoheisel J., *Nucleic Acids Res.*, **2000**, 28, e11.

Berney H., West J., Haefele E., Alderman J., Lane W., and Collins J.K*., Sensors Actuators B*, **2000**, 68, 100.

Blackburn G.F., Shah H.P., Kenten J.H., Leland J., Kamin R.A., Link J., Peterman J., Powell M.J., Shah A., Talley D.B., Tyagi S.K., Wilkins E., Wu T.-G., and Massey R.J., *Clin. Chem.*, **1991**, 37, 1534.

Bonn E.M., Ceres D.M., Drummond T.G., Hill M.G., and Barton J.K., *Nature Biotechnol.*, **2000**, 18, 1096.

Bretz R.L. and Abruña H.D., *J. Electroanal. Chem.*, **1995**, 388, 123.

Bretz R.L. and Abruña H.D., *J. Electroanal. Chem.*, **1996**, 408, 199.

Cai X., Rivas G., Farias P.A.M., Shiraishi H., Wang J., and Palecek E., *Electroanalysis*, **1996**, 8, 753.

Campàs M. and Katakis I., *Spanish Patent Application 200200129*, "Método para la fabricación de chips para la detección de analitos", **2002**.

Caruana D.J. and Heller A., *J. Am. Chem. Soc.*, **1999**, 121, 769.

Caruso F., Rodda E., Furlong D.N., Nikura K., and Okahata Y., *Anal. Chem.*, **1997a**, 69, 2043.

Caruso F., Rodda E., Furlong D.N., and Haring V., *Sensors Actuators B*, **1997b**, 41, 189.

Castellino A.M., *Genome Res.*, **1997**, 7, 943.

Chandler D.P., Stults J.R., Anderson K.K., Cebula S., Schick B.L., and Brockman F.J*., Anal. Biochem.*, **2000**, 283, 241.

Chen W., Martinez G., and Mulchandani A., *Anal. Biochem.*, **2000**, 280, 166.

Cheng Q. and Brajter-Toth A., *Anal. Biochem.*, **1996**, 68, 4180.

Chidsey C.E.D., Bertozzi C.R., Putvinski T.M., and Mujsce A.M., *J. Am. Chem. Soc.*, **1990**, 112, 4301.

Collins M.L., Irvine B., Tyner D., Fine E., Zayati C., Chang C., Horn T., Ahle D., Detmer J., Shen L.-P., Kolberg J., Bushnell S., Urdea M.S., and Jo D.H., *Nucleic Acids Res.*, **1997**, 25, 2979.

Drobyshev A., Mologina N., Shik V., Pobedimskaya D., Yershov G., and Mirzabekov A., *Gene*, **1997**, 188, 45.

Ebersole R.C., Miller J.A., Moran J.R., and Ward M.D., *J. Am. Chem. Soc.*, **1990**, 112, 3239.

Edelstein R.L., Tamanaha C.R., Sheehan P.E., Miller M.M., Baselt D.R., Whitman L.J., and Colton R.J., *Biosens. Bioelectron.*, **2000**, 14, 805.

Fodor S.P.A., Read J.L., Pirrung M.C., Stryer L., Lu A.T., and Solas D., *Science*, **1991**, 251, 767.

Fojta M., Doffková R., and Palecek E., *Electroanalysis*, **1996**, 8, 420.

Frutos A.G., Pal S., Quesada M., and Lahiri J., *J. Am. Chem. Soc.*, **2002**, 124, 2396.

Gentalen E. and Chee M., *Nucleic Acids Res.*, **1999**, 27, 1485.

Georgiadis R., Peterlinz K.P., and Peterson A.W., *J. Am. Chem. Soc.*, **2000**, 122, 3166.

Giesendorf B.A.J., Vet J.A.M., Tyagi S., Mensink E.J.M.G., Trijbels F.J.M., and Blom H.J., *Clin. Chem.*, **1998**, 44, 482.

Giordano B.C., Ferrance J., Swedberg S., Hühmer A.F.R., and Landers J.P., *Anal. Biochem.*, **2001**, 291, 124.

Gudibande S.R., Kenten J.H., Link J., Friedman K., and Massey R.J., *Mol. Cell. Probes*, **1992**, 6, 495.

Guedon P., Livache T., Martin F., Lesbre F., Roget A., Bidan G., and Levy Y., *Anal. Chem.*, **2000**, 72, 6003.

Guschin D., Yershov G., Zaslavsky A., Gemmell A., Shick V., Proudnikov D., Arenkov P., and Mirzabekov A., *Anal. Biochem.*, **1997**, 250, 203.

Hasebe Y., Hamada K., Hirano T., and S. Uchiyama, *Anal. Commun.*, **1997**, 34, 153.

Hashimoto K., Ito K., and Ishimori Y., *Anal. Chem.*, **1994**, 66, 3830.

Hatch A., Sano T., Misasi J., and Smith C.L., *Genetic-Analysis-Biomolecular-Engineering*, **1999**, 15, 35.

Head S.R., Parikh K., Rogers Y.-H., Bishai W., Goelet P., and Boyce-Jacino M.T., *Mol. Cell. Probes*, **1999**, 13, 81.

Healey B.G., Matson R.S., and Walt D.R., *Anal. Biochem.*, **1997**, 251, 270.

Heaton R.J., Peterson A.W., and Georgiadis R.M., *Proc. Natl. Acad. Sci.*, **2001**, 98, 3701.

Hickman J.J., Ofer D., Zou C., Wrighton M.S., Laibinis P.E., and Whitesides G.M., *J. Am. Chem. Soc.*, **1991**, 113, 1128.

Hsueh Y.-T., Smith R.L., and Northrup M.A., *Sensors Actuators B*, **1996**, 33, 110.

Imabayashi S.-I., Iida M., Hobara D., Feng Z.Q., Niki K., and Kakiuchi T., *J. Electroanal. Chem.*, **1997**, 428, 33.

Iqbal S.S., Chambers J.P., Brubaker R.R., Goode M.T., and Valdes J.J., *Mol. Cell. Probes*, **1999**, 13, 315.

Jablonski E., Moomaw E.W., Tullis R.H., and Ruth J.L., *Nucleic Acids Res.*, **1986**, 14, 6115.

Jensen K.K., Ørum H., Nielsen P.E., and Nordén B., *Biochem.*, **1997**, 36, 5072.

Joos B., Kuster H., and Cone R., *Anal. Biochem.*, **1997**, 247, 96.

Katz E. and Solov'ev A.A., *J. Electroanal. Chem.*, **1990**, 291, 171.

Katz E., Itzhak N., and Willner I., *J. Electroanal. Chem.*, **1992**, 226, 357.

Kaway S., Maekawajiri S., and Yamane A*., Anal. Biochem.*, **1993**, 209, 63.

Kenten J.H., Gudibande S., Link J., Willey J.J., Curfman B., Major E.O., and Massey R.J., *Clin. Chem.*, **1992**, 38, 873.

Ketterer T., Stadler H., Rickert J., Bayer E., and W. Göpel, *Sensors Actuators B*, **2000**, 65, 73.

Kleinjung F., Bier F.F., Warsinke A., and Scheller F.W., *Anal. Chim. Acta*, **1997**, 350, 51.

Kolakowski B., Battaglini F., Lee Y.S., Klironomos G., and Mikkelsen S.R., *Anal. Chem.*, **1996**, 68, 1197.

Krznaric D. and Cosovic B., *Anal. Biochem.*, **1986**, 156, 454.

Li P., Medon P.P., Skingle D.C., Lanser J.A., and Symons R.H., *Nucleic Acids Res.*, **1987**, 15, 5275.

Liu X., Farmerie W., Schuster S., and Tan W., *Anal. Biochem.*, **2000**, 83, 56.

Livache T., Roget A., Dejean E., Barthet C., Bidan G., and Téoule R., *Nucleic Acids Res.*, **1994**, 22, 2915.

Livache T., Roget A., Dejean E., Barthet C., Bidan G., and Téoule R., *Synthetic Metals*, **1995**, 71, 2143.

Livache T., Fouque B., Roget A., Marchand J., Bidan G., Téoule R., and Mathis G., *Anal. Biochem.*, **1998**, 255, 188.

Lizardi P.M., Huang X., Zhu Z., Bray-Ward P., Thomas D.C., and Ward D.C., *Nature Genet.*, **1998**, 19, 225.

Lucas S.W. and Harding M.M., *Anal. Biochem.*, **2000**, 282, 70.

Madoz J., Kuznetzov B.A., Medrano F.J., Garcia J.L., and Fernandez V.M., *J. Am. Chem. Soc.*, **1997**, 119, 1043.

Marrazza G., Chianella I., and Mascini M., *Anal. Chim. Acta*, **1999**, 387, 297.

Maskus M. and Abruña H.D., *Langmuir*, **1996**, 12, 4455.

Mikkelsen S.R., *Electroanalysis*, **1996**, 8, 15.

Millan K.M. and Mikkelsen S.R., *Anal. Chem.*, **1993**, 65, 2317.

Millan K.M., Saraullo A., and Mikkelsen S.R., *Anal. Chem.*, **1994**, 66, 2943.

Miller C., Cuendet P., and Grätzel M., *J. Phys. Chem.*, **1991**, 95, 877.

Nakano K., Maeda M., Uchida S., and Takagi M., *Anal. Sci.*, **1997**, 13, 455.

Napier M.E. and Thorp H.H., *Langmuir*, **1997**, 13, 6342.

Napier M.E., Loomis C.R., Sistare M.F., Kim J., Eckhardt A.E., Thorp and H.H., *Bioconjugate Chem.*, **1997**, 8, 906.

Nelson B.P., Grimsrud T.E., Liles M.R., Goodman R.M., and Corn R.M., *Anal. Chem.*, **2001**, 73, 1.

Nikiforov T.T. and Jeong S., *Anal. Biochem.*, **1999**, 275, 248.

Okahata Y., Matsunobu Y., Ijiro K., Mukae M., Murakami A., and Makino K., *J. Am. Chem. Soc.*, **1992**, 8299, 114.

Okahata Y., Kawase M., Niikura K., Ohtake F., Furusawa H., and Y. Ebara, *Anal. Chem.*, **1998**, 70, 1288.

Oliveira-Brett A.M., Serrano S.H.P., Macedo T.A., Raimundo D., Marques M.H., and La-Scalea M.A., *Electroanalysis*, **1996**, 8, 992.

Oliveira-Brett A.M., Serrano S.H.P., Gutz I., La-Scalea M.A., and M.L. Cruz, *Electroanalysis*, **1997**, 9, 1132.

Ontko A.C., Armistead P.M., Kircus S.R., and Thorp H.H., *Inorg. Chem.*, **1999**, 38, 1842.

Ortiz E., Estrada G., and Lizardi P.M., *Mol. Cell. Probes*, **1998**, 12, 219.

Palanti S., Marrazza G., and Mascini M., *Anal. Lett.*, **1996**, 29, 2309.

Pang D.-W. and Abruña H.D., *Anal. Chem.*, **1998**, 70, 3162.

Patolsky F., Katz E., Bardea A., and Willner I., *Langmuir*, **1999**, 15, 370.

Patolsky F., Lichtenstein A., and Willner I., *Angew. Chem. Int.*, **2000a**, 39, 940.

Patolsky F., Ranjit K.T., Lichtenstein A., and Willner I., *Chem. Commun.*, **2000b**, 12, 1025.

Pease A.C., Solas D., Sullivan E.J., Cronin M.T., Holmes C.P., and Fodor S.P.A., *Proc. Natl. Acad. Sci.*, **1991**, 91, 5022.

Piunno P.A.E., Krull U.J., Hudson R.H.E., Damha M.J., and Cohen H., *Anal. Chem.*, **1995**, 67, 2635.

Pividori M.I., Merkoçi A., and Alegret S., *Biosens. Bioelectron.*, **2000**, 15, 291.

Potyrailo R.A., Conrad R.C., Ellington A.D., and Hieftje G.M., *Anal. Chem.*, **1998**, 70, 3419.

Proudnikov D., Timofeev E., and Mirzabekov A., *Anal. Biochem.*, **1998**, 259, 34.

Proudnikov D., Kirillov E., Chumakov K., Donlon J., Rezapkin G., and Mirzabekov A., *Biologicals*, **2000**, 28, 57.

Radtkey R., Feng L., Muralhidar M., Duhon M., Canter D., DiPierro D., Fallon S., Tu E., McElfresh K., Nerenberg M., and Sosnowski R., *Nucleic Acids Res.*, **2000**, 28, e17.

Riccelli P.V., Merante F., Leung K.T., Bortolin S., Zastawny R.L., Janeczko R., and Benight A.S., *Nucleic Acids Res.*, **2001**, 29, 996.

Roget A., Livache T., Marchand J., and Téoule R., *Nucleosides Nucleotides*, **1995**, 14, 943.

Sauerbrey G.Z., *Z. Phys.*, **1959**, 155, 206.

Schwarz F.P., Robinson S., and Butler J.M., *Nucleic Acids Res.*, **1999**, 27, 4792.

Schweitzer B., Wiltshire S., Lambert J., O'Malley S., Kukanskis K., Zhu Z., Kingsmore S.F., Lizardi P.M., and Ward D.C., *Proc. Natl. Acad. Sci.*, **2000**, 97, 10113.

Shchepinov M.S., Udalova I.A., Bridgman A.J., and Southern E.M., *Nucleic Acids Res.*, **1997**, 25, 4447.

Sokol D.L., Zhang X., Lu P., and Gewirtz A.M., *Proc. Natl. Acad. Sci.*, **1998**, 95, 11538.

Sosnowski R.G., Tu E., Butler W.F., O'Connell J.P., and Heller M.J., *Proc. Natl. Acad. Sci.*, **1997**, 94, 1119.

Southern E.M., Maskos U., and Elder J.K., *Genomics*, **1992**, 13, 1008.

Stears R.L., Getts R.C., and Gullans S.R., *Phisiol. Genomics*, **2000**, 3, 93.

Steel A.B., Herne T.M., and Tarlov M.J., *Anal. Chem.*, **1998**, 70, 4670.

Steemers F.J., Ferguson J.A., and Walt D.R., *Nature Biotechnol.*, **2000**, 18, 91.

Stühmeier F., Hillisch A., Clegg R.M., and Diekmann S., *J. Mol. Biol.*, **2000**, 302, 1081.

Svanvik N., Westman G., Wang D., and Kubista M., *Anal. Biochem.*, **2000a**, 281, 26.

Svanvik N., Ståhlberg A., Sehlstedt U., Sjöback R., and Kubista M., *Anal. Biochem.*, **2000b**, 287, 179.

Tang X. and Johansson G., *Anal. Lett.*, **1995**, 28, 2595.

Tatsuma T., Watanabe Y., Oyama N., Kitakizaki K., and Haba M, *Anal. Chem.*, **1999**, 71, 71.

Thelwell N., Millington S., Solinas A., Booth J., and Brown T., *Nucleic Acids Res.*, **2000**, 28, 3752.

Tillib S.V., Strizhkov B.N., and Mirzabekov A.D., *Anal. Biochem.*, **2001**, 292, 155.

Tirado J.D. and Abruña H.D., *J. Phys. Chem.*, **1996**, 100, 4556.

Trabesinger W., Schütz G.J., Gruber H.J., Schindler H., and Schmidt T., *Anal. Chem.*, **1999**, 71, 279.

Umek R.M., Lin S.W., Vieltmetter J., Terbrueggen R.H., Irvine B., Yu C.J., Kayyem J.F., Yowanto H., Blackburn G.F., Farkas D.H., and Chen Y.-P., *J. Mol. Diagn.*, **2001**, 3, 74.

Vo-Dinh T., Alarie J.P., Isola N., Landis D., Winterberg A.L., and Ericson M.N., *Anal. Chem.*, **1999**, 71, 358.

Wallace R.B., Shaffer J., Murphy R.F., Bonner J., Hirose T., and Itakura K., *Nucleic Acids Res.*, **1979**, 6, 3543.

Wallace R.B., Johnson M.J., T. Hirose T., Miyaki T., Kawashima E.H., and Itakura K., *Nucleic Acids Res.*, **1981**, 9, 879.

Wang J., Cai X., Jonsson C., and Balakrishnan M., *Electroanalysis*, **1996a**, 8, 20.

Wang J., Chicharro M., Rivas G., Cai X., Dontha N., Farias P.A.M., and Shiraishi H., *Anal. Chem.*, **1996b**, 68, 2251.

Wang J., Rivas G., Cai X., Shiraishi H., Farias P.A.M., Dontha N., and Luo D., *Anal. Chim. Acta*, **1996c**, 332, 139.

Wang J., Rivas G., and Cai X., *Electroanalysis*, **1997a**, 9, 395.

Wang J., Rivas G., Cai X., Chicharro M., Parrado C., Dontha N., Begleiter A., Mowat M., Palecek E., and Nielsen P.E., *Anal. Chim. Acta*, **1997b**, 344, 111.

Wang J., Rivas G., Parrado C., Cai X., and Flair M.N., *Talanta*, **1997c**, 44, 2003.

Whitcombe D., Theaker J., Guy S.P., Brown T., and Little S., *Nat. Biotechnol.*, **1999**, 17, 804.

Wiltshire S., O'Malley S., Lambert J., Kukanskis K., Edgar D., Kingsmore S.F., and Schweitzer B., *Clin. Chem.*, **2000**, 46, 1990.

Yang D.-F., Wilde C.P., and Morin M., Langmuir, **1996**, 12, 6570.

Yang D.-F., Wilde C.P., and Morin M., Langmuir, **1997a**, 13, 243.

Yang M., McGovern M.E., and Thompson M., *Anal. Chim. Ac*ta, **1997b**, 346, 259.

Yershov G., Barsky V., Belgovskiy A., Kirillov E., Kreindlin E., Ivanov I., Parinov S., Guschin D., Drobishev A., Dubiley S., and Mirzabekov A., *Proc. Natl. Acad. Sci.*, **1996**, 93, 4913.

Yu H., Bruno J.G., Cheng T., Calomiris J.J., Goode M.T., and Gatto-Menking D.L., *J. Biolumin. Chemilumin.*, **1995**, 10, 239.

Zammatteo N., Jeanmart L., Hamels S., Courtois S., Louette P., Hevesi L., and Remacle J., *Anal. Biochem.*, **2000**, 280, 143.

Zhao Y.-D., Pang D.-W., Wang Z.-L., Cheng J.-K., and Qi Y.-P., *J. Electroanal. Chem.*, **1997**, 431, 203.

Zhao Y.-D., Pang D.-W., Hu S., Wang Z.-L., Cheng J.-K., Qi Y.-P., Dai H.-P., Mao B.-W., Tian Z.-Q., Luo J., and Lin Z.-H., *Anal. Chim. Acta*, **1999**, 388, 93.

Zhao H-Q., Lin L., Li J.R., Tang J.A., Duan M.X., and Jiang L., *J. Nanopart. Res.*, **2001**, 3, 321.

Zhou X.C., Huang L.Q., and Li S.F.Y., *Biosens. Bioelectron.*, **2001**, 16, 85.

Zhu Z. and Waggoner A.S., *Cytometry*, **1997**, 28, 206.

Abbreviations

A: adenine

AC: alternating current

AO: acridine orange

bDNA: branched DNA

bpy: 2,2'-bipyridine

C: cytosine

CCD: charge-coupled device

cDNA: complementary DNA

CV: cyclic voltammetry

DNA: deoxyribonucleic acid

DNP: dinitrophenol

dsDNA: double-stranded DNA

EB: ethidium bromide

ECL: electrogenerated chemiluminescence

EDC: 1-ethyl-3-(3-dimethylaminopropyl)carbodiimide hydrochloride

FITC: fluorescein-isothiocyanate

G: guanine

HCMV: human cytomegalovirus

HRP: horseradish peroxidase

IR: infra-red

ITO: indium-tin oxide

LSV: linear sweep voltammetry

mRNA: messenger RNA

NHS: N-hydroxysuccinimide

PCR: polymerase chain reaction

phen: phenanthroline
PNA: peptide nucleic acid
QCM: quartz crystal microbalance
RCA: rolling circle amplification
RNA: ribonucleic acid
rRNA: ribosomal RNA
SAM: self-assembled monolayer
SBH: sequencing by hybridisation
SBP: soybean peroxidase
SERS: surface-enhanced Raman scattering
SNP: single nucleotide polymorphism
SPR: surface plasmon resonance
ssDNA: single-stranded DNA
STM: Scanning Tunnelling Microscopy
T: thymine
TBR: tris(2,2'-bipyridine) ruthenium (II)
T_m: melting temperature
TSA: Tyramide signal amplification
UV: Ultra-Violet
vis: visible
XPS: X-ray photoelectron spectroscopy

1.2. Colloidal gold conjugations and deposition

One of the first studies of colloidal gold systems was reported by Faraday in 1857. He described the stability of colloids in different electrolytes. He observed that the addition of salt changed the solution colour from ruby towards blue and that solid tended to precipitate from the blue liquid. Neither the blue liquid nor the deposits could be changed back to ruby. However, he also demonstrated the protective effect of gelatine and other macromolecules, suggesting that the change induced by changing conditions was “not a change of the gold as gold, but rather a change in the relations of the surface of the particle to the surrounding medium”. His observations were the beginning of colloidal research.

1.2.1. Colloidal gold suspensions characteristics

A colloidal suspension is a dispersed phase (or discontinuous phase) distributed uniformly in a finely divided state in a dispersion medium (or continuous phase). An important characteristic of this kind of suspension is the high interfacial area between the discontinuous and the continuous phase. Additionally, each colloidal particle is made up of a limited number of molecules, and most of them lie at or close to the surface of the particle.

Of interest here are colloidal gold suspensions, where the discontinuous phase is formed by the colloidal gold particles and the continuous phase is the aqueous solution. A colloidal gold particle consists of an elemental gold core with adsorbed ions on its surface, such as Cl^-, $AuCl_2^-$ or citrate ions produced from its synthesis. These ions confer a negative charge on the particle and stabilise the dispersion in an aqueous suspension, preventing aggregation by electrostatic repulsion. Their detectability under light and electron microscopy, as well as the small size, the high stability, the non-toxicity and the possibility to conjugate them to a great variety of biomolecules, make colloidal gold particles suitable as markers (Roth and Binder, 1978). Furthermore, their ability to act as nucleation sites for the electroless deposition of silver enhances their detectability under light microscopy (Danscher and Rytter-Norgaard, 1983; Brada and Roth, 1984; De Waele *et al.*, 1989; Van den Brink *et al.*, 1990; Medalia *et al.*, 1999; and Hainfeld and Powell, 2000).

Most colloidal gold particles have a diameter between 2 and 150nm, depending on the synthesis method. All the synthesis methods are based on the reduction of Au^{3+}, usually in the form of gold trichloride, using different reducing agents and under varying conditions. This reduction produces a supersaturated molecular Au^0 solution and as the Au^0 concentration increases the gold atoms cluster and form seed of nuclei. Particle growth occurs by further deposition of metallic gold upon the nuclei (Slot and Geuze, 1985). The size of the particle depends on the concentration of Au^{3+}, the reducing agent used, its concentration, the reaction time and the hydrodynamics of the reacting mixture. In general terms, strong reductants produce a great number of nuclei and hence rather small particles, and vice versa. For example, small particle sizes (<5nm) are obtained with high

power reductants, such as sodium borohydride (Bonnard *et al.*, 1984) or yellow or white phosphorous (Faulk and Taylor, 1971; Horisberger and Rosset, 1977; and Pawley and Albrecht, 1989), and drastic conditions; medium-sized particles (6-15nm) are formed by treatment with sodium ascorbate (Horisberger and Tacchini-Vonlanthen, 1983 and Albrecht *et al.*, 1988); and larger particles are obtained with sodium citrate and milder conditions (Horisberger and Rosset, 1977; Horisberger, 1979; and Pow and Morris, 1991). Colloidal suspensions are not of uniform size, but instead a Gaussian distribution of sizes is produced (Weisbecker *et al.*, 1996; Mayya *et al.*, 1997; and Goia et Matijević, 1999). The colour of the suspension depends on the particle size, yellow-orange being the suspension of the smallest particles, red the suspension of the midrange particle size, and blue-green the suspension of the largest particles. This observed effect could be explained by Mie's theory (1908), which illustrates the size dependence of extinction by colloidal gold, relating it with the absorption and the scattering of light. On one hand, particles with diameter between 5.2 and 20.0nm absorb at around λ = 520nm, and as the diameter increases beyond 20.0nm, the absorption peak broadens and shifts towards longer wavelengths. On the other hand, scattering of white light by small particles is weak but starts to be important when the diameter is larger than 50nm. The colour of the suspension is the result of both preferential scattering and absorption at longer wavelengths for larger particles.

1.2.2. Stability of colloidal gold suspensions

The DLVO theory, developed independently by Derjaguin and Landau (1941) and Verwey and Overbeek (1948), established the basis of behaviour of colloidal systems in suspension, quantifying the combined effect of short- and long-range forces on the behaviour of this metastable system.

A number of phenomena and physical forces are relevant to the study of colloidal systems and their electrostatic stabilisation. Particles move according to Brownian dynamics subject to inertial, viscous and gravitational force fields. Since the beginning of the century, Einstein and Langevin have set forth the theory describing these phenomena (Einstein, 1906 and Langevin, 1908). This movement is subject to dispersion and repulsive (mainly electrostatic) forces whose balance decides the stability of the suspension. Quantification of dispersive forces was developed by Hamaker in 1937. As for the electrostatic potential, it was not until Gouy (1910) and Chapman (1913) developed their theory relating the potential of the particles with the thickness of the diffuse layer depending on the ionic strength of the electrolyte, that a quantitative description of these phenomena could be made. As mentioned, DLVO theory integrates these effects in a quantitative description of the interparticle potential that in general presents two minima separated by a potential maximum at intermediate distances, as depicted in Figure I.1.

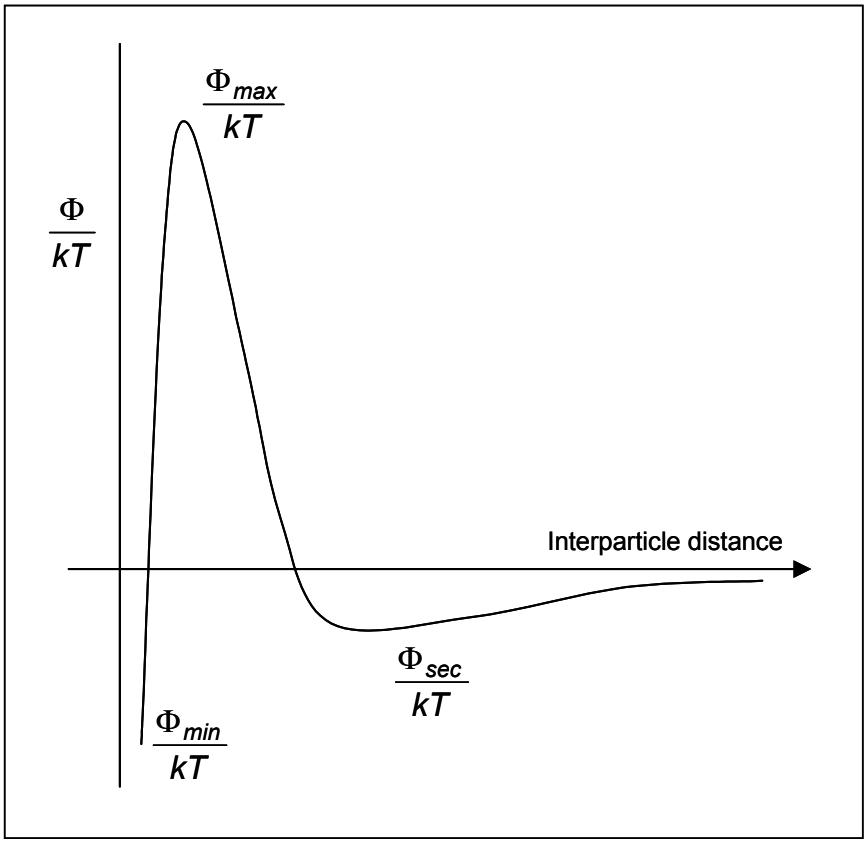

Figure I.1. General presentation of interaction potential of spheres in water.

At low ionic strength the $\frac{\Phi_{max}}{kT}$ is high enough so as to constitute a repulsive barrier that maintains the dispersion stable in the kinetic sense, although is not at thermodynamic equilibrium. An approximation of the interparticle potential expression can be reached for a symmetric electrolyte:

$$\frac{\Phi}{kT} = \frac{8\,a}{z^2 l_b} \tanh^2 \frac{ez\,\Psi_s}{4kT} \exp\left[-\frac{(r-2a)}{l_b}\right] - \frac{aA_{\text{eff}}(0)}{12kT(r-2a)} \qquad \text{(Eq. I.2)}$$

where $\frac{\Phi}{kT}$ is the dimensionless interparticle interaction potential, a is the particle radius, r is the centre-to-centre particle separation, l_b is the Debye length, z is the valence of the particle, e is the fundamental charge, Ψ_s is the particle surface potential, and A_{eff} / kT is the effective Hamaker constant. This expression indicates that Φ_{max} can be made to disappear at $\Phi = -\frac{d\Phi}{dr} = 0$ at decreasing Debye length (l_b). The Debye length can be minimised at increasing ionic strength and the critical salt concentration that brings about the irreversible flocculation can be calculated.

The above analysis leaves out of the picture chemical effects, such as the nature of the electrolyte (for example valence), although it can be accounted for implicitly. Despite this, it is a good starting

point for simple colloidal systems. Still, through the Hamaker constant (A_{eff}), the expression accounts for the properties of the dispersed phase.

Although Eq. I.2 gives a qualitative understanding of colloidal stability, the prediction of the same under particular conditions or the explanation of the instability of small particle colloids requires statistical thermodynamic considerations that lead to the definition of the stability ratio $W = J_0 / J$ where J_0 is the rate of flocculation calculated from the free diffusion of spheres, whereas J is the flux of particles under an arbitrary potential.

Substituting the linearised DLVO description of Φ allows the explicit calculation of W under specified conditions and thus the prediction of stability of a colloidal suspension. It should be noted that W is a dynamic measure of stability that also allows the calculation of the time scale of the formation of doublets that is considered the first event of flocculation. In the 1970s (Honig *et al.*, 1978) the effect of hydrodynamics on flocculation was included in the expressions for W predicting accurately shear effects on colloid stability.

The final modifications of the DLVO theory of relevance to this thesis have to do with the effect of osmotic forces and entropy on colloidal stability. Polymer addition to colloidal suspensions was known to stabilise them. Later observations rationalised the effects of polymers depending on their relation to the dispersed phase (Napper, 1983). Strongly adsorbing polymers change the nature of the surface interaction and depending on their extension in solution can stabilise or destabilise entropically the suspension. Non-adsorbing polymers can increase the osmotic drive for aggregation in the case they are excluded from the interparticle space. Quantitative descriptions of the interparticle potential as modified by the presence of polymers in colloidal systems have been developed (deGennes, 1980, 1982 and 1987).

1.2.3. Colloidal gold conjugation: stabilisation or aggregation?

As mentioned, addition of macromolecules or biomolecules, especially proteins, can protect colloidal gold from aggregation by conjugation to it, preventing cohesion of one particle to another and at the same time converting the lyophobic colloidal gold suspension to a lyophilic one that assumes many of the surface properties characteristics of the protein. However, the eventual stabilisation or destabilisation of the suspension will depend on the properties of the conjugating biomolecule, the extent of conjugation and the characteristics of the solution. The conjugation of biomolecules to colloidal gold depends on three parameters: 1) the electrostatic attraction between the negatively charged particle and the positively charged sites on the biomolecules, 2) the adsorption forces between the metal surface and the hydrophobic pockets on the biomolecule, and 3) the dative binding between gold and sulfhydryl groups, if present in the biomolecule. The temperature, the concentrations of the reagents, the pH and the ionic strength of the media have to be considered during and after conjugation. The optimum pH for conjugation is close to or slightly

above the isoelectric point (pI) of the biomolecule because at this pH the maximum adsorption efficiency and the highest stability are obtained. This point corresponds to the maximal interfacial tension and lowest solubility for the protein, favouring adsorption. If conjugation is attempted at lower pH, aggregation of colloidal gold occurs immediately upon addition of protein, due to the strong electrostatic attraction forces that cause the bonding of one protein to several gold particles. At higher pH, the adsorption is lower due to the higher charge repulsion between the protein and the colloid, and the increased hydration of the biomolecule.

Once the conjugation is concluded, blocking agents are used to block any remaining free sites, usually by adsorption, and to further stabilise the colloidal gold suspension. These blocking agents are also called protective agents. If they are negatively charged, they provide an extra repulsive force to the system, preventing aggregation. If they are positively charged, they can have a detrimental effect if not used in the appropriate concentration.

Usually, the formation of biomolecule-gold conjugates does not affect the biological activity of the biomolecule (Crumbliss *et al.*, 1992). However, alteration of biological activity may occur due to steric effects. In fact, depending on the number of contacts per molecule with the colloidal gold particle and its orientation, the adsorbed biomolecule can partially lose its specific activity or biorecognition capacity.

A variety of biomolecules can be conjugated to gold particles. Several types of proteins and small molecules have been conjugated, such as antibodies (Geoghegan *et al.*, 1977; Slot and Geuze, 1985; De Waele *et al.*, 1989; Lyon *et al.*, 1998; and Seelenbinder *et al.*, 1999), immunoglobulin binding proteins such as protein A (Brada and Roth, 1984 and Slot and Geuze, 1985), avidin (Morris and Saelinger, 1984 and González-García *et al.*, 2000) and streptavidin (Bonnard *et al.*, 1984 and González-García *et al.*, 2000), enzymes (Geoghegan *et al.*, 1977; Crumbliss *et al.*, 1992; and O'Daly *et al.*, 1995), lectins (Benhamou *et al.*, 1988) and alkanethiolates (Weisbecker *et al.*, 1996), as well as DNA (Elghanian *et al.*, 1997; Mucic *et al.*, 1998; and Storhoff *et al.*, 1998), RNA (Medalia *et al.*, 1999) and polymers.

1.2.4. Colloidal gold electrodeposition: the theory

When colloidal particles are charged, externally applied electric fields can cause them to migrate by electrophoresis. This discovery dates from 1809, when Reuss saw that colloidal particles were charged and noted their motion under an electric field. After him, Linder and Picton found that synthetic sols of sulphur, ferrocyanide, gold, silver and platinum were negatively charged, while oxide sols of iron, chromium, aluminium and cerium were positive. In 1940, Hamaker and Verwey postulated that the chief action of the electric field is to move the particles towards the electrode and produce a force that presses the particles together on the surface of the electrode in the same

way as the force of gravity presses them on the bottom of a container. In a more quantitative way, Yang *et al.* (1998) divided the deposition process in four stages:

1. At large distances from the electrode, particle transport is due to convection and migration due to external forces.
2. As a particle approaches the collector within a distance comparable to the particle size, the resulting reduction in particle mobility is due to the particle-wall hydrodynamic interaction.
3. At closer distances to the electrode, apart from hydrodynamic interaction, colloidal forces (Van der Waals and electrostatic interactions) appear. In addition, hydration, steric and hydrophobic forces may also be present and the whole process may be controlled by solution hydrodynamics.
4. When the particle is close to physical contact with the electrode, stochastic effects such as flux due to discrete charges at the collector and particles surfaces, surface heterogeneity, roughness and polymer bridging, may play significant roles. Again, hydrodynamics and particle-to-particle repulsion may play a role in the establishment of the eventual equilibrium.

Several models, like the random sequential adsorption (RSA) model, have been developed and are being refined to account for adsorbed particle interactions (Adamczyk *et al.*, 1994 and 1997, and Adamczyk and Weroński, 1997) and transport mechanisms, such as diffusion, convection, etc., in an effort to describe irreversible colloidal adsorption. Lavalle *et al.* (1999) also modified the RSA model including the diffusion of the particles during deposition, allowing an accurate description of the irreversible deposition process. In this direction, Wojtaszczyk *et al.* (1997) and Faraudo and Bafaluy (1999) modelled the same system taking into account both the transport from the bulk and the interaction with pre-adsorbed particles, which was also useful in describing irreversible colloidal adsorption.

Although the RSA model or modifications can successfully predict the adsorption of colloidal gold particles, during electrodeposition, in the presence of an electrical field, the situation changes. The general belief is that colloidal particles are electrodeposited by an irreversible process, and that mobility on the electrode is unexpected due to both the strong attraction between the positive electrode and the negatively charged colloids. However, Trau *et al.* (1996 and 1997) observed migration and postulated the appearance of an attractive force between deposited like-charged colloidal particles that overcomes the effect of the repulsive forces. This attractive force probably occurs due to electrohydrodynamic effects arising from charge accumulation near the electrodes due to the passage of ionic current through the solution and can, not only lead to particle approach, but also to monolayer or aggregation formation. Böhmer (1996) and Solomentsev *et al.* (1997) observed that electroosmosis effects could also explain particle motion.

1.2.5. Colloidal gold electrodeposition: the practice

Colloidal particle deposition in general is both a well-studied and long-applied technique, for protection of metal surfaces, painting, etc. (Narayan and Narayana, 1979; Celis and Roos, 1982; and Hovestad and Janssen, 1995). Despić and Pavlović (1984) were the pioneers in colloidal gold electrodeposition on electrodes. They took advantage of the electrophoretic mobility of colloidal gold to deposit it on a carbon electrode under an applied potential. They suggested a discharge-controlled process resulting from the oxidation of the oxygen-containing species that had adsorbed on the gold particles and the formation of oxide or oxygen, which could react with the carbon electrode and thus stabilise the deposition. In the same direction, Bailey *et al.* (2000) deposited citrate-stabilised colloidal gold on micro-patterned conductive indium-tin oxide (ITO) substrates by electrophoresis, and examined the optical properties of the patterned films. Whereas in the assembly on thiol-activated surfaces the colloidal gold particles are immobilised in a randomly and low-packed distribution (Grabar *et al.*, 1996), the structure of electrodeposited colloidal gold particles is ordered and close-packed (Giersig and Mulvaney, 1993). As mentioned above, the attractive interaction that overcomes the repulsion between colloids probably comes from electrohydrodynamic and electroosmic effects. This force of attraction can not only make colloidal particles move toward each other, but also form multilayers or agglomerates, as Despić and Pavlović (1984) and Trau *et al.* (1996) observed experimentally. In fact, Zhao *et al.* (2000) observed that higher field strength resulted in more orderly packed structures and higher coverage, probably due to the stronger attractive forces between particles.

Colloidal gold can be used as probe immobilisation tool, when conjugated to a biomolecule, such as GOx (Yabuki and Mizutani, 1995), HRP (O'Daly *et al.*, 1995), xanthine oxidase and bovine carbonic anhydrase (Crumbliss *et al.*, 1992). Combining the electrodeposition with the electrochemical determination of gold by cyclic voltammetry, differential pulse voltammetry or linear sweep voltammetry (Alexander *et al.*, 1978; Despić and Pavlović, 1984; González-García and Costa-García, 1995; Trancoso and Barros, 1989; Dequaire *et al.*, 2000; and González-García *et al.*, 2000), it is possible to determine the conjugate immobilisation on an electrode surface. Furthermore, steady-state amperometry monitoring of the enzymatic substrate consumption or enzymatic activity assay of the conjugates lead to determine if the biomolecule has retained its biological activity after conjugation and deposition under an applied potential, which makes this strategy attractive for the development of amperometric sensors (Crumbliss *et al.*, 1992; O'Daly *et al.*, 1995; and Yabuki and Mizutani, 1995).

The modular approach for DNA chip arrays proposed in the present work, depicted in Scheme I.1, is based on the dual ability of colloidal gold to be electrodeposited on the electrode surface and to be conjugated to biomolecules. Thiol-modified oligonucleotides were conjugated to colloidal gold, and the conjugations resulted in stable and functional DNA-gold nanomodules. In continuation, the

conjugates were selectively electrodeposited on different electrode surfaces, and the depositions were examined by different characterisation techniques. Moreover, the electrodeposited biorecognition modules were functional, i.e. hybridisable. The ability to selectively deposit these nanomodules and the observed functionality after immobilisation make the strategy suitable as a probe arraying method for DNA chips.

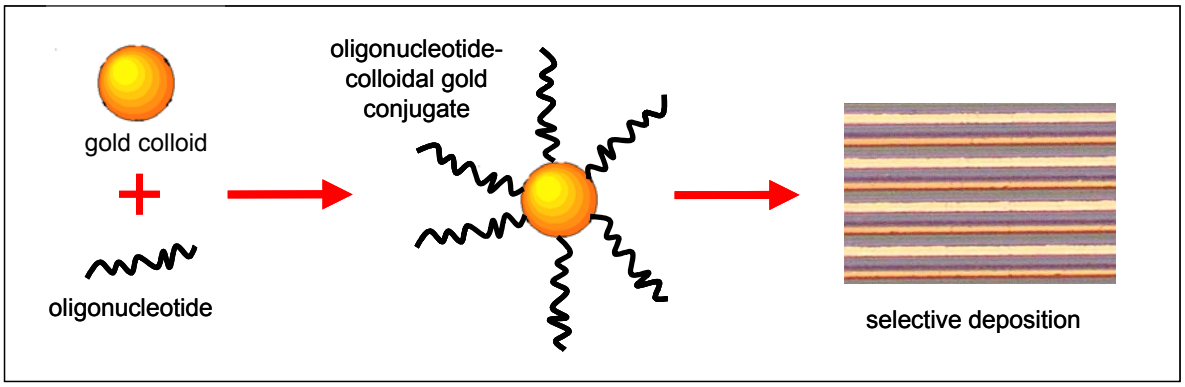

Scheme I.1. Strategy based on the conjugation of oligonucleotides on colloidal gold and the subsequent selective electrodeposition on arrays.

1.2.6. Oligonucleotide-colloidal gold hybridisation

Until now, the gold particle in the oligonucleotide-colloidal gold conjugates has been mainly used as a label in *in situ* hybridisation detection using microscopy (Van den Brink *et al.*, 1990). However, some authors have taken advantage of other colloidal gold properties in conjunction with DNA hybridisation. For example, Mirkin *et al.* (1996) constructed a nanocrystal assembly, forming dimers or trimers by hybridisation. Firstly, they tagged 13nm gold particles with non-complementary oligonucleotides. Afterwards, a duplex DNA with sticky ends complementary to the oligonucleotides on the particles was added. In that moment, aggregation occurred and as consequence a macroscopic network was created. The process could be reversed by changing the temperature above the T_m of the hybridised complementary strands, and the phenomenon was monitored by spectrophotometry. Mucic *et al.* (1998) used colloidal gold particles of different sizes simultaneously to create mixed nanostructures. Similarly, Alivisatos *et al.* (1996) demonstrated that individual 1.4nm gold particles functionalised with oligonucleotides were aligned upon a single strand of DNA in a “head-to-head” of “head-to-tail” fashion, based on the hybridisation event. These works are examples on how oligonucleotide-conjugated colloids are being used as nanomodules to construct nanoarchitectures. Modified colloids as building microblocks or nanomodules are thus becoming a powerful tool to form bottom-up superstructures with many possible applications.

Additionally, oligonucleotide-colloidal gold conjugates have been used to develop highly sensitive DNA detection methods. Reynolds *et al.* (2000) functionalised latex microspheres and gold particles with different oligonucleotide sequences and then introduced the target oligonucleotide into the

sample. When the target was complementary to both probes, the linking event between the gold particles and the latex microspheres resulted in a white-to-red colour change. Their detection limit was 500pM for a 24-base target. Elghanian *et al.* (1997) and Storhoff *et al.* (1998) used the same colloidal gold property but they observed red-to-purple/blue colour change associated to the hybridisation and consequent aggregate and polymeric net formation, which enabled to distinguish target sequences with one-base mismatches, deletions or insertions from the fully complementary ones. They detected about 10 femtomoles of a 30-base oligonucleotide.

Patolsky *et al.* (2000) used colloidal gold as an amplification tool. They labelled oligonucleotides with 12nm colloidal gold particles and used them as amplification probes in the detection of hybridisation on a QCM crystal. Their limit of detection was 100pM, but they could go to lower limits of detection by using a second amplification with dendritic oligonucleotide-colloidal gold structures, which amplified the response by 3 times. Zhao *et al.* (2001) used the same system but with 50nm colloidal gold particles and they obtained a lower detection limit of detection of 10fM.

In the present work, the colloidal gold-DNA conjugates have been used as nanomodules to develop a new and promising DNA arraying method. As it has been mentioned before, the biorecognition modules formed by thiol-modified oligonucleotides conjugated to colloidal gold were functional. In other words, the oligonucleotide sequence was able to recognise its complementary sequence when it was present into the sample. The hybridisation event was examined both colourimetrically and electrochemically, and both techniques reported satisfactory results. Moreover, the DNA sensor was able to discriminate a sequence with 4-point mutations. It is also necessary to mention that this strategy is not useful only to construct DNA arrays, but also to create any multi-sensoric platform, as colloidal gold can be conjugated to any biomolecule, and the selective electrodeposition of the nanomodules does not depend of the kind of biorecognition element.

References

Adamczyk Z., Siwek B., Zembala M., and Belouschek P., *Adv. Colloid. Interface Sci.*, **1994**, 48, 151.

Adamczyk Z., Siwek B., Zembala M., and Weroński P., *J. Colloid. Interface Sci.*, **1997**, 185, 236.

Adamczyk Z. and Weroński P., *J. Colloid. Interface Sci.*, **1997**, 189, 348.

Albrecht R.M., Goodman S.L., and Simmons S.R., *Am. J. Anat.*, **1989**, 185, 149.

Alexander R., Kinsella B., and Middleton A., *J. Electroanal. Chem.*, **1978**, 93, 19.

Alivisatos A.P., Johnsson K.P., Peng X., Wilson T.E., Loweth C.J., Bruchez M.P.Jr., and Schultz P.G., *Nature*, **1996**, 382, 609.

Bailey R.C., Stevenson K.J., and Hupp J.T., *Adv. Mater.*, **2000**, 12 (24), 1930.

Benhamou N., Gilboa-Garber N., Trudel J., and Asselin A., *J. Histochem. Cytochem.*, **1988**, 36, 1403.

Böhmer M., *Langmuir*, **1996**, 12 (24), 5747.

Bonnard C., Papermaster D.S., and Kraehenbuhl, J.-P., in *Immunolabelling for Electron Microscopy*, ed. Elsevier, New York, USA, **1984**, pp. 95-111.

Brada D. and Roth J., *Anal. Biochem.*, **1984**, 142, 79.

Celis P. and Roos J.R., in *Reviews on Coatings and Corrosion*; ed. Parkins R.N., Freund Publishing House Ltd., Tel-Aviv, Israel, **1982**, Vol 5, pp. 1-41.

Chapman D.L., *Phil. Mag.*, **1913**, 25, 475.

Crumbliss A.L., Perine S.C., Stonehuerner J., Tubergen K.R., Zhao J., Henkens R.W., and O'Daly J.P., *Biotechnol. Bioeng.*, **1992**, 40 (4), 483.

Danscher G. and Norgaard J.O.R., *J. Histochem. Cytochem.*, **1983**, 31, 1394.

deGennes P.-G., *Macromolecules*, **1980**, 13, 1069.

deGennes P.-G., *Macromolecules*, **1982**, 15, 492.

deGennes P.-G., *Adv. Colloid Interface Sci.*, **1987**, 27, 189.

Dequaire M., Degrand C., and Limoges B., *Anal. Chem.*, **2000**, 72 (22), 5521.

Derjaguin B.V. and Landau L., *Acta Physicochim.*, **1941**, 14, 633.

Despić A.R. and Pavlović M.G., *J. Electroanal. Chem.*, **1984**, 180, 31.

De Waele M., Renmans W., Segers E., De Valck V., Jochmans K., and Van Camp B., *J. Histochem. Cytochem.*, **1989**, 37 (12), 1855.

Einstein A., *Ann. Physik*, **1906**, 19, 371.

Elghanian R., Storhoff J.J., Mucic R.C., Letsinger R.L., and Mirkin C.A., *Science*, **1997**, 277, 1078.

Faraday M., *Philos. Trans. R. Soc. London*, **1857**, 147, 145.

Faraudo J. and Bafaluy J., *Europhys. Lett.*, **1999**, 46 (4), 505.

Faulk W.P. and Taylor G.M., *Immunochem.*, **1971**, 8, 1081.

Geoghegan W.D. and Ackerman G.A., *J. Histochem. Cytochem.*, **1977**, 25 (11), 1187.

Giersig M. and Mulvaney P, *J. Phys. Chem.*, **1993**, 97, 6334.

Goia D.V. and Matijević E., *Colloids Surfaces A: Physicochem. Eng. Aspects*, **1999**, 146, 139.

González-García M.B. and Costa-García A., *Bioelectrochem. Bioenergetics*, **1995**, 38, 389.

González-García M.B., Fernández-Sánchez C., and Costa-García A., *Biosens. Bioelectron.*, **2000**, 15, 315.

Gouy G., *J. Phys.*, **1910**, 9, 457.

Grabar K.C., Smith P.C., Musick M.D., Davis J.A., Walter D.G., Jackson M.A., Guthrie A.P., and Natan M.J., *J. Am. Chem. Soc.*, **1996**, 118 (5), 1148.

Hainfeld J.F. and Powell R.D., *J. Histochem. Cytochem.*, **2000**, 48 (4), 471.

Hamaker H.C., *Physica*, **1937**, 4, 1058.

Hamaker H.C. and Verwey E.J.W., *Trans. Faraday Soc.*, **1940**, 36, 180.

Honig E.P., Roeberson G.J., and Wiersema, P.H., *J. Colloid. Interface Sci.*, **1971**, 36, 97.

Horisberger M., *Biol. Cell*, **1979**, 36, 253.

Horisberger M. and Rosset J., *J. Histochem. Cytochem.*, **1977**, 25, 295.

Horisberger M. and Tacchini-Vonlanthen M., *Histochem.*, **1983**, 77, 37.

Hovestad A. and Janssen L.J.J., *J. Appl. Electrochem.*, **1995**, 25, 519.

Langevin P., *C. R. Acad. Sci. Paris*, **1908**, 146, 530.

Lavalle P., Schaaf P., Ostafin M., Voegel J.-C., and Senger B., *Prot. Natl. Acad. Sci. USA*, **1999**, 96, 11100.

Lyon L.A., Musick M.D., and Natan M.J., *Anal. Chem.*, **1998**, 70 (24), 5177.

Mayya K.S., Patil V., and Sastry M., *J. Chem. Soc., Faraday Trans.*, **1997**, 93 (18), 3377.

Medalia O., Heim M., Guckenberger R., Sperling R., and Sperling J., *J. Struct. Biol.*, **1999**, 127, 113.

Mie G., *Ann. Phys.*, **1908**, 25, 377.

Mirkin C.A., Letsinger R.L., Mucic R.C., and Storhoff J.J., *Nature*, **1996**, 382, 607.

Morris R.E. and Saenlinger C.B., *J. Histochem. Cytochem.*, **1984**, 32, 124.

Mucic R.C., Storhoff J.J., Mirkin C.A., and Letsinger R.L., *J. Am. Chem. Soc.*, **1998**, 120 (48), 12674.

Napper D.H., *Polymeric Stabilisation of Colloidal Dispersions*, Academic Press, London, United Kingdom, **1983**.

Narayan R. and Narayana B.H., in *Reviews on Coatings and Corrosion*; ed. Yahalom J., Freund Publishing House Ltd., Tel-Aviv, Israel, **1979**, Vol 4, pp. 113-153.

O'Daly J.P., Henkens R.W., Zhan J., and Zhang H., *U.S. Patent 5,391,272*, **1995**.

Patolsky F., Ranjit K.T., Lichtenstein A., and Willner I., *Chem. Commun.*, **2000**, (12), 1025.

Pawley J. and Albrecht R., *Scan. Microsc.*, **1988**, 10, 184.

Pow D.V. and Morris J.F., *Cell Tissue Res.*, **1991**, 264, 299.

Reynolds R.A.III, Mirkin C.A., and Letsinger R.L., *Pure Appl. Chem.*, **2000**, 72 (1-2), 229.

Roth J. and Binder M., *J. Histochem. Cytochem.*, **1978**, 26 (3), 163.

Russel W.B., Saville D.A., and Schowalter W.R., *Colloidal dispersions*, Press Syndicate of the University of Cambridge, Cambridge, United Kingdom, **1989**.

Seelenbinder J.A., Brown C.W., Pivarnik P., and Rand A.G., *Anal. Chem.*, **1999**, 71 (10), 1963.

Slot J.W. and Geuze H.J., *European J. Cell Biol.*, **1985**, 38, 87.

Solomentsev Y., Böhmer M., and Anderson J.L., *Langmuir*, **1997**, 13, 6058.

Storhoff J.J., Elghanian R., Mucic R.C., Mirkin C.A., and Letsinger R.L., *J. Am. Chem. Soc.*, **1998**, 120 (9), 1959.

Trancoso M.A. and Barros J.S., *Analyst*, **1989**, 114, 1053.

Trau M., Saville D.A., and Aksay I.A., *Science*, **1996**, 272, 706.

Trau M., Saville D.A., and Aksay I.A., *Langmuir*, **1997**, 13 (24), 6375.

Van den Brink W., Van der Loos C., Volkers H., Lauwen R., Van den Berg F., Houthoff H.-J., and Das P.K., *J. Histochem. Cytochem.*, **1990**, 38 (3), 325.

Verwey E.J.W. and Overbeek J.T.G., *Theory of the stability of lyophobic colloids*, ed. Elsevier, New York, USA, **1948**.

Weisbecker C.S., Merritt M.V., and Whitesides G.M., *Langmuir*, **1996**, 12 (16), 3763.

Wojtaszczyk P., Bonet Ávalos J., and Rubí J.M., *Europhys. Lett.*, **1997**, 40 (3), 299.

Yabuki S. and Mizutani F., *Denki Kagaku*, **1995**, 7, 654.

Yang C., Dabros T., Li D., Czarnecki J., and Masliyah J.H., *J. Colloid Interface Sci.*, **1998**, 208, 226.

Zhao S.Y., Lei S.B., Chen S.H., Ma H.Y., and Wang S.Y., *Colloid Polym. Sci.*, **2000**, 278, 682.

Zhao H.Q., Lin L., Li J.R., Tang J.A., Duan M.X., and Jiang L., *J. Nanoparticle Res.*, **2001**, 3, 321.

Abbreviations

att: attraction

DLVO: Derjaguin - Landau - Verwey – Overbeek

DNA: deoxyribonucleic acid

GOx: glucose oxidase

HRP: horseradish peroxidase

ITO: indium-tin oxide

rep: repulsion

QCM: quartz crystal microbalance

RNA: ribonucleic acid

RSA: random sequential adsorption

T_m: melting temperature

1.3. Signal amplification: electron transfer kinetics

1.3.1. Hybridisation detection and amplification in DNA sensors

Detection of DNA hybridisation depends on the signal generated by the biorecognition event. One of the problems is that the amount of DNA that has to be detected is at the femtomolar (10^{-15}M) or attomolar (10^{-18}M) level. To solve this problem, samples are subjected to PCR, a technique that increases the amount of DNA in the sample. Different methods can be used to detect hybridisation. In this work, an electrochemical method of transduction was employed. Among the different signal transducers, the electrochemical ones (Millan and Mikkelsen, 1993; Millan *et al.*, 1994; Hashimoto *et al.*, 1994; Kolakowski *et al.*, 1996; Palanti *et al.*, 1996; Wang *et al.*, 1996, 1997a, b, c; Napier and Thorp, 1997; Napier *et al.*, 1997; Marrazza *et al.*, 1999; Caruana and Heller, 1999; Ontko *et al.*, 1999; and Azek *et al.*, 2000) have certain advantages, such as high sensitivity, fast response, robustness, potential for cost savings, miniaturisation, mass production, portability and automatisation of measurement and data processing.

The goal in this work is to develop integrated DNA amperometric array devices. The strategy is based on the integration of probe arraying and target sensing by the same method. It consists of the arraying of biorecognition nanomodules on biochips, by selective electrodeposition of the oligonucleotide-thiol-colloidal gold conjugates on determined sites of the array, and of the measurement of the biorecognition event, using the appropriate electrochemical enzymatic label, whose electron communication with the transducer is usually mediated by a redox compound.

In the amperometric DNA sensors based on redox enzyme-labelled targets, the oxidation current obtained at the electrode is proportional to the amount of enzyme in proximity to the electrode. As the enzyme is the label, this oxidation current will be proportional to the hybridisation yield. An essential prerequisite for the development of such sensors with high sensitivity and fast response is to establish a fast electron transfer from the redox enzyme to the electrode. As it is known, most redox enzymes cannot transfer electrons to the electrode and it is here where mediators play their role. Mediators catalyse the electron transfer between enzymes and electrodes by shuttling electrons between the enzyme active site and the electrode.

For the purposes of the present work, the state-of-the-art on redox electron exchange and the study of electron transfer between biomolecules and mediators are relevant because in a label-dependent detection of hybridisation, one of three possible strategies can be envisioned as shown in Scheme I.2. Any one of these strategies can be combined with one or more enzyme cascades for signal amplification and reagentless operation (as for example when the sample contains the substrate of the immobilised enzyme whose product is substrate for the label enzyme, having the additional advantage that an inverted diffusion layer is created for the label‘s substrate starting at the electrode surface and thus contributing to the possibility of separation-less assays).

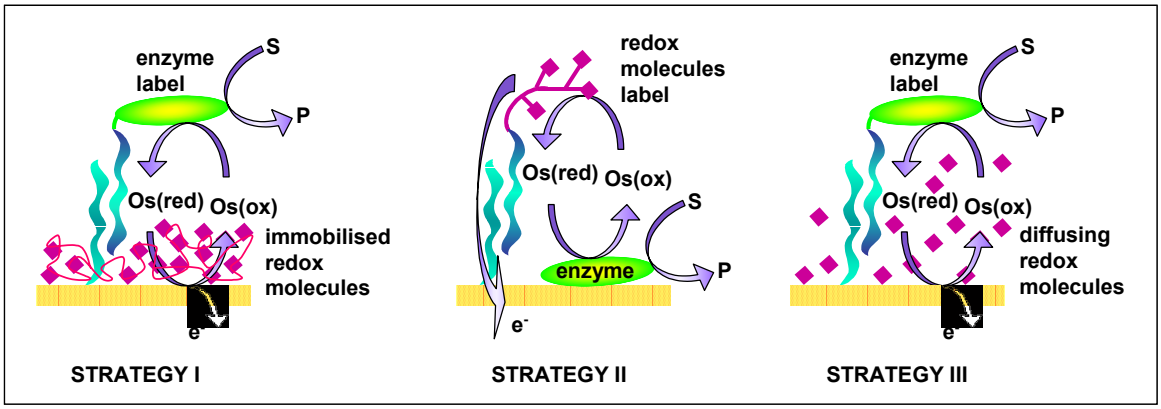

Scheme I.2. Strategies for the electrochemical detection of hybridisation.

In all these strategies, two phenomena involved in electron transport are relevant for the optimum operation of the detection scheme:

a. **Electron tunnelling**: whenever electrons have to "jump" through a distance (be it from the label's position to the electrode surface or from the enzyme active site to the mediator), it is important to take into consideration the Marcus theory of biological electron transfer to predict the electron tunnelling.

b. **Electron exchange kinetics**: when electrons are shuttled through a mediator, it is important to achieve optimum electron exchange rate constants.

In the following, the parameters influencing both phenomena are briefly discussed.

1.3.2. Marcus' theory and mediators' role

For an electron transfer reaction to occur, reactants must approach each other to facilitate electron coupling. The Marcus semiclassical theory (Marcus, 1965 and Marcus and Sutin, 1985) predicts and experiments show that electron transfer rates decay exponentially with distance, when distance exceeds atomic dimensions (>3Å), and that they also depend on the nature of the intervening medium. This dependence can be expressed as:

$$k_{ET} = 10^{13}\, exp\,(-ß(d - 3))\, exp\,(-(\Delta G^{0} + \lambda)^{2} / 4RT\lambda) \qquad \text{(Eq. I.3)}$$

where k_{ET} is the electron transfer rate constant, ß is a constant reflecting the effect of the medium, $-\Delta G^{0}$ is the reaction free energy, related to the driving force, i.e. the formal redox potential difference between the acceptor and the donor, and λ is the Marcus reorganisation energy.

The first application of Marcus' theory in the design of DNA hybridisation detection schemes has to do with the calculation of the possible distance of immobilisation of the label through which electron transfer can still occur at meaningful rates. Numerous works (Closs *et al.*, 1986; Mayo *et al.*, 1986; Lawson *et al.*, 1989; Wuttke *et al.*, 1992; Bjerrum *et al.*, 1995; Langen *et al.*, 1995; Smaley *et al.*,

1995; Gray and Winkler, 1997; and Winkler *et al.*, 1999) have shown the determined values of β to be 0.7-1.6Å^{-1} in biological layers and 0.8-1.1Å^{-1} in saturated alkane bridges. Furthermore, Bretz and Abruña (1995 and 1996) have shown that efficient electron transfer can occur even in 6-bonded monolayers through 6 bonds or through electron jumping in layer-by-layer architectures. The significance of these findings is that Strategy II of Scheme I.2 would only be feasible if the redox moiety could approach the electrode surface at short distances. Since this would require labelling of the proximal end of the target, it is likely that the specificity of the hybridisation event would be affected due to steric and electrostatic interferences of the label. Therefore, work should centre on strategies I and III, each one having relative advantages.

The second application of Eq. I.3 is relevant when studying electron transfer itself: usually enzymes are not able to transfer directly electrons to the electrode surface, due to the poor accessibility of their active site, which is imbedded in the insulating protein shell. One example was reported by Hecht *et al.* (1993), who observed a long funnel in glucose oxidase (GOx), allowing little accessibility to the solvent and with the flavin adenine dinucleotide (FAD) at the bottom. Mediators, immobilised or freely diffusing, somehow establish electrical contact between the enzyme active site and the electrode surface. In the example of GOx, mediators accept electrons from the $FADH_2$, competing with O_2, and afterwards, transfer these electrons to an electrode at a fixed potential where they are regenerated. Scheme I.3 shows these events.

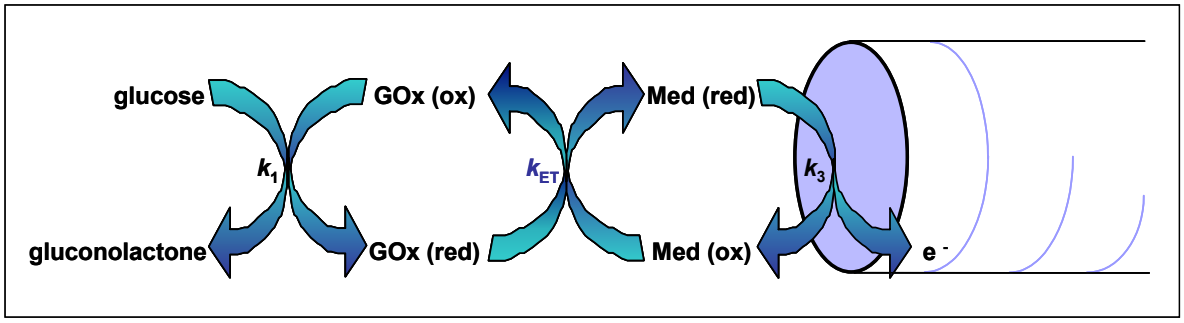

Scheme I.3. Electrochemical transduction of mediated GOx.

In some cases electron transfer between proteins and redox mediators has been observed to occur at very high rates, even at long distances (it is accepted that the mediator cannot reach the enzymatic active site). These high rates may be due to the presence of electron-conducting "pathways" where an electron tunnelling effect is produced. The existence of these "pathways" has been experimentally verified in proteins like cytochrome *c* and myoglobin using semi-synthesised proteins with incorporated redox complexes (Mayo *et al.*, 1986; Wuttke *et al.*, 1992; Casimiro *et al.*, 1993; and Gray and Winkler, 1997). These electron-conducting "pathways" are especially interesting in the DNA hybridisation detection schemes because their presence in the enzyme label can contribute to an increase in the rate constant for the electron transfer reaction with the redox mediator, permitting to obtain higher catalytic currents and lower limits of detection.

1.3.3. Electron transfer rate constant determination

The homogeneous electron transfer rate constant of the reaction between a redox couple and a redox enzyme is thus of interest in the design and improvement of biosensors, be them catalytic or affinity using redox enzyme labels, especially for the implementation of Strategy III in Scheme I.2.

These constants can be determined by cyclic voltammetry, based on the analysis of electrocatalytic reactions described by Nicholson and Shain in 1964. Two criteria must be fulfilled in order to apply their analysis: the electrode reaction of the mediator has to be fast compared to the rate between the mediator and the enzyme, and the substrate (in the case of GOx, glucose) has to be in a saturating concentration to ensure that all the enzyme is in the reduced form. If these hypotheses are fulfilled, the limiting step of the overall mechanism is the reaction between the reduced enzyme and the oxidised mediator.

The theoretical treatment of Nicholson and Shain (1964) is suitable for the EC_{cat} reactions:

$$Enz_{red} + Med_{ox} \longrightarrow Med_{red}$$

$$Med_{red} \longleftrightarrow Med_{ox} + ne^-$$

where Med_{ox} and Med_{red} are the respective redox forms of the mediator and Enz_{red} is the reduced enzyme. This theory provides an equation for the steady-state current, i_{SS}, which is an expression derived from the Savéant and Vianello (1965) equation:

$$i_{SS} = n\,F\,A\,C_{med}\,(D_{med}\,k_{ET}\,C_{enz})^{1/2} \qquad \text{(Eq. I.4)}$$

where i_{SS} is the steady-state current, A is the electrode area, C_{med} is the solution concentration of mediator, D_{med} is the diffusion coefficient of mediator, k_{ET} is the electron transfer rate constant between the enzyme and the mediator, and C_{enz} is the enzyme concentration in solution. This equation predicts a scan rate independent steady-state intensity, and a dependence of this intensity on the square root of the enzyme concentration. Plots of i_{SS} *vs.* $C_{enz}^{½}$ are linear and, according to this equation, provide the k_{ET} values if the other parameters are known.

Many works have been performed to study the “best” enzyme-mediator combination. Although ferrocene and its derivatives were the first mediators used for GOx, due to their high efficiency, stability and pH-independent redox potentials (Cass *et al.*, 1984 and 1985; Green and Hill, 1986; Jönsson *et al.*, 1989; Liaudet *et al.*, 1990; and Bourdillon *et al.*, 1993), other mediators, like derivatives of phenothiazines and phenoxazines, Wurster’s salts, benzoquinones, and cobalt, iron, ruthenium and osmium complexes have also been used (Kulys *et al.*, 1988 and 1994; Scheller *et al.*, 1989; Zakeeruddin *et al.*, 1992; and Fraser *et al.*, 1993). The apparent self-exchange rate constants of the cytochrome *c* heme site have also been studied (Coury *et al.*, 1990, 1991 and 1993). Apart from these electrochemical studies, it is necessary to mention the extensive work on

photo-induced electron transfer carried out by Gray and co-workers (Wherland and Gray, 1976; Crutchley *et al.*, 1984; Mayo *et al.*, 1986; Wuttke *et al.*, 1992; Casimiro *et al.*, 1993; Bjerrum *et al.*, 1995; Winkler and Gray, 1997; Gray and Winkler, 1997; and Winkler *et al.*, 1999), who studied the long-range electron transfer in biological systems, like myoglobin and cytochrome *c*, and helped to understand the electron tunnelling process in proteins. In recent studies, Savéant's group has developed a detailed theoretical model applicable to a large variety of experimental systems, which analysed the competition between substrate and cosubstrate on the kinetic control of the overall process, and its effect on the electrochemical response (Limoges *et al.*, 2002a, b).

In this thesis, a systematic study has been carried out independently varying the global charge and redox potential of several osmium redox complexes, and examining the effect of ionic strength and pH on the electron transfer rate constant to rationally design redox mediators for redox enzymes. These studies provide the information to elaborate enzymatic mechanisms and to rationally design electrochemical signal amplification schemes for affinity sensors.

1.3.4. Electrochemical amplification

As mentioned above, apart from intrinsically increasing the current from the redox system with more efficient mediators, it is possible to amplify the electrochemical signal using enzymatic cascades. Most electrochemical amplification schemes use dehydrogenase enzymes combined with diaphorase (Tang and Johansson, 1995) or tyrosinase (Bauer *et al.* 1996 and 1998) to detect alkaline phosphatase (ALP). The tyrosinase amplification schemes can also be used to detect phenols, although in this case it is also possible to directly oxidise the phenolic compound on the electrode surface and to reduce it using glucose dehydrogenase (GDH) (Rose *et al.*, 2001). ALP has also been detected using GOx as amplifying enzyme (Della Ciana *et al.*, 1995). In this system, *p*-hydroxyphenyl phosphate (HQP) is dephosphorilated and converted to hydroquinone (H_2Q) by ALP. H_2Q is then consumed at the electrode surface but is regenerated by GOx. In a similar way, GOx has been used to recycle and detect pentachlorophenol in contaminated soil (Male *et al.*, 1998). GOx has also been used in combination with GDH to increase the sensitivity for glucose determination in a fermentation bioreactor (Lapierre *et al.*, 1998). Such amplification schemes that include GOx suggest that the results obtained in Chapter V can be applied to rationally design hybridisation signal amplification.

References

Azek F., Grossiord C., Joannes M., Limoges B., and Brossier P., *Anal. Biochem.*, **2000**, 284, 107.

Bauer C.G., Eremenko A.V., Ehrentreich-Förster E., Bier F.F., Makower A., Halsall H.B., Heineman W.R., and Scheller F.W., *Anal. Chem.*, **1996**, 68, 2453.

Bauer C.G., Eremenko A.V., Kühn A., Kürzinger K., Makower A., and Scheller F.W., *Anal. Chem.*, **1998**, 70, 4624.

Bjerrum M.J., Casimiro D.R., Chang I.-J., Di Bilio A.J., Gray H.B., Hill M.G., Langen R., Mines G.A., Skov L.K., Winkler J.R., Wuttke D. S., *J. Bioenerget. Bioelectron.*, **1995**, 27 (3), 295.

Bourdillon C., Demaille C., Moiroux J., and Savéant J.-M., *J. Am. Chem. Soc.*, **1993**, 115, 2.

Bretz R.L. and Abruña H.D., *J. Electroanal. Chem.*, **1995**, 388, 123.

Bretz R.L. and Abruña H.D., *J. Electroanal. Chem.*, **1996**, 408, 199.

Caruana D.J. and Heller A., *J. Am. Chem. Soc.*, **1999**, 121 (4), 769.

Cass A.E.G., Davis G., Francis G.D., Hill H.A.O., Aston W.J., Higgins I.J., Plotkin E.V., Scott L.D.L., and Turner A.P.F., *Anal. Chem.*, **1984**, 56, 667.

Cass A.E.G., Davis G., Green M.J., and Hill H.A.O., *J. Electroanal. Chem.*, **1985**, 190, 117.

Casimiro D.R., Wong L.-L., Colón J.L., Zewert T.E., Richards J.H., Chang I.-J., Winkler J.R., and Gray H.B., *J. Am. Chem. Soc.*, **1993**, 115, 1485.

Closs G.L., Calcaterra L.T., Green N.J., Penfield K.W., and Miller J.R., *J. Phys. Chem.*, **1986**, 90, 3673.

Coury L.A.Jr., Oliver B.N., Egekeze J.O., Sosnoff C.S., Brumfield J.C., Buck R.P., and Murray R.W., *Anal. Chem.*, **1990**, 62, 452.

Coury L.A.Jr., Murray R.W., Johnson J.L., and Rajagopalan K.V., *J. Phys. Chem.*, **1991**, 95, 6034.

Coury L. A. Jr., Yang L., and Murray R. W., *Anal. Chem.*, **1993**, 65, 242.

Crutchley R.J., Walther R.E.Jr., and Gray H.B., *J. Am. Chem. Soc.*, **1985**, 107, 5002.

Della Ciana L., Bernacca G., Bordin F., Fenu S., and Garetto F., *J. Electroanal. Chem.*, **1995**, 382, 129.

Fraser D.M., Zakeeruddin S.M., and Grätzel M., *J. Electroanal. Chem.*, **1993**, 359, 125.

Gray H.B. and Winkler J.R., *J. Electroanal. Chem.*, **1997**, 438, 43.

Green M.J. and Hill H.A.O., *J. Chem. Soc., Faraday Trans.*, **1986**, 82, 1237.

Hashimoto K., Ito K., and Ishimori Y., *Anal. Chem.*, **1994**, 66 (21), 3830.

Hecht H.J., Schomburg D., Kalisz H.M., and Schmid R.D., *Biosens. Bioelectron.*, **1993**, 8, 197.

Jönsson G., Gorton L., and Pettersson L., *Electroanaysis*, **1989**, 1, 49.

Kolakowski B., Battaglini F., Lee Y.S., Klironomos G., and Mikkelsen S.R., *Anal. Chem.*, **1996**, 68 (7), 1197.

Kulys J. and Cénas N.K., *J. Mol. Catal.*, **1988**, 47, 335.

Kulys J., Buch-Rasmussen T., Bechgaard K., Razumas V., Kazlauskaite J., Marcinkeviciene J., Christensen J.B., and Hansen H.E., *J. Mol. Catal.*, **1994**, 91, 407.

Lapierre A.V., Olsina R.A., and Raba J., *Anal. Chem.*, **1998**, 70, 3679.

Lawson J.M., Craig D.C., Paddon-Row M.N., Kroon J., and Verhoeven J.W., *Chem. Phys. Lett.*, **1989**, 164, 120.

Liaudet E., Battaglini F., and Calvo E.J., *J. Electroanal. Chem.*, **1990**, 293, 55.

Limoges B., Moiroux J., and Savéant J.-M., *J. Electroanal. Chem.*, **2002a**, 521, 1.

Limoges B., Moiroux J., and Savéant J.-M., *J. Electroanal. Chem.*, **2002b**, 521, 8.

Male K.B., Saby C., and Luong J.H.T., *Anal. Chem.*, **1998**, 70, 4134.

Marcus R.A., *J. Chem. Phys.*, **1965**, 43, 679.

Marcus R.A. and Sutin N., *Biochim. Biophys. Acta*, **1985**, 811, 265.

Marrazza G., Chianella I., and Mascini M., *Anal. Chim. Acta*, **1999**, 387, 297.

Mayo S.L., Ellis W.R.Jr., Crutchley R.J., and Gray H.B., *Science*, **1986**, 233, 948.

Mikkelsen S.R., *Electroanalysis*, **1996**, 8 (1), 15.

Millan K.M. and Mikkelsen S.R., *Anal. Chem.*, **1993**, 65 (17), 2317.

Millan K.M., Saraullo A., and Mikkelsen S.R., *Anal. Chem.*, **1994**, 66 (18), 2943.

Napier M.E., Loomis C.R., Sistare M.F., Kim J., Eckhardt A.E., and Thorp H.H., *Bioconjugate Chem.*, **1997**, 8 (6), 906.

Napier M.E. and Thorp H.H., *Langmuir*, **1997**, 13 (23), 6342.

Nicholson R.S. and Shain I., *Anal. Chem.*, **1964**, 36, 706.

Ontko A.C., Armistead P.M., Kircus S.R., and Thorp H.H., *Inorg. Chem.*, **1999**, 38 (8), 1842.

Palanti S., Marrazza G., and Mascini M., *Anal. Lett.*, **1996**, 29 (13), 2309.

Rose A., Scheller F.W., Wollenberger U., and Pfeiffer D., *Fresenius J. Anal. Lett.*, **2001**, 369, 145.

Savéant J.-M. and Vianello E., *Electrochim. Acta*, **1965**, 10, 905.

Scheller F.W., Hintsche R., Neuman B., and Bogdanovskaya V., *Studia Biophys.*, **1989**, 132, 93.

Smalley J.F., Feldberg S.W., Chidsey C.E.D., Linford M.R., Newton M.D., and Liu Y.-P., *J. Am. Chem. Soc.*, **1995**, 99, 13141.

Tang X. and Johansson G., *Anal. Lett.*, **1995**, 28 (15), 2595.

Wang J., Rivas G., Cai X., Shiraishi H., Farias P.A.M., Dontha N., and Luo D., *Anal. Chim. Acta*, **1996**, 332, 139.

Wang J., Rivas G., and Cai X., *Electroanalysis*, **1997a**, 9 (5), 395.

Wang J., Rivas G., Cai X., Chicharro M., Parrado C., Dontha N., Begleiter A., Mowat M., Palecek E., and Nielsen P.E., *Anal. Chim. Acta*, **1997b**, 344, 111.

Wang J., Rivas G., Parrado C., Cai X., and Flair M.N., *Talanta*, **1997c**, 44, 2003.

Wherland S. and Gray H.B., *Prot. Natl. Acad. Sci. USA*, **1976**, 73 (9), 2959.

Winkler J.R., Di Bilio A.J., Farrow N.A., Richards J.H., and Gray H.B., *Pure Appl. Chem.*, **1999**, 71 (9), 1753.

Winkler J.R. and Gray H.B., *J.B.I.C.*, **1997**, 2, 399.

Wuttke D.S., Bjerrum M.J., Winkler J.R., and Gray H.B., *Science*, **1992**, 256, 1007.

Yokoyama K. and Kayanuma Y., *Anal. Chem.*, **1998**, 70, 3368.

Zakeeruddin S.M., Fraser D.M., Nazeeruddin M.-K., and Grätzel M., *J. Electroanal. Chem.*, **1992**, 337, 253.

Abbreviations

ALP: alkaline phosphatase

DNA: deoxyribonucleic acid

Enz: enzyme

FAD: oxidised flavin adenine dinucleotide

$FADH_2$: reduced flavin adenine dinucleotide

GOx: glucose oxidase

GDH: glucose dehydrogenase

H_2Q: hydroquinone

HQP: *p*-hydroxyphenyl phosphate

Med: mediator

ox: oxidised

PCR: polymerase chain reaction

red: reduced

SAM: self-assembled monolayer

1.4. Presentation of the thesis

1.4.1. Objective

The objective of this thesis is to demonstrate a new concept of DNA chip arraying and establish an electrochemical method for hybridisation. This concept is based on the construction of biorecognition nanomodules: colloidal gold suspensions modified with quality-controlled probes that are stable for the time scale of manufacturing. These biorecognition nanomodules are subsequently electrodeposited in a directed way that in principle should allow arraying with photolithographic resolution. For the technique to have technological significance, an easy electrochemical hybridisation detection method should accompany the demonstration of arraying.

1.4.2. State-of-the-art

As examined in parts 1.1-1.3, the state-of-the-art in DNA chip arraying is characterised by two kinds of systems: *in situ* synthesis of oligonucleotide probes that allows photolithographic resolution of arraying but is subject to errors and therefore needs redundant probe locations and sophisticated compensation software, and ink-jetting or pin deposition of pre-fabricated probes with significantly lower site density but with controlled probe quality. Between these two extremes exist techniques such as polypyrrolisation or photolithographic patterning of pre-activated and pre-fabricated probes that combine the benefits of both techniques. As an indicator of the capacities of each method, assuming a 128-probe device of 16-nucleotide probes and state-of-the-art manufacturing facilities, and operating at the state-of-the-art resolution for each technique, 195 x 10^3 and 5 devices per cm^2 could be packed by the photolithographic and pin deposition techniques, respectively. The manufacturing capacity could reach 875 x 10^4 and 3.1 x 10^4 devices per hour, respectively. This means that for markets larger than about 80 million devices per year, the photolithographic technique presents a definite advantage despite the higher initial investment required for the manufacturing facilities. Therefore, the answer to the question to which method belongs the future of DNA chips should be that this depends on the product concept. For the high throughput applications (pharmacogenomics, toxicogenomics) probably the pin and ink-jet deposition methods will prove competitive if sample volume is not critical. For genome analysis and sequencing or gene discovery applications probably the photolithographic techniques will prevail. However, if the main driver for the future is diagnostics or decentralised, on site diagnostics at the physician's office, or even, home diagnostics, then the deciding parameters change radically. In that case, low-cost disposable amplification cartridges can be envisioned coupled with one-use chips that have to be produced at the 1-10 euro range. It is improbable that the existing methods could provide such a solution.

Related to the product concept is the need for low detection limits. Fluorescence detection is at its limit with a monolayer of 50-100μm dots even if all the closely-packed monolayer is hybridised with

fluorescence tags. Electrochemical detection limits are in general 4 orders of magnitude higher. It is therefore questionable that the current state-of-the-art in resolution and miniaturisation can be met by the state-of-the-art in detection sensitivity. By enzyme cascades and multi-labelling, both techniques can gain in sensitivity 2 or 4 orders of magnitude. How to achieve this signal manipulation in a way that is reliable and does not interfere with biorecognition is a challenge that meeting it might define the shape of the DNA chips in the future.

Colloidal modification and use that has been chosen as arraying vehicle and immobilisation matrix presents a series of related challenges. Although the last century has been marked by an improved understanding of these metastable systems, they are still far from robust formulations that can be used in a manufacturing setting.

1.4.3. Hypothesis - significance

The basic hypothesis of this thesis is that biorecognition nanomodules can be synthesised in the form of colloidal gold particles modified with oligonucleotide probes. It is aimed that these nanomodules can form stable suspensions. It is further stipulated that they can be selectively arrayed under an electric potential field with photolithographic resolution. Additionally, it is proposed that the first steps be achieved towards proposing a hybridisation detection scheme based on electrochemistry that could yield currents of the order of 1nA from electrodes of diameters smaller than 50μm, assuming fully hybridised monolayers. This task in its entirety (not proposed to be resolved in this thesis) would mean a 5 to 7 order of magnitude signal amplification.

The significance of these propositions is that micrometric arraying will be achieved for DNA chips and an electrochemistry-based manufacturing method will be developed. If at the same time, a reliable and sensitive electrochemical detection method is reached, the technological basis will be in place to achieve low-cost, minimum-volume DNA analysis devices and microsystems. In the process, it is expected that interesting contributions will be made in the areas of colloidal science, bioorganic chemistry and redox bioelectrochemistry.

1.4.4. Methodology

The first task was to establish a reliable DNA immobilisation technique and characterisation methods. For this reason, monolayers were self-assembled simply by immersion of gold electrode surfaces into solutions containing thiol-modified oligonucleotides. The presence and reactivity of these SAMs were characterised by electrochemical, piezoelectric and colourimetric techniques. The hybridisation with enzyme-labelled sequences was verified by hybridisation ELONA assays. This activity is described in Chapter II.

The second task was to prepare functional bionanomodules. The stability of unmodified and modified colloidal gold suspensions was characterised by spectrophotometry. The conjugation of

oligonucleotides to colloidal gold particles was studied by sandwich ELONA assays and fluorescence. The functionality of the conjugated oligonucleotides was demonstrated by hybridisation ELONA assays. Finally, fluorescence was also used to study the thermal stability of the conjugation. This activity is described in Chapter III.

The third task was to achieve and study the selective electrodeposition of biorecognition nanomodules on different electrode surfaces and also to assure that they were functional through hybridisation. Several characterisation methods were used: light and electronic microscopy, spectrophotometry, colourimetry, electrochemistry and piezoelectric techniques, all described in Chapter IV.

Finally, electrochemistry was used to obtain the rate constants for the electron transfer between GOx and osmium complexes as a first step to design efficient amperometric detection techniques by molecular engineering of redox partners. This effort is described in Chapter V.

1.4.5. Most important conclusions

Regarding the preliminary “immobilisation and hybridisation” system, the absorbance from sequences with 4-point mutations was 74 $\pm$ 9% of complementary sequences, indicating the ability of the system to discriminate mutations.

It was found that 8.5mM carbonate, phosphate and citrate buffers gave the best results for the stabilisation of colloidal gold suspensions. High salt concentrations in the colloidal gold suspension produced aggregation, the effect being more important when using salts with divalent counterions. Nevertheless, this effect could be inhibited with 1% of BSA as blocking agent.

The conjugations of two model oligonucleotides to colloidal gold particles were successful and the biorecognition nanomodules were stable and functional under hybridisation temperatures, allowing to differentiate an oligonucleotide with 4-point mutations.

Selective electrodeposition (optimal conditions: +1.2V (*vs.* Ag/AgCl) for 2min) of oligonucleotide-colloidal gold conjugates was demonstrated with a 5μm resolution (limited by the resolution of the photolithographed electrodes), making the strategy suitable for array manufacturing. Additionally, after hybridisation, mutated sequences gave 32% of response compared to complementary ones, proving the viability of the strategy to differentiate 4 mutations in a 19-mer oligonucleotide.

More than 1 order of magnitude of amperometric signal amplification can be achieved by simply engaging in molecular engineering of redox partners.

1.4.6. Limitations and future work

Despite the successful results for the selective deposition, the current intensities from the hybridised sequences were always very close to current intensities from the blanks. This problem has hindered

the evaluation of the percentage of non-specific adsorption compared to selective deposition. This limitation of the electrochemical technique suggests that the effect of the non-specific adsorption could be lower. Consequently, the amplification of the electrochemical signal is required to detect not only the electrodeposition but also the biorecognition event in which a redox enzymatic label is involved. This methodology however did not allow a rational optimisation of the deposition conditions for lack of discrimination. An additional effort has to be made to eliminate any possible non-specific adsorption. Since the non-specific events are a function of shear stress and osmotic phenomena, manipulating the Reynolds number of the mobile phase in contact with the electrode and the solution osmotic parameters is warranted.

The electrochemical quartz crystal microbalance (EQCM), a device that permits label-free monitoring, has been used in preliminary experiments to evaluate the electrodeposition of colloidal gold particles. However, limitations associated with the flaw-less function of the device in the electrochemical mode appeared and this work has not advanced as expected. Once the system is fully set up, this piezoelectric technique will provide useful information, since it is highly sensitive. Additionally, real-time hybridisation measurements will be possible. This technique combined with other concurrent surface analysis techniques (electrochemical SPR) and colloidal phase characterisation (zeta potentials, light scattering) will eventually facilitate rationalised selective deposition and correlate it with suspension properties.